TRANSPORTATION RESEARCH

RECORD

No. 1284

Materials and Construction

Cement, Admixtures, and Concrete 1990

A peer-reviewed publication of the Transportation Research Board

TRANSPORTATION RESEARCH BOARD
NATIONAL RESEARCH COUNCIL
WASHINGTON, D.C. 1990

Transportation Research Record 1284
Price: $16.00

Subscriber Category
IIIB materials and construction

Modes
1 highway transportation
5 other

Subject Areas
25 structures design and performance
32 cement and concrete
33 construction
40 maintenance

TRB Publications Staff
Director of Publications: Nancy A. Ackerman
Senior Editor: Naomi C. Kassabian
Associate Editor: Alison G. Tobias
Assistant Editors: Luanne Crayton, Kathleen Solomon, Norman Solomon
Graphics Coordinator: Diane L. Ross
Office Manager: Phyllis D. Barber
Production Assistant: Betty L. Hawkins

Printed in the United States of America

Library of Congress Cataloging-in-Publication Data
National Research Council. Transportation Research Board.

Cement, admixtures, and concrete, 1990.
p. cm.—(Transportation research record ISSN 0361-1981 ; no. 1284)
ISBN 0-309-05063-4
1. Pavements, Concrete—Testing. 2. Pavements, Reinforced concrete—Testing. 3. Concrete—Additives. I. National Research Council (U.S.). Transportation Research Board. II. Series: Transportation research record ; 1284.
TE7.H5 no. 1284
[TE278]
388 s—dc20
[625.8'4] 90-23855
CIP

Sponsorship of Transportation Research Record 1284

GROUP 2—DESIGN AND CONSTRUCTION OF TRANSPORTATION FACILITIES
Chairman: Raymond A. Forsyth, Sacramento, California

Concrete Section
Chairman: Thomas J. Pasko, Jr., Federal Highway Administration, U.S. Department of Transportation

Committee on Performance of Concrete
Chairman: William P. Chamberlin, Schenectady, New York
M. Arockiasamy, Philip D. Cady, James R. Clifton, Glenn William De Puy, John W. Figg, Richard H. Howe, Inam Jawed, Joseph F. Lamond, Stella L. Marusin, Richard C. Meininger, Roger P. Northwood, John T. Paxton, V. Ramakrishnan, John Ryell, Charles F. Scholer, Richard Karl Smutzer, David Stark, Hollis N. Walker, Robert Warburton, Richard Edwin Weyers, James H. Woodstrom

Committee on Mechanical Properties of Concrete
Chairman: Michael M. Sprinkel, Virginia Transportation Research Council
Archie F. Carter, Jr., J. Harold Deatherage, James T. Dikeou, Wilbur Charles Greer, Jr., Lloyd E. Hackman, Inam Jawed, Kevin Jones, Louis A. Kuhlmann, Joseph F. Lamond, V. M. Malhotra, Richard C. Meininger, Edward G. Nawy, Sandor Popovics, V. Ramakrishnan, Masood Rasoulian, David R. Reidenouer, Gary L. Robson, Robert R. Santoro, Ernest Schrader, Raymond J. Schutz, S. P. Shah, Parviz Soroushian, Peter C. Tatnall, Dan G. Zollinger

Committee on Chemical Additions and Admixtures for Concrete
Chairman: H. Celik Ozyildirim, Virginia Transportation Research Council
William F. Boles, Bernard C. Brown, John W. Bugler, Ramon L. Carrasquillo, Henry H. Duval, Jr., Richard D. Gaynor, W. J. Head, Inam Jawed, Daniel P. Johnston, Louis A. Kuhlmann, T. J. Larsen, Michael F. Pistilli, Joseph H. Pound, V. Ramakrishnan, Lawrence R. Roberts, Philip A. Rosskopf, Raymond J. Schutz, Maris A. Sermolins, A. Haleem Tahir, Suneel N. Vanikar, David Whiting

Federick D. Hejl, Transportation Research Board staff

Sponsorship is indicated by a footnote at the end of each paper. The organizational units, officers, and members are as of December 31, 1989.

Transportation Research Record 1284

Contents

Foreword

The papers in this Record, dealing with various facets of cement, admixtures, and concrete, should be of interest to construction, design, and materials engineers and researchers.

Dossey et al. present regression models to predict pavement concrete properties made with several coarse aggregates using data on the chemical composition of the aggregate as input to the models. Rix et al. suggest that seismic measurements offer a reliable alternative to conventional penetration resistance and cylinder compression testing to determine the properties of portland cement concrete during curing. Oluokun et al. report the results of tests investigating the gain of physical properties of concrete with time. They observed that the first 12 hr after casting was the period of fastest development of physical properties and that the elastic modulus developed much faster than either the tensile or the compressive strength, which developed at approximately the same rate. Leming presents the results of a study to determine and compare properties of high-strength concrete produced with various sets of materials that are available to the North Carolina Department of Transportation. Oloukun et al. investigated the causes of early-age cracking reported in some precast, prestressed, steam-cured structural members at fabrication sites. They report that observed low tensile strength developed in steam-cured test specimens may be partially responsible for the cracking reported during strand release and form stripping. Kudlapur and Nawy investigated the shear interaction between high-strength regular portland cement concrete and cold weather high-strength concretes as is experienced in rehabilitation of bridge decks and other infrastructure systems. Brown discusses the chemistry of the early reactions that occur during the hydration of portland cement concrete. Luciano and Bobrowski propose that sound experimental design principles, rather than three-point curves, be used to determine high-strength concrete mixture proportions that maximize performance while minimizing cost.

Scannell and Clear studied the corrosion characteristics of epoxy-coated reinforcing steel in concrete. After 6.5 years of outdoor exposure in a northern environment, results indicate the epoxy-coated rebars are far more resistant to corrosion-induced damage than uncoated bars. Whiting surveyed highway agencies on the use of penetrating sealers for portland cement concrete. He found a high level of interest in the use of sealers, but actual applications are still limited. He also found that linseed oil is still widely used, although it has been discontinued by many agencies because of its poor long-term performance.

Simons discusses the technique of optimizing various concrete mixes to develop mixes that are easier to produce, provide all of the structural and performance requirements necessary for the project, and are the most cost-effective material for the application. In both examples cited by Simons, fly ash was found to be an important ingredient to the mixtures. Luther reviews high-performance silica fume–modified cementitious repair materials that have been used successfully in North America and Europe. Halstead provides an overview of some of the opportunities and concerns on the use of fly ash as a pozzolan in hydraulic cement concrete for the construction of highways and other transportation facilities.

Prediction of Concrete Properties Using Coarse Aggregate Chemical Composition Data

TERRY DOSSEY, HUMBERTO CASTEDO, AND B. FRANK MCCULLOUGH

Regression models that predict the compressive strength, tensile strength, modulus of elasticity, and drying shrinkage of concrete made with several coarse aggregates are presented in this paper. The findings are part of a comprehensive research study being conducted in Texas for determining the effect of aggregates on the performance of concrete pavements. Using statistical analysis of laboratory test data from concrete samples made with eight commonly used aggregates of known chemical composition, regression models were developed to predict the concrete properties just mentioned. The predicted values were then compared with the laboratory test results, and the models were used to predict the concrete properties of 11 additional untested coarse aggregates also used for pavement construction in Texas. The predicted concrete properties were within the pavement concrete range reported for these types of concrete mixtures. These prediction models can estimate preliminary information for coarse aggregates or coarse aggregate blends from chemical composition data before casting and testing of concrete samples. This will allow for initial screening of proposed new sources of coarse aggregate or tentative blends of new or existing aggregate sources of known chemical composition.

In portland cement concrete (PCC) pavement construction, the importance of using the right type and quality of aggregate cannot be overemphasized because the fine and coarse aggregates occupy roughly 60 to 75 percent of the concrete volume (70 to 80 percent by weight) (*1*). For given environmental conditions, changes in concrete volume stresses depend on modulus of elasticity, thermal properties, and drying shrinkage of the concrete. These concrete properties, as well as wheel load stresses, depend on the tensile strength and modulus of the concrete, which in turn depend largely on the type of coarse aggregate used (*2*). In PCC pavement design, most states do not consider coarse aggregate type as a design variable. However, field observation has shown significant variation in the performance of pavements built with different coarse aggregates (*3*).

The findings reported in this paper are part of results from a comprehensive research study being conducted by the Center for Transportation Research (CTR) of The University of Texas at Austin for the Texas State Department of Highways and Public Transportation (SDHPT) to determine the effects of aggregate types on the performance of concrete pavements.

The Texas SDHPT has recently taken steps to recognize the influence of coarse aggregate type on the performance of concrete pavements. SDHPT has developed PCC pavement designs that incorporate these effects to provide equal performance of pavements made with any type of coarse aggregate (*4*). The large number of aggregate sources in the state that are approved for concrete pavement construction make this consideration important. Sand and siliceous river gravel; limestone; to some extent, granite, basalt, and sandstones; and blends of these aggregates can be used for the construction of concrete pavements in Texas.

Center for Transportation Research, University of Texas at Austin, Austin, Tex. 78712.

OBJECTIVE, APPROACH, AND SCOPE

The objective of this paper is to present the Texas SDHPT approach for fast and simple assessment of pavement concrete properties that can be used with appropriate pavement design procedures. The advantage of this technique is that by using a surrogate test such as the chemical analysis of the coarse aggregate (chemical and mineral composition of the aggregate can be obtained, in most cases, directly from the supplier), one can quickly estimate preliminary concrete properties versus age before expensive laboratory testing. This permits the initial evaluation of proposed new sources of coarse aggregate or blends and can also be used to predict the current performance of aggregates such as limestone, which is quarried from bedded strata and thus may vary significantly in chemical composition, even when quarried from the same source.

The approach taken in this study was to develop regression models for predicting 28-day (256 days for shrinkage) concrete properties from the chemical makeup of the coarse aggregate used to produce the concrete. These models were developed with laboratory test data from concrete made with eight carefully chosen coarse aggregates representing the wide range of aggregates used in Texas pavements.

The interdependence, or correlation, that exists among the various chemical components of the coarse aggregates was determined using chemical composition data from 20 different aggregate types. Once the 28- (or 256-) day models were developed, two models (Models 1 and 2) were proposed to predict the concrete properties at any age using the 28- or 256-day value and the curing age as the sole input.

These prediction equations are limited to modeling properties of concrete mixes made with Type I cement cured at 75°F and 40 percent relative humidity. These curing conditions were chosen to simulate field curing in pavements. The predictions may not be applicable to concrete mixtures made with other types of cement and cured under other conditions.

All of the aggregates tested conform to SDHPT Specification 360. This ensured adequate grading and reduced any effect of aggregate shape. No deleterious aggregates were used, and the models are not intended to predict for them.

TEST RESULTS

Laboratory test results of concrete specimens made with eight different coarse aggregates were obtained using standard ASTM procedures as follows:

		Curing Conditions		
Laboratory Property	*ASTM Standard*	*°F*	*Humidity (%)*	*Curing Time (days)*
Compressive strength	C 39	75	40	1, 3, 7, 28
Tensile strength	C 496	75	40	1, 3, 7, 28
Modulus of elasticity	469	75	40	1, 3, 7, 28
Drying shrinkage	None	75	40	1 through 256

Chemical composition data were obtained for coarse aggregates from 20 different sources using X-ray diffraction, fusion, and coulometric techniques (*5*). The major chemical components of eight commonly used aggregates are reported in Table 1. These aggregates were also used to obtain the pavement concrete properties just listed. The X-ray diffraction results of all aggregates used as part of this study for which chemical composition data were available are presented in Table 2.

DATA ANALYSIS METHODOLOGY

It is generally accepted that the curing rate of concrete depends primarily on the type of cement used and the temperature and humidity conditions experienced during curing (*6*). The use of different types of coarse aggregate, therefore, has the greatest effect on the final strength of the concrete. Because all the concrete specimens cast for this study were mixed and cured identically, any differences (excluding normal material variances, laboratory test repeatability, etc.) in the final properties can be attributed to aggregate influence, with curing rates being similar for all specimens (*7*).

Estimating concrete properties from coarse aggregate chemical composition data was therefore a two-step process. The first phase of the analysis consisted of developing models for predicting 28-day concrete properties from chemical composition. Because drying shrinkage develops more slowly, and because long-term shrinkage data were available for 256-day cured specimens, these long-term values were used in the analysis instead of the 28-day values.

CONCRETE PROPERTIES AT 28 DAYS

Because concrete properties were tested for only the eight aggregates listed in Table 1, there are insufficient degrees of freedom to use all 10 chemical components or their interactions in a standard analysis of variance (ANOVA). A correlation analysis was run instead, as a preliminary step, using the Pearson product-moment correlation (*8*) to determine which chemicals were interdependent or correlated with one another. All 20 aggregates were used to determine these chemical associations. The results indicated that the chemicals belong to the following groups, probably as they exist naturally as ores:

Group 1	*Group 2*	*Group 3*	*Group 4*	*Group 5*
SiO_2	CaO CO_2	MgO	Fe_2O_3 MnO	Al_2O_3 TiO_2 Na_2O K_2O

Further examination of the chemical data revealed a strong negative correlation between Groups 1 and 2, indicating that whenever SiO_2 is present in high concentrations, CaO and CO_2

TABLE 1 COARSE AGGREGATE CHEMICAL ANALYSIS DATA

Source	Aggregate Type		SiO_2	CaO	MgO	CO_2	MnO	Fe_2O_3	Al_2O_3	Na_2O	K_2O	TiO_2	Other
McCelligan	Dolomite	(DL)	6.53	34.9	13.0	42.9	.02	0.21	0.38	0.09	0.26	0.02	1.69
Western-T	S/L	(WT)	68.5	11.4	0.35	8.98	.05	2.64	3.97	0.85	1.1	0.17	1.99
Bridpt+TinTop	L+S/L	(BTT*)	17.53	42.55	0.71	35.65	0.04	0.57	0.56	0.15	0.30	0.04	1.91
Feld (TCS)	Limestone	(LS)	2.56	45.7	5.97	43.3	.01	0.06	0.21	0.14	0.21	0.02	1.82
Fordyce	SRG	(SRG)	93.8	2.23	0.11	1.77	.01	0.76	0.63	0.18	0.32	0.1	0.09
Vega	SRG	(VG)	66.9	11.6	0.39	9.07	.07	2.33	4.22	0.95	1.16	0.19	3.12
Ferris	L/S	(FR)	14.2	42.1	0.43	34.4	.10	3.70	0.87	0.17	0.26	0.06	3.71
Scotland	Granite	(GR)	71.3	1.5	0.63	0.59	.03	1.52	14.3	4.4	3.83	0.29	1.61
TXI-Boonesville		(BO)	5.26	49.8	0.34	40.0	0.03	0.40	0.41	0.06	0.14	0.02	3.54
McCelligan Canyon #2		(DL2)	7.31	35.2	12.4	42.8	0.02	0.21	0.42	0.11	0.29	0.03	1.21
Ferris #2		(FR2)	12.5	42.8	0.44	35.4	0.10	3.56	0.76	0.17	0.28	0.06	3.93
TCP-Cleburne #51		(CL)	18.8	41.3	0.49	34.7	0.05	0.72	0.62	0.19	0.31	0.04	2.78
Ingram Whitehead		(IW)	23.9	38.7	0.44	31.2	0.05	0.77	0.69	0.21	0.32	0.05	3.67
TXI-Tin Top #2		(TT2)	33.6	34.1	0.35	27.9	0.06	0.91	0.74	0.16	0.32	0.05	1.81
Pioneer-Landess Pit		(PI)	14.7	42.8	0.42	34.7	0.09	3.31	0.65	0.15	0.25	0.05	2.88
Jobe-Hueco		(JH)	17.5	41.7	1.62	35.1	0.02	0.45	1.01	0.16	0.35	0.06	2.03
Rainbow-Baker Pit		(RB)	32.8	34.6	0.41	27.9	0.06	0.98	0.69	0.21	0.36	0.05	1.94
A-Rock Brazos River Pit		(BR)	55.6	20.2	0.43	16.4	0.03	0.89	2.31	0.64	0.93	0.11	2.46
Vulcan-Mexico		(VM)	0.27	53.1	0.55	43.8	0.01	0.03	0.23	0.18	0.28	0.04	1.51

* These aggregates combined in a 50/50 blend when tested in the laboratory for concrete properties.

TABLE 2 MINERALOGICAL RESULTS (X-RAY DIFFRACTION)

Source	Aggregate Type	Minerals Found		
		Most Abundant	Second	Third
McCelligan Canyon # 1	DL	Dolomite	Calcite	Quartz
Western-Tascosa	WT	Quartz	Calcite	
Tin-Top # 1	BTT	Calcite	Quartz	
Bridgeport	BTT	Calcite	Dolomite	Quartz
Feld (TCS)	LS	Calcite	Dolomite	Quartz
Fordyce	SRG	Quartz	Calcite	
Vega	VG	Quartz	Calcite	
Ferris # 1	FR	Calcite	Quartz	
Scotland Granite	GR	Quartz	Albite	
TXI-Boonesville	BO	Calcite	Quartz	
McCelligan Canyon # 2	DL2	Dolomite	Calcite	Quartz
Ferris # 2	FR2	Calcite	Quartz	
TCP-Cleburne # 51	CL	Calcite	Quartz	
Ingram Whitehead	IW		Calcite	Quartz
TXI-Tin Top # 2	TT2	Calcite	Quartz	
Pioneer-Landerss Pit	PI	Calcite	Quartz	
Jobe-Hueco	JH	Calcite	Quartz	
Rainbour-Baker Pit	RB	Calcite	Quartz	
A-Rock Brazos River Pit	BR	Calcite	Quartz	
Vulcan-Mexico	VM	Calcite	Quartz	

are not present in an aggregate. It would therefore be unnecessary to include both groups in the statistical analysis. On the basis of these observations, only Groups 2 through 5 were selected as regressors, using the compound present in highest concentration to represent each group. Thus CaO, MgO, Fe_2O_3, and Al_2O_3 were selected as primary regressors. CaO was chosen over CO_2 because a portion of the CO_2 was released from $CaMg(CO_3)_2$ (dolomite) during the high-temperature analysis. This was confirmed by the partial positive correlation between CO_2 and MgO observed in the analysis.

REGRESSION MODELS FOR 28-DAY CONCRETE PROPERTIES

Using the four primary regressors selected and their two-way interactions, a stepwise regression (*8*) was used to determine the best models for 28-day tensile strength, compressive strength, modulus of elasticity, and 256-day drying shrinkage. Drying shrinkage was predicted at 256 days because laboratory measurements were available for all eight tested aggregates at that time. Models were restricted to three or fewer predictors to avoid the artificially high R^2 (and consequent low predictive ability) associated with models with few degrees of freedom (*9*). Calculating regression coefficients resulted in the following models:

$$f_c(28) = -403.2 \cdot \ln(\text{CaO}) + 6.806\ (\text{CaO}/\text{Al}_2\text{O}_3) + 5{,}120.5 \quad (1)$$

$$f_t(28) = -59.238 \cdot \ln(\text{CaO}) + 46.884 \cdot \ln(\text{MgO}) + 1.7159\ (\text{CaO}/\text{MgO}) + 572.2 \quad (2)$$

$$E(28) = -0.4135 \cdot \ln(Al_2O_3) + 0.264 \cdot \ln(MgO) - 0.00948\,(CaO/Al_2O_3) + 4.664 \quad (3)$$

$$Z(256) = 1.8723\,(CaO \cdot Al_2O_3) + 0.1223\,(CaO/Fe_2O_3) - 0.1383\,(CaO \cdot MgO) + 350.6 \quad (4)$$

where

$f_c(28)$ = 28-day concrete compressive strength (psi),
$f_t(28)$ = 28-day concrete tensile strength (psi),
$E(28)$ = 28-day concrete modulus of elasticity (10^6 psi), and
$Z(256)$ = 256-day concrete drying shrinkage (in./in. 10^{-6}).

Scattergrams showing the predicted 28- (or 256-) day pavement concrete properties obtained using Equations 1–4 versus laboratory results are given in Figures 1–4. As shown in these graphs, the average laboratory test values can be accurately predicted using the equations.

TIME-DEPENDENT MODELS OF CONCRETE PROPERTIES

After the 28-day models had been developed, the second phase was to determine a method to estimate the pavement concrete properties for any given curing time, t. If concrete curing time is assumed to be independent of coarse aggregate type, all that is needed is to calculate a normalized curing curve for each of the material properties, adjusting it for each aggregate using the 28-day (256-day, for Z) values predicted by Equations 1–4. Although four curing models were developed, only the best two are presented.

Model 1

The American Concrete Institute (ACI) Committee 209 proposed the following model expressing compressive strength

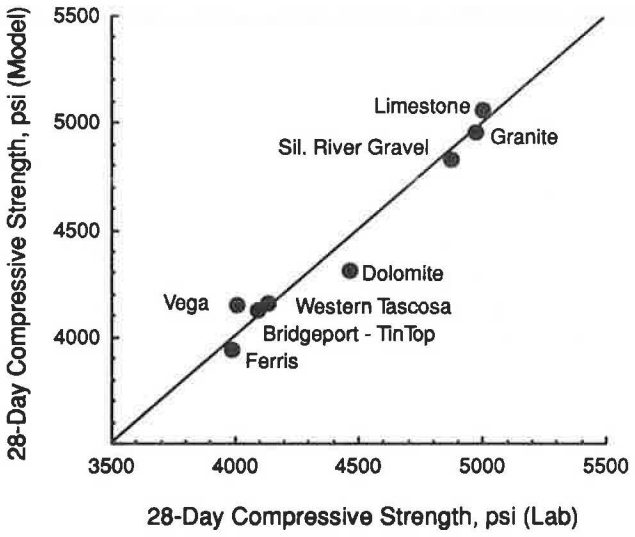

FIGURE 1 Predicted versus actual compressive strength.

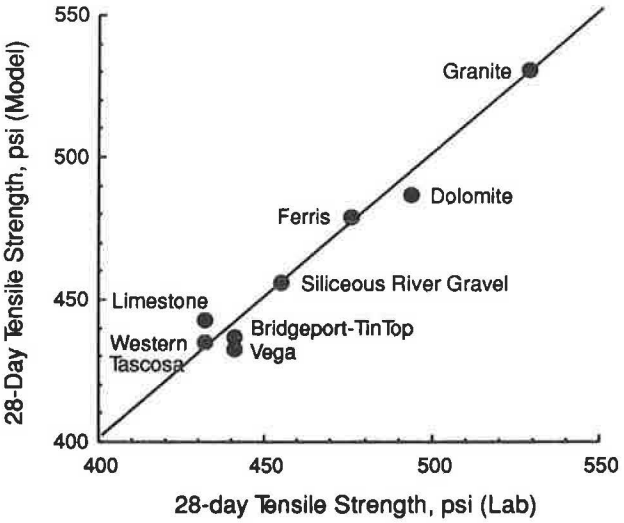

FIGURE 2 Predicted versus actual tensile strength.

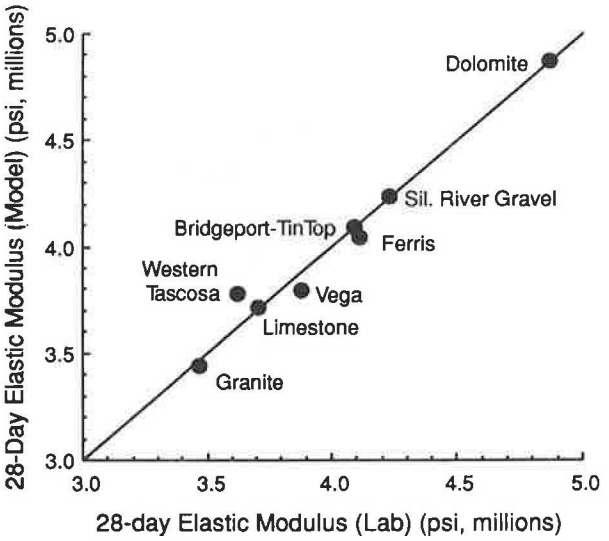

FIGURE 3 Predicted versus actual modulus of elasticity.

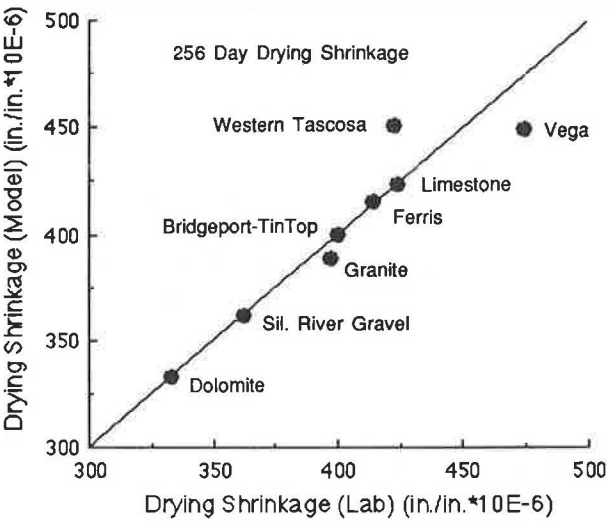

FIGURE 4 Predicted versus actual drying shrinkage.

at time t as a percentage of the 28-day compressive strength for Type I cement moisture cured at 70°F (*10*):

$$f_c(t) = f_c(28)\cdot\left(\frac{t}{4 + 0.85t}\right) \quad (5)$$

In the general form, this equation becomes

$$F(t) = F(28)\cdot\left(\frac{t}{A + Bt}\right) \quad (6)$$

where F is the concrete property function (f_c, f_t, E, or Z) at time t, and A and B are coefficients of curvature, which can be determined by regression. The following time-dependent curves were obtained, averaged for all aggregates:

$$f_c(t) = f_c(28)\cdot\left(\frac{t}{2.1743 + 0.90597t}\right) \quad (7)$$

$$f_t(t) = f_t(28)\cdot\left(\frac{t}{(1.43139 + 0.94156t}\right) \quad (8)$$

$$E(t) = E(28)\cdot\left(\frac{t}{0.43056 + 0.99451t}\right) \quad (9)$$

$$Z(t) = Z(256)\cdot\left(\frac{t}{23.851 + 0.91056t}\right) \quad (10)$$

Model 2

The second successful model form is adapted from one of the prediction equations proposed by CTR research studies (*11*):

$$F(t) = F(28)(A)\cdot(2 - e^{-Bt} - e^{-Ct}) \quad (11)$$

Again, combining concrete property data from all eight aggregates and finding a least-squares fit for A, B, and C, the following property curves were developed:

$$f_c(t) = f_c(28)\cdot(0.50136)\cdot(2 - e^{-0.57677t} - e^{-0.17658t}) \quad (12)$$

$$f_t(t) = f_t(28)\cdot(0.50189)\cdot(2 - e^{-0.19901t} - e^{-1.0597t}) \quad (13)$$

$$E(t) = E(28)\cdot(0.89032)\cdot(2 - e^{-0.004799t} - e^{-1.5282t}) \quad (14)$$

$$Z(t) = Z(256)\cdot(0.52452)\cdot(2 - e^{-0.067464t} - e^{-0.00984t}) \quad (15)$$

Typical curves predicted by Models 1 and 2 are plotted with laboratory data in Figure 5 for compressive strength of concrete (Equations 7 and 12) made with siliceous river gravel as the coarse aggregate, in Figure 6 for tensile strength of concrete (Equations 8 and 13) made with limestone as the coarse aggregate, in Figure 7 for modulus of elasticity of concrete (Equations 9 and 14) made with granite as the coarse aggregate, and in Figure 8 for drying shrinkage of concrete (Equations 10 and 15) made with siliceous river gravel as the coarse aggregate.

Typical predicted values for coarse aggregates that had undergone chemical analysis but not concrete testing are presented in Figure 9 for compressive strength of concrete (Equations 7 and 12) made with limestone/siliceous coarse aggregate (see also Table 2), in Figure 10 for tensile strength of concrete

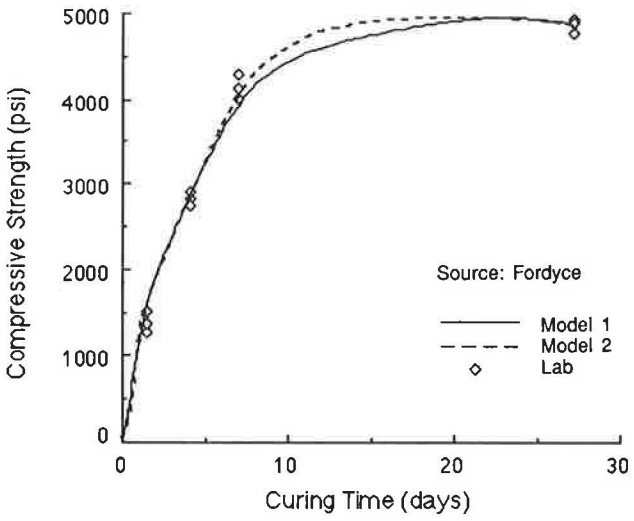

FIGURE 5 Predicted and laboratory compressive strength for PCC made with siliceous river gravel.

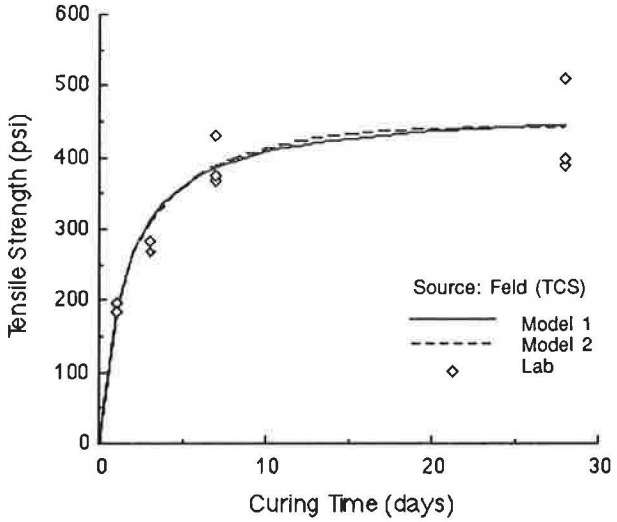

FIGURE 6 Predicted and laboratory tensile strength for PCC made with limestone.

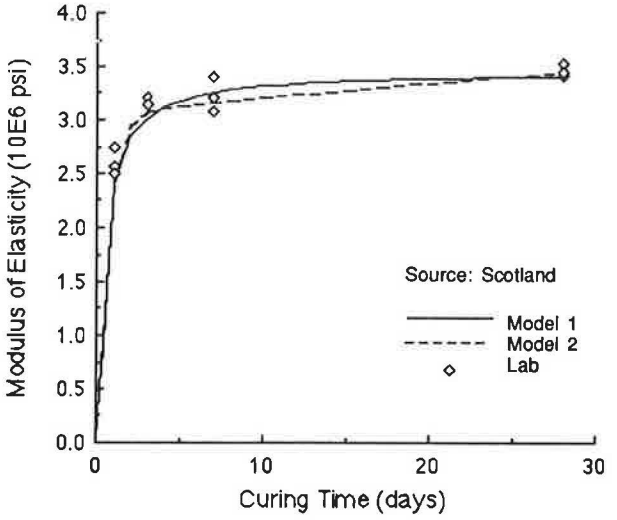

FIGURE 7 Predicted and laboratory modulus of elasticity for PCC made with granite.

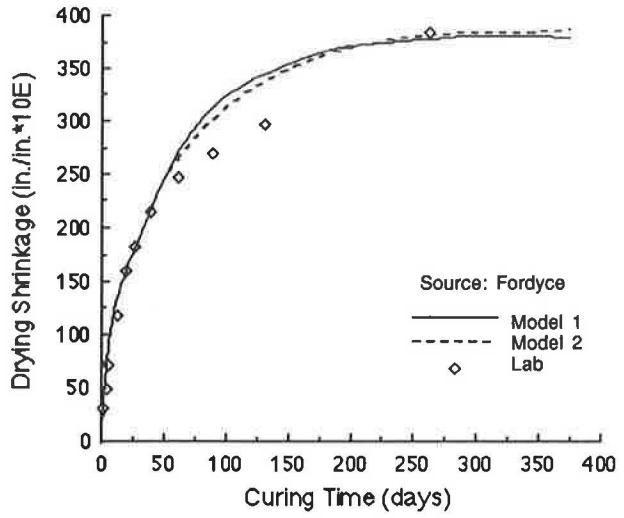

FIGURE 8 Predicted and laboratory drying shrinkage for PCC made with siliceous river gravel.

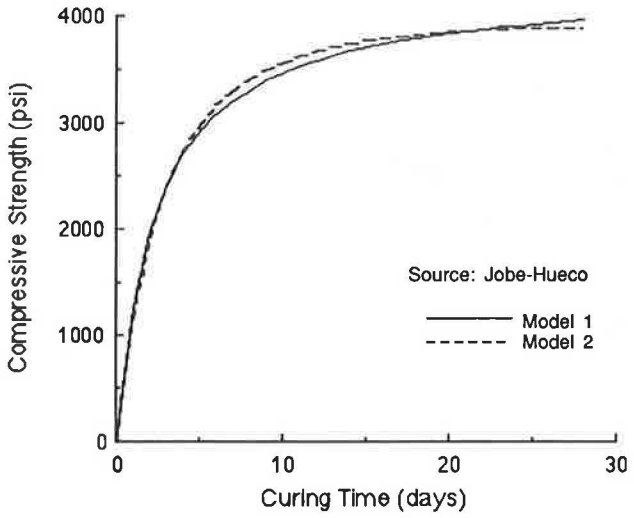

FIGURE 9 Predicted compressive strength for PCC made with limestone-siliceous aggregate.

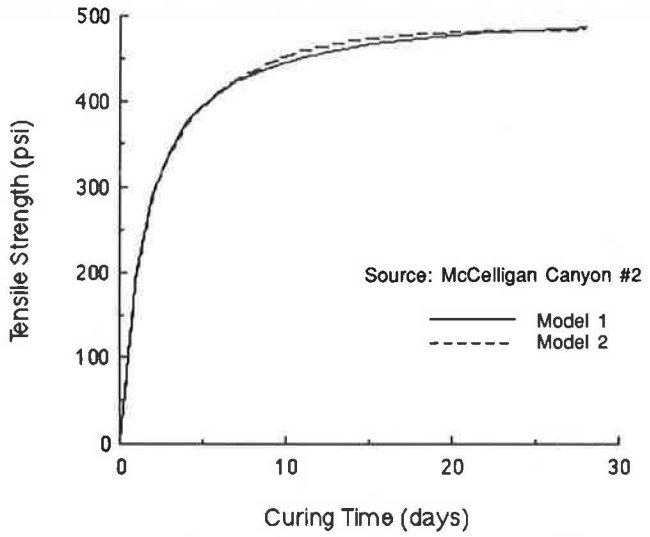

FIGURE 10 Predicted tensile strength for PCC made with dolomite.

(Equations 8 and 13) made with dolomite coarse aggregate, in Figure 11 for modulus of elasticity of concrete (Equations 9 and 14) made with siliceous river gravel coarse aggregate, and in Figure 12 for drying shrinkage of concrete (Equations 10 and 15) made with Mexican limestone coarse aggregate.

CONCLUSIONS

Pavement concrete strength, modulus of elasticity, and drying shrinkage for curing times can be predicted accurately up to 28 days (256 days for shrinkage) using either Model 1 or 2, as demonstrated in Figures 5 through 8. The results from Models 1 and 2 are similar, each providing a reasonable fit, well within the normal material and testing variability demonstrated by the three replicate laboratory data points. In addition, Figures 9 to 12 show reasonable curves for PCC made with coarse aggregates not yet tested in the laboratory for concrete properties. Pavement concrete properties were

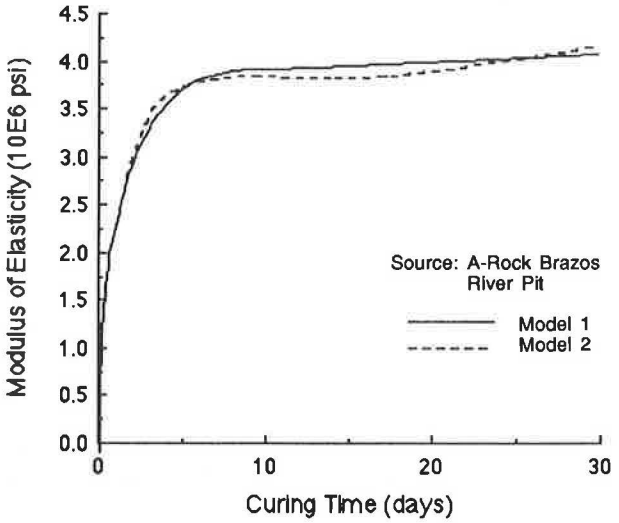

FIGURE 11 Predicted modulus of elasticity for PCC made with siliceous river gravel.

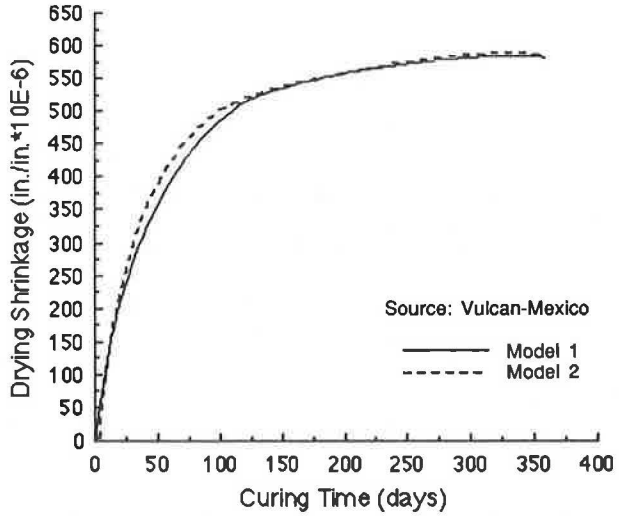

FIGURE 12 Predicted drying shrinkage for PCC made with limestone.

predicted approximately as reported by the suppliers of coarse aggregate (*8*), despite the wide variation in chemical composition and mineralogy of the aggregates investigated (see Tables 1 and 2).

RECOMMENDATIONS

If carefully applied within the inference space of the models (Table 3), either Model 1 or 2 can be used as given to provide a fast and inexpensive preliminary assessment of aggregate performance. Chemical composition data can often be obtained directly from the aggregate supplier. Of course, it is recommended that standard highway department test procedures be followed before any final decision is made regarding aggregate suitability.

Because laboratory testing has been conducted on only eight aggregates to date, testing of additional aggregates should improve the fit and expand the inference space of the model. Other interested organizations can use the approach and procedures outlined here to develop models for the cement types and aggregates of interest to them. For convenience in applying the models presented here, an interactive computer program, CHEM, for IBM PCs and compatibles has been prepared and is available from the authors.

TABLE 3 PERCENTAGE OF CHEMICAL COMPONENTS

	Range	
Compound	High	Low
SiO_2	93.8	2.56
CaO	45.7	1.50
MgO	13.0	0.11
Co_2	42.9	0.59
MnO	0.1	0.01
Fe_2O_3	3.7	0.06
Al_2O_3	14.3	0.21
Ma_2O	4.4	0.09
K_2O	3.8	0.21
TiO_2	0.29	0.02
Other	3.71	0.09

ACKNOWLEDGMENTS

The authors are pleased to acknowledge the support of the Center for Transportation Research, University of Texas at Austin, and the sponsor of the main study, the Texas Department of Highways and Public Transportation, in cooperation with the U.S. Department of Transportation, Federal Highway Administration. The assistance of Jian Lu and Bryan Black is gratefully acknowledged.

REFERENCES

1. S. H. Kosmatka and W. C. Panarese. *Design and Control of Concrete Mixtures*, 13th ed. Portland Cement Association, Skokie, Ill. 1988.
2. D. F. Orchard. *Concrete Technology, Vol. 1: Properties of Materials*, 4th ed. Applied Science Publishers, London, 1979.
3. M. Guiterrez de Velasco and B. F. McCullough. *Summary Report for 1978 CRCP Condition Survey in Texas*. Report 177-20. Center for Transportation Research, University of Texas at Austin, Jan. 1981.
4. M. C. Won. *Mechanistic Analysis of Continuously Reinforced Concrete Pavements Considering Materials Characteristics, Variability and Fatigue*. Ph.D. dissertation. Department of Civil Engineering, University of Texas at Austin, May 1989.
5. T. Dossey. *Prediction of Concrete Properties from Aggregate Chemical Assay*. Tech Memo 422-58. Center for Transportation Research, University of Texas at Austin, May 5, 1989.
6. J. G. MacGregor. *Reinforced Concrete: Mechanics and Design*. Prentice-Hall, Eaglewood Cliffs, N.J., 1988.
7. H. Castedo. *Summary of Laboratory Test Results, Phase I & II—Project 422*. Tech Memo 422-47. Center for Transportation Research, University of Texas at Austin, Feb. 1, 1989.
8. *SAS User's Guide: Statistics*. SAS Institute, Inc. Cary, N.C., 1987.
9. V. L. Anderson and R. A. McLean. *Design of Experiments: A Realistic Approach*. Marcel Dekker, Inc., New York, 1974.
10. ACI Committee 209. Prediction of Creep, Shrinkage and Temperature Effects in Concrete Structures. In *Designing for Creep and Shrinkage in Concrete Structures*. ACI Publication SP-76. American Concrete Institute, Detroit, Mich., 1982.
11. J. Lu, H. Castedo, and B. F. McCullough. *Normalization of Models 1 and 2 for Tensile Strength, Modulus of Elasticity, and Drying Shrinkage of Pavement Concrete Made with Texas Coarse Aggregates*. Tech Memo 422-38. Center for Transportation Research, University of Texas at Austin, Feb. 8, 1989.

Publication of this paper sponsored by Committee on Mechanical Properties of Concrete.

Assessing In Situ Stiffness of Curing Portland Cement Concrete with Seismic Tests

GLENN J. RIX, JAMES A. BAY, AND KENNETH H. STOKOE II

In situ measurement of surface wave velocity using the spectral-analysis-of-surface-waves (SASW) method shows that this type of seismic measurement offers a reliable alternative to conventional penetration resistance and cylinder compression testing for determining the stiffness of portland cement concrete during curing. Both surface wave velocity and penetration resistance exhibit similar rates of increase during the initial stages of curing, suggesting that in situ measurements of wave velocity are potentially useful to assess the degree of curing that has occurred. At later stages of curing, values of Young's moduli calculated from in situ seismic tests agree well with values of Young's moduli from cylinder compression tests for similar curing histories. Advantages of nondestructive and nonintrusive seismic tests like the SASW test are that, unlike penetration resistance and cylinder compression tests, these tests (a) require no samples, (b) can be performed directly on the concrete slab to evaluate spatial variability, and (c) can be performed repeatedly at the same locations at different times during the curing process.

In situ seismic methods are among several methods available to evaluate the elastic moduli of portland cement concrete (PCC) pavements. The spectral-analysis-of-surface-waves (SASW) method, a seismic method using the analysis of dispersed surface waves in a layered system, is particularly well suited for this purpose because the test is nondestructive and nonintrusive (*1*). The SASW method is flexible in that it can be used to (a) provide a detailed modulus profile of the subgrade and base materials during all phases of construction (*2*); (b) provide a profile of the entire pavement system, including the pavement surface layer, during the subsequent life of the pavement (*1*); or (c) evaluate the modulus of only the pavement surface layer rapidly (*3*).

The SASW method has recently been applied to measuring the stiffness of curing concrete in situ. This approach was undertaken because few in situ tests are available for this purpose. The usual practice is to evaluate the degree of curing or "set" of freshly placed concrete using penetration tests on small representative samples (ASTM C 304). During later stages of curing, cylinder compression tests are used to determine the strength and stiffness properties of the concrete (ASTM C 39).

The use of the SASW method to determine the properties of curing PCC in situ is the focus of this paper. Results from tests performed on prototype and full-scale concrete slabs are presented that indicate in situ seismic measurements to be a reliable, alternative means of evaluating the stiffness of curing concrete. Although this paper describes results obtained on pavements, the approach applies equally well to structural concrete.

G. J. Rix, School of Civil Engineering, Georgia Institute of Technology, Atlanta, Ga. 30332. J. A. Bay and K. H. Stokoe, Geotechnical Engineering, University of Texas at Austin, Tex. 78712.

OVERVIEW OF SASW METHOD

The SASW method is an engineering seismic method that uses the dispersive property of surface waves to determine the shear or Young's modulus of pavement components (surface layer, base, and subgrade) in situ. The nondestructive and nonintrusive aspects of the SASW method make it particularly useful for evaluating pavements. Brief descriptions of the dispersive behavior of surface waves in a layered system and the procedure used in SASW testing are presented in the following sections.

Surface Wave Dispersion

To understand how surface waves can be used to determine the modulus profile of a pavement, it is first necessary to understand surface wave dispersion in a layered profile. A dispersive wave is one in which the velocity of propagation varies with frequency (which is the same as saying that velocity varies with wavelength). Surface wave dispersion is caused by the distribution of particle motion with depth. As wavelength increases, particle motion extends to greater depths in the profile as illustrated in Figure 1. The velocities of surface waves are representative of the material stiffness over depths in which there is significant particle motion. For example, the particle motion of a wave that has a wavelength shorter than the thickness of the pavement surface layer is confined to this layer (Figure 1b). Therefore, the wave velocity is influenced by the stiffness of the surface layer and not by the lower layers. The velocity of a wave with a wavelength of several feet is influenced by the properties of the surface layer, base, and subgrade because a significant portion of the particle motion is in these layers (Figure 1c). Thus, by measuring the velocity of surface waves over a wide range of wavelengths, it is possible to assess the stiffness of the layers over a range of depths. However, if one desires only to determine the stiffness of the PCC layer, only wavelengths shorter than the thickness of this surface layer need to be generated and measured.

The objective in SASW testing is to make field measurements of surface wave dispersion (i.e., measurements of sur-

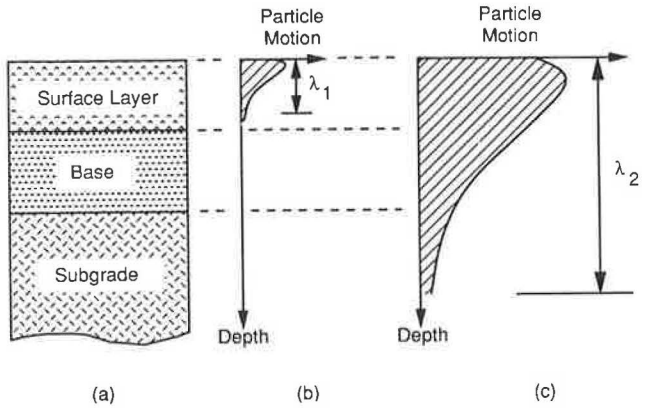

FIGURE 1 Approximate distribution of vertical particle motion with depth for two surface waves of different wavelengths: (a) material profile; (b) shorter wavelength, λ_1; and (c) longer wavelength, λ_2.

face wave velocity, V_R, at various wavelengths, L_R) and then to determine the shear wave velocities of the layers in the profile. These velocities can, in turn, be used to calculate values of shear and Young's moduli using simple relationships from the theory of elasticity as follows:

$$V_s = CV_R \quad (1)$$

$$G = \rho V_{s^2} \quad (2)$$

$$E = 2G(1 + \nu) \quad (3)$$

where

C = function of Poisson's ratio (as given in Table 1),
G = shear modulus,
E = Young's modulus,
V_s = shear wave velocity,
ν = Poisson's ratio, and
ρ = mass density.

SASW Test Procedure

The procedure used to perform an SASW test can be divided into three steps: (a) field testing, (b) dispersion calculations, and (c) inversion. Brief descriptions of each of these steps are now presented.

TABLE 1 VARIATION IN THE RELATIVE VALUES OF SEISMIC WAVE VELOCITIES WITH POISSON'S RATIO

Poisson's Ratio ν	V_S/V_R	V_P/V_R	V_P/V_C
0	1.144	1.618	1.000
0.05	1.132	1.644	1.003
0.10	1.120	1.680	1.011
0.15	1.108	1.727	1.028
0.20	1.098	1.793	1.054
0.25	1.088	1.884	1.095
0.30	1.078	2.017	1.160
0.35	1.070	2.226	1.267
0.40	1.061	2.600	1.464
0.45	1.054	3.495	1.948
0.50	1.047	∞	∞

*V_R = surface (Rayleigh type) wave velocity, V_S = shear wave velocity, V_P = constrained compression wave velocity, and V_C = unconstrained compression wave velocity

Equipment and Field Setup

The general configuration of source, receivers, and recording equipment used in SASW testing in shown in Figure 2. The most common types of sources used on curing concrete slabs have been small hammers lightly striking the surface or piezoelectric transducers placed on the surface. Both of these sources create a transient wave containing a broad range of frequencies. Recently, the use of random input motion with piezoelectric transducers has also been used effectively (*4,5*).

Selection of receivers is based on the range of frequencies that will be used. For profiling curing concrete, piezoelectric accelerometers work well. Testing the hardened PCC layer requires the use of high frequencies (up to 50 kHz) to generate short wavelengths so that the stiffness of the surface layer can be accurately evaluated. Piezoelectric accelerometers, which are coupled rigidly to the pavement with mounting studs, are typically used in this range of frequencies. When the concrete is first placed, surface wave velocities are low (only a few hundred feet per second), and frequencies as low as 500 Hz are used. Fortunately, piezoelectric accelerometers also perform well in this frequency range.

A dual-channel fast Fourier transform (FFT) analyzer is used to record and analyze surface wave motion at the two receivers. This type of analyzer permits real-time field evaluations of the data. Finally, a microcomputer is used to transfer data from the analyzer and to perform dispersion calculations, which are described subsequently.

The spacing between receivers ($D = d_2 - d_1$ in Figure 2) varies according to the range of wavelengths used. In a "general purpose" test in which the goal is to determine the stiffness of all the components of the pavement system using a wide range of wavelengths, several receiver spacings from 0.25 to 16 ft (0.08 to 4.9 m) are used in a single test. For "special purpose" tests in which the goal is to evaluate the stiffness of a single layer (in this case the curing concrete), a limited range of wavelengths is used, and it is possible to employ only one source-receiver setup. For the tests performed in this study, the receiver-to-receiver spacing ranged from about 5 to 12 in. (0.13 to 0.3 m), depending on the thickness of the PCC layer.

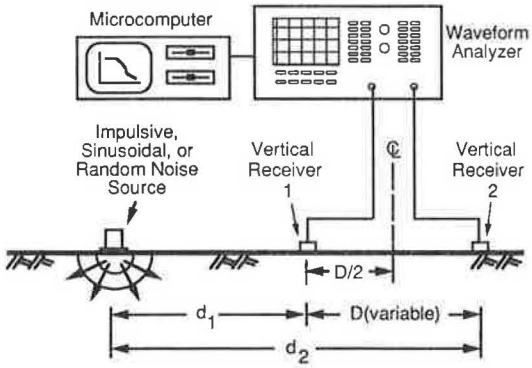

FIGURE 2 General configuration of equipment used in field testing.

Dispersion Calculations

For a given source-receiver spacing, the time histories recorded by the two receivers, $x(t)$ and $y(t)$, are transformed to the frequency domain resulting in the linear spectra of the two signals. The cross-power spectrum of the signals, the coherence function, and the auto-power spectrum of each signal are then calculated using the linear spectra. All calculations are performed in real time by the FFT analyzer.

The key data are the phase of the cross-power spectrum and the coherence function. The coherence function reflects the signal-to-noise ratio and should be nearly equal to one in the range of acceptable data. The phase of the cross-power spectrum, denoted $\theta_{yx}(f)$, is used to calculate the time delay between receivers as a function of frequency from which surface wave velocity and wavelength are then determined.

Two sets of measurements showing the phase of the cross-power spectrum and the coherence function are presented in Figure 3. The first set of measurements, performed soon after placement of the concrete, is shown in Figure 3a, and the second set of measurements, made after the concrete was quite stiff, are presented in Figure 3b. Both sets of measurements were made at the same location on the slab.

Dispersion curves are determined from these measurements as follows. The time delay between receivers is

$$t(f) = \theta_{yx}(f)/2\pi f \tag{4}$$

where the phase angle is in radians and the frequency, f, is in cycles/second. The surface wave phase velocity, V_R, is

$$V_R(f) = (d_2 - d_1)/t(f) \tag{5}$$

and the corresponding wavelength of the surface wave is

$$L_R = V_R/f \tag{6}$$

These calculations yield a dispersion curve (V_R versus L_R) for the receiver spacing.

Examples of dispersion curves measured on two curing concrete slabs are presented in Figure 4. The individual dispersion curves show results from measurements made at var-

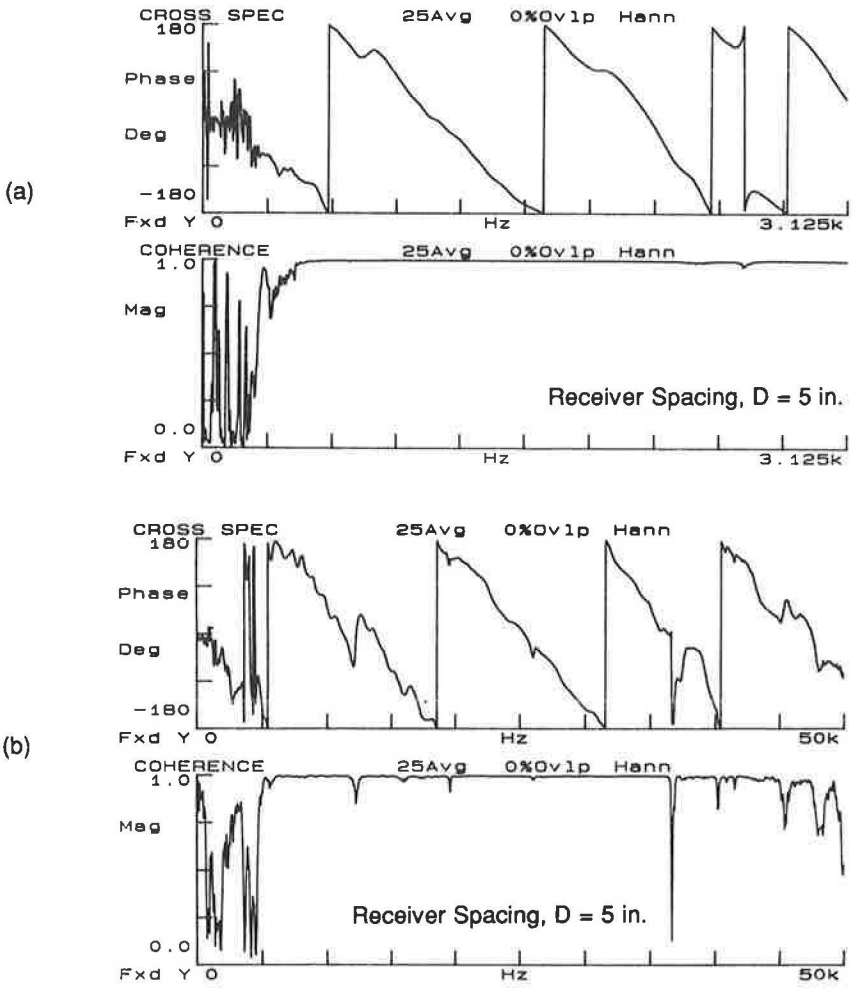

FIGURE 3 Spectral functions measured at Balcones Research Center: (a) measurements performed 255 min after addition of water to cement aggregate mixture and (b) measurements performed 750 min after addition of water to cement aggregate mixture.

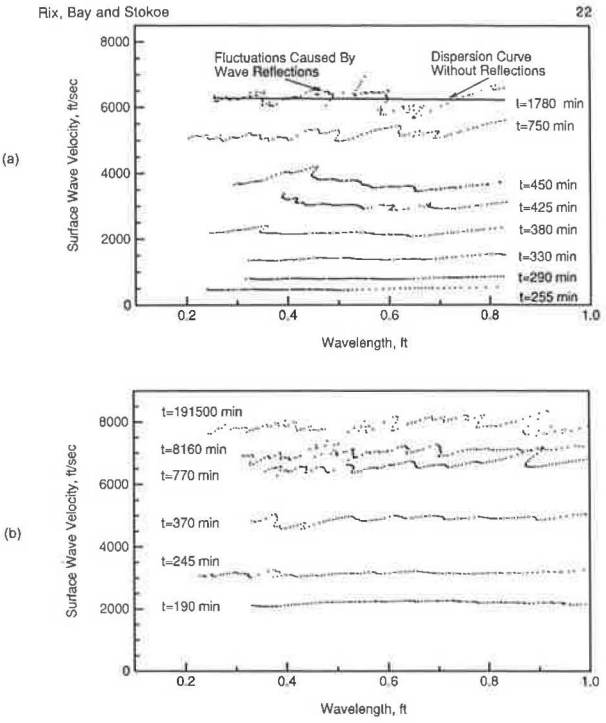

FIGURE 4 Dispersion curves measured on curing concrete slabs at various times after addition of water to the mix: (a) prototype slab at BRC and (b) continuously reinforced PCC pavement section in El Paso, Texas.

ious times. (The measurements shown in Figure 3 were used in constructing two of the dispersion curves shown in Figure 4a.) The most important aspect in Figure 4 is that the individual dispersion curves are nearly constant for values of wavelength less than the slab thickness, indicating that only the curing concrete was sampled and that the stiffness was uniform at any given time. Fluctuations observed in the dispersion curves at large elapsed times result from reflections of shear, compression, and surface waves from the lateral and vertical boundaries of the slab (*5–7*) as discussed in the following.

The dispersion curves in Figure 4 are appropriate for assessing the stiffness of the concrete surface layer using Equations 1–3. If it is necessary to determine the moduli of the base and subgrade in addition to the surface layer, individual dispersion curves from larger receiver spacings would be combined with the curves shown in Figure 4 to form a composite dispersion curve.

Inversion

Inversion is the process of calculating the shear wave velocity (or modulus) profile using the experimental dispersion data. In the inversion process, a theoretical dispersion curve is calculated for an assumed velocity profile and is then compared with the experimental dispersion curve. The assumed velocity profile contains a sufficiently large number of sublayers to define the variation of pavement properties with depth accurately. The theoretical curve is calculated using a modified Haskell-Thomson matrix algorithm (*8–10*). The shear wave velocities and thicknesses of the sublayers in the assumed profile are adjusted by trial and error until a satisfactory match is obtained; the final profile is assumed to represent the actual pavement profile.

If only the stiffness of the pavement surface layer is of concern, it is possible to use a greatly simplified form of inversion. The basis of the simplified method is that, for wavelengths that are less than the thickness of the slab (see Figure 1b), the slab will appear to be a uniform half space if the properties are nearly constant (*3,7,10*). This point is illustrated in Figure 4a in which the phase velocities are nearly constant for measurement times less than about 400 min for wavelengths shorter than the slab thickness. At larger measurement times, the fluctuations in the dispersion curve are caused by wave reflections (*3,5–7*) and a "best-fit" straight line placed through the data most nearly represents the dispersion curve without reflections. For a uniform half space, the shear wave velocity is approximately 1.1 times the surface wave phase velocity. Thus, for short wavelengths, it is possible to estimate the shear wave velocity of the concrete by multiplying the observed surface wave phase velocity by 1.1. For the dispersion curves shown in Figure 4a, this simple calculation yields shear wave velocities ranging from about 550 ft/sec (168 m/sec) at t = 255 min to about 7,000 ft/sec (2,135 m/sec) at t = 1,780 min. The resulting Young's moduli are then 28 ksi (193 MPa) and 3,830 ksi (26,400 MPa), respectively.

It must be emphasized that this simple method of determining shear wave velocity is only applicable to the surface layer. A crude inversion procedure such as this can lead to large errors if it is used to determine the shear wave velocities and elastic moduli of layers other than the surface layer. Also, if a reasonable estimate of Poisson's ratio can be made, the value of C in Equation 1 can be estimated more closely using Table 1 (from the value of 1.1 assumed), and a more accurate value of V_s can be estimated.

CASE HISTORIES

Several sites have been used to evaluate the use of the SASW method for the purpose of determining the stiffness of curing PCC. One of the sites is the Hornsby Bend (HB) test facility, located in Austin, Texas. At this site, a prototype concrete slab was cast on a silty clay subgrade. The slab was unreinforced and had dimensions of 8 by 12 ft (2.4 by 3.7 m) with a nominal thickness of 10 in. (0.25 m). Class S concrete with Type I cement and a maximum aggregate size of 0.75 in. (0.019 m) was used for the slab. The mix was specified to be 6 sacks/yd^3 and 5 gal/sack, with a design 28-day compressive strength of 3,600 psi (24.8 MPa). The slump of the concrete was 1.5 in. (0.04 m). Finishing consisted of vibrating, screeding, and floating. In addition to the slab, twenty-five 6- by 12-in. (0.15- by 0.3-m) cylinders and two penetration resistance samples were cast to perform additional comparative tests.

The second site was a prototype PCC slab cast at the Balcones Research Center (BRC) of the University of Texas. The slab was unreinforced and had dimensions of 6 by 12 ft (1.8 by 3.6 m) and a nominal thickness of 10 in. (0.25 m). The slab was cast on a silty clay subgrade. The mix was specified to have a maximum aggregate size of 1.5 in. (0.038 m),

5 sacks of Type I cement per cubic yard with 25 percent fly ash, a retarder, and an air-entraining admixture.

The third site was a section of Interstate 10 in El Paso, Texas. The tests were performed on a continuously reinforced PCC pavement that was being constructed to widen the expressway. The pavement system consisted of 12 in. (0.3 m) of PCC pavement over 13 in. (0.33 m) of hot-mix asphalt concrete (HMAC) over a silty sand fill. The PCC mix was specified to have a maximum aggregate size of 1.75 in. (0.044 m), 5 sacks/yd^3 with 25 percent fly ash and 5 percent entrained air. Unlike the first two sites, the pavement section in El Paso was continuously reinforced. The presence of the reinforcing steel does not influence the oberved surface wave phase velocity because the diameter of the steel is much smaller (by about 4 times) than the wavelengths used for the measurements.

Variation of Surface Wave Velocity with Time

The fundamental idea behind the use of seismic tests to determine properties of curing PCC is that changes observed in the surface wave velocity or shear wave velocity (and, hence, modulus) during curing are direct indicators of the curing process. To investigate this hypothesis, a series of surface wave tests was performed on the concrete slabs at each location beginning immediately after the slabs were poured and finished, and continuing throughout the time that curing was taking place. Surface wave measurements were conducted using the procedure described previously. Because only the wave velocity of the curing concrete (the surface layer) was of interest, it was possible to use the simplified form of inversion described earlier rather than the more rigorous inversion method.

Examples of the dispersion curves measured on the concrete slab are presented in Figure 4. The dispersion curves were measured at various times after water had been added to the cement-aggregate mixture at the batch plant. The increase in surface wave velocity with time for each of the three sites is shown in Figures 5–7. Clearly, the wave velocity increases very rapidly initially and then begins to level off. Intuitively, this behavior mimics the expected curing process.

An independent series of compression wave measurements was also performed at the BRC slab. As expected, the curing process is also clearly reflected by the increase in compression wave velocity. However, in the authors' experience, the SASW measurements are easier to perform. Values of Poisson's ratio during curing are shown in Figure 8 on the basis of surface and compression wave velocities. The uncured PCC initially is more "fluid-like" and the measured values of Poisson's ratio approach 0.5, which is the expected value for an incompressible fluid. Later, when the PCC has more fully cured, Poisson's ratio is approximately 0.22, which is typical of hardened concrete.

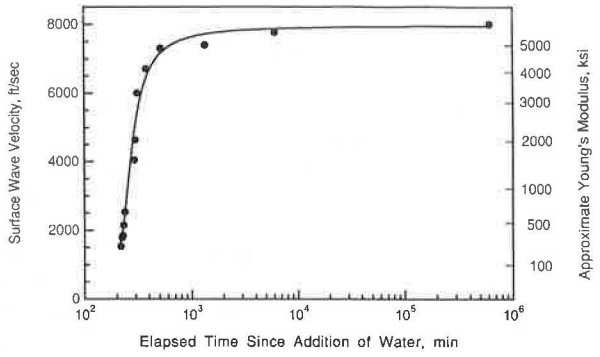

FIGURE 5 Variation in shear wave velocity of PCC layer during curing for Hornsby Bend slab.

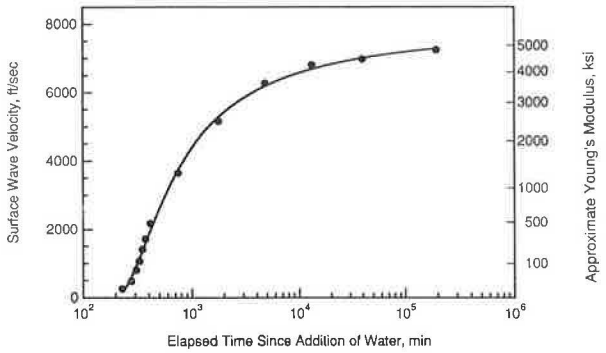

FIGURE 6 Variation in surface wave velocity of PCC layer during curing at Balcones Research Center.

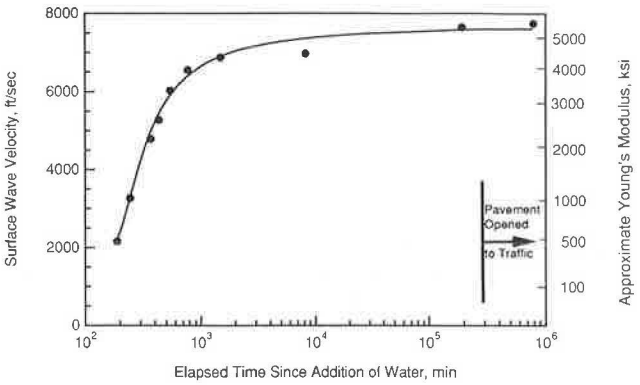

FIGURE 7 Variation in surface wave velocity of PCC layer during curing for pavement at El Paso, Texas.

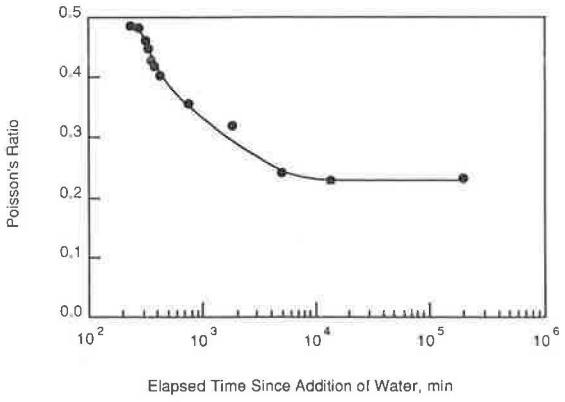

FIGURE 8 Variation in Poisson's ratio of the PCC layer during curing at Balcones Research Center.

Comparison of Seismic Wave Velocity with Penetration Resistance

The penetration resistance of fresh concrete is a common test used to determine to what extent that concrete has cured or, in other words, its set. These tests require a sample of concrete that has been passed through a No. 4 sieve to remove the large aggregate. A cylindrical penetrometer is forced into the sample and the load necessary to cause 1 in. (0.025 m) of penetration is recorded. The load is divided by the cross-sectional area of the penetrometer to calculate the penetration resistance. Initial set is defined as the time at which the penetration resistance is equal to 500 psi (3.45 MPa). Final set occurs when the penetration resistance has increased to 4,000 psi (27.6 MPa). A complete description of the test procedure is given elsewhere (ASTM C 403).

To evaluate the use of surface wave velocity measurements as an alternative to penetration resistance tests for determining set, results of the two tests are plotted together in Figures 9 and 10 for the two sites where both types of tests were performed. At the HB site, initial set occurred 180 min after the addition of water. The time of final set, 300 min, was extrapolated from the final two readings because the sample could not be penetrated following the 3,600-psi (24.8-MPa) reading at 280 min. At the BRC site, initial set occurred 355 min after the addition of water and final set occurred at 386 min. In both cases, penetration resistance and surface wave velocity exhibit similar, rapid rates of increase during the initial stages of curing, indicating that in situ measurements of wave velocity are potentially useful for determining the degree of curing that has occurred in new concrete. Furthermore, seismic tests performed using the SASW test procedure allow the degree of set to be evaluated without the need to cast special samples for this purpose. It is therefore possible to perform more tests on the slab itself, rather than a limited number of tests on samples that have been altered by sieving and may be curing at different rates because they have been separated from the slab.

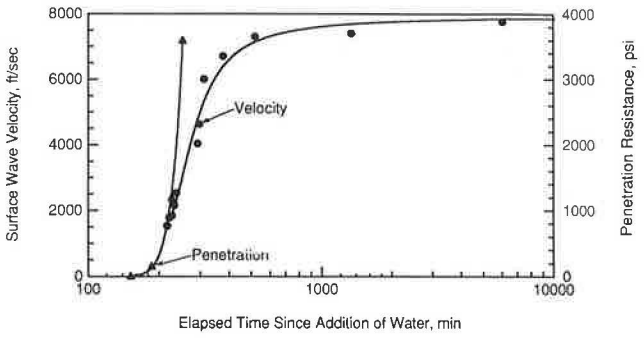

FIGURE 9 Comparison of surface wave velocity and penetration resistance measured during curing of the concrete slab at Hornsby Bend.

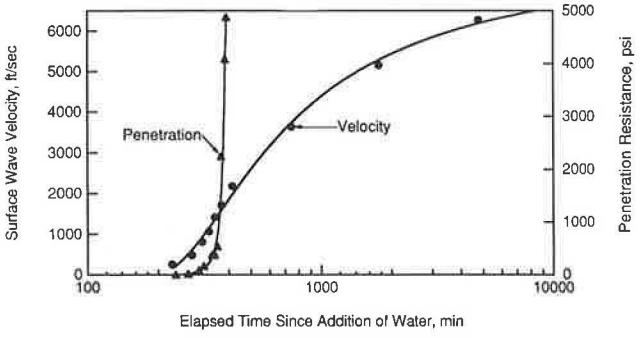

FIGURE 10 Comparison of surface wave velocity and penetration resistance measured during curing of the concrete slab at Balcones Research Center.

Comparison of Seismic Moduli with Secant Moduli from Cylinder Tests

Another use of seismic measurements is to determine the in situ Young's modulus of new concrete without relying on test cylinders. To examine the feasibility of this approach, standard cylinder compression tests (ASTM C 39) were performed on 6- by 12-in. (0.15- by 0.3-m) samples in order to compare Young's moduli from these tests with Young's moduli from seismic tests at the HB slab. Compression tests were performed 1, 3, 7, and 28 days after the slab was cast. The procedure used in this series of tests is as follows: (a) several compression tests were performed to determine the average compressive strength of the cylinders and (b) Young's modulus tests were then conducted on other cylinders using the compressive strength to choose the proper stress level at which to measure the secant Young's modulus. The average compressive strength of the concrete cylinders is given in Table 2. The values in Table 2 are substantially greater than the specified compressive strength, 3.6 ksi, for the slab at HB.

Values of Young's modulus were calculated at 40 percent of the average compressive strength. Examples of typical stress-strain curves used to determine Young's modulus are shown for tests performed at 1 day and 3 days (Figure 11). For each test the strain corresponding to a stress equal to 40 percent of the compressive strength was determined, and this point was then used to calculate the secant Young's modulus from the origin. Young's moduli determined using this method along with the associated strain levels are summarized in Table 3.

Values of Young's moduli were calculated from the results of surface wave velocity measurements using Equations 1–3. An assumed unit weight of 145 lb/ft^3 was used to calculate the shear modulus from the measured values of wave velocity. To convert shear modulus to Young's modulus using Equation 3, values of Poisson's ratio were measured in situ at various

TABLE 2 AVERAGE VALUES OF COMPRESSIVE STRENGTH AT 1, 3, 7, AND 28 DAYS FOR PCC SAMPLES FROM HORNSBY BEND

Elapsed Time (days)	Number of Tests	Range in Compressive Strengths (ksi)	Average Compressive Strength (ksi)
1	2	4.89-4.93	4.91
3	3	5.20-5.74	5.44
7	2	5.69-5.74	5.71
28	4	6.30-6.69	6.47

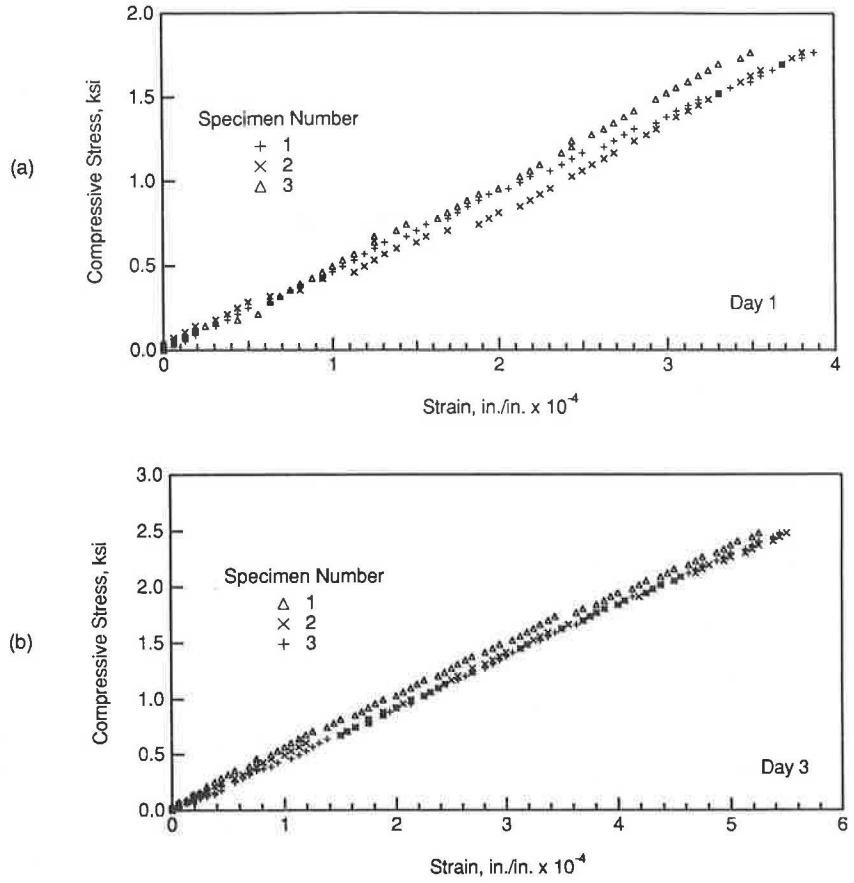

FIGURE 11 Stress-strain curves for Young's modulus tests performed at different times after casting of the slab at Hornsby Bend: (a) three tests performed 1 day after casting and (b) three tests performed 3 days after casting.

TABLE 3 VALUES OF YOUNG'S MODULUS DETERMINED USING CYLINDER TESTS FOR PCC SAMPLES FROM HORNSBY BEND

Elapsed Time (days)	Number of Tests	Average Young's Modulus (1000 ksi)	Average Value of Strain (in /in x 10^{-3})
1	3	4.75	0.38
3	3	4.63	0.47
7	2	4.79	0.48
28	3	4.86	0.54

TABLE 4 COMPARISON OF YOUNG'S MODULI FOR SEISMIC TESTS AND THOSE DETERMINED USING CONVENTIONAL CYLINDER TESTS FROM HORNSBY BEND

Elapsed Time (days)	Modulus from Seismic Tests (1000 ksi)	Modulus from Cylinder Tests (1000 ksi)
1	5.04	4.75
3	5.30	4.63
7	5.60*	4.79
28	5.63*	4.86

* Interpolated from the data in Fig. 5

times during the curing of the concrete by also measuring compression wave velocities. Values of Poisson's ratio presented in Figure 8 for several elapsed times are typical of these values. At times greater than 1 day, the unit weight and Poisson's ratio usually vary within a relatively small range and any errors in assumed values do not have a significant impact on the resulting values of Young's modulus.

Moduli from cylinder compression tests and from in situ seismic measurements at 1 and 3 days are compared in Table 4. Because seismic measurements were not performed at exactly 7 and 28 days, values of moduli at these times were interpolated from Figure 5. Because the trend is well defined in Figure 5, it is believed that there is little error introduced by the interpolation. The two different methods used to determine the moduli compare favorably, as shown in Table 4. One possible reason why the seismic moduli average about 13 percent more than the cylinder moduli is that the concrete in the slab cured at a different rate than did the concrete in the cylinders. If this hypothesis is true, it highlights the advantage of using in situ seismic methods to evaluate curing concrete. Another possible reason that the seismic moduli are slightly greater is that seismic measurements determine the initial tangent modulus at very small values of strain, less than 0.01×10^{-3}, whereas cylinder compression tests determine

the secant modulus at strain levels ranging from 0.38×10^{-3} to 0.54×10^{-3}. Both of these reasons probably contributed to the differences.

As in the case of measurements of set, seismic measurements appear to offer the potential of reliable in situ determinations of the Young's modulus of new concrete without the use of samples. Additional studies that include comparisons for a large number of tests are needed to confirm the results of this feasibility study.

IMPLEMENTATION

The equipment and procedures currently used to make seismic measurements on curing concrete are oriented toward research studies. It is believed, however, that the equipment and simplified procedures used in such studies lend themselves to the development of an automated system for surface wave measurements. With an automated system, measurements of the in situ moduli and estimates of the set could be obtained easily and rapidly by highway agencies or contractors.

CONCLUSIONS

In situ seismic measurements using the SASW method offer a potentially useful alternative to conventional penetration resistance and cylinder compression tests for determining the characteristics of PCC during curing. The SASW method is a nondestructive and nonintrusive method based on the analysis of dispersed surface waves in a layered half space. In addition to the ability to determine the modulus profile of the entire pavement system with the SASW method, it can also be used to evaluate the pavement surface layer rapidly, which makes it particularly useful for measurements on curing concrete pavements.

Several series of tests performed on two research slabs indicated that the surface wave velocity of concrete and the penetration resistance both increase at similar rates during the initial stages of curing. On the basis of these results, it appears that in situ measurements of surface wave velocity can be useful in assessing the degree of curing in fresh concrete. Values of Young's moduli from in situ seismic tests also agree well with the values of Young's moduli measured using cylinder compression tests, indicating the potential usefulness of SASW tests in this area. However, one must be careful when making these comparisons because dissimilar curing processes and strain levels can cause differences between Young's moduli measured by in situ seismic and cylinder compression tests.

One distinct advantage of nondestructive, nonintrusive seismic measurements over conventional penetration resistance and cylinder compression testing is that the need to cast samples can be avoided and that a larger number of tests can be performed on the concrete slab itself.

ACKNOWLEDMENTS

This work was supported by the Texas State Department of Highways and Public Transportation. The authors wish to express their appreciation for this support.

REFERENCES

1. S. Nazarian, K. H. Stokoe II, and W. R. Hudson. Use of Spectral Analysis of Surface Waves Method for Determination of Moduli and Thicknesses of Pavement Systems. In *Transportation Research Record 930*, National Research Council, Washington, D.C., 1983, pp. 38–45.
2. G. J. Rix and K. H. Stokoe II. Stiffness Profiling of Pavement Subgrades. In *Transportation Research Record 1235*, National Research Council, Washington, D.C., 1989, pp. 1–9.
3. J.-C. Sheu, G. J. Rix, and K. H. Stokoe II. Rapid Determination of Modulus and Thickness of Pavement Surface Layer. Presented at the 66th Annual Meeting of the Transportation Research Board, Washington, D.C., 1987.
4. G. J. Rix. *Experimental Study of Factors Affecting the Spectral-Analysis-of-Surface-Waves Method*. Ph.D dissertation. University of Texas at Austin, 1988, 315 pp.
5. J.-C. Sheu. *Applications and Limitations of the Spectral-Analysis-of-Surface-Waves Method*. Ph.D dissertation. University of Texas at Austin, 1987, 280 pp.
6. J.-C. Sheu, K. H. Stokoe II, and J. M. Roesset. *Effect of Reflected Waves in SASW Testing of Pavements*. In *Transportation Research Record 1196*, TRB, National Research Council, pp. 51–61.
7. J. M. Roesset, D.-W. Chang, K. H. Stokoe II, and M. Aouad. Modulus and Thickness of the Pavement Surface Layer from SASW Tests. In *Transportation Research Record 1260*, TRB, National Research Council, Washington, D.C., pp. 53–63.
8. N. A. Haskell. The Dispersion of Surface Waves in Multilayered Media. *Bulletin of the Seismological Society of America*, Vol. 43, 1953, pp. 17–34.
9. W. T. Thomson. Transmission of Elastic Waves Through a Stratified Solid. *Journal of Applied Physics*, Vol. 21, 1950, pp. 89–93.
10. S. Nazarian. *In Situ Determination of Elastic Moduli of Soil Deposits and Pavement Systems by Spectral-Analysis-of-Surface-Waves Method*. Ph.D. dissertation. University of Texas at Austin, 1984, 453 pp.

Publication of this paper sponsored by Committee on Mechanical Properties of Concrete.

Rates of Development of Physical Properties of Concrete at Early Ages

FRANCIS A. OLUOKUN, EDWIN G. BURDETTE, AND J. HAROLD DEATHERAGE

An investigation on the gain of physical properties of concrete with time and experimental results on the development of compressive strength, splitting tensile strength, modulus of elasticity, and Poisson's ratio are reported. The results show that the elastic modulus developed much faster than either the tensile or the compressive strength, which developed at approximately the same rate. Poisson's ratio did not change substantially with either richness of mix or age of concrete and did not vary appreciably with time after 6 hr. The period within the first 12 hr after casting was observed to be the period of fastest development of physical properties.

Pressure on the concrete industry to reduce construction schedules has led to subjecting concrete members to loads long before the conventional 28-day curing period has been completed. This trend in loading has brought about the need for a more thorough understanding of the time rates of development of various physical properties of concrete.

The determination of early-age physical properties of concrete is at the forefront of concrete technology, as evidenced by the formation of an American Concrete Institute (ACI) technical committee (ACI 231) on properties of concrete at early ages. Francis Young, chairman of ACI 231, emphasized the importance of determining how properties (including but not limited to compressive strength) develop in early stages (*1*).

The main objectives of the investigation reported here were as follows: (a) obtain a fundamental understanding of the rate of development of physical properties in concrete, particularly within the first 3 days after casting; and (b) generate data describing the time variation of development of physical properties in concrete with particular reference to the early age of concrete.

This study investigated the development of the following physical property parameters at early ages:

1. Compressive strength (f'_c),
2. Modulus of elasticity in compression (E_c),
3. Splitting tensile strength (f_t), and
4. Poisson's ratio (ν).

These parameters were not chosen randomly; they were selected on the basis of their importance to safe concrete design and construction practices. Compressive strength, to which all other physical strength parameters appear related, is considered the most important physical property of concrete. Compressive strength influences the operation of concrete precasting plants. Release of strands in the precast, prestressed concrete industry without detrimental losses requires a knowledge of compressive strength and tensile strength development. Furthermore, adequate knowledge of these properties is necessary for safe form stripping and early load applications.

The static elastic modulus is another important characteristic of concrete. It is a basic parameter necessary for estimating prestress losses, immediate and time-dependent deformations due to early loading, and tensile strain capacity. Although it is generally assumed that concrete performance is governed primarily by its compression capabilities, tensile strength (which directly influences cracking at prestress release and shear capacity) is important for the appearance and durability of concrete structural members. Variation of tensile strength with time is important in predicting concrete shear strength at different curing times. The variation of static elastic modulus of concrete is also useful in predicting early-age buckling loads of long columns. Knowledge of Poisson's ratio is needed in slab analysis.

The variation of these physical property parameters with time of cure is investigated. Time-dependent variational trends of physical property development at early ages have not been clearly established, especially during the critical first 3 days after casting. A thorough review of literature on this subject is presented by Oluokun (*2*).

EXPERIMENTAL INVESTIGATION PROCEDURE

Fabrication of Test Specimens

Four series of test specimens were cast using Type I cement that satisfied the requirements of ASTM C 150. Aggregates were selected in accordance with the specifications of ASTM C 33. Three of the four series were laboratory mixes prepared in a 7.5-ft^3 capacity mixer, and one was a precast, prestressed concrete producer sample. The 28-day compressive strengths of the concrete mixes used ranged from approximately 4,000 psi to approximately 9,000 psi. The specimens for each series were cast from a single batch of concrete. Standard 6- × 12-in. plastic molds were used in accordance with ASTM C 470, and molding was done according to the specifications of ASTM C 31. The coarse aggregate used was ASTM No. 67 with 100 percent of the crushed stone less than 1 in.; 90 to 100 percent was about ¾ in. The fine aggregate used was crushed limestone. Mix proportions are shown in Table 1.

Department of Civil Engineering, University of Tennessee, Knoxville, Tenn. 37996-2010.

TABLE 1 CONCRETE MIX DATA

Mix ID	Cement Type	Quantities per Cubic Yard of Concrete: Water Gal.	Water lb.	Cement Bags	Cement lb.	Aggregate, lb. Fine	Aggregate, lb. Coarse	Gravimetric Air Content (%)	Water to Cement Ratio	Slump in.
A	I	35.00	292	8.00	752	1,242	1,730	2.0	0.388	3.50
B	I	32.0	267	3.72	350	1,400	1,900	4.50	0.763	3.50
C	I	32.00	267	5.32	500	1,400	1,900	4.50	0.534	2.50
D	I	37.00	309	10.00	940	1,200	1,900	5.00	0.329	1.50

Curing Procedure

Wet burlap was used to cover the molds and specimens until the specimens were removed from the molds. A polyethylene sheet was placed over the burlap to minimize evaporation. At about 20 to 24 hr after casting, specimens were stripped and transferred to the standard moist room where curing continued at about 73°F (23°C) in accordance with ASTM C 192. Because most results on which strength design relations are based were derived from tests performed on moist-cured concrete specimens, moist curing at 73°F was used in this study.

Testing Procedure

Three specimens from each mix were tested for each of the parameters investigated at the ages of 6 hr, 12 hr, 1 day, 2 days, 3 days, 7 days, and 28 days. In all, 200 cylinders were tested.

Compressive Strength, Elastic Modulus, and Poisson's Ratio Tests

The cylinders that were tested for compressive strength also provided the data for static elastic modulus and Poisson's ratio. Before testing and to prevent stress concentration during testing, the specimens were capped with a proprietary compound containing sulfur (ASTM C 617). Compressive strength testing was performed on a 300,000-lb capacity testing machine that is capable of loading at a rate of 20 to 50 lb/in.^{2}/sec (ASTM C 39). Compressive strength tests were performed in uniaxial compression up to failure.

The longitudinal and lateral deformations were measured simultaneously with the compressive strength test by using the Structural Behavior Engineering Laboratories deformation jacket (DJC). This jacket is equipped with six linear variable differential transformer transducers (LVDTs). Three of these LVDTs measure the axial strain and the other three measure the lateral strain. These LVDTs are arranged at 60-degree angles from each other. This arrangement of the LVDTs provided an average of three readings for strains in each direction. This approach reduced the error in strain measurement and ensured a higher degree of accuracy of physical property evaluation. The strains in the two directions were computed using data acquisition software.

The static elastic modulus (Young's modulus) was calculated from the stress-strain diagram. Three different methods are used to do this: the initial tangent method, the secant modulus method, and the chord modulus method. The chord modulus method (ASTM C 469) was used in this study. The chord modulus is calculated from the relation

$$E_c = \frac{S_2 - S_1}{\varepsilon_2 - 0.00005} \tag{1}$$

where

S_2 = stress corresponding to 40 percent of the ultimate stress,
S_1 = stress corresponding to a strain of 0.00005, and
ε_2 = longitudinal strain corresponding to S_2.

Poisson's ratio, the ratio of transverse strain to longitudinal strain, was determined from the relation

$$\nu = \frac{\varepsilon t_2 - \varepsilon t_1}{\varepsilon_2 - 0.00005} \tag{2}$$

where εt_2 and εt_1 were transverse strains at mid-height of the test specimen produced by S_2 and S_1, respectively. S_2, S_1, and ε_2 are the same as defined in Equation 1.

Splitting Tensile Strength

In general, three kinds of test methods are available for estimating the tensile strength of concrete: the direct tension test, the beam or modulus-of-rupture test, and the split-cylinder or Brazilian test.

Previous investigations (*3–7*) have indicated that the split-cylinder method is a more reliable measure of tensile strength than the modulus-of-rupture or beam test. The most important advantage of the split-cylinder test is the approximate uniformity of tensile stress over the diametral area of the test cylinder. Moreover, its simplicity affords the opportunity to test a large number of specimens in a relatively short time.

The split-cylinder test was used in this study (ASTM C 496). The tensile strength was computed from the relation

$$f_t = \frac{2P}{\pi DL} \tag{3}$$

where

f_t = tensile strength (psi),
P = magnitude of load at failure (lb),

D = cylinder diameter (in.), and
L = cylinder length (in.).

PRESENTATION AND DISCUSSION OF TEST RESULTS

The basic test data are summarized in Table 2, which gives the averages of three tests performed at each age.

Data in Table 2 indicate that each of the physical properties investigated increased with age of concrete. As expected, the lower the water-to-cement ratio the higher the value of each of the physical properties at a particular age.

One of the primary objectives of this study was to determine the rate of development of physical properties of concrete at early ages. The compressive and the splitting tensile strengths and the elastic moduli were normalized by dividing them by their respective 28-day values from a 73°F cure because the 28-day values of these physical properties obtained from concrete, moist cured at 73°F, are the acceptable standard reference values. These normalized values for each mix, when plotted against age of concrete (Figures 1–4), can be used to compare the rates of development of each of these physical properties with their 28-day values.

For the concrete mixes investigated in this study, as shown in Figures 1–4, the rate of the elastic modulus development is faster at early ages (first 3 days), but relatively slower than that of both the tensile and the compressive strengths at later ages. The rate of development of the tensile and compressive strengths is not appreciably different at the later ages.

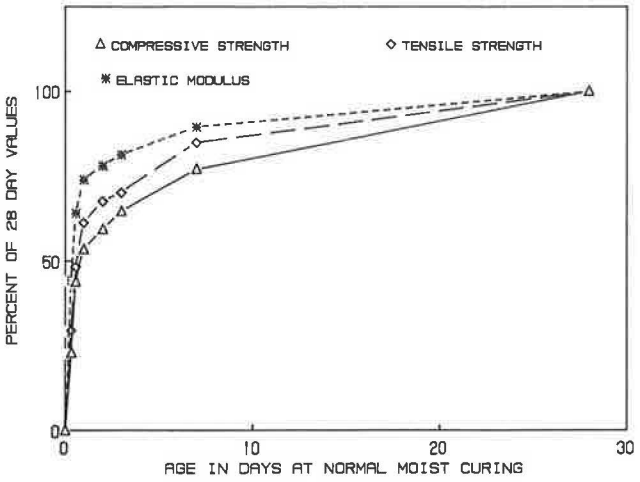

FIGURE 1 Comparison of physical property development using normalized values: Mix A, moist cured.

The variations in the development of the various physical properties of concrete become more obvious when a particular property developed is plotted against curing period in a bar chart (Figures 5–7). These charts show the rates of development for the first 3 days using the normalized values of each parameter investigated. It can be seen in these figures that the development of physical properties in concrete is

TABLE 2 SUMMARY OF TEST RESULTS

	Mix A (w/c = .388)				Mix B (w/c = .763			
Age	Average fc (psi)	Average Ec (10^6 psi)	Average ft (psi)	Average ν	Average fc (psi)	Average Ec (10^6 psi)	Average ft (psi)	Average ν
6 Hrs	1,548	2.2677	177	0.1374	188	0.4123	16	0.1316
12 Hrs	2,942	3.2875	289	0.1876	669	1.9446	69	0.1959
24 Hrs	3,596	3.7994	366	0.1839	1,134	2.3731	155	0.1982
2 Days	3,979	4.0057	405	0.1834	1,768	2.8145	182	0.1990
3 Days	4,339	4.1840	420	0.1862	2,075	3.1370	277	0.1876
7 Days	5,176	4.5960	507	0.1948	2,694	3.5527	305	0.1924
28 Days	6,720	5.1316	597	0.1875	4,060	4.5592	455	0.1856
	Mix C (w/c = .534)				Mix D (w/c = .329)			
Age	Average fc (psi)	Average Ec (10^6 psi)	Average ft (psi)	Average ν	Average fc (psi)	Average Ec (10^6 psi)	Average ft (psi)	Average ν
6 Hrs	382	0.8465	31	0.1512	1,461	2.2303	121	0.1440
12 Hrs	1,772	2.7774	193	0.1805	3,882	4.0707	361	0.1814
24 Hrs	2,709	3.2357	281	0.1895	5,211	4.5243	481	0.1886
2 Days	3,466	3.7396	415	0.1907	6,413	5.0901	583	0.1878
3 Days	3,840	3.8448	447	0.1909	6,702	5.1368	607	0.1834
7 Days	5,140	4.4385	563	0.1819	7,268	5.2512	630	0.1832
28 Days	6,402	4.9785	690	0.1901	8,842	5.8440	768	0.1902

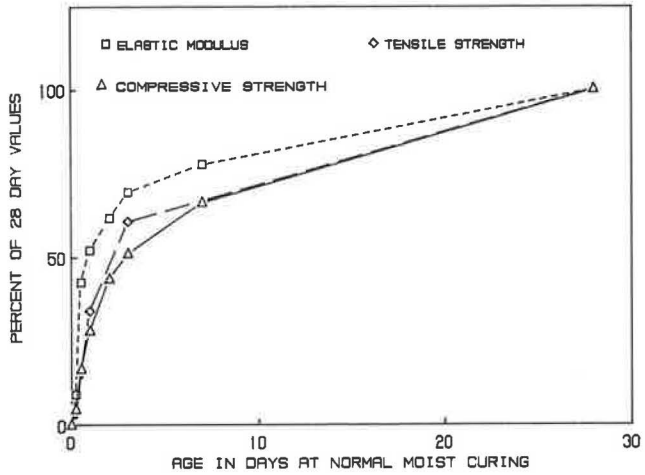

FIGURE 2 Comparison of physical strength development using normalized values: Mix B.

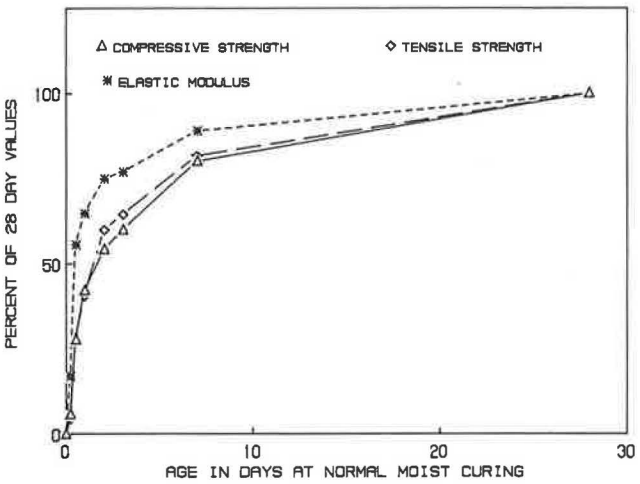

FIGURE 3 Comparison of physical property development using normalized values: Mix C.

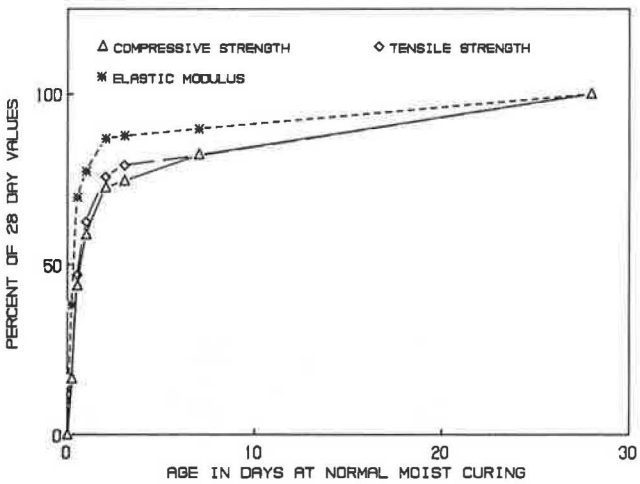

FIGURE 4 Comparison of physical property development using normalized values: Mix D.

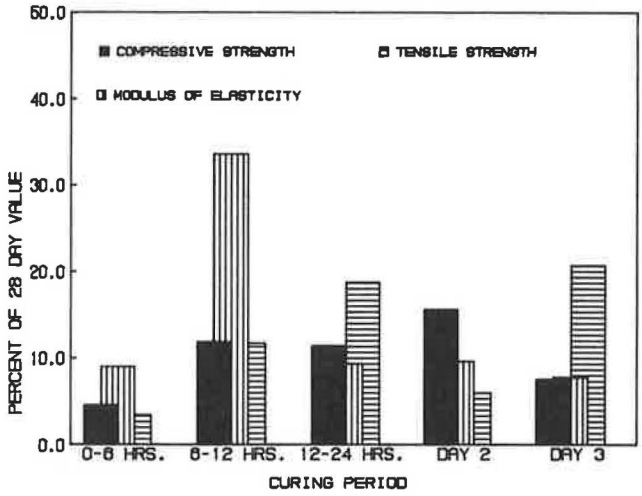

FIGURE 5 Periodic development of physical properties: Mix B.

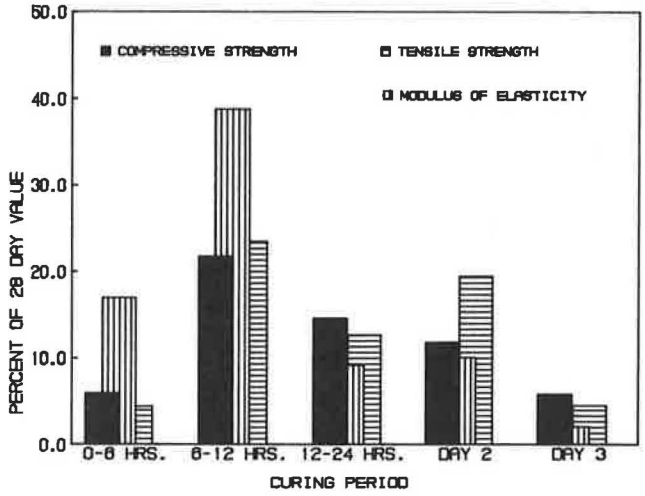

FIGURE 6 Periodic development of physical properties: Mix C.

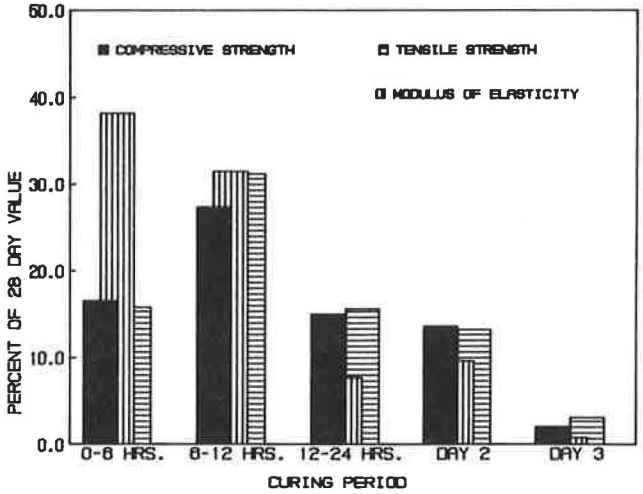

FIGURE 7 Periodic development of physical properties: Mix D.

fastest within the first 12 hr after casting, specifically within 6 to 12 hr for normal- and medium-strength concrete and 0 to 12 hr for high-strength concrete. In all mixes the elastic modulus developed the fastest, and the tensile and the compressive strengths developed at about the same rate, generally with less than 5 percent difference.

By the end of the first 12 hr after casting, the percentage of the 28-day value of the elastic modulus developed (Figures 3–6) varied from 42.7 in normal-strength (4,000-psi) concrete through 55.8/64.1 in medium-strength (6,000- to 7,000-psi) concrete to 70.0 in high-strength (about 9,000-psi) concrete. Within the same period, the percentage of the 28-day value of the tensile strength developed varied from 15.2 through 28.0 to 47.0 in normal-, medium-, and high-strength concrete, respectively, whereas that of the compressive strength varied from 16.5 through 27.7 to 43.9 in normal-, medium-, and high-strength concrete, respectively. The differences between the rates of development of each of these physical properties narrowed with increasing age. After 12 hr (Figures 5–7) the rate of elastic modulus development decreased faster than those of the compressive and the tensile strengths. The fastest drop in the rate of elastic modulus development occurred between 12 and 24 hr after casting in all mixes. After 12 hr the rates of development of the tensile and compressive strengths were slightly higher than that of the elastic modulus. Rate differences continued to narrow considerably after 24 hr. By the end of the third day after casting, the percentages for the elastic modulus changed to 69.5, 77.2/81.6, and 87.9 for normal-, medium-, and high-strength concrete, respectively. In the same period the percentages for the tensile strength became 60.7, 64.7/70.4, and 79.0, and those for the compressive strength rose to 51.1, 60.0/64.6, and 74.6 for the normal-, medium-, and high-strength concretes, respectively.

Figures 8 through 10 compare rates of development of each of the physical properties as affected by mix richness. Generally, the richer the mix, the higher the rate of development of all the physical properties. Figures 11 through 13 compare rates of physical property development at early ages as affected by richness of concrete mix. They show that the richer the mix, the faster the rate of physical property development

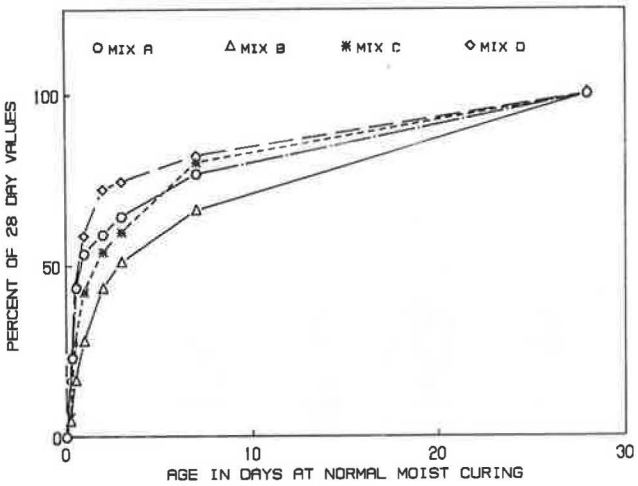

FIGURE 8 Comparison of compressive strength development using normalized values.

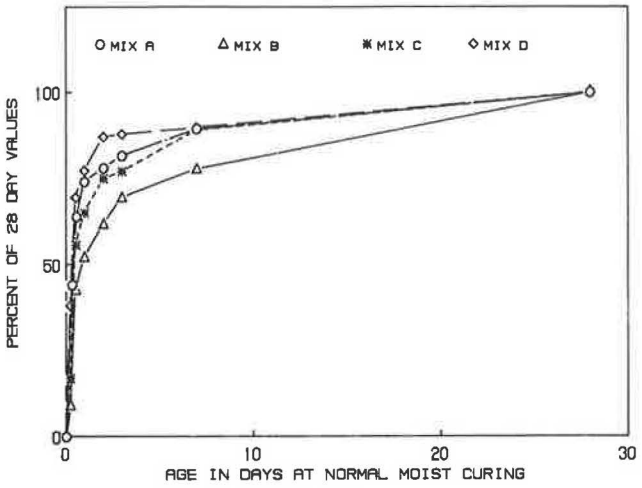

FIGURE 9 Comparison of elastic modulus development using normalized values.

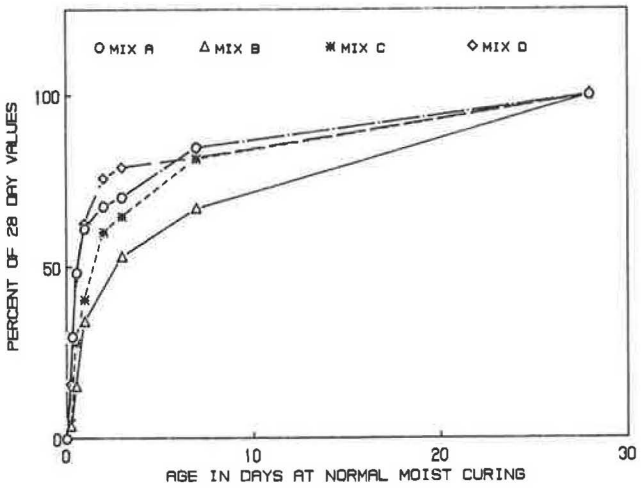

FIGURE 10 Comparison of tensile strength development using normalized values.

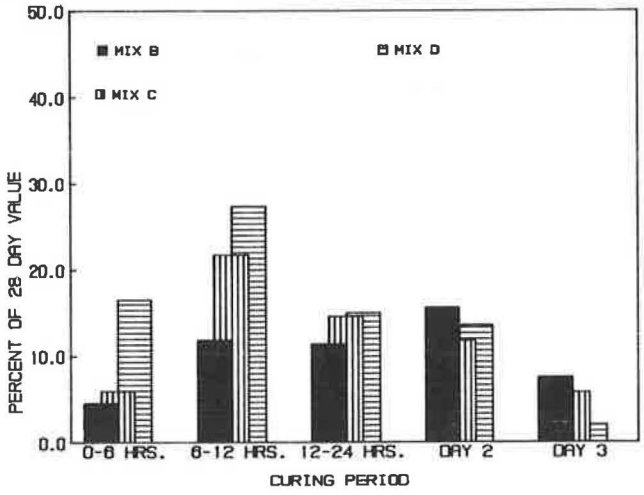

FIGURE 11 Comparison of compressive strength development (first 3 days).

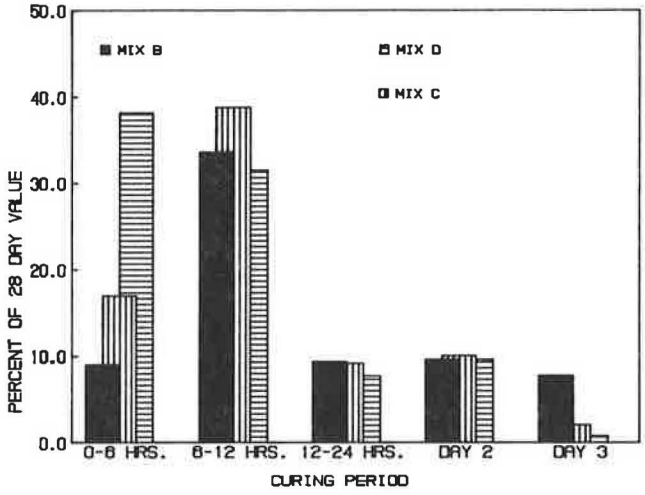

FIGURE 12 Comparison of elastic modulus development (first 3 days).

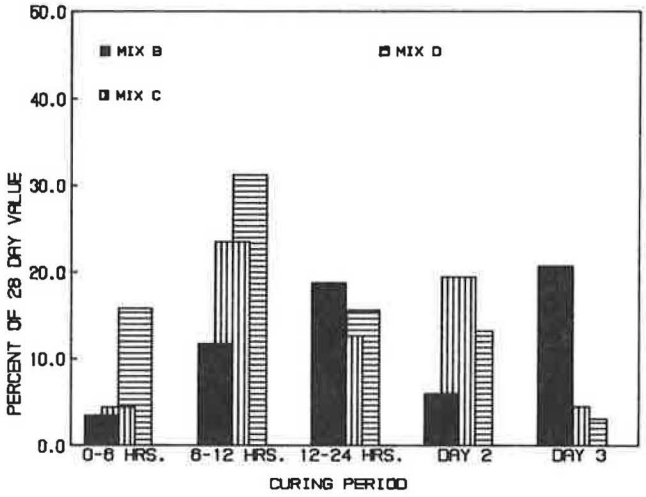

FIGURE 13 Comparison of tensile strength development (first 3 days).

within the first 12 hr after casting. This period is followed by periods of slower rates of development; and the richer the mix, the slower the rate of physical strength development, particularly after the first 2 days of casting. The rate of the elastic modulus development, which was fastest during the first 12 hr, dropped off most rapidly afterwards. That the rate of strength development at early ages is proportional to the richness of the mix is not surprising, because rate of hydration on which physical property development at early ages depends increases with concrete mix richness.

Poisson's ratio was found to be insensitive to mix proportion and richness of mix and to age of concrete above 6 hr (Table 2). In all the mixes tested, low Poisson's ratios ranging from 0.1316 through 0.1512 were obtained at 6 hr. It is the authors' opinion that whether a concrete mix is really concrete at the age of 6 hr is highly debatable. It is clear that at 6 hr concrete is still somewhat plastic, and its properties are still very much in their initial stages of formation. It can be concluded from this study that the Poisson's ratio of concrete is relatively insensitive to the age of concrete. This observation about Poisson's ratio agrees with earlier observations made by Higginson (*8*) and Klink (*9*).

CONCLUSIONS

In general, all the physical properties were found to develop fastest within the first 12 hr after mixing. This period of relatively rapid physical property development coincides with the period of most vigorous hydration reaction. It was also found that the elastic modulus developed fastest during the early ages, whereas the tensile strength developed just slightly faster than the compressive strength. It was observed that the faster the early-age development of a particular physical property, the slower its development at later ages. Consequently, the elastic modulus with the fastest early-age development was found to be slowest in development at ages greater than 3 days. This observation was in agreement with earlier observations by Lew and Reichard (*10*). Poisson's ratio was found to be insensitive to both the age and the richness of concrete mix.

It is evident that the values of physical properties used in concrete design are never fully developed at early ages. The relatively low physical properties at early ages could partly account for the cracking and other serviceability problems observed when concrete structures are subjected to substantial early-age loading. The early-age cracking reported by Buckner and Turner (*11*), Fergundo et al. (*12*), and Furr and Fouad (*13*), and the cracking observed at the time of strand release in prestressed deck panels by Barnoff and Rainey (*14*), Barnoff and Orndorff (*15*), and the Federal Highway Administration are, in the authors' opinion, at least partially attributable to the relatively low tensile strength of concrete at strand release. Also, the excessive immediate and long-term deformations observed by Fu and Gardner (*16*) and Shah et al. (*17*) when concrete structures were subjected to substantial early-age construction loads are attributable, at least in part, to the relatively low values of the physical properties of concrete at early ages.

REFERENCES

1. ACI Technical Committee 231. *Properties of Concrete at Early Ages*. SP-95. American Concrete Institute, Detroit, Mich., 1986.
2. F. A. Oluokun. *Investigation of Physical Properties of Concrete at Early Ages*. Ph.D. dissertation. University of Tennessee, Knoxville, 1989, pp 16–59.
3. R. L'Hermite. Actual Ideas About the Technology of Concrete. *Annals of the Technical Institute of Building and Public Works*, Paris, 1959, pp. 115–116.
4. D. J. McNeely and S. D. Lash. Tensile Strength of Concrete. *Journal of the American Concrete Institute*, Vol. 60, No. 6, 1963, pp. 751–761.
5. S. P. Shah and S. H. Ahmad. Structural Properties of High Strength Concrete and Its Implications for Precast Prestressed Concrete. *Journal of Prestressed Concrete Institute*, Vol. 30, No. 6, 1985, pp. 92–119.
6. M. H. Wills. Early Assessment of Concrete Quality by Accelerated Compression Development with Heat. *Journal of Testing Evaluation*, Vol. 24, 1975, pp. 251–262.
7. J. F. Young and M. Sidney. *Concrete*. Prentice-Hall, Inc., Englewood Cliffs, N.J., 1981.
8. E. C. Higginson. Effect of Steam Curing on the Important Prop-

erties of Concrete. *Journal of the American Concrete Institute*, Vol. 58, No. 3, 1961, pp. 281–298.
9. S. A. Klink. Aggregates, Elastic Modulus and Poisson's Ratio of Concrete. *Journal of the American Concrete Institute*, Vol. 83, No. 6, 1986, pp. 961–965.
10. H. S. Lew and T. W. Reichard. Mechanical Properties of Concrete at Early Ages. *Journal of the American Concrete Institute*, Vol. 75, No. 10, 1978, pp. 533–542.
11. C. D. Buckner and H. T. Turner. Performance of Full-Span Panel-Form Bridges Under Repetitive Loading. In *Transportation Research Record 903*, TRB, National Research Council, Washington, D.C., 1983, pp. 45–52.
12. F. E. Fergundo, H. Tabatabai, K. Soongswang, J. M. Richardson, and E. G. Callis. Precast Panel Composite Bridge Deck. *Concrete International: Design and Construction*, Vol. 7, No. 5, 1985, pp. 59–65.
13. H. L. Furr and F. H. Fouad. *Bridge Slab Concrete Placed Adjacent to Moving Live Loads*. Report FHWA/TX-81-11+266-IF. FHWA, U.S. Department of Transportation, 1981.
14. R. M. Barnoff and D. L. Rainey. *Laboratory Tests of Prestressed Concrete Deck Planks and Deck Plank Assemblies*. Report 2. Pennsylvania Transportation Institute, Pennsylvania State University, University Park, 1974.
15. R. M. Barnoff and J. A. Orndorff. *Construction and Testing of an Experimental Prestressed Concrete Bridge*. Report 1. Pennsylvania State University, University Park, 1974.
16. H. C. Fu and N. J. Gardner. Effect of High Early-Age Construction Loads on Long Term Behavior of Slab Structures. In *Properties of Concrete at Early Ages*. SP-95. American Concrete Institute, Detroit, Mich., 1986
17. S. P. Shah, R. A. Miller, and T. E. Virding. Early-Age Shear Strength of Reinforced Concrete Beams. In *Properties of Concrete at Early Ages*. SP-95, American Concrete Institute, Detroit, Mich., 1986.

Publication of this paper sponsored by Committee on Mechanical Properties of Concrete.

Comparison of Mechanical Properties of High-Strength Concrete Made with Different Raw Materials

MICHAEL L. LEMING

Properties of high-strength concrete can vary significantly depending on the specific raw materials used and the strength levels attained. Data on these characteristics are needed by agencies such as departments of transportation that must consider construction alternatives with various materials and develop plans on the basis of economics as well as engineering properties. Results are presented of a study to determine the properties of high-strength concrete produced with several sets of materials. These materials represent those used in structures built under North Carolina Department of Transportation control. Data obtained included compressive strength, creep, shrinkage, elastic modulus, modulus of rupture, and splitting tensile strength of high-strength concrete produced from a variety of sources and types of materials. Rudimentary cost comparisons were also made.

Practical use of high-strength concrete—concrete with a compressive strength in excess of 6,000 pounds per square inch (psi)—was rare until the 1960s. The compressive strength of commercially available concrete has increased over time (*1*,*2*), however, and high-strength concrete is now reasonably available in many locations.

The ultimate strength level, related mechanical properties, and cost-effectiveness of high-strength concrete are strongly influenced by the raw materials used. Data on characteristics, ranges, and typical properties of such concretes are required for informed planning by agencies such as departments of transportation, which must design, build, and maintain concrete structures produced from many different materials, particularly aggregates. Considerations must include economic factors as well as engineering properties.

PURPOSE

Other studies (*3*) have investigated the effects on concrete performance in Texas of different cements, fly ashes, and aggregate characteristics, primarily using dense limestone. This study was conducted to determine the mechanical properties of high-strength concrete using materials that are commonly available and are representative of many materials used in structures built under the control of the North Carolina Department of Transportation (NCDOT).

Results are presented for compressive strength, modulus of rupture, splitting tensile strength, elastic modulus, creep, and drying shrinkage of concretes produced from various sources and with various types of materials. Simple cost comparisons are also given.

Department of Civil Engineering, Campus Box 7908, North Carolina State University, Raleigh, N.C. 27695-7908.

OVERVIEW OF INVESTIGATION

Initially a series of small laboratory batches was produced to determine proportions of specific raw materials for further study. The mixes selected were labeled the "B" series.

Ten B-series mixes were investigated. Aggregate combinations from the coastal, piedmont, and mountain regions were selected. Three mineral admixtures were chosen that are reasonably available to concrete producers in North Carolina: a fly ash, a granulated blast furnace slag, and a silica fume slurry product.

A high-absorbency, crushed-shell limestone and a manufactured limestone sand were chosen from the coastal region near Wilmington, North Carolina (Castle Hayne). A crushed granite with gneiss, schist, and traces of mica with a natural silica sand was selected from the piedmont area near Raleigh, North Carolina. A partially crushed gravel was selected from the Asheville, North Carolina (Swannanoa), area in the mountains and combined with a natural silica sand.

A fourth coarse aggregate was selected for its potential to produce high-strength concrete. This was a diabase and came from the Durham, North Carolina (piedmont), area. It was used in combination with silica sand from nearby Raleigh.

Sands selected were reasonable to use with the coarse aggregates selected. All aggregates complied with NCDOT specifications. (See Table 1.)

Type I portland cement was used in this phase, because it is standard for most work in North Carolina. Although differences in brands of portland cement were found in earlier work, these were not critical. Therefore, only one brand of cement was used.

Chemical admixtures (retarders and high-range water reducers) were limited to one brand. Small variations in the dosage of these admixtures were not found to be critical, compared with differences caused by aggregates or cementitious materials. Therefore, selection of a specific combination and dosage of chemical admixtures was done on a case-by-case basis, according to the quantities, sources, and types of other raw materials; desired plastic concrete properties; and environmental conditions.

TABLE 1 AGGREGATE CHARACTERISTICS

Source	Type	Mix	Specific Gravity (SSD)	Absorption (%)	Fineness Modulus	Dry Rodded Unit Weight
Fine Aggregate						
Raleigh	Silica, natural	B-1, B-3x, B-4, B-5	2.63	0.4	2.56	—
Castle Hayne	Carbonate, manufactured	B-2A	2.63	1.2	2.84	—
Lilesville	Silica, natural	B-2B	2.62	0.4	2.84	—
Coarse Aggregate						
Raleigh	No. 67, silicious, crushed	B-1, B-3x, B-5	2.62	0.6	—	97.7
Castle Hayne	No. 67, carbonate, crushed	B-2A	2.49	2.6	—	76.3
Swannanoa	No. 67, silicious gravel	B-2B	2.69	1.0	—	98.7
Durham	No. 78M, silicious, crushed	B-2C, B-4	2.77	0.4	—	102.6

MIX DESIGNATION, PRODUCTION, AND COMPOSITION

The B-series mixes were produced in one of two ways. One was a laboratory mix with a volume of approximately 3.5 ft^3 batched in a drum mixer. The other type was a 2- to 3-yd^3 batch produced at a local ready-mixed concrete, "dry batch" plant, located 15 to 20 min by truck from the laboratory where specimens were taken. Mix characteristics are presented in Table 2.

The control mix, B-1, was similar to the NCDOT State Class AA mix, with a higher cement factor. It was produced at the dry batch plant, with aggregate from Raleigh.

Mixes B-2A, B-2B, and B-2C (the B-2x subseries) were made with different aggregates. The binder was composed of approximately 585 lb/yd^3 of Type I cement and 365 lb/yd^3 of granulated blast furnace slag (ASTM C 989 Grade 120) plus a high-range water reducer (ASTM C 494 Type F). This amounted to a slag content of 38.5 percent by weight of total cementitious material, or over 60 percent by weight of cement.

Mix B-2A was produced with the manufactured sand and crushed shell limestone from the coast. Mix B-2B was produced with the partially crushed gravel from the mountains. Both aggregates conformed to ASTM C 33 size No. 67 specification. The B-2C mix was produced with high-strength coarse aggregate, an NCDOT size No. 78 M, uniformly graded ½-in. nominal maximum size diabase from Durham. The B-2x mixes were produced in the laboratory. Test results are presented in Table 3.

Mixes B-3A, B-3B, B-3C, and B-3D (the B-3x subseries) used the same aggregate (from Raleigh) as was used in the control mix. The binder composition was different for each.

Mix B-3A used the same cementitious materials (slag) and proportions as was used in the B-2x subseries. B-3B was a fly ash mix (Class F) and B-3C contained silica fume in a slurry form. B-3D was an air-entrained version of B-3A. The

TABLE 2 MIX INGREDIENTS AND CHARACTERISTICS

Mix	B-1[1]	B-2A	B-2B	B-2C	B-3A[1]	B-3B[1]	B-3C[1]	B-3D[1]	B-4[1]	B-5
[2]Cement	712	586	591	580	589	620	788	590	762	765
Slag		368	371	365	361			370		
Ash						280				200
Fume							157		152	
[3]HRWR		15	15	15	15	10	14	8	15	10
Retarder	4				2	1.5	1.5	1.5	2	
[4]Aggregate	R	CH	SL	D	R	R	R	R	R	R
quantity	1740	1680	1690	1660	1760	1760	1720	1710	1710	1720
[5]w/c ratio	0.42	0.30	0.29	0.29	0.29	0.29	0.30	0.28	0.29	0.28
Slump (in)	3 1/2	5 1/2	10 1/2	10 1/2	10 1/2	10 1/2	8 1/4	2 1/4	6 1/2	6 1/2
Air (%)	5.0	2.4	1.2	1.0	1.0	1.0	1.0	1.7	5.9	1.9

[1]from a ready mixed plant, [2]Cement => Type I; Slag => granulated blast furnace slag; Ash => fly ash; Fume => silica fume (slurry); quantities in pounds per cubic yard, [3]HRWR => high range water reducer; Retarder: retarding admixture; quantities in ounces per hundred pounds of cementitious material, [4]w/c => water/cementitious material ratio, [5]Aggregate: R => Raleigh; CH => Castle Hayne; SI_4 => Swannanoa, Lilesville; D => Durham; quantities of coarse aggregate in pounds per cubic yard

TABLE 3 SUMMARY DATA: AGGREGATE EFFECTS

Mix	B-1 [2]		B-2A	B-2B	B-2C	B-3A [2]
Aggregate	R		CH	SL	D	R
Cement	712		586	591	580	589
Slag			368	371	365	361
w/c ratio	0.42		0.30	0.29	0.29	0.29
Air (%)	5.0		2.4	1.2	1.0	1.0
Compressive Strength (psi) (4" x 8", steel molds, except B-1 with both sizes)						
	4x8	6x12				
7 days	6380	---	7350	5890	8780	9590
28 days	7710	6930	9420	7350	10,920	11,570
1 year	9160	8720	10,220	9680	13,030	13,170
Modulus of Rupture (psi) (6" x 6" x 18" beams, third point loading)						
28 days	680		1060	1100	1580	1345
1 year	775		1155	1145	1675	1380
Splitting Tensile (psi) (6" x 12")						
28 days	415		425	430	550	485
1 year	485		645	490	615	645
Elastic Modulus (million psi) (6" x 12")						
28 days	4.07		4.98	4.03	6.52	4.97
1 year	4.40		5.72	4.50	6.59	5.66
Specific Creep (millionths/psi) (6" x 12", except B-1 with both sizes)						
	0.34	0.28	0.16	0.19	0.16	0.13
Shrinkage (microstrain)						
	526		439	454	375	343

[1] see Table 2 for more details [2] ready mixed, R => Raleigh; CH => Castle Hayne; SL => Swannanoa, Lilesville; D => Durham;

B-3x mixes were produced at the concrete batch plant. (See Table 4.)

Mix B-4 had the highest compressive strength. The coarse aggregate used in this mix was the No. 78 M diabase from Durham, North Carolina. The fine aggregate was the same as that used in the B-3x subseries. Silica fume in slurry form was used. This mix was produced in the laboratory. (See Table 5.)

B-5 was another fly ash mix used to examine additional curing effects. B-5 was produced in the laboratory.

The weights of silica fume are weights of the slurry, which contains approximately 50 percent solids (by weight). Percentages of mineral admixtures used are percents by weight of total cementitious material. A high-range water reducer was used in all mixes (except B-1) to obtain the desired workability. A retarding admixture was successfully used to control slump loss in the B-1 and B-3x mixes that had been produced in the summer at the ready-mixed concrete batch plant.

A minimum water content of 260 to 280 lb/yd^3 was found to reduce excessive stickiness of these high-strength concretes, where W/C ratio is water to cementitious material.

Standard procedures for sampling, curing, and testing concrete were followed except where noted. Test results for compressive strength were the average of three specimens each. Modulus of rupture, splitting tensile strength, and elastic modulus values were the average of two specimens each.

Compressive strengths were obtained from 4- by 8-in. specimens cast in steel molds, except B-1, which gives results for both sizes of cylinders. Elastic modulus and splitting tensile strength were determined from 6- by 12-in. cylinders. Modulus of rupture was determined from 6- by 6- by 30-in. prisms.

Creep was determined on the basis of 4- by 8-in. cylinder specimens rather than 6- by 12-in. specimens, except the B-1 mix, which used both. Drying shrinkage values were determined from 4- by 4- by 11-in. prisms.

Comparisons of mechanical properties are presented in Tables 6 and 7.

OBSERVATIONS AND DISCUSSION

Slump Control

Slump loss of the plant-batched mixes using a high-range water reducer was successfully controlled by also using a retarding and water-reducing admixture (ASTM C 494 Type D). The concrete was redosed with high-range water reducer as needed. No excessive retardation was noticed.

TABLE 4 SUMMARY DATA: BINDER EFFECTS

Mix	B-1 [2]	B-3A [2]	B-3B [2]	B-3C [2]	B-3D [2]	B-5
[2] Cement	712	589	620	788	590	765
Mineral Admix		361 Slag	280 Ash	157 Fume	370 Slag	208 Ash
HRWR		15	10	14	8	10
Retarder		4	2	1.5	1.5	1.5
w/c ratio	0.42	0.29	0.30	0.28	0.29	0.28
Air (%)	5.0	1.0	1.0	1.7	5.9	1.9
Compressive Strength (psi) (4" x 8")						
7 days	6380	9590	5510	9730	6110	na
28 days	7710	11,570	7360	12,240	7990	8780
1 year	9160	13,170	10,620	13,610	9990	11,090
Modulus of Rupture (psi) (6" x 6" x 18" beams, third point loading)						
28 days	680	1345	820	1150	1200	na
1 year	775	1380	860	1225	(1020)	na
Splitting Tensile (psi) (6" x 12")						
28 days	415	485	390	505	475	na
1 year	485	645	435	695	530	580
Elastic Modulus (million psi) (6" x 12")						
28 days	4.07	4.97	4.07	4.91	4.29	4.52
1 year	4.40	5.66	4.72	5.53	4.53	4.89
Specific Creep (millionths/psi) (6" x 12")						
	0.28	0.13	0.33	0.11	0.20	0.28
Shrinkage (microstrain)						
	526	343	541	280	463	348

[1] See Table 2 for more details [2] ready mixed

TABLE 5 SUMMARY DATA: SELECTED MIXES, HIGH STRENGTH, AND CONTROL

Mix	B-1 [2]	B-3A [2]	B-4
Cement	712	589	762
Mineral Admix		361 Slag	152 Fume
HRWR		15	15
Retarder		4	2
Aggregate	Raleigh	Raleigh	Durham
w/c ratio	0.42	0.29	0.27
Air (%)	5.0	1.0	4.5
Compressive Strength (psi) (4" x 8", steel molds)			
7 days	6380	9590	11,980
28 days	7710	11,570	15,570
1 year	9160	13,170	17,710
Modulus of Rupture (psi) (6" x 6" x 18" beams, third point loading)			
28 days	680	1345	1660
1 year	775	1380	1700
Splitting Tensile (psi) (6" x 12")			
28 days	415	485	800
1 year	485	645	835
Elastic Modulus (million psi) (6" x 12")			
28 days	4.07	4.97	6.98
1 year	4.40	5.66	7.12
Specific Creep (millionths/psi) (6" x 12")			
	0.34	0.13	0.16
Shrinkage (microstrain)	526	343	358

[1] See Table 2 for more details [2] ready mixed

TABLE 6 SUMMARY DATA: COMPARISON OF AGGREGATE EFFECTS

Mix	B-1 [2]	B-2A	B-2B	B-2C	B-3A [2]
Aggregate	R	CH	SL	D	R
Cement	712	586	591	580	589
Slag		368	371	365	361
w/c ratio	0.42	0.30	0.29	0.29	0.29
Air (%)	5.0	2.4	1.2	1.0	1.0
Compressive Strength Gain (psi and percent: 28 to 365 days)					
psi	1450	800	2330	2110	1600
percent gain	19	8	32	19	14
Modulus of Rupture divided by the square root of compressive strength					
28 days	8.2	10.9	12.8	15.1	12.5
1 year	8.3	11.4	11.6	14.7	12.0
Splitting Tensile Strength divided by the square root of compressive strength					
28 days	5.0	4.4	5.0	5.3	4.5
1 year	5.2	6.4	5.0	5.4	5.6
Elastic Modulus: ratio of value predicted by ACI recommended equations (based on compressive strength) to measured value					
ACI 318					
28 days	1.17	1.11	1.21	0.91	1.23
365 days	1.21	1.01	1.25	0.99	1.16
ACI 363					
28 days	1.06	0.98	1.10	0.79	1.07
365 days	1.08	0.88	1.10	0.85	0.99

[1] See Table 2 for more details, [2] ready mixed

TABLE 7 COMPARISON OF BINDER EFFECTS WITH HIGH-STRENGTH MIX

Mix	B-3A [1]	B-3C [1]	B-3D [1]	B-5	B-4
Cement	589	788	590	765	762
Mineral Admix	361 Slag	157 Fume	370 Slag	208 Ash	157 Fume
w/c ratio	0.29	0.28	0.29	0.28	0.27
Air (%)	1.0	1.7	5.9	1.9	4.5
Compressive Strength Gain (psi and percent: 28 to 365 days)					
psi	1600	1370	2000	2310	2140
percent gain	14	11	25	26	14
Modulus of Rupture divided by the square root of compressive strength					
28 days	12.5	10.4	13.4	na	13.3
1 year	12.0	10.5	na	na	12.8
Splitting Tensile Strength divided by the square root of compressive strength					
28 days	4.5	4.6	5.3	na	6.4
1 year	5.6	6.0	5.3	5.5	6.3
Elastic Modulus: ratio of value predicted by ACI recommended equations (based on compressive strength) to measured value					
ACI 318					
28 days	1.23	1.29	1.19	1.18	1.02
365 days	1.16	1.20	1.26	1.23	1.07
ACI 363					
28 days	1.07	1.11	1.07	1.05	0.86
365 days	0.99	1.03	1.10	1.07	0.89

[1] See Table 2 for more details, [2] ready mixed

Compressive Strength

Aggregate had a profound influence on compressive strength. Compressive strengths at 28 days with the same binder but different aggregates ranged from just over 7,000 psi to well over 11,000 psi.

Differences in compressive strength due to mineral admixture type and quantity were equally significant. Compressive strength at 28 days with the same good quality aggregate ranged from over 7,000 to over 12,000 psi.

Increasing the total air content from 1 percent to almost 6 percent resulted in about 5 percent compressive strength loss for each percent increase in air content (see Mixes B-3A and B-3D, Table 4).

Elastic Modulus

The ACI 318 equation for elastic modulus

$$E = 57{,}000 \cdot \sqrt{f_c} \text{ psi} \quad (1)$$

can yield unconservative values for concrete with compressive strengths in excess of 8,000 psi (*1*,*4*). An alternative equation was suggested by Martinez et al. (*3*) and reported elsewhere (*1*) for 3,000 to 12,000 psi concrete:

$$E = (40{,}000 \cdot \sqrt{f_c}) + 1{,}000{,}000 \text{ psi} \quad (2)$$

This equation gave much closer results to experimental values, even up to 18,000 psi. Variation was still substantial, however. These results are presented in Figure 1. The values of the elastic moduli predicted by Equations 1 and 2 are shown as solid lines. The actual measured values, obtained from high-strength concrete from the B series, are shown as points. The points marked *m* are for data at 28 days (1 month). The points marked *Y* are for data at 365 days (1 year).

Modulus of Rupture

The modulus of rupture of Mix B-3D at 1 year is less than that at 28 days. The modulus of rupture at 28 days appears consistent with other data. The 1-year test is believed to be in error.

The modulus of rupture may be estimated as the square root of compressive strength times a constant, typically 7.5 to 12. For high-strength concrete, the value of 11.7 has been suggested by Carrasquillo et al. (*5*) and reported elsewhere (*1*) for 3,000- to 12,000-psi concrete.

Values ranged from 10 to 15 in this study. Best-fit analysis gave a value of 11.6 for strengths up to 18,000 psi. The standard error of the estimate was in excess of 200 psi, however. There was virtually no difference between strength values at either 28 days or 1 year.

Splitting Tensile Strength

Values of the splitting tensile strength from this series ranged from a low of less than 400 psi to a high of well over 800 psi. The ratio of split cylinder strength to square root of compressive strength for this project ranged from 4.2 to 6.4. Regression produced a value of 5.3. ACI 363 yields a value of 7.4.

Reasons for the difference between the results of this project and the results cited in ACI 363 are not known. Differences in aggregate source and type may play a role. The difference in test specimen size or strength level may also be important.

The standard error of the estimate of the splitting tensile strength was almost 80 psi. As with modulus of rupture, there was no significant difference in the relationship between compressive strength and splitting tensile strength for data at 28 days and 1 year.

Drying Shrinkage

The drying shrinkage of the high-strength concretes tested ranged from less than 300 to well over 500 μstrain. Drying shrinkage strains of the high-strength concretes were less than the drying shrinkage strain of the control mix. The mix with the highest compressive strength did not have the lowest shrinkage.

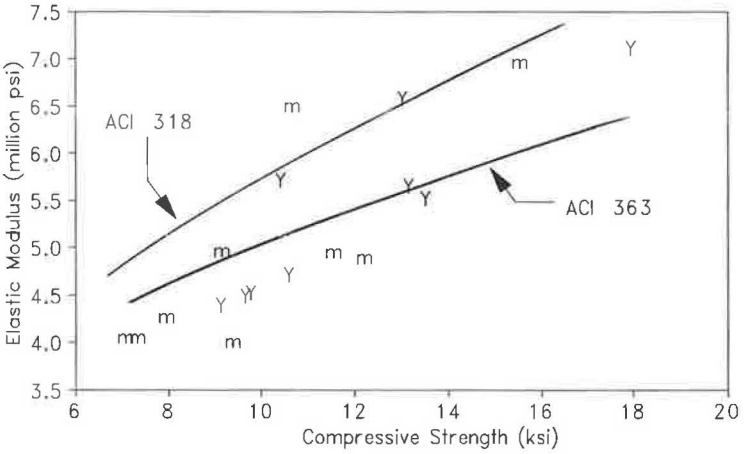

FIGURE 1 Elastic modulus and ACI equations: test versus predicted values.

Comparing concrete made with the same aggregate, but different paste composition (slag and silica fume, B-3A and B-3C, Table 4), the difference in shrinkage was about 60 μstrain. Comparing concrete made with different aggregates (see B-3C and B-4, Table 7), the difference in shrinkage was similar, about 80 μstrain.

Multiple linear regression of paste volume and the inverse of compressive strength versus drying shrinkage proved interesting. Except for the mixes containing fly ash, drying shrinkage (in microstrain with a standard error of 45 μstrain) could be estimated from

$$\varepsilon_{sh} = 321 \cdot Vp + \frac{30{,}000}{fc} - 2{,}690 \cdot \frac{Vp}{fc} - 3{,}130 \qquad (3)$$

where Vp is the volume of paste (in cubic feet per cubic yard) and fc is the compressive strength at 28 days (in kips per square inch).

Nasser and Al-Manaseer (*6*) conclude that shrinkage of plain concrete is nearly the same as concrete with fly ash and superplasticizers. Although the absolute values found are similar to theirs, differences were found that were linked to the mineral admixture used. The fly ash mixes had a higher drying shrinkage than that predicted by this formula.

Because differences in percent mineral admixture were tied directly to the type of mineral admixture used, the effect of changes in percent mineral admixture on the shrinkage strain was indistinguishable from the effect of the mineral admixture itself.

Creep

The specific creep of the control mix was almost 20 percent higher for the 6- by 12-in. specimens than for the 4- by 8-in. specimens (B-1, Table 3).

As with drying shrinkage, variation in specific creep depended on paste composition, strength levels, and aggregate source. The effect of the aggregate source was pronounced.

For mixes made with the same aggregate (Raleigh), but different paste composition [slag (B-3A) and silica fume (B-3C), Table 4], the difference in specific creep was only 0.02 millionths per psi. Both mixes had similar strength levels. Comparing two other mixes [slag (B-2C) and silica fume (B-4), Tables 5 and 6] made with the same aggregate (Durham), there was no measured difference in specific creep, even with a difference in compressive strength over 5,000 psi.

Comparing the difference between mixes made with the same paste composition but different aggregates (B-3C and B-4, Table 7), the difference in shrinkage was 0.05 millionths per psi. In this case the stronger mix (by over 3,000 psi), with smaller aggregate, had the higher creep.

A model to predict specific creep was developed using multiple regression. As with shrinkage, the fly ash mixes did not fit the model.

The following model provided the best fit of the data:

$$\text{Specific creep} = 0.770 - \frac{6.06}{fc} - \frac{4.05}{E} + \frac{39.7}{(fc \cdot E)} \qquad (4)$$

Specific creep is in millionths of an inch per inch per psi, fc is compressive strength in kips per square inch, and E is the elastic modulus in million pounds per square inch. The standard error in the forecast is about 10 percent, excluding the fly ash mix data.

The mixes containing only portland cement, or those with slag or silica fume, conform to the model, whereas mixes with fly ash were significantly different from the model predictions.

Curing conditions for B-5 were altered to adjust for differences in rate of strength gain of fly ash mixes. Moist curing was extended for B-5 for a total of 42 days. Storage in 50 percent relative humidity before loading was maintained according to ASTM standards. The creep of this mix was also significantly different from that predicted by the model, however.

As with drying shrinkage, the values obtained in this study, including the fly ash mixes, are within typical expected ranges (*7*). The fly ash mixes are simply different.

Drying shrinkage and specific creep were highly correlated for all mixes.

COST CONSIDERATIONS

Comparison of concrete mixes in terms of cost per cubic yard is not meaningful when 4,000- or 5,000-psi concrete is compared with 10,000- or 12,000-psi concrete, because of substantial differences in design criteria or life-cycle costs. For concretes with significantly different compressive strengths, dollars per 1,000 psi are somewhat better for comparison.

Raw material costs cannot, by themselves, provide a realistic basis for estimating the price of high-strength concrete. Although operating costs and delivery costs may change only slightly, both profit margins and risk assessments will generally increase.

Profit margins may increase as competitors drop out of bidding on high-strength concrete work. Accurate contingency factors will be largely unknown until more historical data have been developed on high-strength concrete, so estimates will tend to be high. Rigorous quality control and quality assurance programs will be required.

An accurate estimate of high-strength concrete cost is therefore possible at best only for a well-defined set of conditions. If these limits are recognized, however, estimates are still useful and available for comparison.

Costs of several representative mixes were calculated using the following assumptions (for mineral admixtures in the quantities used):

- \$10/ton—aggregates;
- \$60/ton—portland cement;
- \$8/gal—high-range water reducers;
- \$30/yd^3—silica fume (slurry); and
- \$6/yd^3—granulated blast furnace slag.

Normal operating and delivery costs are assumed to be \$15/yd^3 although this depends heavily on distance to the job. Additional quality control and a more sophisticated quality assurance program by the supplier could be estimated to cost from \$10 to \$20/yd^3 on a moderately sized job. Additional charges for profit and contingency are assumed to be 10 percent for commodity-grade concrete and 20 percent for high-strength concrete. These figures were derived on the basis of estimates from previous experience made by the author.

A standard commodity-grade concrete for use by the NCDOT would cost, under these assumptions, about $50/yd³, which is reasonably accurate. Concrete costs reported for 19,000 psi were $120/yd³ in Seattle, not including research (*8*). The cost in dollars per cubic yard of selected mixes along with the value in dollars per cubic yard per 1,000 psi compressive strength at 28 days are as follows:

Mix	*Cost ($/yd³)*	*Value ($/yd³)/ksi*
B-3A	90	7.8
B-3C	120	10.3
B-4	120	7.7
"Standard"	50	10.0
Seattle	120	6.3

These assumptions are useful only for general comparison; their accuracy is obviously limited.

The cost for small projects or those a considerable distance from existing plants may be much more expensive. In some locations, the production of concrete with compressive strengths of 12,000 to 15,000 psi may not be possible without importing aggregate. Depending on the distance and the quantities involved, the cost of the concrete could easily increase by $35 to $50/yd³.

Because a considerable portion of the life-cycle cost of a structure depends on the durability of materials used in construction, cost analysis must also consider the effect of increased durability of high-strength concrete.

CONCLUSIONS

Concretes with compressive strengths in excess of 10,000 psi are possible using several different types of materials from or available at a reasonable price in North Carolina. The mechanical properties vary significantly depending on the source, type, and proportions of raw materials used.

The production of such concrete on a commercial basis from a dry batch concrete plant was found to be possible with minor changes in quality control procedures normally used in a well-run operation. Production of concrete with compressive strength in excess of 12,000 psi from a dry batch plant was found to be possible only with additional constraints on material selection and production procedures plus a detailed quality control and quality assurance program.

The W/C ratio is not an effective predictor of strength for high-strength concrete made with significantly different aggregates or paste composition.

Even moderate air contents reduce the compressive strength of high-strength concrete significantly.

The equations given in ACI 363 for prediction of elastic modulus and of modulus of rupture on the basis of compressive strength provide values that agree reasonably well with those determined experimentally.

Indirect, or splitting, tensile strength was found to be a significantly lower percentage of compressive strength than results reported in other work.

Creep and drying shrinkage were significantly influenced by aggregate type as well as binder composition. Fly ash was found to have a different effect on creep and drying shrinkage than the more reactive mineral admixtures used.

Specific creep values for the high-strength concrete in this study were found to be significantly less than those of conventional-strength concrete.

Estimates of the cost of high-strength concrete on the basis of dollars per cubic yard per thousand pounds per square inch compare favorably with those for conventional-strength concrete.

ACKNOWLEDGMENTS

The data presented here are from work conducted by the Department of Civil Engineering, North Carolina State University, sponsored by NCDOT. This work is entitled, "Properties of High Strength, An Investigation of High-Strength Concrete Characteristics using Materials in North Carolina." Appreciation is also expressed to the staff of the NCDOT Materials and Test Unit for their assistance and to Thomas Tallman, Frank Altimore, Miguel Salandra, and Roberto Nunez for their work as Research Assistants.

REFERENCES

1. ACI Committee 363. State of the Art Report on High Strength Concrete. *ACI Journal*, Vol. 81, No. 4, July-Aug. 1984, pp. 364–411.
2. C. D. Johnston. Fifty Year Developments in High Strength Concrete. *Journal of the Construction Division*, ASCE, Vol. 101, No. 4, Dec. 1975, pp. 801–818.
3. S. Martinez, A. H. Nilson, and F. O. Slate. *Spirally Reinforced High-Strength Concrete Columns*. Research Report 82-10. Department of Structural Engineering, Cornell University, Ithaca, N.Y., Aug. 1982.
4. M. B. Peterman and R. L. Carrasquillo. *Production of High Strength Concrete*. Research Report 315-1F. Center for Transportation Research, Bureau of Engineering Research, University of Texas at Austin, Oct. 1983.
5. R. L. Carrasquillo, F. O. Slate, and A. H. Nilson. Properties of High Strength Concrete Subject to Short-Term Loads. *ACI Journal*, Vol. 78, No. 3, May-June 1981, pp. 171–178.
6. K. W. Nasser and A. A. Al-Manaseer. Creep of Concrete Containing Fly Ash and Superplasticizer at Different Stress/Strength Ratios. *Journal of the American Concrete Institute*, Vol. 83, No. 4, July-Aug. 1986, pp. 668–673.
7. ACI Committee 209. Prediction, Creep, Shrinkage and Temperature Effects in Concrete Structures. *ACI Journal*, Vol. 81, No. 4, July-Aug. 1984, pp. 364–411.
8. M. Ralston and R. Korman. Economical Composite System Is Stiffened with Record 19,000-psi Mix. *Engineering News Report*, Vol. 222, No. 7, Feb. 16, 1989, pp. 44–53.

Publication of this paper sponsored by Committee on Mechanical Properties of Concrete.

Concrete Physical Property Development at Early Ages: the Influence of Steam Curing

FRANCIS A. OLUOKUN, EDWIN G. BURDETTE, AND J. HAROLD DEATHERAGE

Results of tests carried out to investigate the causes of early-age cracking reported in some precast, prestressed, steam-cured structural members are reported. Cracks have been observed at the fabrication site even before structures are put into use. An investigation was conducted into the development of concrete physical properties at early ages when the concrete is steam cured. Properties investigated were compressive strength, elastic modulus, splitting tensile strength, and Poisson's ratio. A prestressed concrete producer sample was used in the fabrication of conventional 6- × 12-in. cylinder test specimens. Test results were obtained for 8 hr, 14 hr, 1 day, 2 days, 3 days, 7 days, and 28 days. Tests were carried out on both steam-cured and companion standard moist-cured specimens for comparison. Steam curing was found to be beneficial to the development of all the physical properties only at early ages. The beneficial effect was found to be the least lasting on the tensile strength development in which the benefit appeared to have ceased even before steam curing was discontinued. This resulted in lower tensile strength values for the steam-cured specimens when compared with the values for their standard moist-cured companions. The observed low tensile strength developed in steam-cured specimens may be responsible, at least partially, for the cracking reported during strand release and form stripping at prestressing plants.

Steam curing is a relatively new curing method that is used mostly by the precast, prestressed concrete industry. The relatively recent introduction of precast, prestressed concrete into different areas of the concrete construction industry has brought pressure on the prestressing plants to produce concrete at a faster rate than can be accommodated by normal curing methods. This demand on the precast, prestressed plants has necessitated an economic daily turnaround of molds that can only be achieved through an accelerated curing procedure. The most commonly used method to achieve accelerated curing is the low-pressure steam-curing method in which concrete is cured with saturated steam at atmospheric pressure, necessarily at temperatures below 100°C (212°F). Its primary purpose is to accelerate concrete compressive strength development so that prestressing strands can be released, forms can be stripped and reused at frequent intervals, and concrete products can be stored or put to use at an early age. Since the use of steam curing at atmospheric pressure began about 60 years ago, considerable experimental work has been undertaken to investigate its effects on concrete strength development.

Recently, it has been observed that some of the steam-cured prestressed structural members are developing cracks even before they are put into use. This early-age cracking has been reported by several researchers (*1–5*) and has been attributed to relatively low values of physical properties developed during the early ages. Cracking has also been reported during routine inspections at the prestressed concrete plant. In most cases, these cracks develop during prestressing at the time of form removal when concrete has not attained its specified design strength.

Although it is generally accepted by researchers (*6–9*) that steam curing accelerates compressive strength development, the effects of steam curing on the early-age development of other properties like elastic modulus, splitting tensile strength, and Poisson's ratio have not been precisely defined. Higginson (*7*) reported that elastic modulus increased with compressive strength and that Poisson's ratio showed nearly the same value for all ages and curing conditions. Hanson (*6*) pointed out that the optimum steam-curing conditions for modulus of elasticity and tensile strength would differ from those required for optimum compressive strength. The U.S. Bureau of Reclamation as well as many researchers (*6–10*) have observed that the greatest acceleration in compressive strength gain and minimum loss in ultimate strength were obtained at steam-curing temperatures between 120° and 165°F.

It has not been established that the stated optimum steam-curing condition for compressive strength development is equally beneficial to either elastic modulus development or tensile strength development at early ages. An understanding of elastic modulus development is required for the estimation of prestress losses and for calculation of immediate and long-term deformations due to early loading.

Although it is generally assumed that concrete performance is mostly governed by its compression capabilities, tensile strength (which directly influences cracking at prestress release) and shear capacity are important with respect to the appearance and durability of concrete structural members. Variation of tensile strength with time is an important factor in predicting concrete shear strength at different curing times. This study investigated the effects of the steam-curing conditions (as used by typical prestressing plants) on the development of the important physical properties at early ages.

Department of Civil Engineering, University of Tennessee, Knoxville, Tenn. 37996-2010.

EXPERIMENTAL INVESTIGATION PROCEDURE

Fabrication of Test Specimens

Test specimens were fabricated from a precast, prestressed concrete producer sample. The 28-day compressive strength of the concrete mix was approximately 6,000 psi. The specimens were cast from a single batch of concrete. Standard 6- × 12-in. molds were used in accordance with ASTM C 470, and molding was done according to the specifications of ASTM C 31. The coarse aggregate used was ASTM No. 67 with 100 percent of the crushed stone less than 1 in. (of this, 90 to 100 percent was about ¾ in.). Fine aggregate was crushed limestone. Concrete mix proportions were as follows (per cubic yard of mix):

- Type I portland cement, 752 lb;
- Coarse aggregate, 1,730 lb;
- Fine aggregate, 1,242 lb; and
- Water, 292 lb.

Curing Procedure

Wet burlap was used to cover the molds and specimens until the specimens were removed from the molds. A polyethylene sheet was placed over the burlap to minimize evaporation.

Both moist and steam curings were used for the precast, prestressed producer sample. Steam curing as practiced by typical prestressing plants was used. The presteaming period was 5 hr, and the rate of temperature rise was about 40°F per hour up to a maximum temperature of about 130°F. The total steaming period was 15 hr.

For comparison, companion specimens were moist cured at standard conditions. About 20 to 24 hr after casting, specimens were stripped and transferred to the standard moist room where curing continued at about 73°F (23°C) in accordance with ASTM C 192. Most of the test results on which strength design relations are based were performed on moist-cured concrete specimens; hence the choice of moist curing at 73°F in this study.

Testing Procedure

Three specimens from each mix were tested for each of the parameters investigated at 6 hr, 12 hr, 1 day, 2 days, 3 days, 7 days, and 28 days.

Compressive Strength, Elastic Modulus, and Poisson's Ratio Tests

The cylinders that were tested for compressive strength also provided the data for static elastic modulus and Poisson's ratio. Before testing, and to prevent stress concentration during testing, the specimens were capped with a proprietary compound containing sulfur in accordance with the specifications of ASTM C 617. Compressive strength testing was performed on a 300,000-lb capacity testing machine that is capable of loading at a rate of 20 to 50 psi/sec (ASTM C 39). Compressive strength tests were performed in uniaxial compression to failure.

Simultaneous with the compressive strength test, the longitudinal and lateral deformations were measured with the Structural Behavior Engineering Laboratories deformation jacket. This jacket is equipped with six linear variable differential transformer transducers (LVDTs). Three of these LVDTs measure the axial strain and the other three measure the lateral strain. These LVDTs provided an average of three readings for strains in each direction. This approach reduced the error in strain measurement and ensured a higher degree of accuracy of physical property evaluation. The strains in the two directions were computed using data acquisition software.

The compressive strength (S) was calculated from the relation

$$S = P/\pi r^2 \tag{1}$$

where P is load at failure and r is the radius of the specimen.

The static elastic modulus (Young's modulus) was calculated from the stress-strain diagram. The chord modulus is calculated from the relation

$$Ec = \frac{S_2 - S_1}{\varepsilon_2 - 0.00005} \tag{2}$$

where S_2 is the stress corresponding to 40 percent of the ultimate stress, S_1 is the stress corresponding to a strain of 0.00005, and ε_2 is the longitudinal strain corresponding to S_2.

Poisson's ratio, the ratio of transverse strain to longitudinal strain, is determined from the relation

$$\mu = \frac{\varepsilon t_2 - \varepsilon t_1}{\varepsilon_2 - 0.00005} \tag{3}$$

where εt_2 and εt_1 are transverse strains at mid-height of the test specimen produced by S_2 and S_1, respectively. S_2, S_1, and ε_2 are the same as defined in Equation 2.

Splitting Tensile Strength

In general, three kinds of test methods are available for estimating the tensile strength of concrete: the direct tension test, the beam or modulus-of-rupture test, and the split-cylinder or Brazilian test.

Previous investigations (*11–15*) have indicated that the split-cylinder method is a more reliable measure of tensile strength than the modulus-of-rupture test. The most important advantage of the split-cylinder test is the approximate uniformity of tensile stress over the diametral area of the test cylinder. Moreover, its simplicity affords the opportunity to test a large number of specimens within a relatively shorter period of time.

The split-cylinder test was used in this study in accordance with the specifications of ASTM C 496. The tensile strength was computed from the relation

$$f_t = \frac{2P}{\pi DL} \tag{4}$$

where f_t is the tensile strength in pounds per square inch, P is the magnitude of load at failure in pounds, and D and L are the cylinder diameter and length, respectively, in inches.

PRESENTATION AND DISCUSSION OF TEST RESULTS

Tests were performed to investigate the influence of steam curing on the elastic modulus, the splitting tensile strength, Poisson's ratio, and the compressive strength developments at early ages. Test results are summarized in Table 1.

Figures 1 and 2 present a comparison of compressive strength development in steam- and moist-cured concretes. As expected, these figures indicate that steam curing significantly accelerated the strength development within the first day. At the end of the first day (when steam curing was discontinued), the rate of gain in strength in the steam-cured concrete diminished. In fact, there was little (184 psi) gain in strength between the end of the first day and the third day. Moist-cured concrete gained strength steadily and, by the third day, it developed more compressive strength than steam-cured concrete. At 7 and 28 days, moist-cured concrete continued to develop higher compressive strengths than steam-cured concrete. This result completely agrees with observations made by other researchers mentioned earlier.

Steam curing appears to have a more lasting effect on elastic modulus development than on development of the compressive strength. The results presented in Figures 3 and 4 show that steam curing was beneficial within the ages of 1 to 3 days. The greatest increase in the elastic modulus development was observed shortly after steam curing had been discontinued. Then, on the seventh day of curing, the moist-cured value of elastic modulus became slightly higher than the steam-cured value. Beyond the age of 7 days, the elastic modulus of moist-cured concrete developed faster than that of steam-cured concrete. This fact indicates that the benefit of steam curing to the elastic modulus development is limited to the first 3 days and that steam curing is detrimental to the elastic modulus development at ages above 3 days.

Tensile strength development benefits least. As presented in Figures 5 and 6, steam curing benefited tensile strength development only up to about 14 hr. Furthermore, it appears that the beneficial effect of steam curing on tensile strength ceased even before steam curing was discontinued. By the end of the first day (when strands are usually released), moist-cured concrete had developed more tensile strength than steam-cured concrete. Thereafter, and up to 28 days, moist-cured concrete consistently developed higher values of tensile strength than steam-cured concrete. As stated earlier, tensile strength controls resistance to cracking at prestress release. The relatively slow rate of tensile strength development in steam-cured concrete may be responsible, at least partially, for the

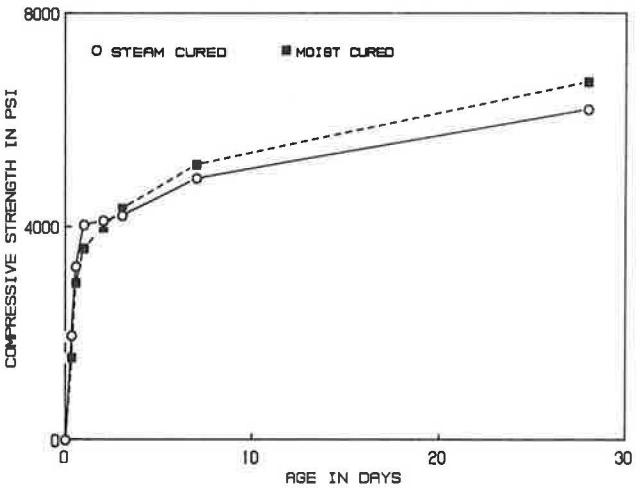

FIGURE 1 Comparison of compressive strength development in moist- and steam-cured concrete.

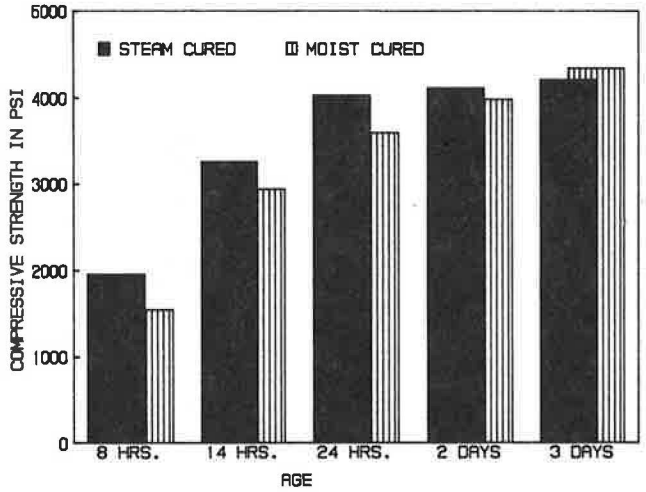

FIGURE 2 Compressive strength development in moist- and steam-cured concrete: first 3 days.

TABLE 1 SUMMARY OF TEST RESULTS

Age	Steam fc (psi)	Moist fc (psi)	Steam Ec (10^6 psi)	Moist Ec (10^6psi)	Steam ft (psi)	Moist ft (psi)	Steam ν	Moist ν
8 Hrs	1,957	1,548	2.4586	2.2677	243	177	0.1438	0.1374
14 Hrs	3,259	2,942	3.3438	3.2875	336	289	0.1841	0.1876
24 Hrs	4,025	3,596	4.2926	3.7994	346	366	0.1815	0.1839
2 Days	4,111	3,979	4.3537	4.0057	391	405	0.1805	0.1834
3 Days	4,029	4,339	4.4744	4.1840	398	420	0.1807	0.1862
7 Days	4,904	5,176	4.5816	4.5960	444	507	0.1906	0.1948
28 Days	6,198	6,720	4.7224	5.1316	534	597	0.1961	0.1875

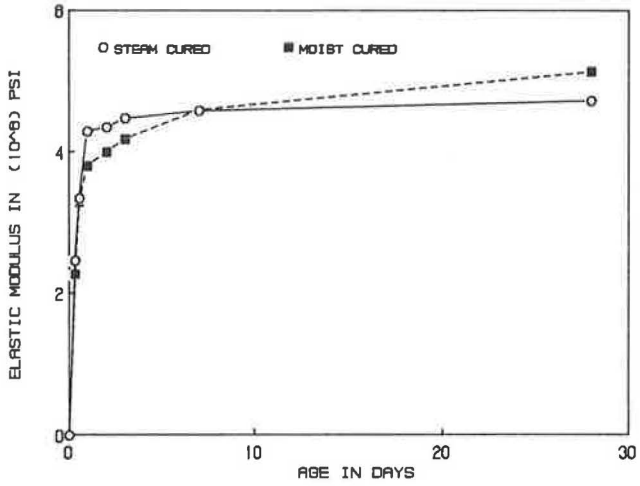

FIGURE 3 Comparison of elastic modulus development in moist- and steam-cured concrete.

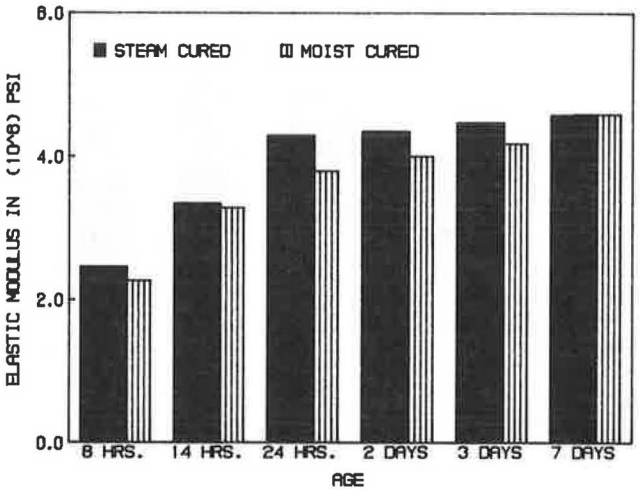

FIGURE 4 Elastic modulus development in moist- and steam-cured concrete: first 7 days.

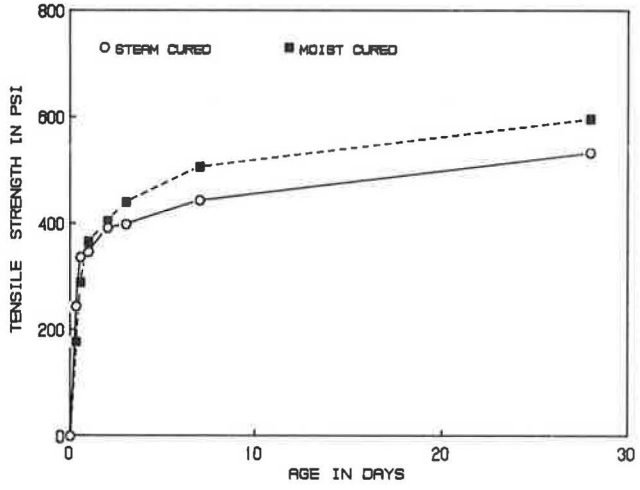

FIGURE 5 Comparison of tensile strength development in moist- and steam-cured concrete.

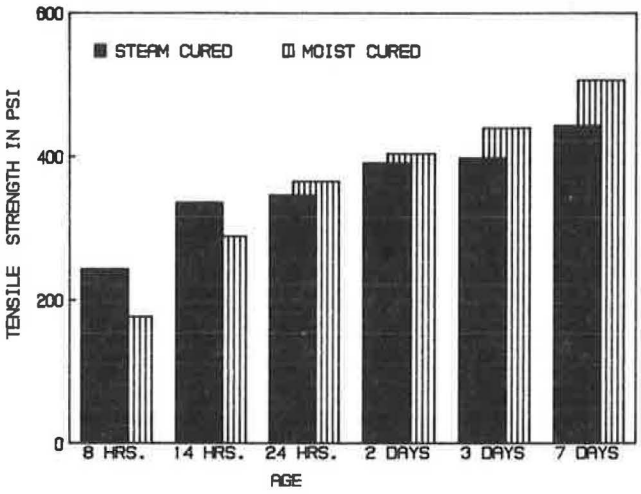

FIGURE 6 Tensile strength development in moist- and steam-cured concrete: first 7 days.

cracking that has been reported in precast, prestressed bridge deck panels during strand release and form removal. Although a difference of 20 psi in the tensile strength values at 1 day may not be statistically significant, it could be detrimental to the ability of concrete to resist cracking at this early age. Moreover, the steam-cured value was lower than that of moist-cured concrete.

Other factors arising from the defective detensioning procedures and improper handling of structures may contribute to early-age cracking. However, the properties of concrete that may contribute to cracking in steam-cured concrete are the concern in this paper.

Using the 28-day moist-cured values as standard, Table 2 presents the various physical properties developed at each testing age as percentages of the respective 28-day values. The detrimental effect of steam curing on physical property development is most pronounced with tensile strength, as evidenced by the percentage of the 28-day moist-cured values developed by each property.

Taking the moist-cured value for each variable at each testing age as an acceptable standard, the effect of steam curing on each property is depicted in Figures 7–9. Points above the reference line represent increases in property development due to steam curing, whereas points below the reference line indicate reductions in physical property development resulting from steam curing. Figure 10 presents the increase or decrease in property development caused by steam curing. The data presented in Figure 10 show that the higher the percentage increase in development of a property at early ages, the less lasting the beneficial effect of steam curing.

As can be seen in Table 3, Poisson's ratio was found to be insensitive to steam curing. Generally, the measured Poisson's ratio was virtually the same value for all ages and conditions of cure. This observation agrees with the previous observations of Hanson (*6*), Higginson (*7*), and Klink (*16*).

CONCLUSIONS

1. Steam curing as used by typical prestressing plants is not equally beneficial to the development of all the physical properties at early ages.

TABLE 2 INCREMENTAL PHYSICAL PROPERTY DEVELOPMENT (STEAM CURED)

	Compressive Strength			Elastic Modulus			Tensile Strength		
Age	Compressive Strength (psi)	$\frac{fcx}{fc}$ (%)	Incremental $\frac{fcx}{fc}$ (%)	Elastic Modulus (10^6 psi)	$\frac{Ecx}{Ec}$ (%)	Incremental $\frac{Ecx}{Ec}$ (%)	Tensile Strength (psi)	$\frac{ftx}{ft}$ (%)	Incremental $\frac{ftx}{ft}$ (%)
8 hrs	1,957	29.12	29.12	2.4586	47.91	47.91	243	40.70	40.70
14 hrs	3,259	48.50	19.38	3.6542	71.21	23.30	336	56.28	15.58
1 day	4,025	59.90	11.40	4.2926	83.65	12.44	346	57.96	1.68
2 days	4,112	61.19	1.29	4.3537	84.84	1.19	391	65.49	7.53
3 days	4,209	62.63	1.44	4.4744	87.19	2.35	398	66.67	1.18
7 days	4,904	72.98	10.35 (2.59/day)	4.5816	89.28	2.09 (0.52/day)	444	74.37	7.70 (1.93/day)
28 days	6,198	92.23	19.25 (0.92/day)	4.7224	92.03	2.75 (0.13/day)	534	89.45	15.08 (0.72/day)

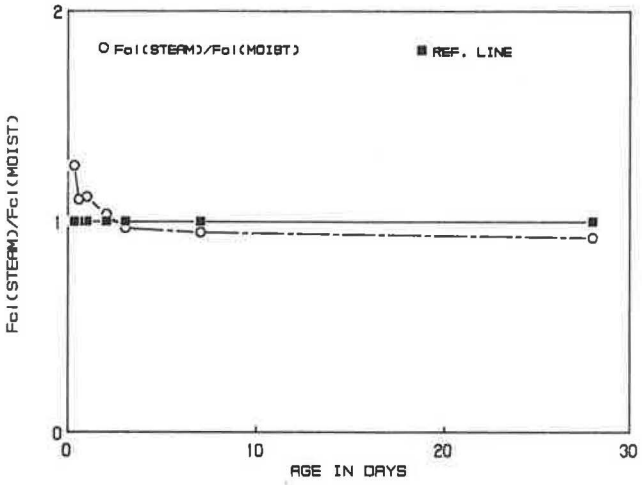

FIGURE 7 Normalized compressive strength for steam cure versus age.

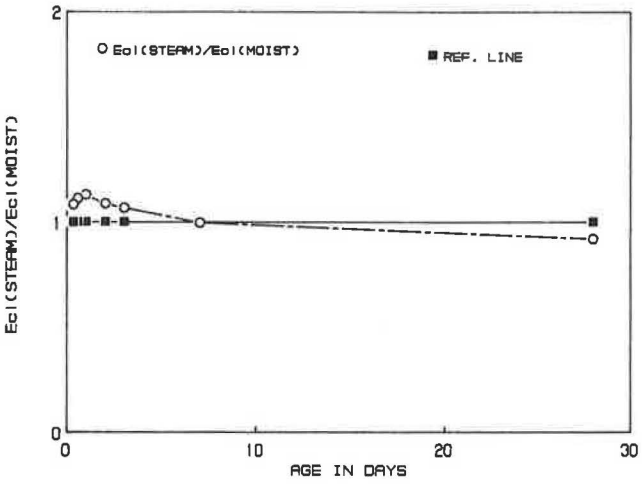

FIGURE 8 Normalized elastic modulus for steam cure versus age.

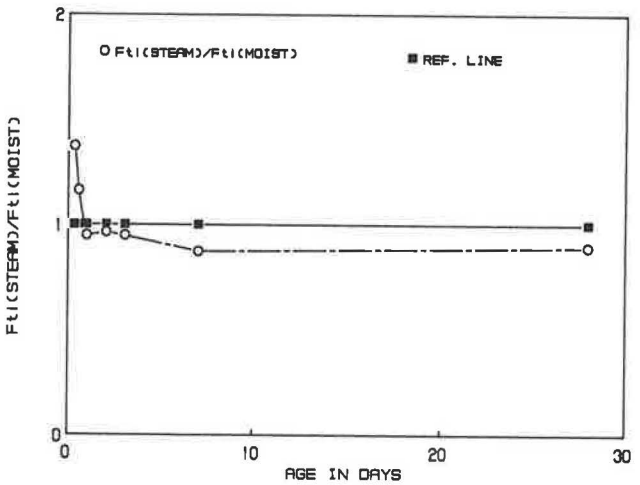

FIGURE 9 Normalized tensile strength for steam cure versus age.

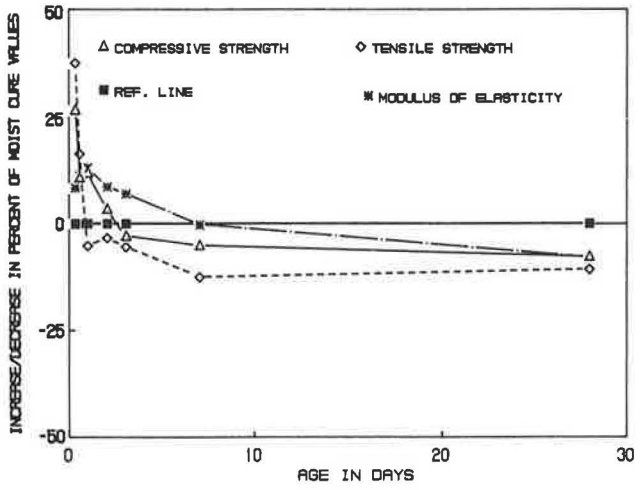

FIGURE 10 Increase or decrease in physical property development (moist-curing values) resulting from steam curing.

TABLE 3 INCREMENTAL PHYSICAL PROPERTY DEVELOPMENT (MOIST CURED)

	Compressive Strength			Elastic Modulus			Tensile Strength		
Age	Compressive Strength (psi)	fcx/fc (%)	Incremental fcx/fc (%)	Elastic Modulus (10^6 psi)	Ecx/Ec (%)	Incremental Ecx/Ec (%)	Tensile Strength (psi)	ftx/ft (%)	Incremental ftx/ft (%)
8 hrs	1,548	23.03	23.03	2.2677	44.19	44.19	177	29.63	29.63
14 hrs	2,942	43.78	20.75	3.2875	64.06	19.87	289	48.40	18.77
1 day	3,596	53.51	9.73	3.7994	74.04	9.98	366	61.24	12.84
2 days	3,979	59.21	5.70	4.0057	78.06	4.02	405	67.78	6.54
3 days	4,339	64.56	5.35	4.1840	81.53	3.47	420	70.37	2.59
7 days	5,176	77.02	12.46 (3.12/day)	4.5960	89.56	8.03 (2.01/day)	507	84.94	14.57 (3.64/day)
28 days	6,720	100.00	22.98 (1.09/day)	5.1316	100.00	10.44 (0.50/day)	597	100.00	15.06 (0.72/day)

2. Steam curing was found to be highly beneficial to the development of the elastic modulus and compressive strength but somewhat detrimental to the development of tensile strength at early ages. This detrimental effect may account for, at least partially, the early-age cracking that has been reported during strand release and form removal.

3. The optimum recommended steam-curing temperature for compressive strength development is not necessarily the optimum temperature for the development of either the elastic modulus or the splitting tensile strength. Investigations into the establishment of a possible optimum steam-curing temperature, which will equally benefit these three major physical properties, should be done. An optimum standard might mitigate the cracking and other serviceability problems associated with steam curing.

REFERENCES

1. R. M. Barnoff and J. A. Orndorff. *Construction and Testing of an Experimental Prestressed Concrete Bridge*. Report 1. Pennsylvania State University, University Park, 1974.
2. R. M. Barnoff and D. L. Rainey. *Laboratory Tests of Prestressed Concrete Deck Planks and Deck Plank Assemblies*. Report 2. Pennsylvania Transportation Institute, Pennsylvania State University, University Park, 1974.
3. C. D. Buckner and H. T. Turner. Performance of Full-Span Panel-Form Bridges Under Repetitive Loading. In *Transportation Research Record 903*, TRB, National Research Council, Washington, D.C., 1983.
4. P. E. Fergundo, H. Tabatabai, K. Soongswang, J. M. Richardson, and E. G. Callis. Precast Panel Composite Bridge Deck. *Concrete International: Design and Construction*, Vol. 7, No. 5, 1985, pp. 59–65.
5. L. H. Jones and H. L. Furr. *Study of In-Service Bridges Constructed with Prestressed Panel Sub Decks*. Research Report 145-1. Texas Highway Department, Austin, 1963.
6. J. A. Hanson. Optimum Steam Curing Procedure in Precasting Plants. *Journal of the American Concrete Institute*, Vol. 60, No. 1, 1963, pp. 75–99.
7. E. C. Higginson. Effect of Steam Curing on the Important Properties of Concrete. *Journal of the American Concrete Institute*, Vol. 58, No. 3, 1961, pp. 281–298.
8. A. G. A. Saul. Principles Underlying the Steam Curing of Concrete at Atmospheric Pressure. *Magazine of Concrete Research*, Vol. 2, No. 6, 1951, pp. 127–140.
9. J. J. Shideler and W. H. Chamberlin. Early Strength of Concrete as Affected by Steam Curing Temperatures. *Journal of the American Concrete Institute*, Vol. 46, No. 6, 1949, pp. 273–288.
10. G. J. Verbeck and L. E. Copeland. *Some Physical and Chemical Aspects of High-Pressure Steam Curing*. SP No. 32. American Concrete Institute, Detroit, Mich., 1972, pp. 1–13.
11. R. L'Hermite. Actual Ideas About the Technology of Concrete. *Annals Technical Institute of Building and Public Works*, Paris, 1959, pp. 115–116.
12. D. J. McNeely and S. D. Lash. Tensile Strength of Concrete. *Journal of the American Concrete Institute*, Vol. 60, No. 6, 1963, pp. 751–761.
13. S. P. Shah and S. H. Ahmad. Structural Properties of High Strength Concrete and Its Implications for Precast Prestressed Concrete. *Journal of Prestressed Concrete Institute*, Vol. 30, No. 6, 1985, pp. 92–119.
14. C. C. Wiley. Effect of Temperature on Strength of Concrete. *Engineering News Record*, Vol. 102, No. 5, 1929, pp. 179–181.
15. J. F. Young and M. Sidney. *Concrete*. Prentice-Hall, Inc., Englewood Cliffs, N.J., 1981.
16. S. A. Klink. Aggregates, Elastic Modulus and Poisson's Ratio of Concrete. *Journal of the American Concrete Institute*, Vol. 83, No. 6, 1986, pp. 961–965.

Publication of this paper sponsored by Committee on Mechanical Properties of Concrete.

Shear Interaction of High-Strength Two-Layered Concretes at Early Ages Placed in Subfreezing Temperatures

SHIVAPRASAD T. KUDLAPUR AND EDWARD G. NAWY

There are few studies on the early-age performance of high-strength cold weather concretes and their shear strength interaction in cold weather. Shear strength characteristics of high-strength cold weather concrete in subfreezing temperatures is the topic of this paper. Tests were conducted on cylinders and L-shaped push-off specimens to determine the early-age shear interlock and shear frictional resistance between high-strength regular portland cement concrete and cold weather high-strength concretes in the rehabilitation of bridge decks and other infrastructure systems. Results validate previous findings on polymer-modified concretes: the American Concrete Institute code limits on the shear-friction strength are too conservative even at early ages of high-strength cold weather concretes and need to be modified.

Previous investigations have identified materials and methods to repair concrete bridges in subfreezing winter conditions (*1*,*2*). A preliminary screening phase was performed to select potentially suitable materials from among 17 materials identified by a literature survey (Phase I). On the basis of Phase I results, five products representing four generically distinct materials were selected for further investigation. The selected materials were two methylmethacrylate (MMA)-based polymer concretes, one water-based and one non-water-based magnesium phosphate concrete, and one polyurethane-based polymer concrete. These materials were studied in depth in Phase II, which included cylinder compressive strength tests, cylinder shear bond strength tests, static and cyclic flexural tests of patched prism specimens, corrosion and durability tests of patched prism specimens, and static and cyclic flexural tests of patched slab specimens.

PERFORMANCE TESTING

Cylinder Tests

Three cylinders of each specimen type were tested in compression for compressive and slant shear strengths at 24 hr and 7 days after casting, and curing in the cold room for the full period. Two sets of cylinders were cast out of each of the two MMA-based materials—one with and one without gravel. Results of the cylinder compressive strengths are shown in Figure 1. It can be observed that all materials possess strength at early age. Gain in strength for the MMA samples containing stone, M1(G) and M2(G), at 24 hr is about 86 percent of their final strength, whereas this value is about 91 percent for magnesium phosphate concrete. MMA mixes behave differently with and without stone. Whereas MMA mixes with stone increase in strength with age, the neat MMA mixes (without stone) decrease with age. The reduction of strength with age of MMA without stone can be attributed to microcracking caused by differential shrinkage. The slant shear strengths for dry-patched and moist-patched specimens are presented in Figure 2. These results provide a comparative measure of shear bond. They also indicate that all the materials possess a reasonable amount of good bond strength at an early age. The reduction of strength with age of MMA materials without stone is again apparent. Gravel-containing MMA concrete shows a gain of only 5.23 percent of bond strength after 24 hr, whereas magnesium phosphate concrete exhibits about 47 percent gain in bond strength.

Rutgers University—The State University of New Jersey, P.O. Box 909, Piscataway, N.J. 08855. *Current affiliation:* S. T. Kudlapur, Jablonski & Mead Associates, 1200 MacArthur Blvd., Mahwah, N.J. 07430.

Flexure Tests

Prism specimens for flexure tests (both static and fatigue) were patched in the cold room with patching materials prepared according to manufacturers' instructions. The patch surfaces were as formed and untreated. Specimens were tested at 7 days of age. Three patch depths were used to assess the effect of patch boundary on the response: shallow, half depth, and full depth. The shallow patches (depth 0.5 in.) with MMA materials did not contain stone but other depths contained ⅜ in. stone. Results of flexure tests indicated that the flexural strengths of the patched specimens were comparable with those of the control specimens.

Freeze-Thaw Tests

Durability tests were performed on patched prism specimens by subjecting them to 300 freeze-thaw cycles (ASTM C 666, Procedure A). Three patch depths were tested. Weight and half-cell potential were measured before cycling and at intervals not greater than 36 cycles. Half-cell readings were taken adjacent to each patch boundary. The results indicated that all materials other than water-based magnesium phosphate showed better freeze-thaw durability than the parent concrete. Observations on the corrosion of reinforcement in freeze-thaw specimens following break-up of specimens indicated substantial corrosion at the patch boundaries of all materials tested.

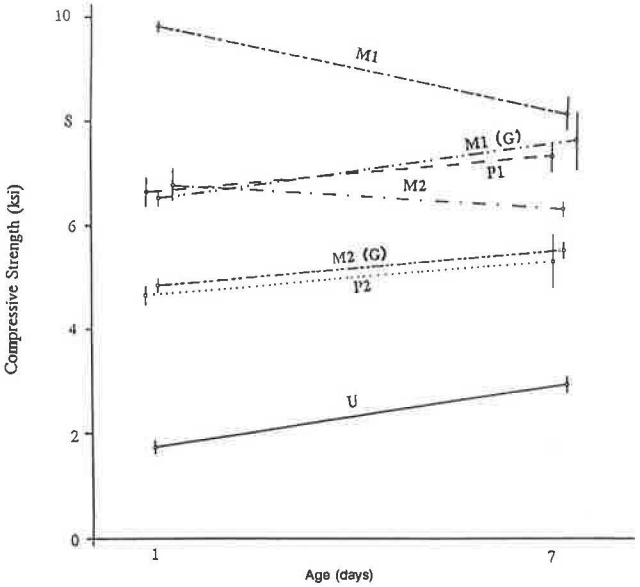

M1, M2--MMA-based polymer concretes
M1(G), M2(G)--MMA-based polymer concretes with 3/8 in. gravel satisfying ASTM C 33 (pea gravel)
P1, P2--water and non-water-based magnesium phosphate concretes
U--Polyurethane polymer concrete

FIGURE 1 Cylinder compressive strength test results.

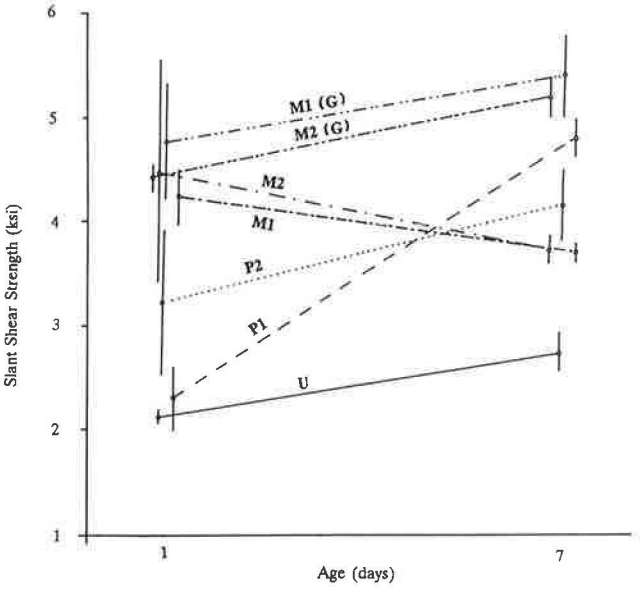

(a) Dry Patched Specimens

M1, M2--MMA-based polymer concrete
M1(G), M2(G)--MMA-based polymer concrete with 3/8 in. pea gravel satisfying ASTM C33
P1, P2--Water and non-water-based magnesium phosphate concretes
U--Polyurethane polymer concrete

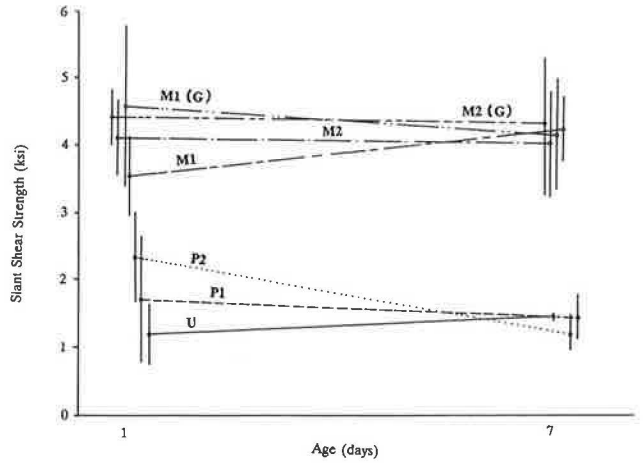

(b) Moist Patched Specimens

M1, M2--MMA-based polymer concrete
M1(G), M2(G)--MMA-based polymer concrete with 3/8 in. pea gravel satisfying ASTM C33
P1, P2--Water and non-water-based magnesium phosphate concretes
U--Polyurethane polymer concrete

FIGURE 2 Cylinder slant shear strength test results.

Summary

The program consisted of a series of factorial experiments. The factors tested were material type, age, and repair depth. The effects of these factors were assessed with an analysis of variance. MMA-based materials and magnesium phosphate-based materials were thus identified as performing satisfactorily at subfreezing temperatures. The MMA-based materials exhibited superior performance over the magnesium phosphate-based materials, particularly on measures of freeze-thaw performance. As far as handling is concerned, magnesium phosphate-based materials showed distinct advantages over the volatile and odorous MMA-based materials.

PRESENT INVESTIGATION

This study concerns the shear transfer mechanism of cold weather repair materials, specifically, the conditions under which failure of interacting bonded surfaces takes place between precast and cast in situ elements in buildings and concrete bridges and in patched sections in bridge deck slabs. Examples are the interface between a precast beam and a cast-in-place floor slab or a vertical plane at the upper reentrant corner of a corbel when repair is necessary under subfreezing conditions. Suitable materials with their shear transfer performance characteristics are needed to repair the damaged structural components. Prediction and knowledge of early-age shear strength at subfreezing temperatures are essential if concrete has to be installed in cold weather.

Current literature describes the shear friction mechanism and dowel action of initially cracked or uncracked regular concrete (*3–8*) or epoxy-modified polymer concrete (*9–11*) bonded to regular concrete surfaces. This investigation was designed to assess the applicability of these results to cold weather repair materials cast at cold temperatures. The two MMA concretes discussed at the beginning of this paper were selected for study on the basis of their overall satisfactory performance. This paper focuses on shear transfer of regular high-strength concrete with (a) MMA-based polymer concrete and (b) magnesium phosphate-based concrete at cold temperatures. The load-deformation behavior of these materials under shearing loads is presented and analyzed.

The main objectives of this investigation were to

1. Determine the early-age shear strength characteristics and shear transfer properties of the MMA polymer concrete and magnesium phosphate concretes cast at subfreezing temperatures at their interaction surface with the parent concrete;

2. Verify the applicability of the "shear friction theory" to the calculation of the direct shear strength using these two repair materials;
3. Evaluate the necessary constants of the theoretical expressions; and
4. Check the validity of the American Concrete Institute (ACI) code limits for high-strength cold weather concretes.

EXPERIMENTAL INVESTIGATION OF THE SHEAR TRANSFER MECHANISM

Materials, Mix Proportion, and Fabrication

Typical test specimens are shown in Figure 3. The shape and size of these specimens were chosen on the basis of successful results obtained for epoxy-modified polymer concrete (*9–11*). When such specimens are loaded axially, shear is produced on the shear plane. By providing adequate longitudinal and end reinforcement, it is assumed that only a negligible moment is produced on the shear plane and that the specimen would fail in shear along the shear plane. The end reinforcement also prevents the top and bottom heads from failing. Actually, the top and bottom heads are elastic in nature. Hence, the loads applied induce flexural stresses of small magnitudes in cold jointed surfaces. If horizontal clamps are used to prevent this rotation, unmeasurable but significant compressive stresses will be induced in the specimen. Thus this was not done. It was therefore assumed that these flexural stresses are negligible in cold jointed surfaces and that the specimen is subjected to pure shear failure. In practice, there is no one test set-up that produces pure shear failure.

In this study, the shear reinforcing strength was varied for both the bar size and the spacing. The bar sizes used were either W4.5 high-strength wire of diameter 0.24 in. or No. 3, as shown in Figure 3. One series of specimens with no transverse reinforcement and three series with transverse shear reinforcement were tested. These are termed specimens with no transverse reinforcement, with light, medium or moderate, and heavy transverse reinforcement, respectively, with vary-

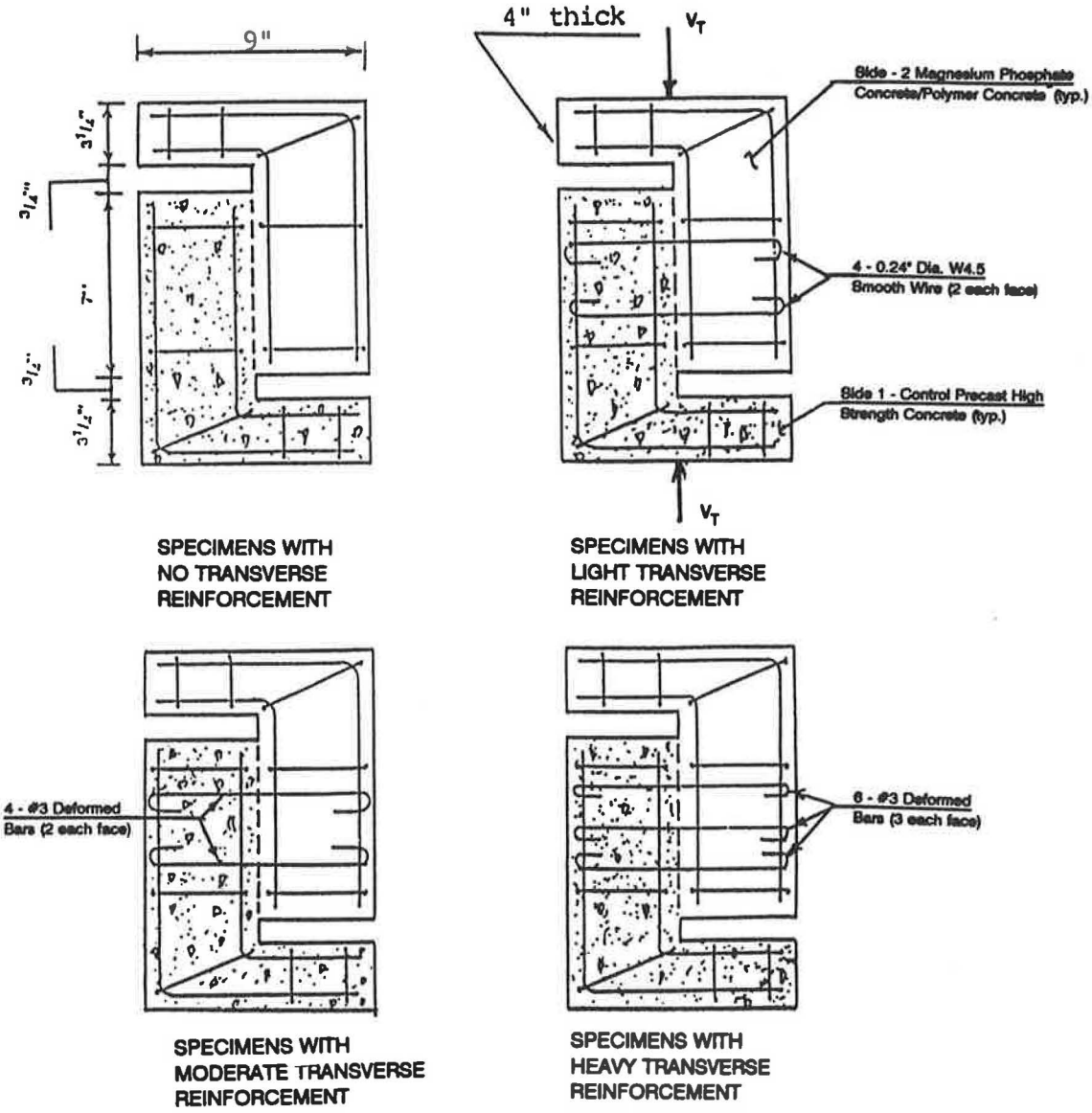

FIGURE 3 Push-off shear test specimens.

ing magnitude of reinforcing steel. "Light," "moderate or medium," and "heavy" are used to indicate different degrees of reinforcement only. The transverse reinforcement crossed the shear plane at 90 degrees. The bar spacings are not shown because they do not have any effect on the shear transfer strength (*7*).

A high-strength concrete mix developed at Rutgers University civil engineering laboratory was used for the control and precast half of the test specimens. This concrete was made from Type III portland cement, ⅜-in. maximum size coarse aggregate, and natural river sand with a fineness modulus of 2.61 for the fine aggregate. The coarse aggregate was washed before use and sand was used in its natural, partially presoaked condition with appropriate allowances for the absorption characteristics. Microsilica, superplasticizer, and a low water-to-cement ratio were used to obtain a high-strength concrete. All test specimens and cylinders were air cured for 24 hr in the mold under polyethylene sheets and then stored in the moisture curing room. The 4- × 8-in. cylinders were tested at 28 days and yielded compressive strengths of 12,000 to 14,500 psi. The test specimens were cured for 30 days before the other half was cast. The second half of the specimens was cast with magnesium phosphate and MMA polymer concrete, following the manufacturers' instructions, in the cold room at a temperature of 15° to 20°F. These were tested at 1, 3, and 7 days of age. The control specimens were included for comparison of shear behavior of cold concretes cast with precast regular concretes.

Instrumentation and Testing of Specimens

In all the specimens reinforced with transverse bars, the steel strains were measured by electric strain gauges mounted a small distance away from the shear plane. Two strain gauges were used for specimens with light and moderate transverse reinforcement, whereas the heavily reinforced specimens carried three gauges on three of the six transverse bars. The vertical slip and the horizontal crack width were measured by linear variable differential transformers (LVDTs) mounted on the specimens as shown in Figure 4 and connected to a Hewlett Packard data acquisition computer system. All the specimens were tested by using a compression testing machine (Figure 5).

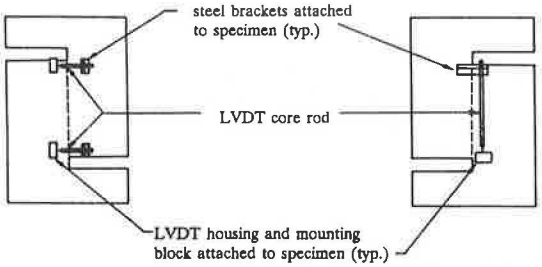

(i) Crack width measurement instrumentation (rear face) (ii) Vertical slip measurement instrumentation (front face)

FIGURE 4 Instrumentation details.

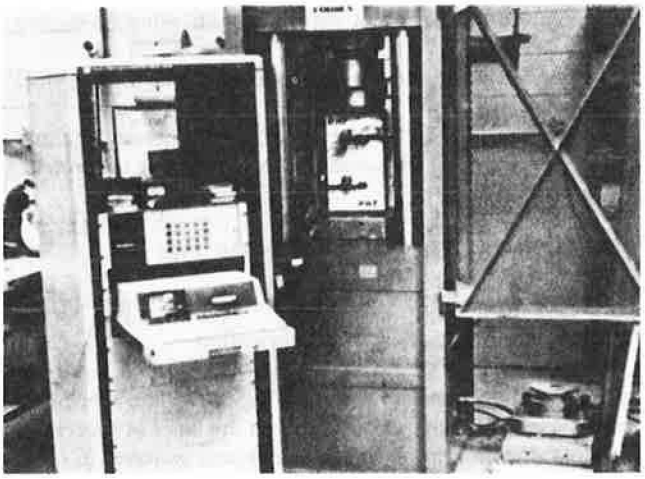

FIGURE 5 Test setup.

SHEAR TRANSFER MECHANISM THEORY FOR CONCRETE

A concrete element offers four types of shear resistance for shear transfer capacity (*11*): intrinsic bond shear resistance V_b (*12*), shear friction resistance V_f (*3,5–7,13*), aggregate interlock mechanism V_i (*8,14*), and dowel action resistance V_d (*15*).

Figure 6 shows a concrete element subjected to a shearing load and Figure 7 shows the dowel shear transfer test config-

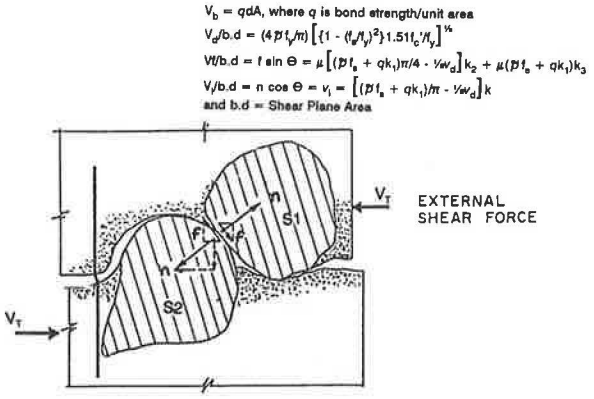

(i) Aggregate Interlock Forces

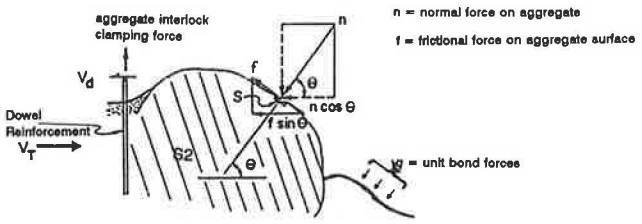

(ii) Force Components

FIGURE 6 Idealized element in shear resistance through friction ($f \sin \theta$), aggregate interlock ($n \cos \theta$), and dowel action (V_d).

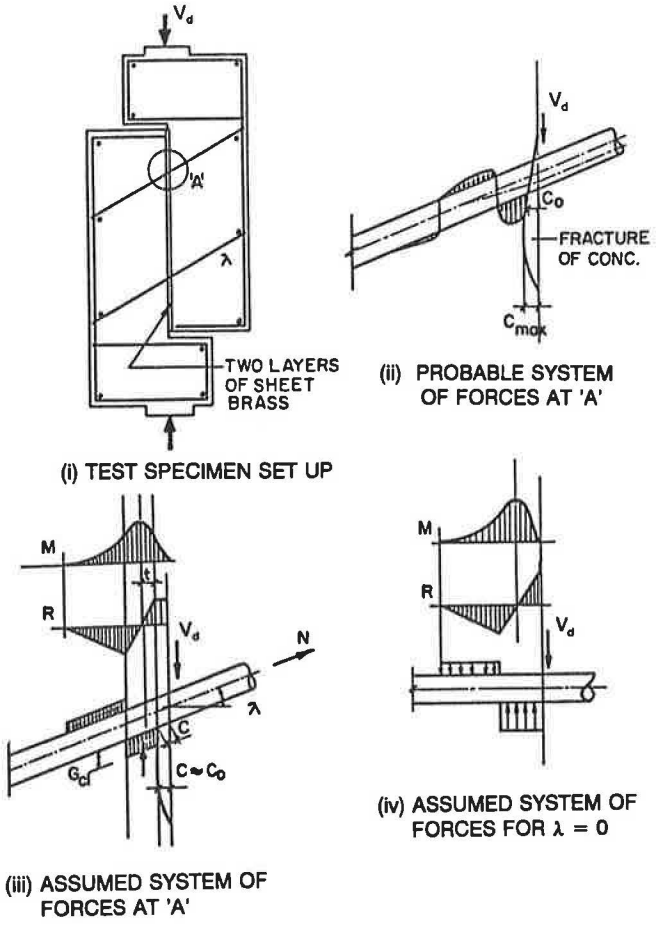

FIGURE 7 System of forces and test configuration for the evaluation of dowel shear transfer strength, *I* (*15*).

uration for evaluating V_d (*15*). Under these loading conditions, initial resistance is offered by the intrinsic bond. When the element cracks, slipping takes place along the shear plane and the shear plane faces are forced to separate. The relative displacement of the concrete on the two sides of the plane produces strains in the reinforcement crossing the shear plane. The result of the forces induced in the reinforcement will have a component parallel to the plane resisting the applied shear and a component normal to the plane that produces a compressive force across the plane. This compressive force produces a frictional resistance to sliding between the faces of the plane, thus opposing the applied shear. The relative movement of the concrete on opposite sides of the plane also subjects the reinforcing steel to a shearing action. The resistance of the reinforcing steel to this shearing action is called dowel action and also contributes to the shearing resistance. Further resistance is provided by aggregate interlock resulting from the interlocking action of the aggregates at the failure plane. Summing up the components of these forces in the horizontal direction yields

$$V_t = V_b + V_f + V_d + V_i \tag{1}$$

Bond shear strength is an intrinsic property of a given concrete mass or epoxy polymer-modified concrete (*9*,*15*). Extending the analogy to MMA polymer concrete and magnesium phosphate concrete, the bond shear resistance can be represented as $V_b = qdA$, where q is the strength per unit bond area. If the ratio of the bond area to the total shear area is k_1, the average bond shear strength is given by

$$v_b = qk_1 \tag{2}$$

Dulacska (*15*) has developed an expression for the load that is transferred by dowel action and is given as

$$V_d = \zeta d_b^2 \Gamma f_y \cdot C \sin\lambda \{(1 + \sigma_c/(3\zeta\omega^2 f_y C \sin^2\lambda))^{1/2} - 1\} \tag{3}$$

where

V_d = shear force transferred by dowel action,
ζ = dowel resistance ratio = $\{1 - (N/N_y)^2\}$ = $\{1 - (f_s/f_y)^2\}$,
N = tensile force in the dowel bar = $A_s f_s$,
N_y = tensile yield force = $A_s f_y$,
d_b = diameter of transverse bar,
ω = constant (0.05),
f_y = steel yield stress,
C = coefficient of local compression of concrete = 4,
λ = angle between transverse bar and the perpendicular to the shear plane (Figure 5b), and
σ_c = cube strength of concrete ($= 1.13\, f'_c$).

Rearranging the terms in the above expression gives

$$V_d = \{(\zeta d_b^2 \omega f_y C \sin\lambda)^2 + [\sigma_c(\zeta d_b^2 \omega f_y C \sin\lambda)^2]/[3\zeta\omega^2 f_y C \sin^2\lambda]\} - \zeta d_b^2 \omega \sin\lambda \tag{4}$$

If a transverse bar crosses the shear plane at 90 degrees, $\lambda = 0 \rightarrow \sin\lambda = 0$

$$V_d = (\zeta d_b^4 f_y C \sigma_c/3)^{1/2} = d_b^2 (\zeta f_y C \sigma_c/3)^{1/2} \tag{5}$$

If n is the number of transverse bars crossing the shear plane with diameter d_b and $d_b^2 = 4A_s/\pi$, substituting for the known terms from above, the total shear force becomes

$$nV_d = (4nA_s/\pi)\,[\{1 - (f_s/f_y)^2\}1.51 f'_c f_y/3]^{1/2} \tag{6}$$

Shear stress over the cross section area bd is given by

$$v_d = nV_d/bd$$

If shear reinforcement ratio is denoted by $\bar{\rho}$, which is equal to nA_s/bd, then dowel action shear resistance is

$$v_d = (4\bar{\rho} f_y/\pi)\,[\{1 - (f_s/f_y)^2\}1.51 f'_c/f_y]^{1/2} \tag{7}$$

Shear resistance due to frictional force (*9–11*) is given by

$$v_f = \mu[(\bar{\rho}f_s + qk_1)\pi/4 - {}^1/_2 v_d]k_2 + \mu(\bar{\rho}f_s + qk_1)k_3 \quad (8)$$

and shear resistance due to aggregate interlock (*9–11*) is given by

$$v_i = [(\bar{\rho}f_s + qk_1)/\pi - {}^1/_2 v_d]k_2 \quad (9)$$

where

μ = coefficient of friction,
k_1 = ratio of bond area to total shear area,
k_2 = ratio of projected area of aggregate to the total shear plane cross-sectional area,
k_3 = ratio of the area unoccupied by the aggregates to that of the total shear at the shear plane $\approx 1 - k_1 - k_2$, and
q = bond shear strength per unit area.

Adding all the components of shear resistance and rearranging terms yields

$$v_t = qk_1 + (4\bar{\rho}f_y/\pi)[\{1 - (f_s/f_y)^2\}1.51f'_c/f_y]^{1/2}[1 - (k_2/2)(1 + \mu)] + (\bar{\rho}f_s + qk_1)\{\mu k_3 + k_2\pi(\mu/4 + 1/\pi^2)\} \quad (10)$$

In this expression, the constant terms ½, $\pi/4$, π, and so on are known to represent the shape of the aggregates in the concrete matrix.

Members with No Shear Transfer Reinforcement

Substituting $\bar{\rho} = 0$ in the expression for total shear resistance, Equation 10 reduces to

$$v_t = qk_1 + qk_1[\mu k_3 + k_2\pi(\mu/4 + 1/\pi^2)] = \text{a constant} \quad (11)$$

Because every term in this expression is a constant for a given surface, v_t is a constant and is termed the "apparent cohesive strength" and is nothing but the bond strength of the materials. In regular concrete and magnesium phosphate concrete joints this magnitude of shear resistance is small and is consistent with the test results. But in polymer concrete, because MMA is a liquid with low viscosity, it flows freely into all the microcracks and forms a polymer matrix by bridging all the cracks. This action induces compressive stress against the plane and helps in the development of additional shear strength through friction and aggregate interlock mechanisms and hence a higher total shear strength for MMA concrete.

Members with Transverse Shear Reinforcement

When specimens with transverse reinforcement are subjected to shear along the shear plane, slipping takes place, thereby inducing stresses in the transverse steel. This transverse steel has been found to develop its yield strength at ultimate as indicated by the readings of the electric strain gauges at the onset of ultimate stress. It is therefore reasonable to assume that at ultimate loads, the strain in reinforcement normal to the shear plane is equal to its yield strain and, hence, the stress is equal to the yield stress. Substituting f_y for f_s in the expression for v_t in Equation 10

$$v_t = (qk_1) + (\bar{\rho}f_y + qk_1)\{\mu k_3 + k_2\pi(\mu/4 + 1/\pi^2)\} \quad (12)$$

Grouping the constant terms will yield

$$v_t = \bar{\rho}f_y\{\mu k_3 + k_2\pi(\mu/4 + 1/\pi^2)\} + qk_1\{1 + \mu k_3 + k_2\pi(\mu/4 + 1/\pi^2)\} \quad (13)$$

$$v_t = \bar{\rho}f_y\mu' + c' \quad (14)$$

where

$\mu' = \{\mu k_3 + k_2\pi(\mu/4 + 1/\pi^2)\}$
$c' = (qk_1)(1 + \mu')$

Let I be the shear reinforcing index $= \bar{\rho}f_y$. Then

$$v_t = I\mu' + c' \quad (15)$$

In Equation 15, c' is the apparent cohesion: the shear resistance resulting from bond action, which is the same as the shear strength for cases with no shear reinforcement. The term μ' is called the apparent coefficient of friction and combines the effect of friction with aggregate interlock actions. Equation 15 is similar to those developed by Hermanson and Cowan (*16*) and ACI (*17*) given by $v_t = I\mu$. Hermanson and ACI apparently did not account for the shear bond strength. Equation 15 is the same as the equations Ukadike (*11*) and Nawy (*9,10*) developed for moderate reinforcement by neglecting the dowel action, assuming that its contribution is negligible after the yielding of transverse steel. By the strain gauge results, transverse steel reached its yield at the onset of ultimate and were stressed beyond their yield values in most of the specimens. This yielding of transverse steel is caused by the separation of the shear plane faces. Therefore, at ultimate strength, the compressive force across the crack after the separation of the shear plane faces is just the yield force in the reinforcement. The frictional resistance to shear along the crack is then equal to this force multiplied by the coefficient of friction of the concrete. The apparent coefficient of friction, μ' in Equation 15, therefore, includes this frictional shear resistance in addition to dowel action and aggregate interlock shear resistances.

DISCUSSION OF RESULTS

Behavior of Test Specimens Under the Action of Shear Loads

Specimens with no transverse reinforcement for both the magnesium phosphate and the polymer concretes exhibited similar modes of failure of vertical slippage along the shear plane. Specimens with light reinforcement experienced rupture of one to two steel bars at and beyond yield loads. Moderately and heavily reinforced specimens, on the other hand, failed

in a ductile manner at strain levels greater than their yield strains and while in the strain hardening stage. Neither vertical cracks nor spalls were noticed for either of the two nonreinforced and lightly reinforced concrete specimens (Figure 8). Although the moderate and heavily reinforced magnesium phosphate concrete specimens showed material spalls on the cast-in-place half at ultimate loading conditions, the similarly reinforced polymer concrete specimens exhibited regular concrete spalls (Figures 9 and 10). No noticeable difference in test specimen behavior was observed at different ages for the same material and reinforcement.

Effect of Age

Effect of age on shear transfer strength is presented in Figure 11 for magnesium phosphate and polymer concretes with various levels of reinforcement. Most of the shear transfer strength of the magnesium phosphate concrete, with or without reinforcement, is attained at 24 hr; further gain in strength is insignificant thereafter. In contrast, MMA polymer concrete specimens of similar geometry show some gain in shear transfer strength between 24 hr and 7 days. As the amount of shear reinforcement increases, a gradual gain in shear transfer strength

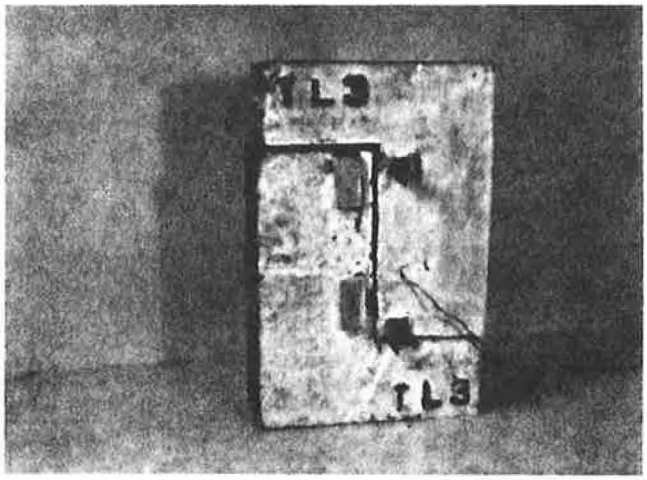

FIGURE 8 Typical failure of TN, TL, PN, and PL specimens (slippage along the shear plane).

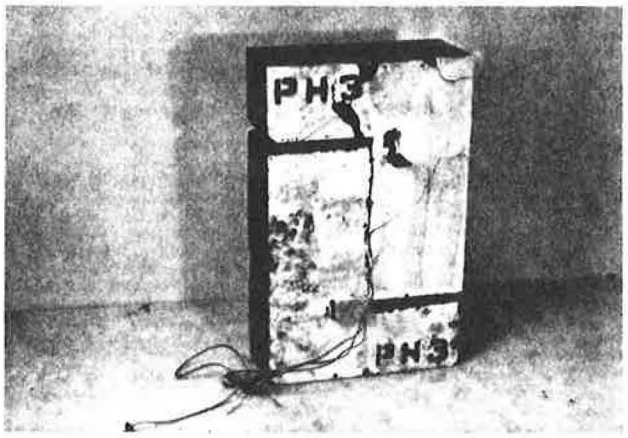

FIGURE 9 Typical failure of PM and PH specimens (spalling of magnesium phosphate concrete).

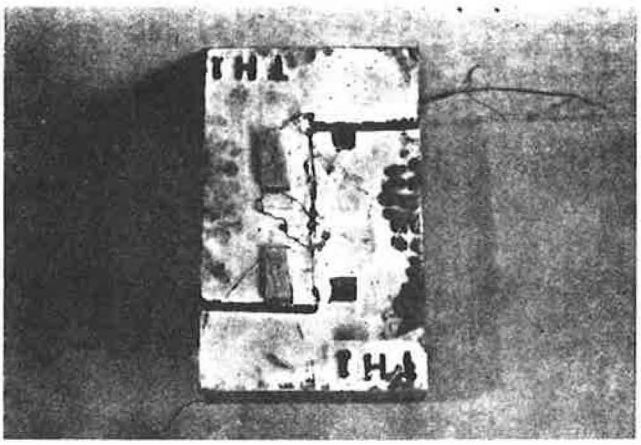

FIGURE 10 Typical failure of TM and TH specimens (spalling of regular concrete).

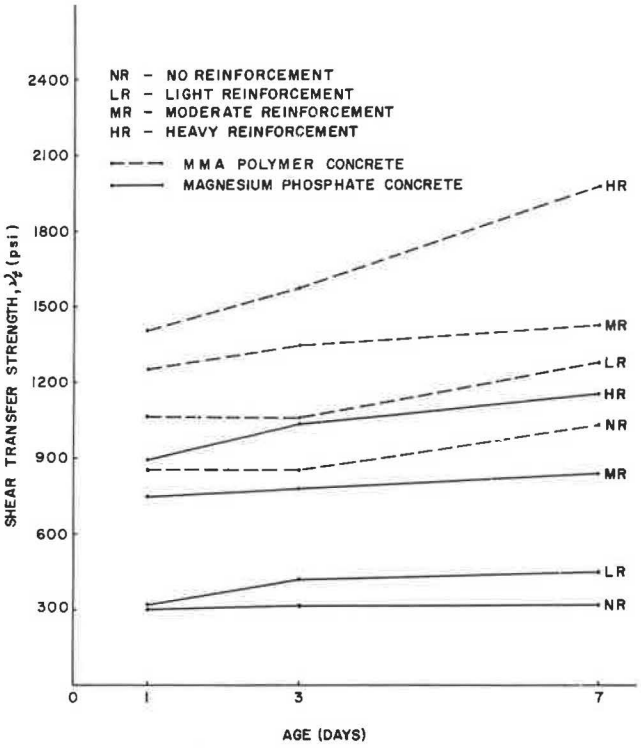

FIGURE 11 Effect of age on shear transfer strength for cold concretes with and without shear reinforcement.

is attained in both the magnesium phosphate and polymer concretes, as shown by the increasing slopes of the plots in Figure 10. This is a result of the increased dowel action contribution to the shear strength at the respective age levels. The 3-day cured specimens illustrate the behavior of the materials at an intermediate time between 1 and 7 days. Therefore, a limited number of specimens were tested at 3 days of age (Tables 1 and 2).

Effect of Shear Reinforcement

The effect of shear reinforcement on shear transfer strength is shown in Figure 12. The slopes of the shear reinforcing

TABLE 1 PUSH-OFF SPECIMEN TEST RESULTS FOR MAGNESIUM PHOSPHATE CONCRETE SPECIMENS

Specimen Identification Code	Shear Reinforcing Strength (psi)	Shear Transfer Capacity (psi)	Number of Test Specimens	Failure Mode
PN1	-	303	2	vertical movement along the shear plane
PN3	-	313	1	
PN7	-	321	2	
PL1	258	321	2	same as above with yielding of transverse
PL3	258	429	1	steel
PL7	258	446	2	
PM1	644	750	2	light diagonal cracking, vertical movement along
PM3	644	786	1	the shear plane, light spalling of magnesium
PM7	644	839	2	phosphate concrete plus steel yield
PH1	965	893	2	light diag. cracking, vert. movement along
PH3	965	1036	1	the shear plane, moderate spalling of magnes-
PH7	965	1143	2	ium phosphate concrete plus steel yield

Notations:

P = Magnesium Phosphate concrete

N = Specimens without any transverse shear reinforcement

L,M,H = Specimens with light, moderate and heavy transverse shear reinforcement respectively

1,2,3 = Specimens cured for 1, 3 and 7 days respectively at 15-20^0 F.

index versus transfer strength line plotted for magnesium phosphate concrete specimens at different ages are almost flat up to a shear reinforcing index of 250 psi. Thus, to take advantage of the dowel action contribution to shear transfer strength of the magnesium phosphate concrete, a minimum shear reinforcing index of 250 psi has to be used. Polymer concrete specimens, on the other hand, appear to gain in strength progressively from the onset of loading.

Figure 10 also gives a plot of the relationship between shear reinforcing index and transfer strength of the control specimens. These specimens represent monolithic construction without cold joints in contrast with the magnesium phosphate and the polymer concrete specimens. Hence, as was expected, shear transfer strength of the control specimens exceeded that of the test specimens by 1,125 percent for magnesium phosphate concrete specimens and 322 percent for polymer concrete specimens due to the monolithic structure of the total control specimen cross section.

Load Deformation Behavior (Slip and Crack Width)

Nonreinforced Specimens

Most related research reports that failure of *nonreinforced* push-off specimens with cold jointed shear plane surfaces is not accompanied by much slip. In this investigation, however, LVDT readings for both the magnesium phosphate and polymer nonreinforced concrete specimens did measure finite slips. Results are presented in Figure 13 for magnesium phosphate concrete and polymer concrete specimens. The variations of slip with applied shear stress are linear up to ultimate loads, at which point the specimens encountered sudden failure. The ultimate slip at 7 days (0.00144 in. at 321 psi stress) for magnesium phosphate concrete is almost twice its slip value at 24 hr (0.000848 in. at 303 psi stress). The magnesium phosphate concrete appears to become more ductile with age. Whereas the variation of slip for polymer concrete specimens with age

TABLE 2 PUSH-OFF SPECIMEN TEST RESULTS FOR MMA POLYMER CONCRETE SPECIMENS

Specimen Identification Code	Shear Reinforcing Strength (psi)	Shear Transfer Capacity (psi)	Number of Test Specimens	Failure Mode
TN1	-	857	2	vertical slip along the shear plane
TN3	-	857	1	
TN7	-	1036	2	
TL1	258	1071	2	same as above with yielding of steel
TL3	258	1071	1	
TL7	258	1286	2	
TM1	644	1250	2	light diagonal tension cracking accompanied
TM3	644	1357	1	by regular concrete spalling plus yielding
TM7	644	1429	2	of steel
TH1	965	1393	2	light diag. tension cracking accompanied
TH3	965	1571	1	by regular concrete spalling plus yielding
TH7	965	1964	2	of steel

Notations: *T = Methyl methacrylate based polymer concrete*

N = Specimens without any transverse shear reinforcement

L,M,H = Specimens with light, moderate and heavy transverse shear reinforcement respectively

1,2,3 = Specimens cured for 1, 3 and 7 days respectively at 15-20^0 F.

TABLE 3 PUSH-OFF SPECIMEN TEST RESULTS FOR CONTROL SPECIMENS

Specimen Identification Code	Shear Reinforcing Strength (psi)	Shear Transfer Capacity (psi)	Number of Test Specimens	Failure Mode
CN	-	1536	2	light to heavy diag. tension cracking, w/concrete
CL	258	1571	2	compression spalling, typical shear failure, plus
CM	644	1964	2	yielding of steel in CL, CM & CH specimens
CH	965	2286	2	

Notations: *C = Control specimens*

N = Specimens without any transverse shear reinforcement

L,M,H = Specimens with light, moderate and heavy transverse shear reinforcement respectively

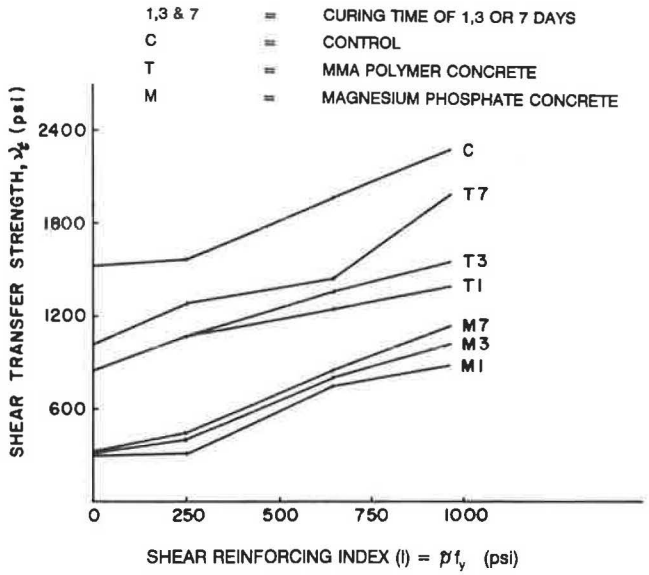

FIGURE 12 Effect of shear reinforcement on shear transfer strength.

was relatively insignificant, indicating that polymer concrete specimens do not exhibit noticeable change in deformation behavior after 24 hr, most of the shear transfer strength contribution for these nonreinforced specimens comes from bond, namely, cohesive strength resulting from high adhesion to the precast concrete. Also, the slip of magnesium phosphate concrete specimens decreases after 3 days. The ultimate slip values for polymer concrete at 1 and 7 days were 0.00789 in. and 0.00824 in., respectively. This indicates that polymer concrete material is several times more ductile than magnesium phosphate concrete material.

Reinforced Specimens

Typical variations of slip and crack width versus shear stress for reinforced specimens are presented in Figure 14 for magnesium phosphate concrete and Figure 15 for polymer concrete specimens. Only results for moderately reinforced specimens are presented because they are typical of all the reinforced specimens. The reinforced test specimens showed very small values of slip and crack width until the formation of the initial vertical cracks along the shear plane. After the development of this crack, both slip and crack width values increased at a faster rate; however, these specimens were still able to carry additional load until ultimate. Increased ductile behavior was observed for slip and crack width with increase in reinforcement levels. Close examination of the slip and crack width plots (Figures 14 and 15) for reinforced specimens indicates that they are similar in pattern. The reliability of the LVDT and the strain gauge readings thus concur. At ultimate load, the maximum slip and crack width values for magnesium phosphate concrete specimens were 0.0638 in. and 0.0043 in., respectively, and for polymer concrete specimens 0.0743 in. and 0.00329 in., respectively. These values point out the similarity in behavior of the two types of cold weather concretes investigated.

A characteristic common to the reinforced specimens is that the rate of increase in slip and crack width appears to vary inversely with the shear reinforcing index. The higher the shear reinforcing index, the lower is the slip and crack width for a given applied shearing load level. An explanation can be given for such behavior of the reinforced specimens. As a reinforced test specimen is loaded, the transverse reinforcing steel is subjected to tensile stresses resulting in development of compressive stresses in the material of the two halves. As the amount of shear reinforcement increases, the force generated in the steel and the surrounding concrete material increases. This confining force is what is responsible for the reduction in deformation.

Performance Comparison of Magnesium Phosphate and Polymer Concretes

Figure 16 presents a comparison of the early-age gain in strength of the two cold weather concrete types. Both concretes exhibit similar trends in strength gain with an increase in reinforcement. The slope of the dotted envelope on the bar plots in both concretes appears to be the same for all ages. The monolithically cast control specimens with similar percentage of reinforcement exhibit higher strength than both the cold weather concretes because of the homogeneity and absence of planes of weakness that the other specimens have. The polymer concrete specimens appear to be considerably stronger than the magnesium phosphate concrete in transferring shearing stresses.

Correlation of the Derived Theory with Experimental Results

A least squares analysis of the test data resulted in the following values of the constants c' and μ' in the expression for total shear transfer capacity v_t in Equation 15:

Age (days)	*Magnesium Phosphate Concrete*		*MMA Polymer Concrete*	
	c'	μ'	c'	μ'
1	248	0.68	890	0.54
3	279	0.78	869	0.74
7	278	0.88	1,015	0.89

For control specimens, the constants are $c' = 1{,}458$ and $\mu' = 0.817$.

These constants are plotted against experimental values in Figure 17 to check their validity. In Figure 17a theoretical and experimental values for the constant c' (cohesive bond strength) are shown for both types of cold weather concretes. There is good agreement between the theoretical and experimental plots for c'. Figure 17b presents a comparison of theoretical and test results for μ' (apparent coefficient of friction) for both types of cold weather concretes. For polymer concrete, 3-day test results appear to be somewhat variable. This probably resulted from the limited number of tests conducted at the 3-day age level. If the 3-day test results are ignored, the polymer concrete test results agree fairly well with the theoretical values.

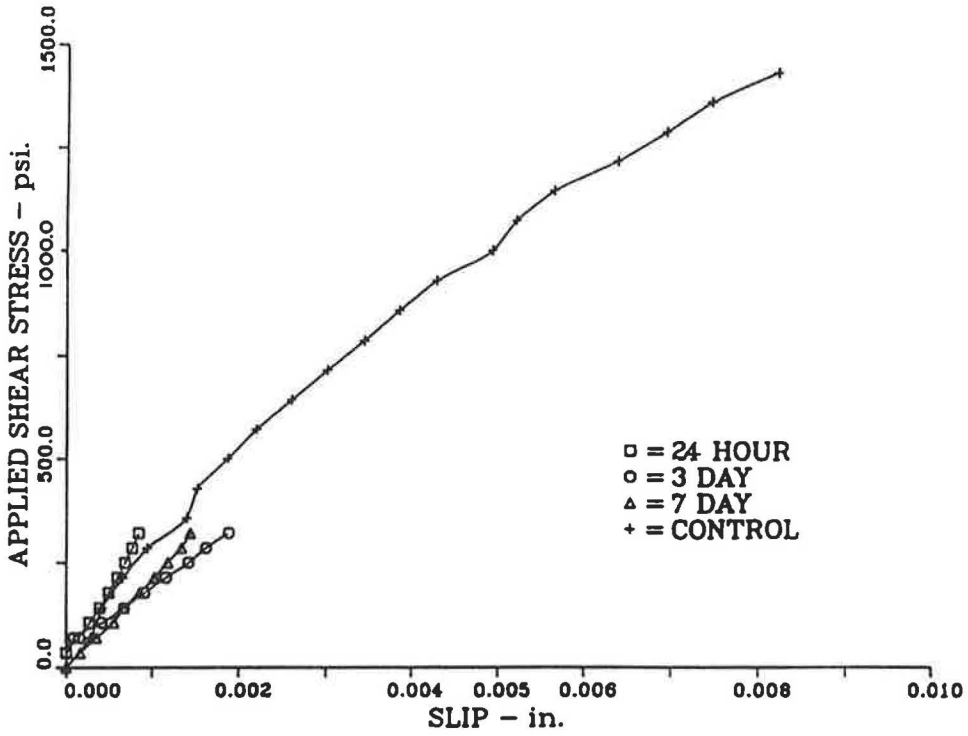

(a) Magnesium Phosphate Concrete Specimens

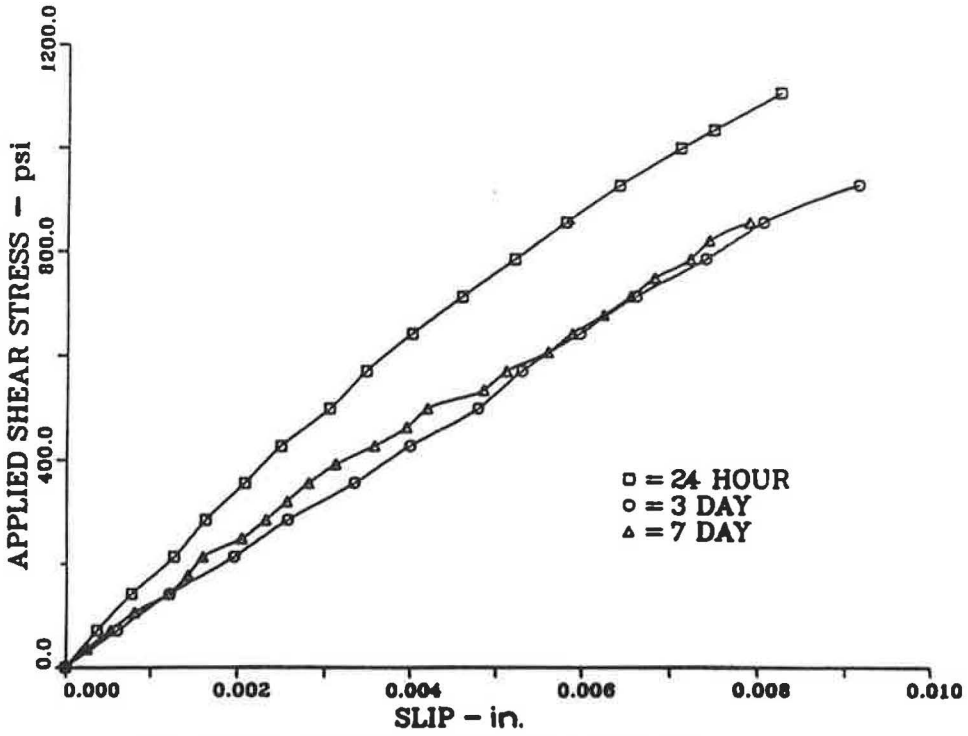

(b) MMA Polymer Concrete Specimens

FIGURE 13 Typical variation of slip with applied shear stress at different ages for nonreinforced specimens.

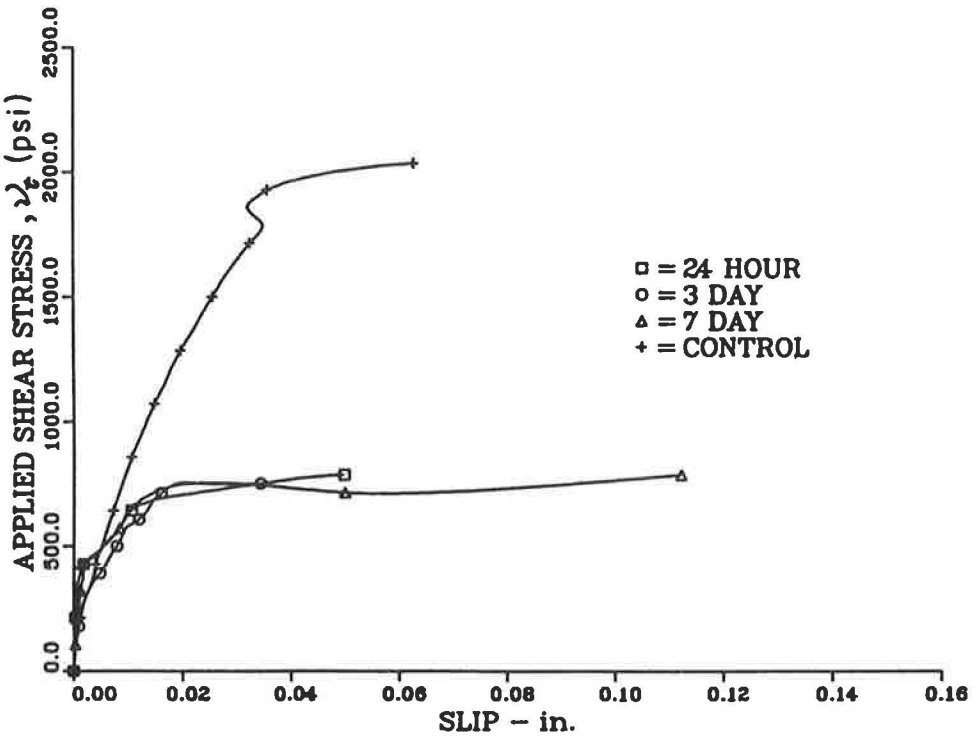

(a) Magnesium Phosphate Concrete Specimens

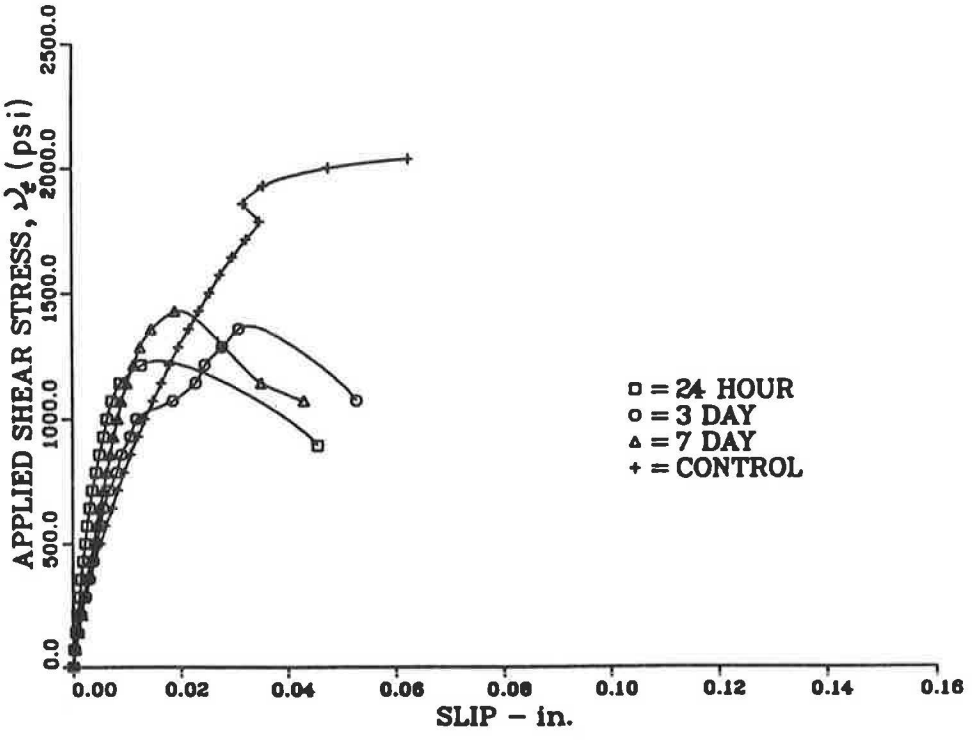

(b) Polymer Concrete Specimens

FIGURE 14 Typical variation of slip with applied shear stress of different ages for moderately reinforced specimens.

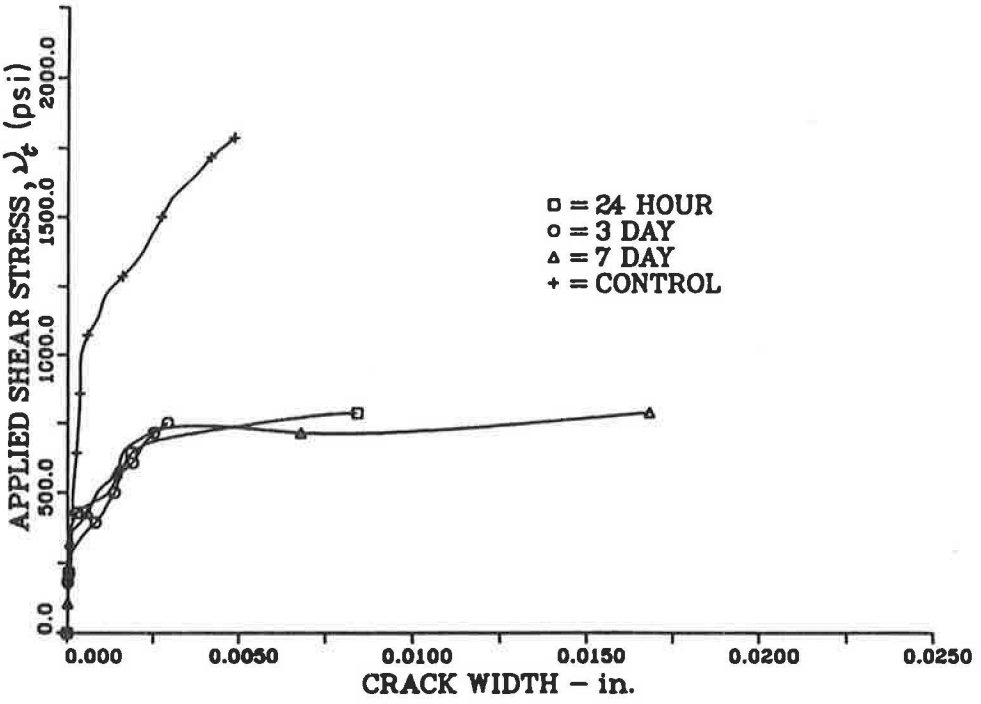

(a) Magnesium Phosphate Concrete Specimens

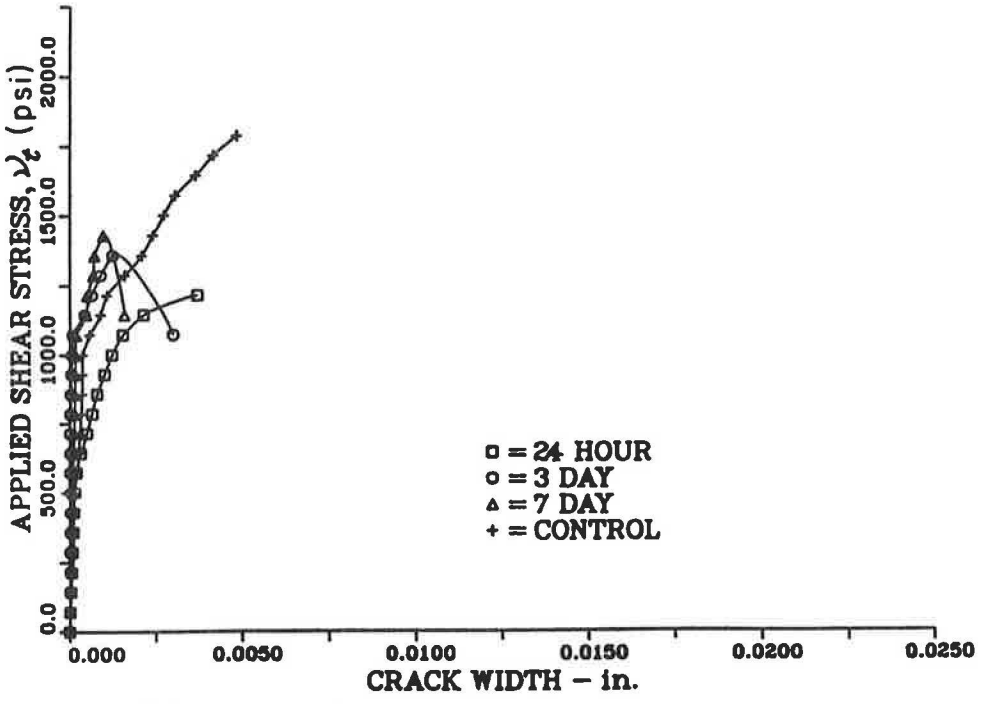

(b) Polymer Concrete Specimens

FIGURE 15 Typical variation of crack width with applied shear stress at different ages for moderately reinforced specimens.

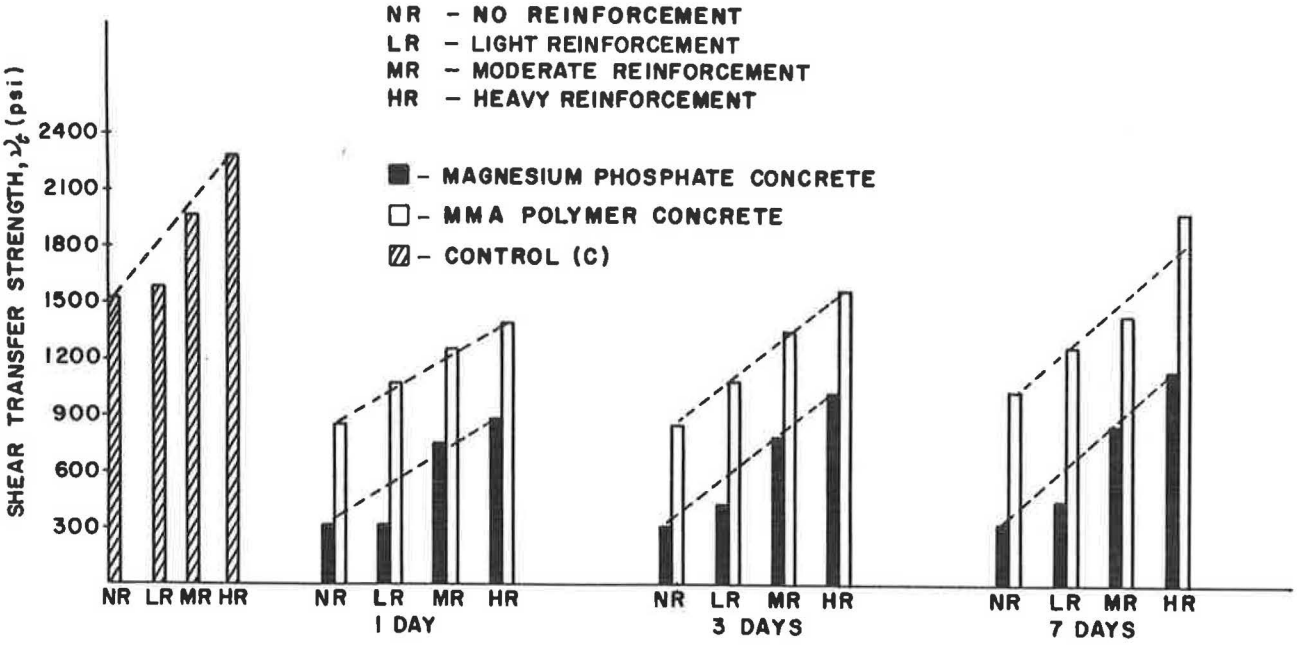

FIGURE 16 Comparison of shear transfer strengths of the cold weather concretes.

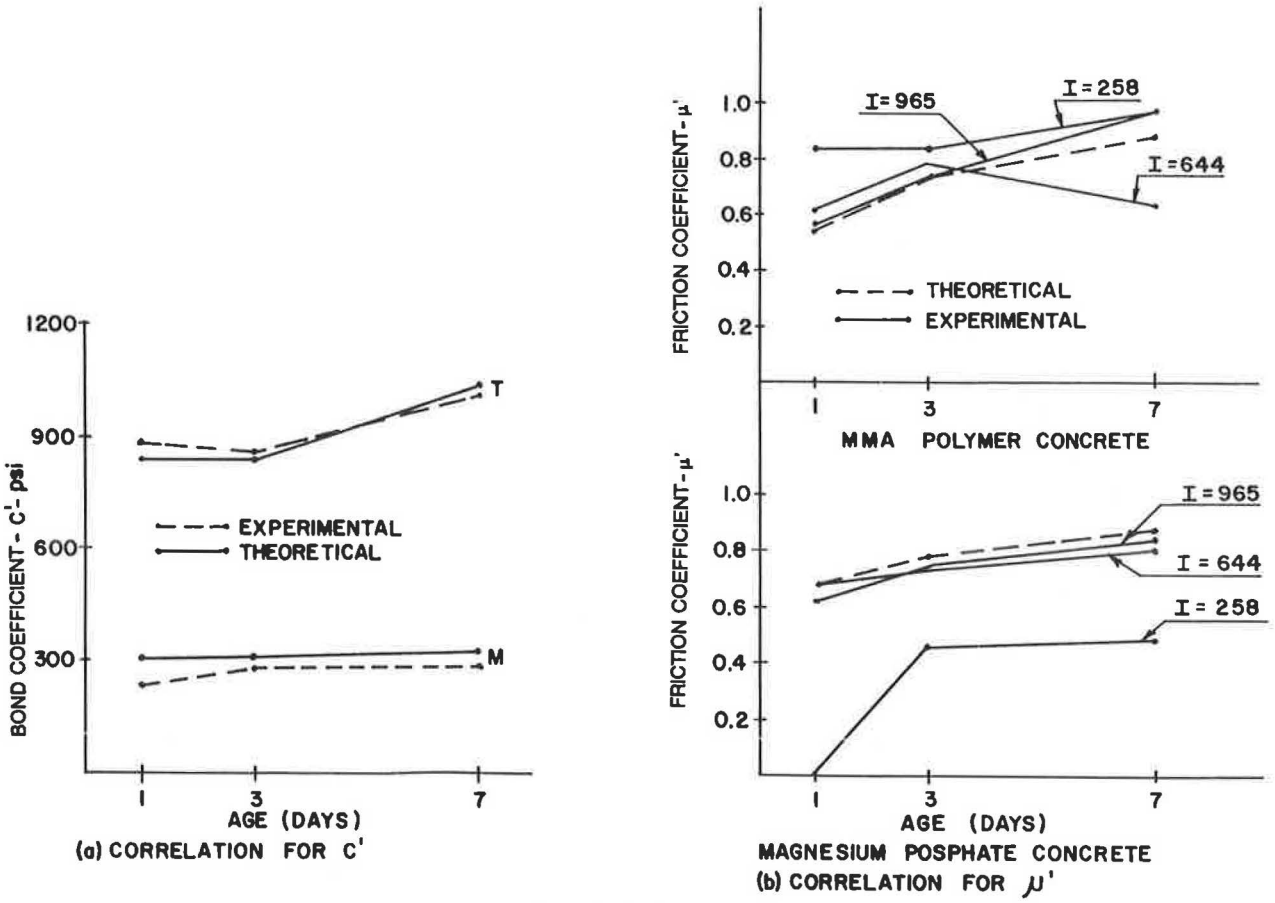

FIGURE 17 Comparison of test results with theoretically derived constants.

Proposed Design Expressions for Shear Transfer Capacity

On the basis of the equation for total shear stress, v_t, Equation 15, $v_t = c' + \mu' I$, and introducing the constants of experiment derived for the two materials and age levels, the following expressions are presented. They are applicable for the design of concrete structural composite sections made of two-layered concretes in subfreezing temperatures having a precast parent regular concrete of strengths up to and exceeding 12,000 psi.

- Magnesium phosphate concrete new layer
  —For early loading conditions based on 1-day test results: $v_t = 248 + 0.68\ I$;
  —For long-term loading conditions based on 7-day test results: $v_t = 277 + 0.88\ I$;
  In the above expressions a minimum of 250 psi for I is recommended.
- MMA polymer concrete new layer
  —For early loading conditions based on 1-day test results: $v_t = 890 + 0.54\ I$;
  —For long-term loading conditions based on 7-day test results: $v_t = 1015 + 0.89\ I$.

Upper Limit for Ultimate Shear Transfer Strength

Because the transverse shear reinforcement becomes very heavy, the theoretical shear resistance due to bond, dowel, friction, and aggregate interlock action becomes greater than the actual shear stress that would cause its failure. The crack in the shear plane locks up in these cases and the behavior and ultimate strength then become the same as that of a monolithically cast specimen. Ultimate shear strength depends on the strength of the weaker of the precast or cold weather concrete material. On the basis of Han-Chin Wu's theory, the upper bound for the ultimate shear transfer capacity is (*11*)

$$v_t = [1.5f'^2_{t2} + 1.426f'_t I - 0.075I^2]^{1/2}$$

where f'_t is the tensile splitting strength of precast or cast in situ concrete, whichever is less.

Because of the material failure of the test specimens at a reinforcement index level of 965 psi, the upper limit for the sum of both components c' and $\mu' I$ can be set at 2,200 psi for polymer concrete and 1,100 psi for magnesium phosphate concrete cast against regular parent concretes of strength up to and in excess of 12,000 psi.

Comparison with ACI Code Provisions for Shear Transfer Strength

Section 11.7 of the ACI Building Code (*17*) lists methods for the design of cross sections subjected to shear transfer at interfaces between dissimilar materials. These provisions allow design for shear transfer based on the shear friction theory proposed by Birkeland and Birkeland (*3*) and Mast (*5*). A comparative study of ACI expression 11.26 for ultimate shear transfer strength, $v_t = 0.85\phi\ \bar{\rho} f_y \mu$ ($\mu = 0.6$ to 1.4) with the experimental results is presented in Figure 18 for both the

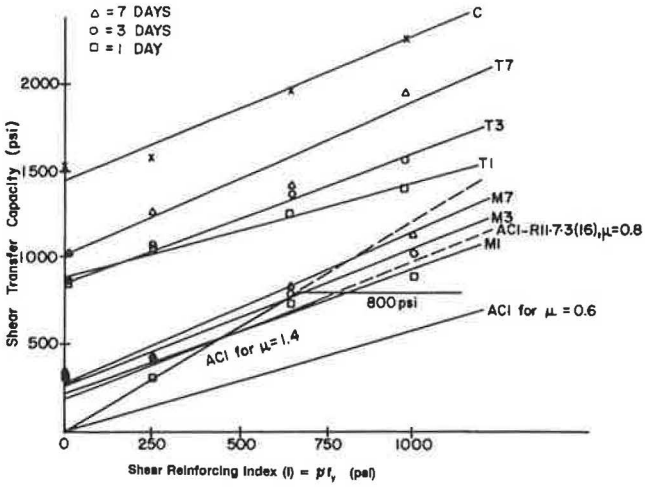

FIGURE 18 Shear transfer capacity versus shear reinforcing strength of magnesium phosphate concrete and MMA polymer concrete and comparison with ACI values.

cold jointed surfaces of cold weather concretes ($\mu = 0.6$) in test specimens and monolithically cast regular concretes ($\mu = 1.4$) in control specimens. In this expression 0.85 is the shear strength reduction factor. Also presented in this figure is the comparison of the test results with the ACI Commentary equation (1b) under section R11.7.3, $v_t = 0.85\ (0.8\ A_s f_y + bdK_1)$, where 0.8 is the coefficient of friction, 0.85 is the shear strength reduction factor, and $K_1 = 400$ psi for normal concrete.

Shear transfer strengths predicted by ACI Equation 11.26 are initially conservative at both the early and late ages for both types of cold weather concretes. This is because the ACI formulations disregard the contribution of apparent cohesive shear transfer strength. At higher values of shear reinforcing strength, the ACI values are in good agreement at all ages of magnesium phosphate concrete, but are conservative for polymer concretes. The control concrete specimens cast under normal weather conditions developed stresses much higher than the two ACI expressions. From the above discussion, it is very clear that MMA polymer concrete can develop shear stresses just by shear and bond in excess of the ACI upper limit of 800 psi even at early ages, whereas the magnesium phosphate concrete can develop the same at early ages with shear reinforcement strengths of 700 psi and greater.

The comparison also validates the previous findings by Nawy and Ukadike (*9*) that the ACI code underestimates the shear transfer strength for polymer concrete layered systems cast under normal weather conditions.

CONCLUSIONS

1. This experimental investigation has identified two types of high-strength cold weather concretes suitable for repairing early-age structural components in subfreezing temperatures and subjected to shearing loads. The two types of concretes are (a) magnesium phosphate concrete (water activated) and (b) MMA polymer concrete. The shear transfer capacity in such concrete elements can be expressed as $v_t = I\mu' + c'$. For a composite element of magnesium phosphate concrete

or polymer concrete cast at subfreezing temperatures against a 12,000-psi conventional precast concrete, the following constants are proposed:

	Magnesium Phosphate Concrete		*MMA Polymer Concrete*	
	c'	μ'	c'	μ'
After 24 hr	248	0.68	890	0.54
After 7 days	278	0.88	890	0.89

Maximum shear transfer capacity for polymer concrete can be taken as 2,200 psi and for magnesium phosphate concrete as 1,100 psi with the parent concrete strength of 1,200 psi or more.

2. At an early age of 24 hr, shear transfer strength of 900 psi and 1,400 psi can be obtained for magnesium phosphate and polymer concretes, respectively, with a reinforcing index of 965 psi.

3. A minimum shear reinforcing index of 250 psi is recommended for magnesium phosphate concrete to take advantage of the contribution of shear reinforcement to shear transfer strength.

4. Both types of cold weather concretes display essentially similar behavior in controlling shear displacements (slip and crack width) at varying ages and transverse reinforcement. The nonreinforced polymer concrete specimens are about five times more ductile than magnesium phosphate concrete specimens with no reinforcement. The pattern of displacements is comparable with that of monolithically cast regular concrete specimens.

5. The changes in slip and crack width vary inversely with the shear reinforcing index.

6. Comparison of the derived expressions and constants from the experimental investigation with the section 11.7 of the ACI building code provisions for ultimate shear transfer strength validates the previous findings by Nawy and Ukadike (*9*) on polymer concretes. ACI underestimates the shear transfer strength at early ages, even for cold weather concretes. Shear stresses in excess of the ACI upper limit of 800 psi can be developed even at early ages with appropriate concrete strengths and reinforcement by cold weather concretes.

ACKNOWLEDGMENTS

The authors wish to acknowledge the support of the FHWA and New Jersey Department of Transportation in funding the initial phase of the project. This work was done by the first author under the direction of the second author in partial fulfillment of requirements for a Ph.D. This project was conducted at the Concrete Research Laboratory of Rutgers, The State University of New Jersey.

REFERENCES

1. E. G. Nawy, A. Hanaor, P. N. Balaguru, and S. Kudlapur. Early Strength of Concrete Patching Materials at Low Temperatures. In *Transportation Research Record 1110*, TRB, National Research Council, Washington, D.C., 1987, pp. 24–33.
2. S. Kudlapur, A. Hanaor, P. N. Balaguru, and E. G. Nawy. *Repair of Bridge Deck Structures in Cold Weather*. Final Report. Department of Civil Engineering, College of Engineering, Rutgers University, Piscataway; N.J. Department of Transportation, Trenton, Aug. 1987, 218 pp.
3. P. W. Birkeland and H. W. Birkeland. Connections in Precast Concrete Construction. *ACI Journal*, Vol. 63, No. 3, March 1966, pp. 345–368.
4. B. Bresler and K. S. Pister. Strength of Concrete Under Combined Stresses. *ACI Journal*, Vol. 55, No. 9, Sept. 1958, pp. 321–345.
5. R. F. Mast. Auxiliary Reinforcement in Precast Concrete Connections. *Proceedings of the American Society of Civil Engineers*, Vol. 94, No. ST6, June 1968, pp. 1485–1504.
6. A. H. Mattock. Design Proposals for Reinforced Concrete Corbels. *Prestressed Concrete Institute Journal*, Vol. 21, No. 3, May-June 1976, pp. 2–26.
7. A. H. Mattock and N. M. Hawkins. Shear Transfer in Reinforced Concrete—Recent Research. *Prestressed Concrete Institute Journal*, Vol. 17, No. 2, March-April 1972, pp. 55–75.
8. T. Paulay and P. J. Loeber. Shear Transfer by Aggregate Interlock. In *ACI Publication SP-42: Shear in Reinforced Concrete*, American Concrete Institute, Detroit, Mich., 1974, pp. 129–166.
9. E. G. Nawy and M. M. Ukadike. Shear Transformation in Concrete and Polymer Modified Concrete Members Subjected to Shearing Loads. *Journal of Testing and Evaluation*, Vol. 11, No. 2, March 1983, pp. 89–98.
10. E. G. Nawy, M. M. Ukadike, and J. Sauer. High Strength Field Polymer Modified Concrete. *Journal of the Structural Division*, ASCE Vol. 103, No. ST-12, Dec. 1977, pp. 2307–2322.
11. M. M. Ukadike. *Durability, Strength and Shear Transfer Characteristics of Polymer Modified Concretes for Concrete Structural Systems*. Ph.D thesis. Rutgers University, Piscataway, N.J., 1978, pp. 132–150.
12. N. C. Palle and T. P. H. Nielsen. Modal Determination of the Effect of Bond Between Coarse Aggregate and Mortar on the Compressive Strength of Concrete. *ACI Journal*, Vol. 66, No. 1, Jan. 1969, pp. 69–72.
13. J. A. Hofbeck, I. A. Ibrahim, and A. H. Mattock. Shear Transfer in Reinforced Concrete. *ACI Journal*, Vol. 66, No. 2, Feb. 1969, pp. 119–128.
14. S. D. Poli, P. G. Gambarova, and C. Karakoc. Aggregate Interlock Role in R. C. Thin-Webbed Beams in Shear. *Journal of the Structural Division*, ASCE, Vol. 113, No. ST-1, Jan. 1987, pp. 1–17.
15. H. Dulacska. Dowel Action of Reinforcement Crossing Cracks in Concrete. *ACI Journal*, Vol. 69, No. 12, Dec. 1972, pp. 754–757.
16. B. R. Hermanson and J. Cowan. Modified Shear Friction Theory for Bracket Design. *ACI Journal*, Vol. 71, No. 2, Feb. 1974, pp. 55–57.
17. *Building Code Requirements for Reinforced Concrete and Commentary—ACI 318R-89*. American Concrete Institute, Detroit, Mich., Nov. 1989, 353 pp.

Publication of this paper sponsored by Committee on Mechanical Properties of Concrete.

Early-Age Cement Hydration Reactions

PAUL WENCIL BROWN

The chemistry of the early reactions that occur during the hydration of the phases in portland cement concrete are considered. Desirable concrete properties are gained because of hydration of the cement. If pozzolanic or latent hydraulic admixtures are present, additional hydration reactions will contribute to strength development. The rate and products of cement hydration may be influenced by the presence of these or of chemical admixtures. Although emphasis is placed on portland cement concrete, reactions in other cements are briefly discussed.

At the time of mixing, fresh concrete contains cement, fine aggregate, coarse aggregate, and water. In addition, chemical and mineral admixtures may be present. Chemical admixtures include accelerating, retarding, water-reducing, or air-entraining admixtures; mineral admixtures include pozzolans, such as fly ash and silica fume, and blast furnace-slag.

Concrete gains desirable mechanical properties principally as a result of the hydration of the cement present. However, if pozzolanic or latent hydraulic admixtures are present, additional hydration reactions will contribute to strength development.

The rate of cement hydration, the composition of the products of hydration, and the morphologies of these hydration products may be influenced by the presence of such mineral admixtures as well as by the presence of chemical admixtures.

The chemistry of the early reactions that occur during the hydration of the phases in portland cement concrete are considered. Early reactions are considered to be those that begin in the first 28 days after mixing. Although emphasis is placed on portland cements, reactions in blended cements, regulated set cements, shrinkage-compensating cements, and high-alumina cements are briefly discussed.

PORTLAND CEMENTS

Five types (I–V) of portland cement are designated in ASTM C 150 (*1*). These contain five major compounds whose proportions vary with cement type. Four of the compounds, which include impure forms of tricalcium silicate and dicalcium silicate, an aluminate phase, and a ferrite phase, are formed during the pyroprocessing of cement. A fifth compound, calcium sulfate, is added during the grinding of portland cement clinker. This compound may be present as anhydrite, $CaSO_4$; as calcium sulfate hemihydrate, $CaSO_4 \cdot \frac{1}{2}H_2O$; or as dihydrate or gypsum, $CaSO_4 \cdot 2H_2O$.

Department of Materials Science and Materials Research Laboratory, Pennsylvania State University, University Park, Pa. 16802.

BLENDED CEMENTS

Eight types of blended cement, containing pozzolan or slag, along with portland cement are designated in ASTM C 595. Pozzolans are a source of reactive silica and, although they are not typically hydraulic in themselves, pozzolans consume calcium hydroxide liberated during cement hydration with the formation of additional binder phase. Commonly used pozzolanic materials include power plant fly ash, silica fume, and certain natural pozzolans. Granulated blast furnace slag is vitrified by rapid quenching and is a latent hydraulic material. The highly alkaline environment of concrete pore solution activates the hydration of slag.

HYDRATION REACTIONS IN MODEL SYSTEMS SIMULATING PORTLAND-BASED CEMENTS

Very Early Reactions

Although the consumption of all the anhydrous phases present in cement initiates at the time of mixing, some hydration reactions end very early. This may occur as a result of the rapidity of these reactions, because the reacting anhydrous solids are finely ground and immediately available to react with the liquid phase or because only a minor amount of the reacting phase is present. Hydration of calcium oxide, reaction of calcium sulfate hemihydrate to form gypsum, and the formation of syngenite may be categorized in this way.

Hydration of Free Lime

Virtually all portland cement contains minor amounts of anhydrous calcium oxide, CaO. Calcium oxide is present as a result of both the proportioning of the raw materials in the manufacture of cement and the nature of the pyroprocessing process. In the manufacture of cement, sources of calcium oxide and silica are finely ground, mixed, and pyroprocessed. During the pyroprocessing step, the calcium oxide and silica initially react to form dicalcium silicate, leaving excess calcium oxide. Tricalcium silicate forms as a result of the reaction of dicalcium silicate with calcium oxide. Often this reaction does not completely consume all the calcium oxide available. The calcium oxide present in cement is called "free lime" and reacts rapidly with water to form calcium hydroxide according to

$$CaO + H_2O \rightarrow Ca(OH)_2 \quad (1)$$

This reaction is expansive in that the solid volume of a mole of calcium hydroxide exceeds that of a mole of calcium oxide by a factor of about 2. The occurrence of this reaction while concrete is in a plastic stage is of little consequence in terms of the dimensional stability of the structure in question. However, in improperly pyroprocessed cements containing high amounts of free lime, undesirable expansion is possible. If all the free lime in a cement is not immediately available to the mixing water, its hydration cannot occur until the anhydrous phases surrounding the grains of free lime have been consumed. Should this occur to a significant extent after the concrete has hardened, the expansion associated with the hydration of the free lime could lead to crack development.

Hydration of Calcium Sulfates

One or more forms of calcium sulfate (anhydrous, hemihydrous, or dihydrous) are interground with cement clinker to control the rate at which the aluminate phases in portland cement hydrate. The chemical formulas for these compounds are as follows:

Type	*Formula*	*Compound*
Anhydrous	$CaSO_4$	Anhydrite
Hemihydrate	$CaSO_4 \cdot \frac{1}{2}H_2O$	Plaster of Paris
Dihydrate	$CaSO_4 \cdot 2H_2O$	Gypsum

Anhydrous calcium sulfate is classified into two types according to its dissolution rate. The terms "soluble anhydrite" and "insoluble anhydrite" have come to be used to indicate the rate at which a particular anhydrous $CaSO_4$ dissolves. In some instances naturally occurring anhydrite or anhydrite formed by the dehydration of gypsum or hemihydrate may dissolve very slowly. If the anhydrite dissolution rate is less than that necessary to control the rate of aluminate hydration, the anhydrite is considered to be insoluble.

Even if gypsum is interground with cement clinker, the heat generated during grinding is frequently sufficient to cause the gypsum to dehydrate to hemihydrate. In extreme instances dehydration may also result in anhydrite formation. During the batching of concrete, both soluble anhydrite and hemihydrate will react with the mixing water to form gypsum as follows:

$$CaSO_4 + 2H_2O \rightarrow CaSO_4 \cdot 2H_2O \quad (2)$$

$$CaSO_4 \cdot \tfrac{1}{2}H_2O + 1.5H_2O \rightarrow CaSO_4 \cdot 2H_2O \quad (3)$$

Figure 1 shows relative rates at which hemihydrate converts to gypsum, depending on temperature (*2*). At the fineness of hemihydrate used in this experiment, the conversion is virtually complete by 30 min at 25 and 41°C, and by about 1 hr at 5°C. Because calcium sulfates are relatively soft, they are easily ground and tend to occur as fine particles or as layers on the surfaces of the cement particles. Thus, the hydration of hemihydrate tends to be complete at shorter times than those typically required for initial set of concrete. In some instances the conversion of hemihydrate to gypsum can result in a phenomenon called "false set," which occurs when the gypsum crystals that have formed result in an apparent set of the mix. Gypsum crystals tend to form as hexagonal needles and their needlelike shape contributes to the occurrence of

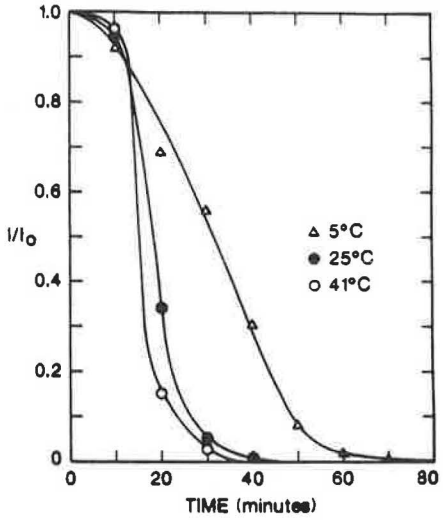

FIGURE 1 Relative rates of conversion of hemihydrate to gypsum depending on temperature.

false set. However, if the mixing process is continued beyond the completion of the hemihydrate-to-gypsum conversion process, the viscosity of the mixture decreases. This is called mixing through false set.

Syngenite Formation

Syngenite is a potassium sulfate–calcium sulfate double salt having the formula $K_2SO_4 \cdot CaSO_4 \cdot H_2O$. Syngenite formation may rapidly occur in cements containing calcium langbeinite, $2CaSO_4 \cdot K_2SO_4$, according to (*3*)

$$2CaSO_4 \cdot K_2SO_4 + nH_2O \rightarrow$$

$$CaK_2(SO_4)_2 \cdot H_2O + CaSO_4 \cdot 2H_2O \quad (4)$$

and lead to accelerated set. Flash set has, for example, been observed in cements to which K_2CO_3 has been added (*4*). Syngenite formation is favorable in pore solutions where the concentration of potassium exceeds 0.35 molar (*5*). This is not uncommon in cements produced in the United States, especially in those containing alkali sulfates.

The occurrence of set associated with syngenite formation is, as in the case of gypsum formation, in part a result of the morphology of syngenite. Syngenite has a needlelike habit and syngenite crystals are capable of causing a loss in plasticity by bridging water-filled spaces. It is not unreasonable that syngenite has sometimes been confused for ettringite; both have generally similar morphologies and strong x-ray diffraction peaks over the same angular ranges (*6*). Syngenite should persist as a stable phase in concrete until the concentration of sulfate in solution becomes depleted through the formation of ettringite.

Silicate Hydration

The silicate phases collectively constitute about 80 weight percent of portland cement. These phases are impure trical-

cium silicate, $3CaO{\cdot}SiO_2$, called alite, and impure dicalcium silicate, $2CaO{\cdot}SiO_2$, called belite. It is the hydration reactions of these silicate phases that are primarily responsible for the development of concrete strength. Alite and belite hydrate to form the same hydration products, calcium silicate hydrate (C-S-H) and calcium hydroxide. However, both the rates of reaction and the relative proportions of the hydration products formed are quite different. The rate of alite hydration is significantly more rapid than that of belite. The relative rates of hydration of the various phases in portland cement are qualitatively shown in Figure 2 (*7*).

The hydration reactions for these phases may be expressed as follows, once calcium hydroxide has precipitated:

$$3CaO{\cdot}SiO_2 + 5.3H_2O \rightarrow 1.7CaO{\cdot}SiO_2{\cdot}4H_2O + 1.3Ca(OH)_2 \quad (5)$$

$$2CaO{\cdot}SiO_2 + 4.3H_2O \rightarrow 1.7CaO{\cdot}SiO_2{\cdot}4H_2O + 0.3Ca(OH)_2 \quad (6)$$

During the early stages of alite or belite hydration, the stoichiometry of the calcium silicate hydrate varies as shown in Figure 3 (*8*). [First-formed C-S-H will have a lime-to-silica ratio near 0.8. Because this ratio is less than 3, the solution will become enriched in calcium. C-S-H formed subsequently will have higher lime-to-silica ratios. These are determined

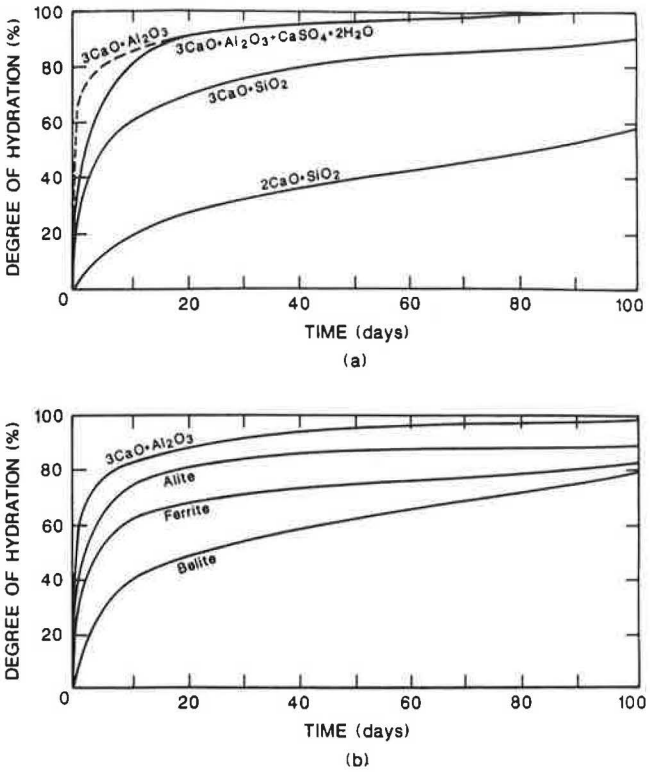

FIGURE 2 Degree of hydration versus time for (a) pure cement phases and (b) those phases in portland cement.

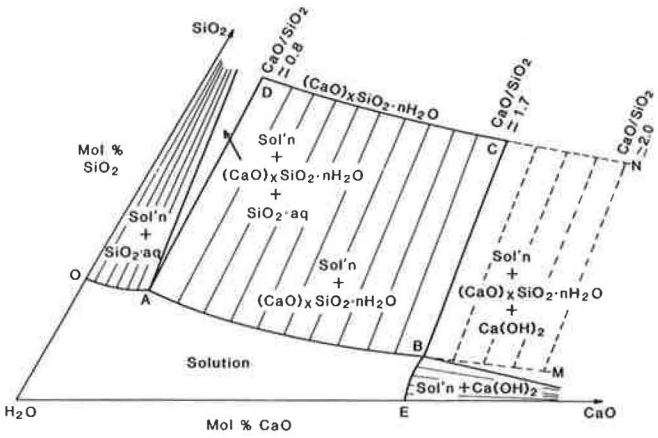

FIGURE 3 Water-rich portion of the ternary system CaO-SiO_2-H_2O.

by the equilibria with the solution. Eventually the solution composition will reach Point *B*. When this invariant point is reached, the C-S-H forming will be at equilibrium with a solution also saturated with respect to $Ca(OH)_2$ and will have a lime-to-silica ratio of about 1.7.] Dissolution of tricalcium silicate or dicalcium silicate continues until the solution becomes supersaturated with respect to calcium silicate hydrate. The calcium silicate hydrate that initially precipitates has a calcium-to-silica ratio near 0.83. This is far lower than the value of 1.7 shown in Equations 5 and 6. Because the calcium-to-silica ratio of the calcium silicate hydrate is always less than that in the anhydrous dicalcium silicate or tricalcium silicate, the solution becomes enriched with calcium as hydration proceeds. To maintain equilibrium, the calcium-to-silica ratio in the C-S-H also increases. Eventually, the solution becomes supersaturated with respect to calcium hydroxide. However, the initial precipitation of this phase does not occur until the calcium hydroxide concentration in solution is about 1.5 times saturation. The calcium-to-silica ratio of the C-S-H responds to the calcium hydroxide supersaturation by reaching a value possibly as high as 2. Eventually, as calcium hydroxide does precipitate and its concentration in solution approaches saturation, the system shown in Figure 3 approaches the invariant Point *B*, and the calcium-to-silica ratio of the C-S-H reaches about 1.7. Thus, the values for the calcium-to-silica ratio given in Equations 5 and 6 assume that this invariant point has been reached.

Using tricalcium silicate as an example, a more general equation describing silicate hydration may be written as follows:

$$3CaO{\cdot}SiO_2 + mH_2O \rightarrow (CaO)_xSiO_2{\cdot}nH_2O + (3 - x)Ca(OH)_2 \quad (7)$$

This equation indicates the variability in the composition of the C-S-H in response to the prevailing solution composition and, along with a companion equation for the hydration of dicalcium silicate, is more relevant to the hydration of the silicate phases in cement than are Equations 5 and 6. Variation in solution composition may be expected during cement

hydration depending on the amount of free lime present, the presence of pozzolans or slag, as well as the concentration of the alkalis, sodium, and potassium in solution.

In addition to the compositional changes that occur during the hydration of the silicate phases in cement, mechanistic and morphological changes occur. Indeed, the latter two changes are closely related. From a mechanistic standpoint, tricalcium silicate hydration occurs in three stages. The first of these is responsible for the onset of the induction period and is the result of the formation of a layer of C-S-H on the surfaces of the hydrating particles. The formation of this layer causes hydration to become diffusionally controlled, with the rate of tricalcium silicate hydration depending on the rate of diffusional transport through this layer. The rate of hydration during this stage is slow and does not appear to be strongly dependent on fineness (*9*). This period of hydration is called the "induction period." Eventually this layer becomes unstable and a morphological transformation to an acicular, cauliflower-like, C-S-H hydration product occurs (*10*). The specific reason for this transformation remains a matter of speculation; however, there is evidence to suggest that it is associated with a polymerization reaction in which monomeric silicate tetrahedra in the C-S-H condense to form dimers (*11*).

Once the initial layer of C-S-H has undergone the transformation to an acicular product, the anhydrous tricalcium silicate particle surfaces are again exposed to the solution. This results in the onset of a period of rapid hydration, referred to as the "acceleratory period." A significant fraction of the alite in cement is consumed during the acceleratory period with the actual amount consumed depending on the fineness of the cement. However, the acceleratory period eventually comes to an end and the rate of hydration decreases again as the small particles of tricalcium silicate are consumed and as the layers of hydration products around the larger particles thicken. A transition to a "postacceleratory period" is complete when the layers of C-S-H surrounding the hydrating particles are sufficiently thick to cause hydration to again become diffusionally controlled. It appears that the hydration rate during this period is independent of fineness (*12*). Thus, in the hydration of cement, it appears that the primary difference in behavior between a Type I or a Type II and a Type III cement lies in the amount of hydration that occurs during the acceleratory period and that grinding to higher fineness contributes principally to the amount of hydration occurring during the acceleratory period.

Aluminate Hydration

The percentage of the aluminate phase in portland cements may vary from essentially zero in so-called "zero C_3A cements" to as high as 14 percent or more.

The aluminate phase in cement is generally considered to be an impure form of tricalcium aluminate. The principal substitution that affects the stoichiometry of the aluminate phase is that of sodium for calcium. However, in cements the composition of the aluminate phase may also depart significantly from that of tricalcium aluminate because of the quenching of nonequilibrium compositions during cooling.

Tricalcium aluminate is a highly reactive phase. If tricalcium aluminate is mixed with water at room temperature, the rate of heat evolution associated with its rapid hydration may be sufficient to cause the water to boil. The rapidity of this reaction leads to a phenomenon in concrete called "flash set." Flash set results because the products of aluminate phase hydration cause a stiffening of the fresh concrete. Premature stiffening associated with aluminate hydration makes placement and finishing difficult. The use of gypsum to control flash set goes back over a century to the studies of Michaelis in 1870 (*13*). The mechanism by which the hydration of the aluminate phase in cement is retarded in the presence of gypsum has remained a matter of debate (*14*). However, it is generally recognized that retardation is associated with the formation of ettringite, $3CaO \cdot Al_2O_3 \cdot 3CaSO_4 \cdot 32H_2O$. The reaction of tricalcium aluminate in the presence of gypsum to form ettringite may be written as follows:

$$3CaO \cdot Al_2O_3 + 3CaSO_4 \cdot 2H_2O + 26H_2O \rightarrow 3CaO \cdot Al_2O_3 \cdot 3CaSO_4 \cdot 32H_2O \quad (8)$$

The amount of calcium sulfate interground with cement clinker is carefully proportioned to ensure that ettringite formation does not continue to any significant extent after about one day, when the concrete has started to gain strength. The formation of ettringite is an expansive reaction. The expansion associated with ettringite formation is acceptable when concrete is in a plastic state and the formation of ettringite needles may indeed contribute to set. It is usually undesirable that an expansive reaction occur in hardening concrete because dimensional instability and cracking may result. There are two reasons why ettringite formation is expansive. First, the solid volume of the ettringite product phase exceeds the sum of the solid volumes of the tricalcium aluminate and gypsum reactant phases. Second, ettringite needles tend to bridge pores in the hardening concrete. Once an ettringite needle has bridged a pore, its continued growth will generate a tensile stress on the pore walls. These internal tensile stresses may eventually lead to crack formation.

A mechanism proposed for the retardation of tricalcium aluminate hydration in the presence of gypsum involves the rapid formation of a layer of ettringite around the hydrating tricalcium aluminate grain. However, the molar volume of the ettringite is much larger than that of the tricalcium aluminate from which it has formed. This results in stresses that lead to cracking of the ettringite layer. As the cracks are filled by additional reaction product, more cracks form. Eventually all the gypsum is consumed. When this occurs, ettringite reacts with the remaining unhydrated tricalcium aluminate to form the monosulfate phase, $3CaO \cdot Al_2O_3 \cdot CaSO_4 \cdot 12H_2O$, according to

$$2(3CaO \cdot Al_2O_3) + 3CaO \cdot Al_2O_3 \cdot 3CaSO_4 \cdot 32H_2O + 4H_2O \rightarrow 3(3CaO \cdot Al_2O_3 \cdot CaSO_4 \cdot 12H_2O) \quad (9)$$

Supporting this mechanism is the observation that tricalcium aluminate hydration is not effectively retarded in the absence of ettringite formation (*15*). On the other hand, the needlelike morphology of ettringite is not in accord with that of a phase that forms an effective diffusion barrier and thereby controls

the rate of tricalcium aluminate hydration. Recent work elucidating the phase relationships in the system CaO-Al_2O-$CaSO_4$-H_2O may reconcile this (*8,16*). Formation of ettringite from tricalcium aluminate results in the existence of local equilibria in the interfacial region between the hydrating particle and the solution. At the exterior of the interfacial region ettringite is in equilibrium with the solution. Inside the ettringite layer is a layer of the monosulfate phase. Inside that is a layer of calcium aluminate hydrates, and inside that, on the anhydrous surface, is a layer of alumina gel. It is suggested that, in analogy with the induction period in the hydration of tricalcium silicate, it is the transport processes across the alumina gel layer that control the rate of tricalcium aluminate hydration. Although an ettringite layer exists at the surface of the hydrating particle, it in itself is not a diffusional barrier; rather its existence allows the formation of an alumina gel diffusional barrier at the tricalcium aluminate interface.

If the hydration of one mole of tricalcium aluminate is carried out in the presence of three moles of gypsum, the reaction proceeds according to Equation 8 and the final product is ettringite. If hydration is carried out in the presence of one mole of gypsum, the reaction proceeds according to Equation 9 and the final product is monosulfate. At gypsum-to-tricalcium aluminate mole ratios greater than 1 but less than 3, a mixture of ettringite and monosulfate forms. At gypsum-to-tricalcium-aluminate mole ratios less than unity, all the available sulfate in the system will have reacted to form monosulfate according to Equation 9 before the anhydrous tricalcium aluminate has been consumed. In this case a third set of hydration reactions involving the formation of calcium aluminate hydrates will occur as follows:

$$2(3CaO\cdot Al_2O_3) + 21H_2O \rightarrow 2CaO\cdot Al_2O_3\cdot 8H_2O + 4CaO\cdot Al_2O_3\cdot 13H_2O \quad (10)$$

Because all the available sulfate has already been consumed, the hydration reaction represented by Equation 10 involves only the formation of calcium aluminate hydrates. Although the formation of the hydrates $2CaO\cdot Al_2O_3\cdot 8H_2O$ and $4CaO\cdot Al_2O_3\cdot 13H_2O$ is kinetically favored, these hydrates are metastable with respect to the hydrate $3CaO\cdot Al_2O_3\cdot 6H_2O$ at above about 15°C. As a consequence, $2CaO\cdot Al_2O_3\cdot 8H_2O$ and $4CaO\cdot Al_2O_3\cdot 13H_2O$ will eventually transform to the stable phase $3CaO\cdot Al_2O_3\cdot 6H_2O$ according to

$$2CaO\cdot Al_2O_3\cdot 8H_2O + 4CaO\cdot Al_2O_3\cdot 13H_2O \rightarrow 2(3CaO\cdot Al_2O_3\cdot 6H_2O) + 9H_2O \quad (11)$$

The situation is somewhat different for portland cement when silica and ferric oxide are available. In cement, the calcium aluminate hydrate $3CaO\cdot Al_2O_3\cdot 6H_2O$ may form solid solutions with a calcium ferrite hydrate and silica. The general formula for this solid solution may be written as

$$3CaO\cdot\{(Al_2O_3)_x\cdot(Fe_2O_3)_{(1-x)}\}_z\cdot SiO_{2(1-z)}\cdot(6 - 2z)H_2O$$

Ferrite Phase Hydration

The relative abundance of the ferrite phase in portland cements is in the same range as that of the aluminate phase or slightly lower. In the pure system, CaO-Al_2O_3-Fe_2O_3, the ferrite phase is actually a solid solution having a generalized composition of $Ca_2Fe_{(2-x)}Al_xO_5$ where x varies between 0 and 0.6. The hydration behavior of the compound tetracalcium aluminoferrite, $4CaO\cdot Al_2O_3\cdot Fe_2O_3$, has often been regarded as representative of the behavior of ferrite solid solutions in general. However, in cement, as with the aluminate phase, a variety of substitutions may occur in the ferrite phase, and this, coupled with quenching-in of nonequilibrium compositions, can result in ferrite phase compositions remote from tetracalcium aluminoferrite.

Of the four major phases in portland cement, the hydration of the ferrite phase is the least well understood. Investigations (*17–19*) of the hydration of tetracalcium aluminoferrite in the presence of gypsum have reported the following hydration reactions, respectively:

$$3(4CaO\cdot Al_2O_3\cdot Fe_2O_3) + 12CaSO_4\cdot 2H_2O + mH_2O \rightarrow 4(3CaO\cdot\{0.75Al_2O_3\cdot 0.25Fe_2O_3\}\cdot 3CaSO_4\cdot 32H_2O) + 2Fe_2O_3\cdot nH_2O \quad (12)$$

$$3(4CaO\cdot Al_2O_3\cdot Fe_2O_3) + 12CaSO_4\cdot 2H_2O + mH_2O \rightarrow (3CaO\cdot\{0.64Al_2O_3\cdot 0.36Fe_2O_3\}\cdot 3CaSO_4\cdot 32H_2O) + 1.56Fe_2O_3\cdot nH_2O + 0.36Al(OH)_3 \quad (13)$$

$$4CaO\cdot Al_2O_3\cdot Fe_2O_3 + 6CaSO_4\cdot 2H_2O + 2Ca(OH)_2 + mH_2O \rightarrow 2(3CaO\cdot\{0.5Al_2O_3\cdot 0.5Fe_2O_3\}\cdot 3CaSO_4\cdot 32H_2O) \quad (14)$$

These reactions suggest a variable stoichiometry for the ettringite-like hydration product. However, a recent investigation (*20*) has shown that early hydration of C_4AF in gypsum and lime-gypsum solutions results in the formation of iron-free ettringite and a calcium ferrite gel according to

$$4CaO\cdot Al_2O_3\cdot Fe_2O_3 + 3CaSO_4\cdot 2H_2O + mH_2O \rightarrow 3CaO\cdot Al_2O_3\cdot 3CaSO_4\cdot 32H_2O + CaFe_2O_3\cdot nH_2O \quad (15)$$

HYDRATION REACTIONS IN PORTLAND CEMENTS

The reactions described for the pure phases or their combinations to a large extent also occur in portland cements. There are, however, important differences both in the rates of reac-

tion and in the compositions and morphologies of the hydration products.

None of the major phases in portland cement are pure; all are solid solutions. Although the nature of the substitutions varies, all these solid solutions contain alkalis. As a consequence, except for the very earliest reactions, hydration in cement occurs at pH values higher than would occur in the model systems. This affects both the stabilities and the compositions of the hydration products that form. For example, if a cement pore solution contains alkali hydroxides in sufficient concentration, the alkali-silica reaction will occur. However, hydration of a mixture of pure phases in the presence of reactive aggregate will not lead to the alkali-silica reaction.

Although the hydration of cement produces significant amounts of calcium hydroxide, very little is observed in the pore solutions extracted from cements. This is because the common ion effect with potassium and sodium hydroxides depresses the calcium ion concentration. On the other hand, there is sufficient calcium present to preclude the formation of the hydrated calcium aluminate phase, $2CaO \cdot Al_2O_3 \cdot 8H_2O$. Rather, the phase $4CaO \cdot Al_2O_3 \cdot 13H_2O$ forms. Other effects associated with elevated alkali hydroxide concentrations in solution include a decrease in the stability of ettringite and, as discussed previously, a tendency for syngenite to form.

Major differences may occur in the hydration of the aluminate and ferrite phases when the behavior of the pure phases and the analogous phases in portland cement are compared. Figure 2 suggests that the ferrite phase in cement is rather slow to react. On the other hand, it has been observed that the hydration of the phase tetracalcium aluminoferrite with gypsum occurs at a higher rate than that of tricalcium aluminate with gypsum (P. W. Brown, unpublished data). The reason for this difference is that the hydration reaction of the ferrite phase is strongly retarded in the presence of calcium hydroxide, whereas that of the aluminate phase is only mildly retarded.

The hydration of both the ferrite and the aluminate phases in cement is affected by the competition of the C-S-H for sulfate. In cement the molar ratio of calcium sulfate-to-(aluminate + ferrite) is about 0.7. Thus, monosulfate phases and hydrated calcium aluminate/ferrite phases would be expected to be the terminal phases associated with aluminate and ferrite phase hydration. However, a small percentage of the silicate in C-S-H can be replaced by sulfate (*21*), and the formation of a sulfate substituted C-S-H results in the decomposition of the monosulfate phases in cements. Finally, as mentioned above, silicate also substitutes in the hydrated calcium aluminate/ferrite phases. As a consequence, the terminal aluminate and ferrite phases in portland cement are hydrogarnets.

EARLY HYDRATION REACTIONS IN MODIFIED PORTLAND CEMENTS AND NONPORTLAND CEMENTS

Blended Cements

The principal difference between the hydration of portland and blended cements is that the calcium hydroxide liberated during silicate hydration reacts with the additives containing reactive silica to produce additional C-S-H. This reaction is called the pozzolanic reaction, which can be described by the following equation:

$$SiO_2 + Ca(OH)_2 + mH_2O \rightarrow (CaO)_xSiO_2 \cdot nH_2O \quad (16)$$

It is not possible to predict the stoichiometry of the C-S-H while the pozzolanic reaction is occurring, but compositional analyses of C-S-H in the vicinity of reacting fly ash particles indicate the C/S ratio to be in the range of 1.2 to 1.4. This represents an averaged value because the C/S ratio at the ash particle–(C-S-H) interface is probably near 0.83, as Figure 3 would suggest, whereas the C/S ratio of the C-S-H at the (C-S-H)–pore solution interface is probably near 1.7. If, when the pozzolanic reaction has reached completion (i.e., the source of reactive silica has been completely consumed) there is calcium hydroxide remaining, the C/S ratio of the C-S-H should eventually reach about 1.7. If, on the other hand, the available calcium hydroxide is consumed and there is still unreacted silica present, the C/S ratio of the C-S-H formed because of the pozzolanic reaction will be less than 1.7.

Shrinkage-Compensating and Regulated-Set Cements

It was mentioned that the amount of calcium sulfate interground with portland cement clinker is proportioned to preclude ettringite formation after about the first day of hydration. Although the expansive reaction associated with ettringite formation can be accommodated while concrete is in a plastic state, the occurrence of an expansive reaction in hardened concrete used in ordinary construction is undesirable. There are, however, exceptions to this and cements have been formulated based, in part, on the formation of ettringite. These cements fall into two general categories—shrinkage-compensating and regulated-set cements.

Shrinkage-compensating cements are formulated so that an expansive reaction compensates for the drying shrinkage typical in portland cement concretes. In cements of this type, ettringite is formed as a result of the reaction between gypsum and the compound $4CaO \cdot 3Al_2O_3 \cdot SO_3$ according to the reaction

$$4CaO \cdot 3Al_2O_3 \cdot SO_3 + 8CaSO_4 \cdot 2H_2O + 6CaO + 80H_2O \rightarrow 3(3CaO \cdot Al_2O_3 \cdot 3CaSO_4 \cdot 32H_2O) \quad (17)$$

Shrinkage-compensating cements are also referred to as expansive cements or self-stressing cements.

Regulated-set cements contain the compounds that react rapidly with sources of calcium sulfate to form ettringite. The early strength gain in regulated-set cements is associated with ettringite formation. After ettringite formation has reached virtual completion, reaction of the silicate phases results in continued strength gain. In one class of regulated-set cements, $11CaO \cdot 7Al_2O_3 \cdot CaF_2$ is added. This compound is rapidly hydraulic and ettringite is rapidly formed when a source of calcium sulfate is present. In a second class, the compound $4CaO \cdot 3Al_2O_3 \cdot SO_3$ is present but in higher proportion than that used in shrinkage-compensating cements.

High-Alumina Cement

High-alumina cement is a nonportland cement composed essentially of monocalcium aluminate, $CaO \cdot Al_2O_3$. The hydration reaction in this cement is

$$CaO \cdot Al_2O_3 + 10H_2O \rightarrow CaO \cdot Al_2O_3 \cdot 10H_2O \quad (18)$$

High-alumina cement offers the desirable features of high early strength and resistance to chemical attack. The source of resistance to chemical attack is the fact that the calcium aluminate hydrate formed is of low basicity and is not attacked by mild acids.

High-alumina cements perform adequately providing the exposure condition does not promote the conversion of the monocalcium aluminate hydrate to tricalcium aluminate hexahydrate. This conversion reaction may be written as follows:

$$3(CaO \cdot Al_2O_3 \cdot 10H_2O) \rightarrow 3CaO \cdot Al_2O_3 \cdot 6H_2O + 2Al_2O_3 \cdot 3H_2O + 18H_2O \quad (19)$$

The monocalcium aluminate hydrate phase becomes increasingly unstable with respect to tricalcium aluminate hexahydrate as the temperature is increased above room temperature. This conversion reaction leads to a loss of strength that has resulted in structural failures (*22*).

Miscellaneous Cements

A variety of cements used for specialized applications, such as white cements, oil well cements, alinite cements, and so forth have not been considered in this paper. In addition, the above discussion of blended, shrinkage-compensating, regulated-set, and high-alumina cements is not intended to be comprehensive and reference may be made to a variety of sources regarding these types of cements (*19,23–26*).

ACKNOWLEDGMENT

The author gratefully acknowledges the support of the Air Force Office of Scientific Research, Electronic and Materials Science Directorate.

REFERENCES

1. Cement; Lime; Gypsum. *Annual Book of ASTM Standards*, Vol. 04.01, 1986.
2. P. W. Brown and P. LaCroix. The Kinetics of Ettringite Formation. *Cement and Concrete Research*, Vol. 19, 1989, pp. 879–884.
3. Z. T. Jugovic and J. L. Gilliam. Early Hydration Reactions in Abnormal Setting Cements. *Journal of Materials*, Vol. 3, 1968, pp. 517–537.
4. E. M. M. G. Niâl. The influence of Alkali-Carbonate on the Hydration of Cement. Presented at 5th International Congress on the Chemistry of Cement, Vol. II, 1968, pp. 472–486.
5. F. E. Jones. The Quinary System CaO-Al_2O_3-$CaSO_4$-K_2O-H_2O at 25°C. *Journal of Physical Chemistry*, Vol. 44, 1944, pp. 356–378.
6. P. W. Brown et al. The Hydration of Tricalcium Aluminate and Tetracalcium Aluminoferrite in the Presence of Calcium Sulfate. *Materials and Structures*, Vol. 19, No. 110, 1986, pp. 137–147.
7. S. Mindness and J. F. Young. *Concrete*. Prentice-Hall, Englewood Cliffs, N.J., 1981.
8. P. W. Brown. The Implications of Phase Equilibria on Hydration in the Tricalcium Silicate-Water and the Tricalcium Aluminate-Gypsum-Water Systems. Presented at 8th International Congress on the Chemistry of Cement, Vol. III, 1986, pp. 231–238.
9. P. W. Brown, E. Franz, G. Frohnsdorff, and H. F. W. Taylor. Analysis of the Aqueous Phase During Early Tricalcium Silicate Hydration. *Cement and Concrete Research*, Vol. 14, 1984, pp. 257–262.
10. J. Ings and P. W. Brown. Early Hydration of Single Crystals of Tricalcium Silicate. *Cement and Concrete Research*, Vol. 13, 1983, pp. 843–848.
11. S. A. Rodger et al. A Study of Tricalcium Silicate Hydration from Very Early to Very Late Stages. In *Microstructural Development During Cement Hydration* (L. Struble and P. W. Brown, eds.), Materials Research Society, Pittsburgh, Pa. (in press), pp. 13–20.
12. P. W. Brown. The Influence of Particle Size Distribution on the Kinetics of Tricalcium Silicate Hydration. *Journal of the American Ceramic Society*, Vol. 72, No. 10, 1989, pp. 1829–1832.
13. W. Michaelis. Cited in H. Kanare. Optimum Sulfate in Portland Cement. In *Cements Research Progress—1984* (J. F. Young, ed.), American Ceramic Society, Westerville, Ohio, 1985.
14. P. W. Brown et al. The Hydration of Tricalcium Aluminate and Tetracalcium Aluminoferrite in the Presence of Calcium Sulfate. *Materials and Structures*, Vol. 19, No. 110, 1986, pp. 137–47.
15. M. Collepardi et al. Tricalcium Aluminate Formation in the Presence of Lime, Gypsum, and Sodium Sulfate. *Cement and Concrete Research*, Vol. 8, 1978, pp. 571–580, 1978.
16. P. W. Brown. Phase Equilibria and Cement Hydration. In *The Materials Science of Concrete*, American Ceramic Society, Westerville, Ohio, 1989.
17. M. Fukuhara et al. Mechanism and Kinetics of C4AF Hydration with Gypsum. *Cement and Concrete Research*, Vol. 11, 1981, pp. 407–414.
18. E. Andreeva and R. Sanzhaasuren. Investigation of the Processes of Chemical Interaction on Aqueous Suspensions of Tetracalcium Aluminoferrite in the Presence of Gypsum Dihydrate (English translation). *Colloid Journal USSR*, Vol. 39, 1977, 197–202.
19. J. Bensted. The Hydration of Portland Cement. In *Advances in Cement Technology* (S. D. Ghosh ed.), Pergamon Press, New York City, 1983, pp. 307–347.
20. P. W. Brown. Early Hydration of Tetracalcium Aluminoferrite in Gypsum and Lime-Gypsum Solutions. *Journal of the American Ceramic Society*, Vol. 70, 1987, pp. 493–496.
21. D. Menetrier, I. Jawed, and J. Skalny. Effect of Gypsum on C3S Hydration. *Cement and Concrete Research*, Vol. 10, 1980, pp. 697–702.
22. *High Alumina Cement Concrete in Buildings*. Current Paper CP34/74. Building Research Establishment, Garston, England, April 1975.
23. Expansive Cement Concretes—Present State of Knowledge. *Journal of the American Concrete Institute*, ACI Communication 223, Vol. 67, 1970, pp. 583–610.
24. F. Lea. *The Chemistry of Cement and Concrete*. Chemical Publishing Company, New York City, 1971.
25. A. Neville and P. J. Wainwright. *High Alumina Cement Concrete*. Wiley, New York City, 1975.
26. S. Mindness and J. F. Young. *Concrete*. Prentice-Hall, Englewood Cliffs, N.J., 1981.

Publication of this paper sponsored by Committee on Mechanical Properties of Concrete.

Using Statistical Methods To Optimize High-Strength Concrete Performance

JOHN J. LUCIANO AND GREGORY S. BOBROWSKI

Sound experimental design principles, rather than three-point curves, can be employed to determine high-strength concrete mixture proportions that maximize performance while minimizing cost. Important issues on experimental design and empirical modeling are discussed. Graphical methods illustrate how high compressive strengths can be obtained for a wide range of costs—and how to get the most for your money. An example is given using a classical experimental design. It greatly reduces the number of concrete mixes that otherwise would have been necessary to obtain information on five variables that change simultaneously. This experiment illuminates the effect of the silica fume addition percentage and the high-range water reducer dosage on 28-day compressive strength and raw material cost. Contour plots are provided to demonstrate the usefulness of a statistical approach.

One of the best reasons for using concrete is that it is a forgiving conglomerate. The proper assemblage of cement, sand, stone, water, and admixtures yields a product that has engineering properties useful for various structures. Traditionally, a good mixture proportion is determined by a combination of field experience and simple experimentation. For example, after some simple laboratory batches are made, field mixes are run using three different cement factors and the desired performance is obtained by interpolating from the best-fit curve to the data. Certainly this method will eventually generate a suitable mixture proportion.

However, increased attention to the front end of this process will often pay large dividends when one is ready to make field-sized trial batches to simulate job conditions. When one considers the small price of trial batches compared with production costs, it makes good sense to understand how raw materials work together.

Understanding the effects and synergisms of the materials is particularly important for high-strength concrete mix proportioning. Reducing the water-cementitious ratio as low as possible yet maintaining a certain workability level for the least cost is the goal to be pursued.

The challenge is to ascertain how to assimilate the effects of the cement, aggregates, and admixtures (and their interactions) on each response variable. It will then be possible to execute sound judgment when mix proportions are determined for high-strength concrete.

A statistical strategy will certainly not replace valuable scientific knowledge and experience pertaining to concrete technology. However, experimental design and statistics can be used to complement a researcher's understanding of particular materials. Sound experimental design principles can help determine high-strength concrete mixture proportions that optimize performance and cost.

Master Builders, Inc., 23700 Chagrin Boulevard, Cleveland, Ohio 44122-5554.

THE DILEMMA

Concrete comes from the Latin word *concretus*, which means "grown together." When hydration (the chemical reaction between water and the cementitious material) occurs, the cement paste encompasses the aggregate like glue. To obtain high-strength concrete, the idea is to recreate a large rock by cementing together its broken pieces (*1*).

Scientific knowledge coupled with practical experience usually provides a good starting point. For example, it is known that strength failure occurs in concrete because of limitations associated with (a) Cement paste, (b) Coarse aggregate, and (c) Paste-to-aggregate bond (*2*). Consequently, it is known that the amount and quality of the cement paste have an important bearing on concrete performance. Similarly, the amount, shape, size, and quality of the coarse aggregate significantly affect the engineering properties of concrete. Finally, the importance of the bond between the two cannot be underestimated.

Because concrete is a mixture, there are many ways to assemble its components. The dilemma arises when one considers how to optimally combine the ingredients. ACI 363R-84 comments briefly on optimization (*3*):

> A principal consideration in establishing the desired cement content will be the identification of combinations of materials which will produce optimum strengths. Ideally, evaluations of each potential source of cement, fly ash, liquid admixture, and aggregate in varying concentrations would indicate the optimum cement content and optimum combination of materials. Testing costs and time requirements usually have limited the completeness of the testing programs, but particular attention has been given to evaluation of the brand of cement to be used with the class and source of pozzolan, if a pozzolan is to be used.

Admittedly, when all reasonable combinations of materials are considered, the task of evaluating them can be formidable. Certainly it would be quite impractical to attempt to test more than a small fraction of these combinations. What is needed is an organized strategy that will facilitate navigation through the complex process of optimizing concrete mix proportions.

DESIGNING THE EXPERIMENT

Fortunately, the principles of experimental design provide the framework for an organized strategy. The combination of

careful determination of objectives, experimental design, controlled laboratory testing, thorough analysis, and field evaluation usually yields favorable results.

The first step is to determine what objectives are to be met. This may sound so obvious that it is not worth mentioning. However, many researchers collect data without a clear understanding of their goal. Before work begins, there must be a focused objective in mind. At this point, specific questions should be formulated that can be answered from experimentation. The minimum requirement for success is always knowing what the target is.

As soon as the goals are clear, the researcher can move to the next step—setting up the experimental design or designs. The appropriate experiment will depend on the complexity of the situation, minimum information desired, resources, and time. For example, it may be appropriate to run a simple experiment that compares the mortar compressive strength of several locally available cements. After this experiment has been run, the cement that performs best can be used in a later evaluation. This sequential experimentation serves to reduce the number of variables for more detailed experimentation in the future.

To construct the experimental design, the response variables and the experimental region must be determined. The response variables are simply measured variables that depend on the values of the independent variables. Examples of response variables are initial set time compressive strength and modulus of elasticity. The independent variables are the controlled variables that are intentionally changed to affect the responses. Examples of independent variables are cement factor, water-to-cement ratio, and admixture dosage. The experimental region is the geometric space jointly defined by the independent variables and their respective levels. For example, the effect of the cement factor and water-to-cement ratio on compressive strength is to be evaluated by varying the cement factor between 700 and 900 lb/yd^3 and the water-to-cement ratio between 0.25 and 0.35. The experimental region for this example would simply be a square that contains the following four combinations:

Cement Factor	*Water-to-Cement Ratio*
700	0.25
700	0.35
900	0.25
900	0.35

The interior of this region is where the response values for specific combinations of independent variables are to be predicted. Two levels for a given independent variable allow for the estimation of a linear trend through the experimental region. Three or more levels allow for the estimation of nonlinear trends through the experimental region.

After the number of independent variables and their expected trends have been determined, an efficient way to specify the experimental mixes needs to be ascertained. For example, if five independent variables were under study, with each effect best estimated by a nonlinear trend through the experimental region, then $3^5 = 243$ mixes could be specified, considering all possible combinations. Clearly, however, it would be impractical to conduct this experiment. The correct course of action here would be to conduct an experiment on a relatively small fraction of the total possible combinations. The goal behind experimental design is to obtain the maximum amount of information from the least amount of resources.

Before the experiment can be conducted, some additional information must be obtained. First, it is necessary to understand what the experimental unit (the basic unit to which a treatment is applied) is for each response in the study. Examples of experimental units include compressive strength cylinders, length change beams, and setting time proctors.

Second, it is absolutely critical to ensure that a good estimate of experimental error is available after the study has been run because there is variation in experimental results resulting from known and unknown factors. This variation is sometimes referred to simply as "noise." A simple example may be helpful here. Suppose a large batch of concrete is made and several cylinders are fabricated. After 28 days, when these cylinders are broken, all of them will not have identical compressive strengths. This results from experimental error. In other words, even though all the specimens represent the same concrete there are some nuisance factors that cause the test results to be different. Possibly the loading rate changed or the cylinders were tested slightly off-center. Certainly it is possible that factors not only outside the experimenter's control but also beyond his knowledge influence experimental results. The simple truth is that experimental error is a natural occurrence irrespective of how careful one is in collecting data. As long as the amount of experimental error is understood, a logical determination of the independent variable effects can be made. Without understanding of the experimental error, it is extremely difficult to develop logical inferences from the data. Drawing conclusions from data without knowing the experimental error is like making decisions by flipping a coin in a dark room.

One concept related to estimating experimental error is blocking. It is common to expect certain unavoidable sources of variation. Blocking is a tool to reduce experimental error by grouping similar experimental units with respect to the response variable or variables. In essence, the blocking variable removes one or more sources of variability that would otherwise have been captured in the experimental error. Suppose, for instance, the interest is to compare the compressive strength of two cements. Further suppose that on one day four mixes were made with each cement, and on a second day four additional mixes were made with each cement. Now clearly the day-to-day effect (which includes material, environmental, and personnel changes) would affect the ability to discriminate effectively between the two cements. If this source of variation was removed by mixing all cement on one day, then the comparison between the cements would become more powerful. This is the benefit of adding a blocking variable.

Another important concept relating to experimental design is randomization. Essentially, randomization is a statistical method to distribute the order of experimental runs to prevent systematic bias from contaminating study results. It is helpful to view randomization as insurance against unwanted sources of variation. For example, suppose that one desires to examine the effect of adding 5, 7, 9, and 11 percent of a mineral admixture to the mix design. If this work was performed outdoors in the order of increasing addition percentages, then the influence of temperature may introduce a systematic bias. Here the mixes run early in the morning will, all other things

being equal, have a lower concrete temperature, and hence hydrate more efficiently and yield higher compressive strengths than the mixes run later under higher temperature conditions. Consequently, the effect of the addition percentage would be partially masked by the temperature effect.

Unfortunately, applying randomization is not a natural thing to do. However, suppose in the previous example that the four different addition percentages were mixed throughout the day. If 12 mixes were to be run (three mixes per level), one possible randomized order would be 7, 9, 5, 9, 11, 11, 7, 5, 7, 11, 9, and 5 percent. The effect of temperature would tend to cancel out among the different levels of admixture addition percentages. This is what makes randomization so effective; bias tends to be removed by cancellation, whether external sources of variation can be anticipated or not. Even if no lurking sources of variation exist, the cost of randomization is at most a little inconvenience. On the other hand, it is apparent that using randomization can easily save an experiment that is otherwise doomed to failure. The moral of the story is (*4*)

> Block what you can control,
> Randomize what you cannot control.

CONDUCTING THE EXPERIMENT

After experimental design issues have been addressed, it is time to conduct the experiment. For this step there is no substitute for a team of individuals who are highly skilled in concrete mix proportioning and testing. Those who understand how variations in raw materials (age, grading, composition, specific gravity, etc.), temperature, mixing, handling, compacting, curing, and testing affect performance are necessary. The mixes need to be proportioned to ensure the proper yield. The guidelines given in ACI 211.1, 211.2, and 211.3 (*5*) are helpful for this stage.

After mix proportioning is complete and a set of batch weights is available, the mixes can be made according to the specifications of the experimental design. The air content, slump, and unit weight should always be measured in addition to the other response variables of interest. Each mix should be made in as similar an environment as possible. If not, these uncontrolled environmental variables can confuse the results of a study, rendering an experiment totally worthless. Collecting information without external biases is critical to understanding the data.

ANALYZING THE EXPERIMENT

No matter how much care is taken to execute an experiment, some erroneous values inevitably appear on the data sheets. Before any serious analysis is performed, data should be screened to eliminate numbers that are grossly wrong. However, if there are doubts concerning the validity of any data value, it should be left alone. Simple scatter plots and linear regression analysis as well as common sense will prepare the data for a formal analysis. This process serves to identify simple, detectable errors (such as a transposition of digits or a calculation error).

The next step is to model each response of interest using statistical methods. It is understood that the complex processes involving cement hydration could never be exactly modeled. The idea is to develop models that approximate each response in the region of interest without bias. For example, if the number of days per month was to be modeled, a mathematical model to calculate the value exactly could be employed. However, a simpler yet unbiased model would be using 30.5 as an approximation to the number of days in a month. It is not as good as a more sophisticated model, but it will be correct to within ½ day more than 90 percent of the time. In this situation God's complex model cannot be accessed, so the phenomenon is approximated using mathematical building blocks; generally, the greater the number of building blocks, the better the approximation.

Regression is a powerful statistical technique that is useful in the modeling of data when the exact mathematical relationship between a response variable and a set of independent (predictor) variables is not known. Regression results in a model that optimizes the fit between the data and a criterion. Generally, the model minimizes the squared differences between the actual response values and the values predicted by the regression equation.

After each response has been represented, the statistical model undergoes some "quality" tests. This series of tests checks that the model is an appropriate representation of the data that are being fit. For example, if the model estimated the number of days per month at 40, the model would probably be less than satisfactory because it would always overestimate the correct value. The statistical model sought is one that is not biased in any direction. Consequently, it is crucial to examine predicted values for each data value to ensure that no systematic bias is present. Clearly all models are wrong in some sense, because they are approximations. A statistical model is considered good when it describes a high percentage of the variability without exhibiting systematic deviations from the actual data.

When the models successfully undergo these quality checks, the estimates obtained from these equations assuredly yield reasonably unbiased approximations for each response within the region of interest. An optimization program can now be built. This computer program allows data to be simulated by iterating through each of the independent variables in small steps. The values of the independent variables are plugged into the statistical models yielding predicted values for each response. Raw material costs are also incorporated in this program so that mixes can be generated, each with a specific performance and cost.

Model values are then written to a data set where they can be sorted by various ranges of performance criteria. For example, mixes with a given set time and compressive strength could be sorted by cost. Each point surviving this "final cut" is a suitable candidate to meet the original objectives.

The major assumption is that the statistical models provide adequate approximations to the various responses. Fortunately this assumption can be checked to some extent. However, there are two additional assumptions that must be made. First, it is assumed that no major raw material variations occur. For example, if the study was performed using only Class C fly ash, a substitution involving Class F fly ash could (and does) make a big difference. Second, it must be assumed

that relative performance differences observed in the laboratory also occur in the field. Generally speaking, this is a valid assumption. The only time that this should be a concern is when laboratory work poorly simulates the large scale batches or the actual delivery time involved.

It is also important to consider other variables that are not being measured. For example, a mix may be generated that would yield the necessary performance and cost-effectiveness to be a workable solution. However, the amount of cementitious material may be so high that in practice it would be unworkable. Someone who understands concrete well would be able to eliminate choices that obviously would not be feasible.

The last step is to make and test final mix recommendations. On paper the analytical process yields a scientific choice to improve performance while restricting the cost. The safe course of action at this point is to validate this empirical work by running full-scale batches.

EXAMPLE

Many industries have the luxury of obtaining information on their response variables within a very short period. Unfortunately, with concrete, much of the data on standard hardened properties does not become available until 28 days. Often this precludes sequential experimentation. Consequently, it becomes important to design experiments that carefully blanket the region of interest.

The central composite design is a classical experimental design that enables an experimenter to estimate linear and quadratic trends for each of the independent variables under study. The easiest way to begin to understand these designs is to view them geometrically. Figure 1 presents the experimental region for a three-variable central composite design. The cube portion of this design consists of $2 \times 2 \times 2 = 2^3 = 8$ vertices (corners) that allow the estimation of linear trends for each of the three independent variables. The six axial (star) points protruding from each face of the cube provide five levels for each independent variable. These are included to determine the quadratic (nonlinear) trends present for each variable. The points in the center of each cube are replicates that enable the estimation of pure experimental error. This pure error is used to assess the significance of any model's lack of fit. Any good text on experimental design or response surface methods provides the necessary information to work through the actual design and analysis of this type of experiment. A good statistician would be invaluable here.

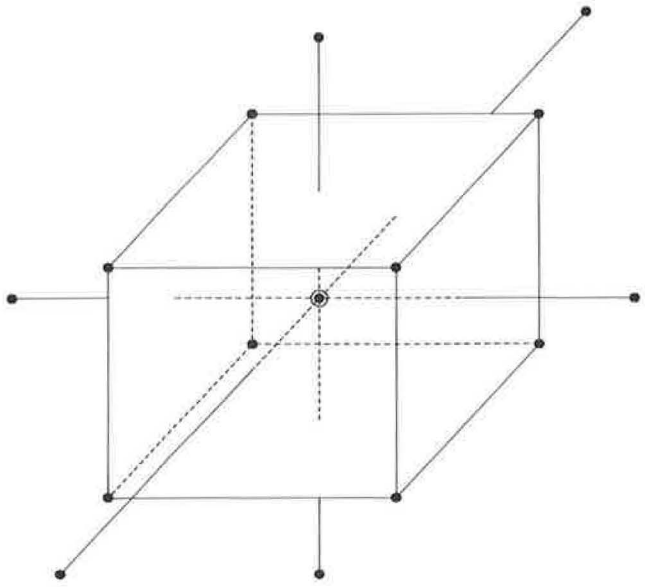

FIGURE 1 Three-factor central composite design.

As an example, Table 1 provides the mix design data for a modified five-variable central composite design, blocked across 3 days. The five factors that were intentionally changed were

- Cement quantity (lb/yd^3),
- Silica fume (addition percent),
- High-range water reducer (HRWR) dosage (oz/100 lb of cement + silica fume),
- Coarse aggregate content (lb/yd^3), and
- Coarse aggregate type or blend.

Before the experiment was run, the cement was tested for false set characteristics using ASTM C 359 and ASTM C 451. Furthermore, the aggregates were analyzed in accordance with ASTM C 29-87, C 40-84, C 127-84, C 128-84, and C 136-84a to determine unit weight, voids, impurities, specific gravity, absorption, and sieve analysis. After this material analysis was performed, the water-to-cementitious ratio was allowed to vary to obtain a slump of 10 ± 1 in.

The relationship between 28-day compressive strength and the water-to-cementitious ratio for this set of materials is presented in Figure 2. The 28-day compressive strength as a function of cost is depicted in Figure 3. Actually, cost does not predict or determine compressive strength. However, this graph illustrates that one can achieve a particular level of strength for a wide range of raw material costs. The desire here is to produce the intended strength for the minimum cost. A cost-effective combination of raw materials that minimize the water-to-cementitious ratio needs to be determined.

It is admittedly difficult to understand a data table that is in a randomized order. Figures 4–6 represent creative attempts to illuminate the patterns contained in the data. Each of these graphs contains values averaged across coarse aggregate content and limestone percentage of the course aggregate. Therefore, the six axial values are averages of one mix; the cube vertices (corners) are averages of two mixes; and the center is an average of 11 mixes. To understand the HRWR effect, it is necessary to look from the bottom to the top of the diagram. For example, in Figure 4 the 2.5-oz dose yielded a 28-day compressive strength of 6,880 psi. A 15-oz dose yielded average 28-day strengths of 8,660, 9,700, 7,600, and 9,070 psi depending on the amount of cement and silica fume added to the mixture proportions. A 27.5-oz dose provided average compressive strengths of 9,480, 12,210, and 12,950 psi, again depending on the cement and silica fume amounts. A 40-oz dose generated average strengths of 9,600, 11,270, 12,160, and 12,590 psi, whereas a 52.5-oz dose registered 11,780 psi.

If none of the independent variables affected the strength, all the values in the circles would be approximately equal.

TABLE 1 CONCRETE MIXTURE PROPORTIONS—DAY 1

MIX	CEMENT (LB./YD.)	SILICA FUME ADDITION %	HIGH RANGE WATER REDUCER (OZ./CWT.)	COARSE AGGREGATE CONTENT (LB./YD.)	COARSE AGGREGATE BLEND	SAND CONTENT (LB./YD.)
1	650	15	40.0	2050	SILICA GRAVEL	990
2	800	10	27.5	1900	50:50 BLEND	1017
3	950	5	40.0	1750	LIMESTONE	1103
4	650	5	15.0	2050	SILICA GRAVEL	988
5	650	5	15.0	1750	LIMESTONE	1301
6	800	10	27.5	1900	50:50 BLEND	1021
7	950	5	40.0	2050	SILICA GRAVEL	742
8	650	15	40.0	1750	LIMESTONE	1352
9	950	15	15.0	2050	SILICA GRAVEL	277
10	800	10	27.5	1900	50:50 BLEND	1020
11	950	15	15.0	1750	LIMESTONE	665

MIX	SLUMP (IN.)	AIR CONTENT %	WATER/ CEMENT+FUME RATIO	28 DAY COMPRESSIVE STRENGTH	RAW MATERIAL COST A ($/YD.)
1	10.0	1.4	0.31	12428	65.94
2	9.8	2.7	0.30	12322	60.28
3	10.8	2.4	0.26	11515	63.26
4	9.0	1.2	0.40	8652	46.89
5	9.3	3.3	0.44	8657	38.54
6	10.3	2.2	0.31	11773	60.26
7	10.3	1.4	0.25	11019	71.50
8	9.5	2.7	0.33	11892	57.66
9	9.5	1.5	0.36	8341	73.55
10	9.8	1.8	0.29	12166	60.34
11	9.8	1.6	0.38	9803	65.25

A
RAW MATERIAL COSTS ASSUME CEMENT=$60/TON, SILICA FUME=$300/TON, SAND=$5/TON, LIMESTONE=$7/TON, SILICA GRAVEL=$15/TON & HRWR=$6/GALLON.

B
MIX 20 COULD NOT BE MADE TO APPROPRIATE SLUMP SPECIFICATION OF 10" +/- 1"

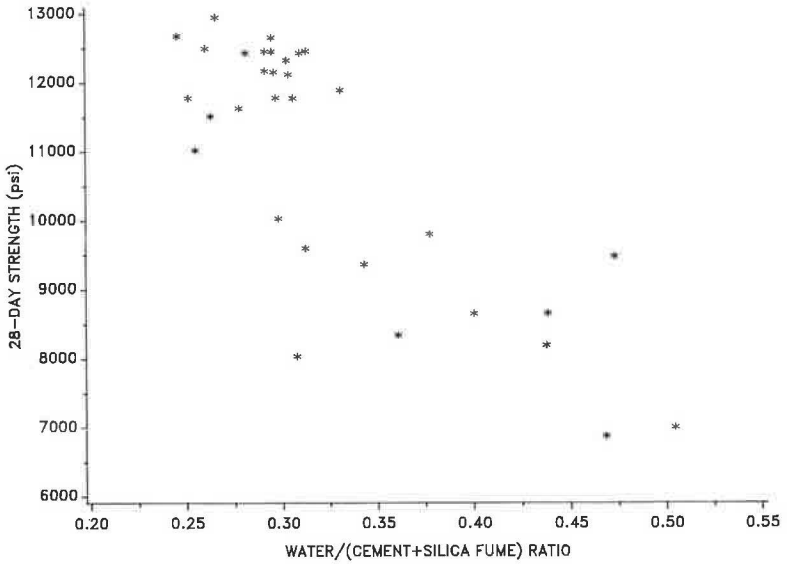

FIGURE 2 Relationship between 28-day compressive strength (psi) and water-to-(cement + silica fume) ratio.

TABLE 2 CONCRETE MIXTURE PROPORTIONS—DAY 2

MIX	CEMENT (LB./YD.)	SILICA FUME ADDITION %	HIGH RANGE WATER REDUCER (OZ./CWT.)	COARSE AGGREGATE CONTENT (LB./YD.)	COARSE AGGREGATE BLEND	SAND CONTENT (LB./YD.)
12	800	10	27.5	1900	50:50 BLEND	1005
13	950	5	15.0	2050	LIMESTONE	638
14	950	5	15.0	1750	SILICA GRAVEL	903
15	800	10	27.5	1900	50:50 BLEND	999
16	650	15	15.0	1750	SILICA GRAVEL	1060
17	650	15	15.0	2050	LIMESTONE	757
18	950	15	40.0	2050	LIMESTONE	658
19	650	5	40.0	1750	SILICA GRAVEL	1381
20 B	650	5	40.0	2050	LIMESTONE	
21	800	10	27.5	1900	50:50 BLEND	1001
22	950	15	40.0	1750	SILICA GRAVEL	859

MIX	SLUMP (IN.)	AIR CONTENT %	WATER/ CEMENT+FUME RATIO	28 DAY COMPRESSIVE STRENGTH	RAW MATERIAL COST A ($/YD.)
12	10.0	2.5	0.29	12453	60.34
13	10.0	2.5	0.34	9366	51.41
14	10.0	2.4	0.30	10029	58.03
15	10.3	2.3	0.30	11777	60.31
16	9.3	1.0	0.44	8192	55.06
17	9.5	1.5	0.50	7004	48.41
18	9.8	2.1	0.26	12498	79.23
19	10.3	2.9	0.31	9597	53.78
20 B	.	.	.	.	.
21	10.0	2.4	0.29	12445	60.32
22	11.0	2.5	0.25	12676	85.67

A
RAW MATERIAL COSTS ASSUME CEMENT=$60/TON, SILICA FUME=$300/TON, SAND=$5/TON, LIMESTONE=$7/TON, SILICA GRAVEL=$15/TON & HRWR=$6/GALLON.

B
MIX 20 COULD NOT BE MADE TO APPROPRIATE SLUMP SPECIFICATION OF 10" +/- 1"

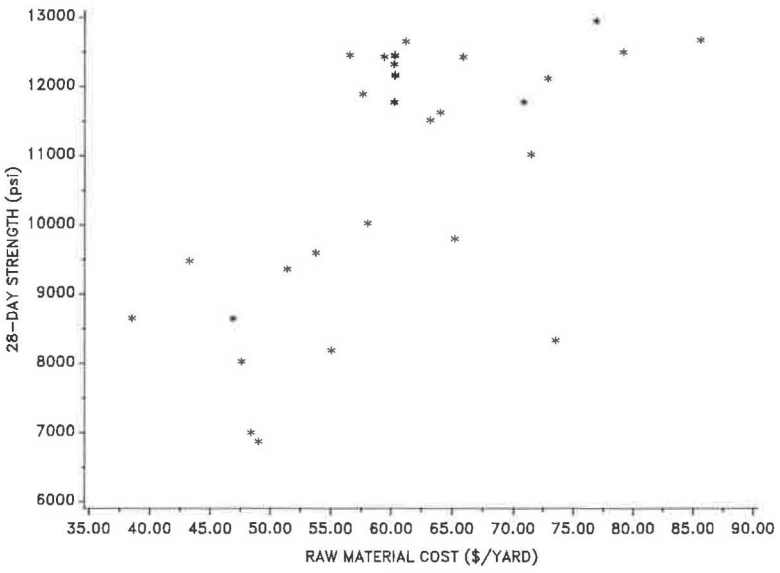

FIGURE 3 Relationship between 28-day compressive strength (psi) and raw material cost ($/yd).

TABLE 3 CONCRETE MIXTURE PROPORTIONS—DAY 3

MIX	CEMENT (LB./YD.)	SILICA FUME ADDITION %	HIGH RANGE WATER REDUCER (OZ./CWT.)	COARSE AGGREGATE CONTENT (LB./YD.)	COARSE AGGREGATE BLEND	SAND CONTENT (LB./YD.)
23	800	0	27.5	1900	50:50 BLEND	1123
24	500	10	27.5	1900	50:50 BLEND	1312
25	800	10	52.5	1900	50:50 BLEND	1094
26	800	10	27.5	1900	LIMESTONE	1033
27	800	10	27.5	1900	50:50 BLEND	1003
28	800	10	2.5	1900	50:50 BLEND	633
29	1100	10	27.5	1900	50:50 BLEND	574
30	800	10	27.5	2200	50:50 BLEND	744
31	800	10	27.5	1900	SILICA GRAVEL	999
32	800	20	27.5	1900	50:50 BLEND	860
33	800	10	27.5	1600	50:50 BLEND	1329

MIX	SLUMP (IN.)	AIR CONTENT %	WATER/ CEMENT+FUME RATIO	28 DAY COMPRESSIVE STRENGTH	RAW MATERIAL COST A ($/YD.)
23	9.8	1.7	0.31	8033	47.60
24	9.0	1.3	0.47	9483	43.28
25	10.5	2.8	0.25	11778	70.88
26	10.0	1.8	0.31	12458	56.59
27	9.8	1.9	0.30	12155	60.32
28	9.0	2.3	0.47	6876	49.02
29	11.0	1.8	0.27	12946	76.96
30	9.8	1.4	0.29	12654	61.25
31	10.0	1.8	0.28	11624	64.05
32	9.5	2.1	0.30	12118	72.92
33	10.0	3.0	0.28	12428	59.47

A
RAW MATERIAL COSTS ASSUME CEMENT=$60/TON, SILICA FUME=$300/TON, SAND=$5/TON, LIMESTONE=$7/TON, SILICA GRAVEL=$15/TON & HRWR=$6/GALLON.
B
MIX 20 COULD NOT BE MADE TO APPROPRIATE SLUMP SPECIFICATION OF 10" +/- 1"

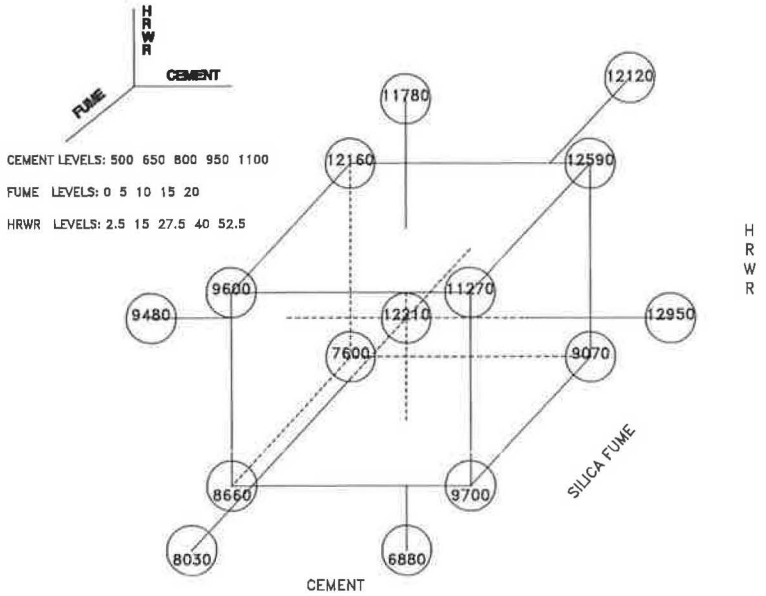

FIGURE 4 Three-dimensional representation of 28-day compressive strength (psi) as a function of cement, silica fume percent, and high-range water reducer dosage.

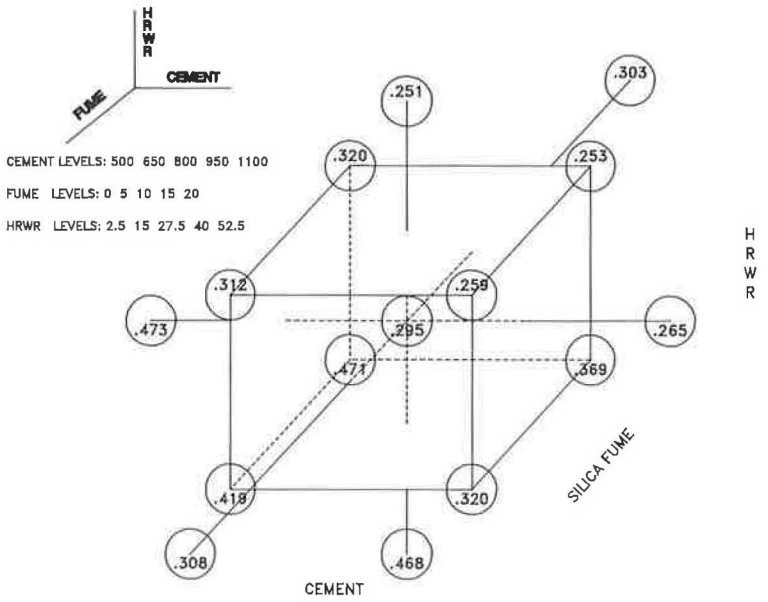

FIGURE 5 Three-dimensional representation of water-to-(cement + silica fume) ratio as a function of cement, silica fume percent, and high-range water reducer dosage.

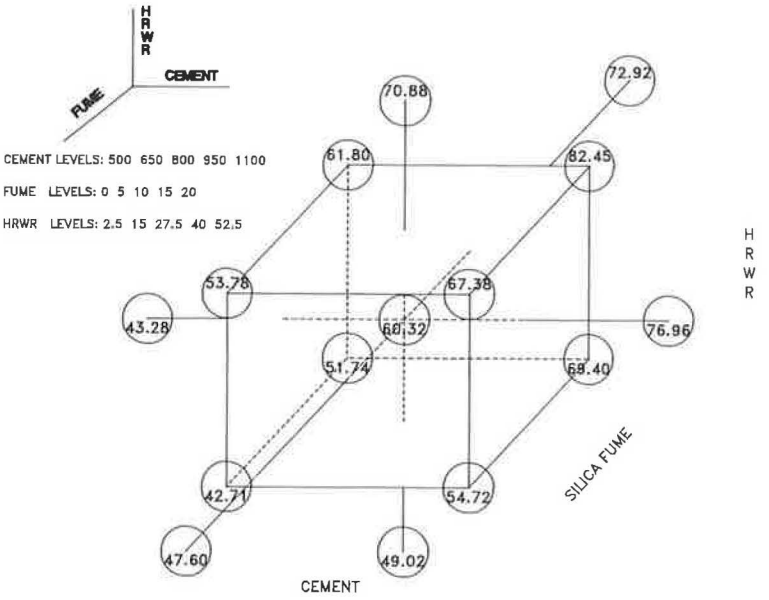

FIGURE 6 Three-dimensional representation of raw material cost ($/yd) as a function of cement, silica fume percent, and high-range water reducer dosage.

However, data in Figure 4 show considerable fluctuation in the compressive strength. In particular, to produce high compressive strength, the selection of the HRWR dose and silica fume addition percentage levels is critical. Too much silica fume without the proper HRWR dosage will hinder performance. Figure 5 illuminates this fact by displaying the water-to-cementitious ratio patterns throughout the region, and Figure 6 displays the raw material costs for these combinations.

For these graphs, actual data values have been used to help visualize what is occurring in this experiment. It is necessary to model the data to approximate the response surface. Probably the best way to understand a response surface is to observe a weather forecaster showing the various temperatures across the United States. These temperatures are analogous to the actual data values obtained from an experiment. Often a contour map that color-codes temperatures by regions is shown. This is, in fact, a response surface. It is these response surfaces that are approximated with statistical models.

Now suppose that the objective is to determine the mixture proportions in the laboratory that will generate 12,000 psi for the least cost. Further suppose that it is known from the lab work, that a mix containing 800 lb of cement and 1,900 lb of

coarse aggregate split 50:50 between silica and limestone will lower the water demanded to optimize performance. Figures 7 and 8 provide the 28-day compressive strength and raw material cost response surfaces, respectively.

The 28-day strength response surface contours illustrate how compressive strength improves as the HRWR dosage and silica fume addition percentage are increased in tandem within the experimental region. Increasing one without the other will only serve to increase cost, not performance. Because both the strength and cost contours increase from the lower left to the upper right, the optimum is easily found to be the area to the lower left of the 12,000–13,000 contour band. This corresponds to a mix containing around 27 oz per hundredweight of an HRWR in combination with 7 ½ percent silica fume added to the 800 lb of cement.

The values contained in the cost contour bands are without variance because cost is a perfect mathematical function of its individual constituents. On the other hand, compressive

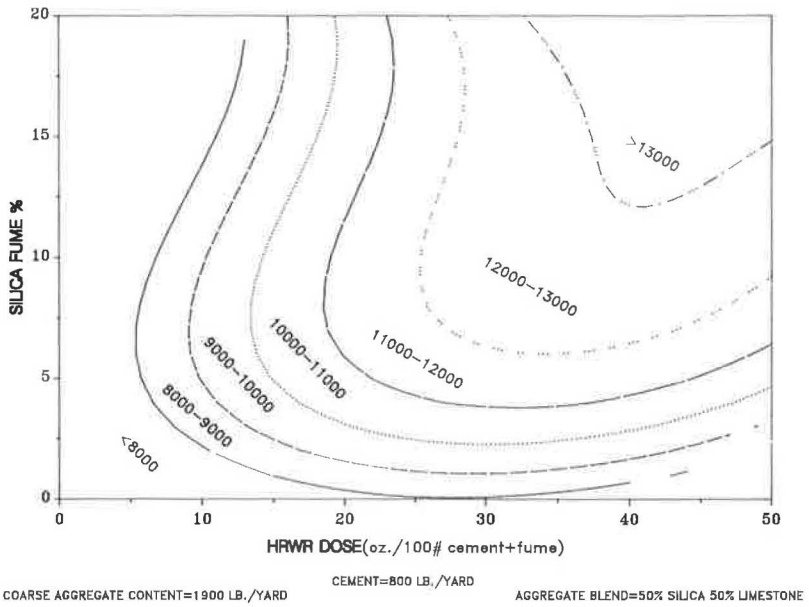

FIGURE 7 Contour plot showing the relationship between 28-day compressive strength (psi) as a function of silica fume percent and high-range water reducer dosage.

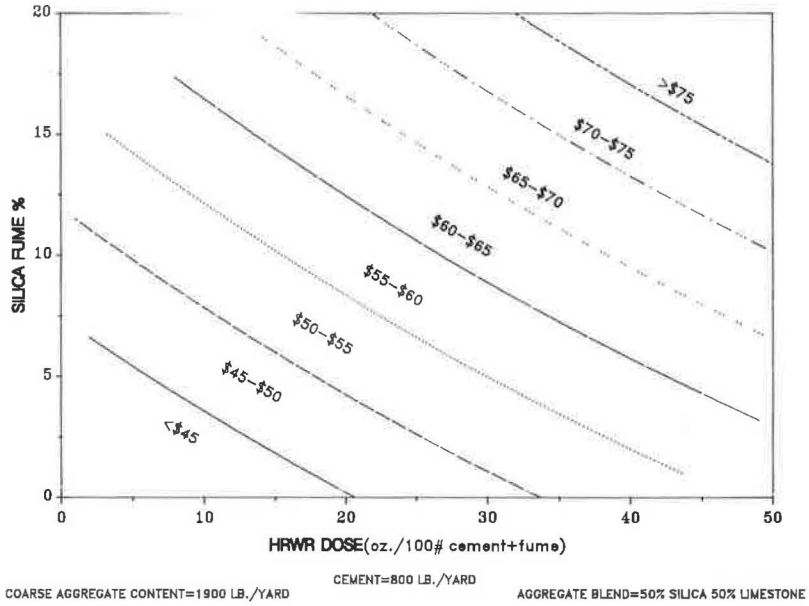

FIGURE 8 Contour plot showing the relationship between raw material cost ($/yd) as a function of silica fume percent and high-range water reducer dosage.

strength is a random variable with a certain level of variance. Consequently, the values contained inside the strength contour bands are predicted values based on the statistical model. Therefore, as stated earlier, it is important to test the recommended mixture proportions to confirm that the desired performance is met.

For this example, it was demonstrated that a graphical approach combined with statistical methods provided a simple solution to a rather complex problem. For more complicated scenarios, a graphical approach would have to be supplemented by an optimization program that would iterate through each of the independent variables.

SUMMARY

The following steps should be taken to optimize high-strength concrete mixes:

1. Discuss specific study objectives,
2. Determine response variables and the experimental region,
3. Develop the experimental design,
4. Conduct the experiment and collect the data,
5. Screen and analyze the data,
6. Build and check statistical models,
7. Create an optimization program,
8. Make mix recommendations, and
9. Test mix recommendations in full-scale batches.

It has been shown how the statistical procedures can facilitate a difficult job. Good analysis coupled with well-chosen graphs can elucidate patterns in the data that would otherwise not be recognized. Sound statistical practices can indeed maximize performance while minimizing cost.

ACKNOWLEDGMENT

The authors wish to acknowledge with thanks the very helpful work of James R. DelGado, manager, for supervising the data collection, and his staff for their diligent work.

REFERENCES

1. *Concrete Fundamentals and Proportioning*. Master Builders. Cleveland, Ohio, 1980, pp. 5–8.
2. N. L. Howard and D. M. Leatham. The Production and Delivery of High-Strength Concrete. *Concrete International*, April 1989, p. 27.
3. State-of-the-Art Report on High-Strength Concrete. *ACI Manual of Concrete Practice*, ACI 363R-84, American Concrete Institute, Detroit, Mich.
4. G. E. P. Box, J. S. Hunter, and W. G. Hunter. *Statistics for Experimenters*. John Wiley & Sons, Inc., New York City, 1978, p. 103.
5. Standard Practice for Selecting Proportions for Normal, Heavyweight, and Mass Concrete; Structural Lightweight Concrete; No-Slump Concrete. In *ACI Manual of Concrete Practice*, ACI 211.1, 211.2, 211.3. American Concrete Institute, Detroit, Mich.

Publication of this paper sponsored by Committee on Mechanical Properties of Concrete.

Long-Term Outdoor Exposure Evaluation of Concrete Slabs Containing Epoxy-Coated Reinforcing Steel

WILLIAM T. SCANNELL AND KENNETH C. CLEAR

Corrosion characteristics of straight epoxy-coated reinforcing steel (which met AASHTO and ASTM specifications) in concrete were studied. Specimens were exposed outdoors in a northern environment for more than 6.5 years, including about 3.1 years of salting cycles with a 3 percent sodium chloride solution. Straight epoxy-coated bars were evaluated when they were used in both mats and when they were used in the top mat only. An additional study variable was the use of uncoated bars in both mats. Results indicated that epoxy-coated rebars are many times more resistant to corrosion-induced damage than uncoated bars when embedded in salt-contaminated concrete and coupled to coated or uncoated bars in salt-free concrete. Overall best performance was achieved when the bars in both mats were epoxy coated. An observed softening of the coating in top- and bottom-mat bars after long-term exposure in the highly alkaline environment is also discussed.

For more than a decade, epoxy-coated reinforcing steel has been effective in reducing or preventing chloride-induced corrosion in bridges and other concrete structures. Widespread acceptance of this technology is exemplified by the current use of epoxy-coated bars in most state highway bridges (*1*). An evaluation of 22 Pennsylvania bridge decks with epoxy-coated reinforcing steel and black (uncoated) steel indicated good performance through 10 years of service (*2*). Although 4 of the 11 decks with uncoated bars showed corrosion-induced concrete deterioration, none of the 11 decks constructed with epoxy-coated bars showed any visual signs of corrosion-induced deterioration.

The widespread use of epoxy-coated reinforcing steel and the excellent field performance in deicing-salt environments are not surprising. It is well known that corrosion of reinforcing steel in concrete (excluding that associated with carbonation) requires sufficient chloride ions, oxygen, and moisture at the steel surface. One therefore can prevent or retard corrosion by eliminating one or more of these factors. Early research by the National Bureau of Standards (NBS) and the Federal Highway Administration (FHWA) indicated that reinforcing bars, coated with select powdered epoxies by an electrostatic spray process after bar cleaning, performed well in salt-contaminated concrete (*3,4*). Such coated rebars were resistant to high rates of corrosion and thus early-age deterioration of the surrounding concrete because the pressures generated by expansive corrosion products were minimized. The primary advantage of an epoxy coating is that it acts as a barrier that prevents chloride ions from reacting at the steel surface. Further, by increasing the electrical resistance between neighboring coated steel, an epoxy coating reduces the magnitude of macroscopic corrosion cells responsible for extensive early bridge deck deterioration (*5*).

Kenneth C. Clear, Inc., 201 Davis Drive, Unit GG, Sterling, Virginia 22170.

Laboratory studies generally concur that epoxy-coated reinforcing steel in concrete contaminated by chloride is superior to bare reinforcing steel in preventing corrosion (*3–6*). It was further determined that epoxy-coated reinforcement was most successful if all the reinforcement was coated as compared with only the upper mat steel and the black lower mat steel (*5,6*). Quality control during the coating application process and subsequent handling of the fabricated bars is of the utmost importance. Strict adherence to ASTM A 775 and AASHTO M 284 specifications is required to effectively use epoxy-coated steel to prevent or reduce the damaging effects of chloride-induced corrosion.

Despite positive laboratory and field performance studies, however, premature corrosion-related deterioration has recently been observed on several bridge substructures incorporating epoxy-coated reinforcement. These structures are located in the Florida Keys and were constructed 6 to 9 years ago (*1,7*). Many field and laboratory investigations are being conducted to determine the cause of the unexpected corrosion (*8,9*).

To address the overall performance of epoxy-coated reinforcing steel in salt-contaminated concrete, the results of a more than 6.5 year, outdoor exposure, comparative study of coated and uncoated reinforcing steel are presented.

EXPERIMENTAL PROCEDURE

Ten 1- × 2-ft concrete slabs, 6-in. thick, were fabricated in September 1982. The slab design is shown in Figure 1. Nine of the slabs were reinforced with four 30-in.-long bars on the top level and six 30-in.-long bars on the bottom level. The remaining slab was unreinforced. Of each bar, 24 in. is embedded in the slabs, with the remainder extending from the two edges. No connections between bars are present inside the concrete. This setup facilitates external connection of the top bars separately from the bottom bars and the subsequent monitoring of the corrosion current flowing between the mats. Earlier FHWA research indicated that such macroscopic corrosion cells, in which a macrocathode on the bottom-mat rebar in salt-free concrete drives corrosion of uncoated top-mat steel in salty concrete, are primarily responsible for rapid corrosion-induced deterioration (*4*).

Reinforcing steel (No. 5, Grade 60) from one production lot was used for all slabs. A portion of the bars was epoxy coated, using Scotchkote 214, in accordance with Maryland Department of Transportation, AASHTO M 284-81, and ASTM D 3963-81 specifications. The bars were plant-coated as part of a normal field production run (i.e., no special coating or handling was used). The coated and uncoated bars were chosen randomly from the production lot for use in each slab. Before being cast in concrete, coated bars were evaluated for coating thickness and number of holidays and cut areas. Coating thickness was measured (using a Mikrotest Model II thumbwell magnetic gauge calibrated according to National Bureau of Standards guidelines) at three locations on each side of each bar along the portion that was to be embedded in concrete. The number of holidays and cut areas was determined using a 67.5-volt Tinker-Rasor Model M-1 holiday detector. The concrete used for all slabs complied with 1982 Virginia Department of Highways specifications for high-quality bridge deck concrete, except that a higher-than-normal air content was used as additional insurance against deicer scaling. Table 1 provides details on this concrete mix design, which exhibited a water-to-cement ratio of 0.42. Clear concrete cover over the top-mat reinforcing steel was 1.0 in. Slab fabrication was accomplished from one 2.5-yd³ ready-mix batch. The slabs were then cured for 7 days using wet burlap and polyethylene.

Three groups of three slabs each were fabricated with the following variables:

- Epoxy-coated bars in both mats;
- Epoxy-coated bars in the top mat and black steel (uncoated) bars in the bottom mat; and
- Black steel bars in both mats.

An additional unreinforced slab was also included.

After fabrication and curing, reinforcement in each slab was made electrically continuous using external wiring, and the top and bottom mats were connected through a resistor and switch to monitor the macrocell corrosion current [flowing between the top (anode) and bottom (cathode) rebar] and the AC resistance between the rebar mats in the uncoupled mode (see Figure 1). The sides of each slab and all exposed steel were then coated with epoxy and ½-in. diameter holes were drilled to a 3-in. depth in each slab to measure bottom-mat electrical half-cell potential. To introduce chloride at the level of the top steel, dams were placed around the top surface

TABLE 1 CONCRETE MIX DESIGN

Cement (Portland Type I, ASTM C150)	635 lbs/cu yd
Coarse aggregate (Crushed limestone)	1928 lbs/cu yd
Fine aggregate (silica sand)	1146 lbs/cu yd
Water reducing/retarding agent (Daratard 17, ASTM C494)	13.5 oz/cu yd
Water	268.5 lbs/cu yd
Slump	4 inches
Air content (Admixture Daravair, ASTM C494)	9.5%
Water/cement ratio	0.42

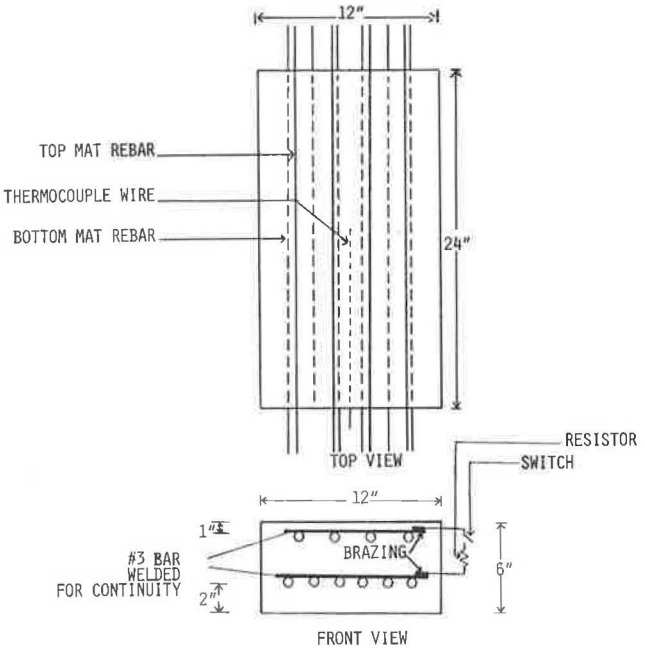

FIGURE 1 Specimen design.

of each slab for salt ponding. The surface around the bottom-mat potential wells was built up using plastic pipe and polymer mortar to prevent salt solution from entering the holes.

From initial testing in November 1982 through December 1985—3.1 years—all slabs were subjected to weekly exposure cycles of 3 days of ponding with a 3 percent sodium chloride solution followed by 4 days of natural weathering with the solution removed. At select intervals, chloride content versus depth was determined on the unreinforced slab according to AASHTO T-260. Salting was terminated in December 1985 because large quantities (more than 10 lb/yd³) of chloride were present at the top rebar level. The dams on the slab surfaces were then removed and subsequent exposure was to natural weathering only. A bar graph showing rebar level chlorides defined at various times during the salting cycles is presented in Figure 2.

The results represent an exposure period of more than 6.5 years. The corrosion characteristics of the slabs were periodically monitored using macrocell corrosion current measurements, AC electrical resistance measurements (between the rebar mats when uncoupled), and top- and bottom-mat electrical half-cell potentials. In addition, concrete temperature was recorded with each data set. The macrocell corrosion current for each slab was measured as the voltage drop across the resistor installed between the rebar mats.

Throughout the test period the slabs were exposed above ground at the Kenneth C. Clear, Inc. outdoor exposure facility located in Herndon, Virginia, a suburb of Washington, D.C. Following the exposure period, a full-depth core was obtained from one slab representing each variable. Each core contained a portion of the top and bottom steel. The cores were saw cut and split open to expose the bars. Visual examinations were then conducted to determine relative corrosion activity and to investigate any physical changes in the epoxy coating.

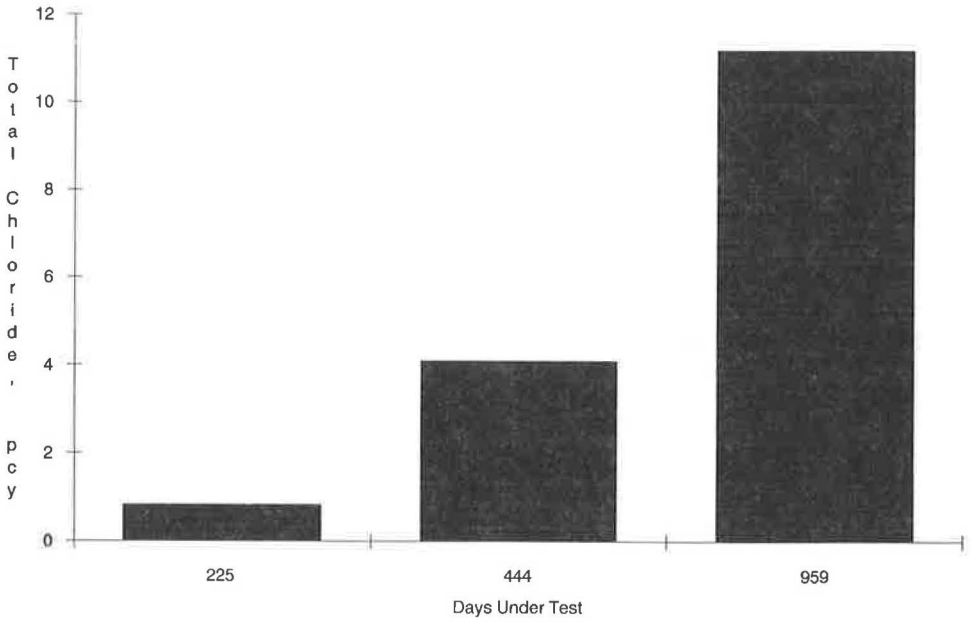

FIGURE 2 Rebar level chloride versus time.

RESULTS AND DISCUSSION

Coating thickness measurements, obtained before casting at three locations on each side of each bar along the portion that would be embedded in concrete (i.e., 24 measurements for each top mat and 36 measurements for each bottom mat), are summarized in Table 2. The average coating thickness was 9.9 mils with a range of 4.1 to 21.5 mils.

Table 3 presents the total number of holidays and cut areas on each mat of coated rebar. There are four bars in each top mat (8 lineal ft) and six bars in the bottom mat (12 lineal ft). The top mat average was 3.5 holidays and cut areas per lineal ft of bar and the bottom mat average was 2.7, for an overall average of 3.3. Most were, of course, not visible to the unaided eye.

The macrocell corrosion current parameter is a direct measure of the electrons released by the macrocell corrosion process and therefore provides a direct measure of macrocell corrosion activity. Microcell corrosion (i.e., anodes and cathodes are present on the same bar with corrosion activity but no current flows between the mats) probably occurs also, but macrocell corrosion has been reported as the main cause of rapid corrosion-induced deterioration. Also, corrosion current is dependent on concrete temperature, primarily because of the effect of temperature on resistance. Therefore, all macrocell corrosion current and mat-to-mat resistance data were adjusted to 70°F equivalents using the known resistance of the current shunt, concrete temperature at measurement, and formulas provided by Clear (*10*).

Figures 3 and 4 present the average adjusted (i.e., 70°F) macrocell corrosion current versus time for the three variables studied. For epoxy-coated bars in both mats (Figure 3), the average corrosion current was zero or negligible (less than 10 μA) for the test duration (overall average was 0.61 μA). Slabs with epoxy-coated bars in the top mat only (Figure 3) started with zero corrosion current and after about 0.4 year of salting, variable but very low corrosion currents were measured (overall average was 3.23 μA). Slabs with black steel in both mats (Figure 4) began to show measurable corrosion currents 0.2 year into the study. After 1.2 years of salting, corrosion currents increased drastically, averaging 886.87 μA through 3.7 years. Values were frequently more than 40 times the maximum current measured in the slabs with epoxy-coated bars in the top mat only and more than 100 times that for the slabs with epoxy-coated bars in both mats. Macrocell currents remained at high levels through the remaining test period,

TABLE 2 COATING THICKNESS

Slab Number	Variable	Coating Thickness, mils: Top Mat Ave.	Top Mat Range	Bottom Mat Ave.	Bottom Mat Range
1	Epoxy Both Mats	12.8	5.1 to 21.5	10.2	5.4 to 19.5
2	Epoxy Both Mats	12.2	8.0 to 19	10.1	7.2 to 17.5
3	Epoxy Both Mats	9.2	5.0 to 16	9.5	4.8 to 15.5
4	Epoxy Top Only	9.5	6.0 to 15.5	--	--
5	Epoxy Top Only	8.6	4.3 to 13	--	--
6	Epoxy Top Only	7.3	4.1 to 12	--	--
	All Epoxy Coated	9.9	4.1 to 21.5	9.9	4.8 to 19.5

TABLE 3 HOLIDAYS AND CUT AREAS

Slab Number	Variable	Total Holidays And Cut Areas: Top Mat	Bottom Mat
1	Epoxy Both Mats	22	34
2	Epoxy Both Mats	8	35
3	Epoxy Both Mats	35	29
4	Epoxy Top Mat Only	30	--
5	Epoxy Top Mat Only	31	--
6	Epoxy Top Mat Only	55	--
48	Epoxy Top Mat Only	17	--

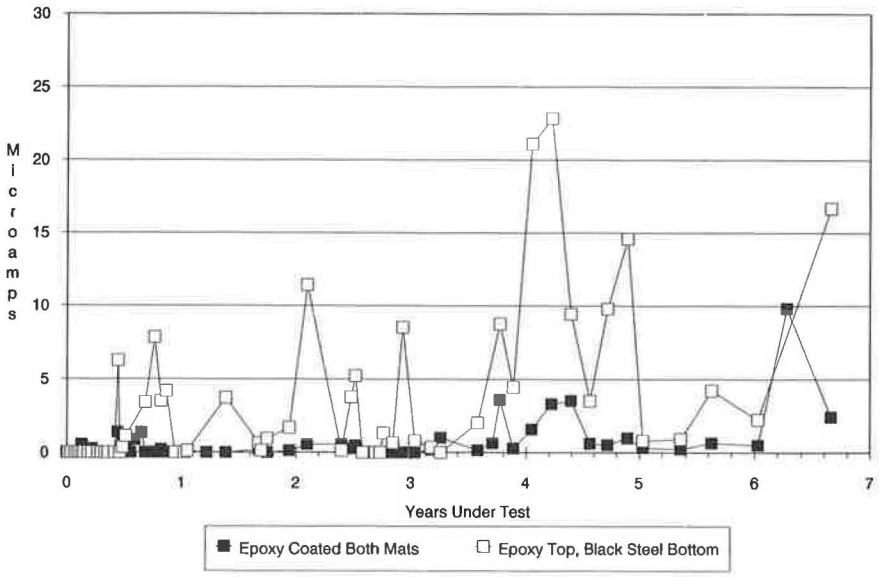

FIGURE 3 Average macrocell corrosion current (70°F) versus time.

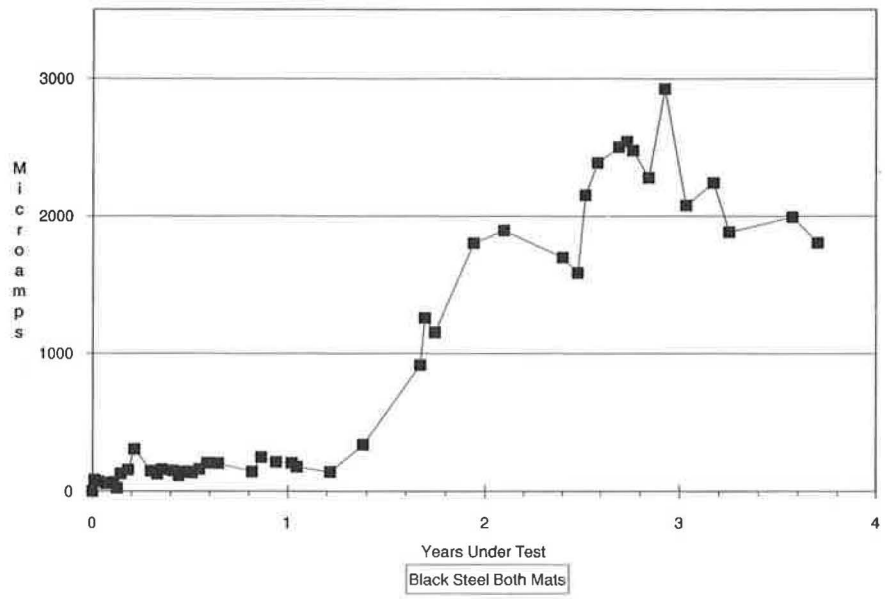

FIGURE 4 Average macrocell corrosion current (70°F) versus time.

although a decreasing trend was seen after about 3.7 years of testing as severe corrosion-induced cracking allowed chloride access to the bottom steel. These data support the results reported by Clear et al. (*5*) on nonspecification epoxy-coated bars in concrete with a higher water-to-cement ratio. They concluded that epoxy-coated reinforcing steel in salty concrete should be significantly more resistant to corrosion-induced concrete damage than uncoated steel. It was further reported that epoxy-coated bars perform best when all continuous bars are epoxy coated as compared with bars in one mat coated or bars in both mats uncoated (average corrosion current with bars in both mats uncoated was about 11 times greater than in the case of bars in the top mat only and 41 times greater than in the case of bars both mats coated).

Figure 5 plots the average adjusted mat-to-mat resistance versus time for the three cases studied. Both the slabs with epoxy-coated bars in the top mat only and in the top and bottom mats exhibited average resistances about two orders of magnitude higher than the slabs with black steel in both the top and bottom mats at the start of the test. Further, the slabs with epoxy-coated bars in the top mat and in both mats showed a marked increase in resistance with time. Overall test averages were 22 ohms for the slabs with the black steel bars in both mats, 2,151 ohms for the slabs with epoxy-coated bars in the top mat only, and 1,911 ohms for the slabs with epoxy-coated bars in both the top and bottom mats. These data indicate that (a) corrosion protection afforded by epoxy-coated reinforcing steel primarily results from its inherent

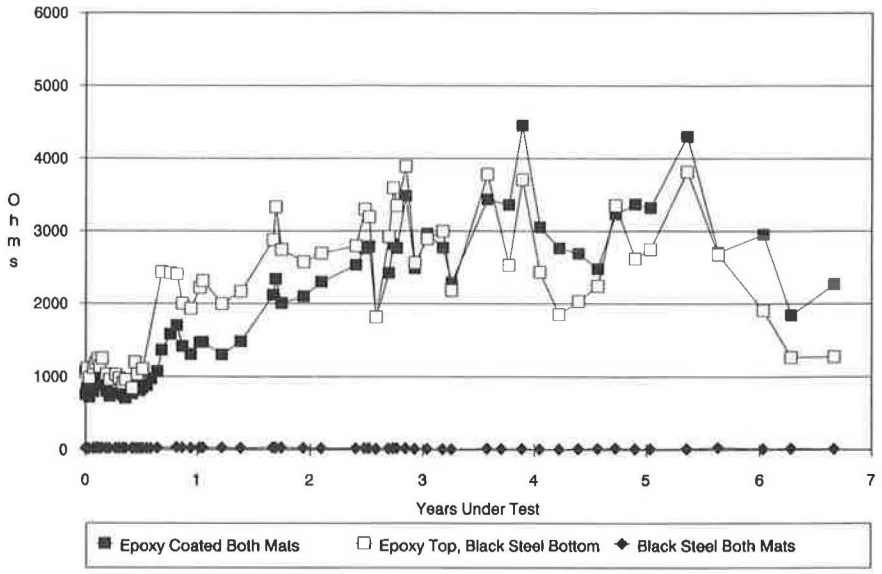

FIGURE 5 Average resistance (70°F) versus time.

effect on increasing the macrocorrosion cell resistive path, and (b) there is no observable tendency for the coating to deteriorate when embedded in salt-contaminated concrete in the long term (i.e., resistance did not decrease with time). Average top-mat potentials [millivolts copper-copper sulfate reference halfcell (CSE)] versus time and average potential differences (i.e., average bottom-mat potential minus average top-mat potential) versus time for the three variables evaluated are presented in Figures 6 and 7, respectively. For slabs with epoxy-coated rebars, the average top-mat potentials for years 1 through 6.66 were −226 mV for the epoxy top mat only slabs and −335 for the epoxy both mat slabs. During the middle portion of testing, epoxy both mats slabs showed average top-mat potentials in the range of −350 to −450 mV CSE. The average potential difference shows a general increase with time to values in the range of 200 mV (overall average for years 1 through 6 was 171 mV). However, as discussed previously, the macrocell corrosion currents have remained near zero. Thus, these data tend to support previous findings that, although corrosion will occur at small breaks in the coating once critical quantities of chloride penetrate, its magnitude is so low that significant iron consumption and tensile stresses high enough to crack the concrete will not occur for very long periods of time (*5*). Performance of the epoxy top mat only slabs has been similar to that of epoxy both mat slabs except that average top-mat rebar potentials are generally more positive in epoxy top mat only slabs. In the case when the bars in both mats were coated, more negative potentials were undoubtedly exhibited because of oxygen starvation (cathodic polarization), whereas such was not the case when the bottom mat was uncoated. Potential differences were similar throughout the test period (overall average for epoxy top

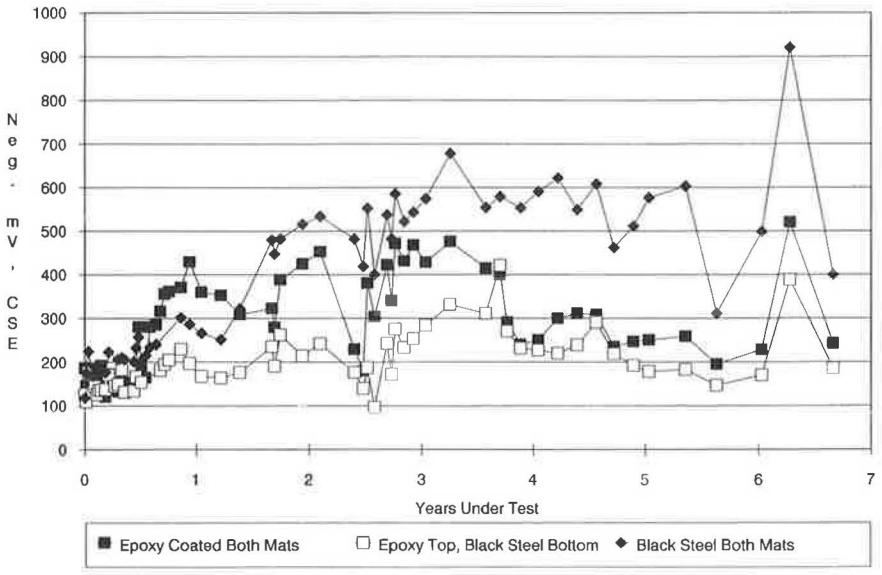

FIGURE 6 Average top mat potential versus time.

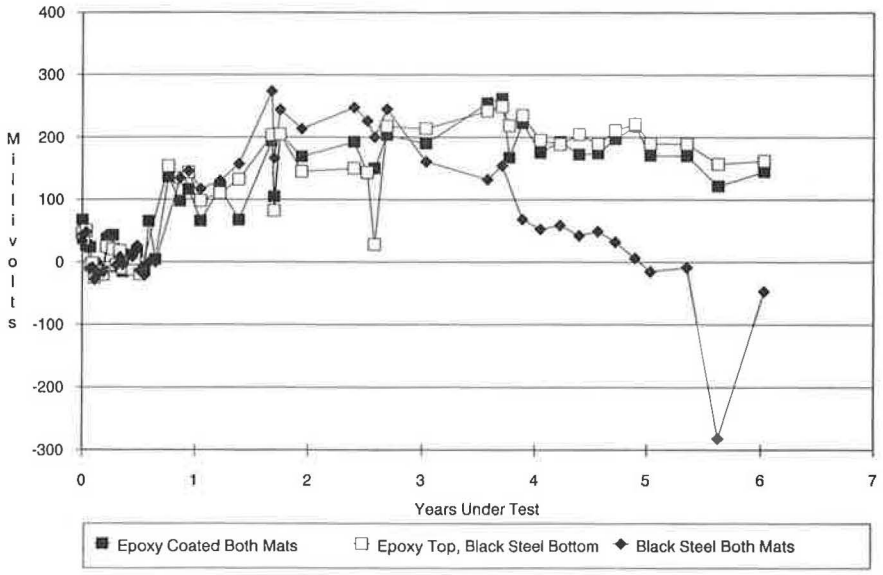

FIGURE 7 Average potential difference versus time.

mat only slabs for years 1 through 6 was 176 mV). Macrocell corrosion currents remained at low values throughout the test period, although at times they were about 5 to 10 times higher than the epoxy both mat slabs. Thus, these data indicate that specification epoxy-coated bars perform best when all bars are coated, although both variables (i.e., epoxy-coated bars in both mats and epoxy-coated bars in the top mat only) provide significantly enhanced resistance to corrosion-induced concrete damage as compared with uncoated steel (average top-mat potential and potential difference for years 1 through 3.7 was −486 and 191 mV, respectively). The decreasing trend in potential difference (average bottom-mat potential minus average top-mat potential difference) (Figure 7) for this variable was the result of corrosion activity on the bottom steel caused by chloride migration through large surface cracks. The formation of liquid corrosion product that does not lead to spalling is possible, particularly in a crevice or coating undercutting situation, although this was not seen on the full-depth cores as discussed in the following.

Figures 8 and 9 show the surface condition of each group of slabs after more than 6.5 years of outdoor exposure, including about 3.1 years of salt ponding. The *x*'s on the slab surfaces designate top-mat potential monitoring locations and the circular mounds on the slab surfaces represent the bottom-mat potential wells discussed previously. No surface cracking, staining, or other deterioration was found on any of the slabs containing epoxy-coated bars in both mats or epoxy-coated bars in the top mat only. However, extensive surface cracking and staining can be seen on the slabs containing black steel bars in both mats. Fine corrosion-induced cracking and minor staining were first observed on these slabs after only 0.9 year into the study.

Upon completion of the exposure period, full-depth cores representing each variable were obtained from one slab. These cores were then autopsied to determine the relative extent of corrosion-induced damage, if any, and the overall physical condition of the epoxy-coated bars. Figures 10 through 12 are photographs typical of those taken during autopsies. The top-mat steel in both the epoxy-coated both mats and epoxy top mat only situations exhibited similar results (Figures 10 and 11). There was no visible corrosion product at the rebar-concrete interface or beneath the coating (steel was bright and clean) when it was scraped off with a utility knife. No visible deterioration was observed on the coating itself; however, the coating was more easily removed from these specimens as compared with bar with a retained original coating that had never been embedded in concrete. Hence, the coating softened somewhat during exposure, but no obvious detrimental effects were discerned and there was no observed tendency for undercutting of the coating by corrosion. Similar results were found on the coated bottom-mat bar for the epoxy-coated both mats variable (Figure 10). Very minor corrosion was observed on the uncoated bottom bar in the epoxy top mat only situation (Figure 11).

Extensive corrosion product and section loss were observed on the top-mat steel representing the uncoated both mats variable (Figure 12). This was expected because of measured macrocell corrosion currents, half-cell potentials, and visual surface condition. Minor corrosion was found on the bottom-mat bar from the same variable.

CONCLUSIONS

The test program showed that straight specification epoxy-coated rebars are more resistant to corrosion-induced damage than uncoated bars when embedded in salt-contaminated concrete and coupled to coated or uncoated bars in salt-free concrete for over 6.5 years in an outdoor northern environment. Overall, best performance is achieved when the bars in both mats are epoxy coated. Active corrosion, as indicated by macrocell corrosion currents and half-cell potentials, occurred (presumably at small breaks in the coating) when the epoxy-coated bars were in the top mat only and when the bars in both mats were epoxy coated; however, the magnitudes of corrosion were so low (40 times lower than black

FIGURE 8 Surface condition after exposure. (Top: both mats coated; bottom: top mat only.)

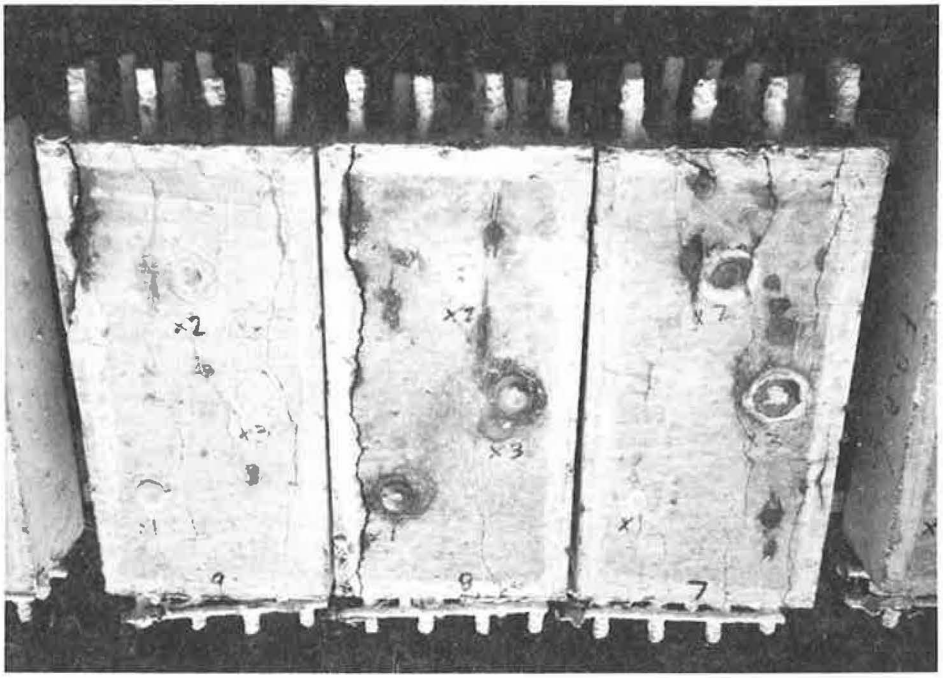

FIGURE 9 Surface condition after exposure (both mats uncoated).

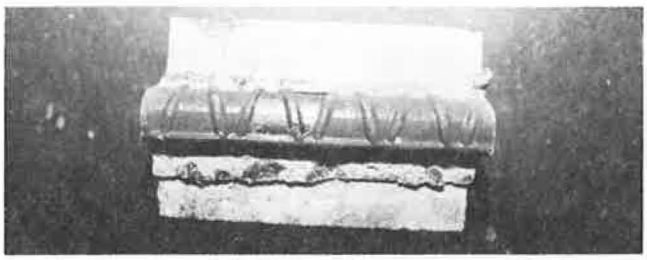

FIGURE 10 Autopsy photographs. (*Top*: top bar, epoxy-coated bars in both mats. *Middle*: bottom bar, epoxy-coated bars in both mats. *Bottom*: epoxy-coated rebar trace).

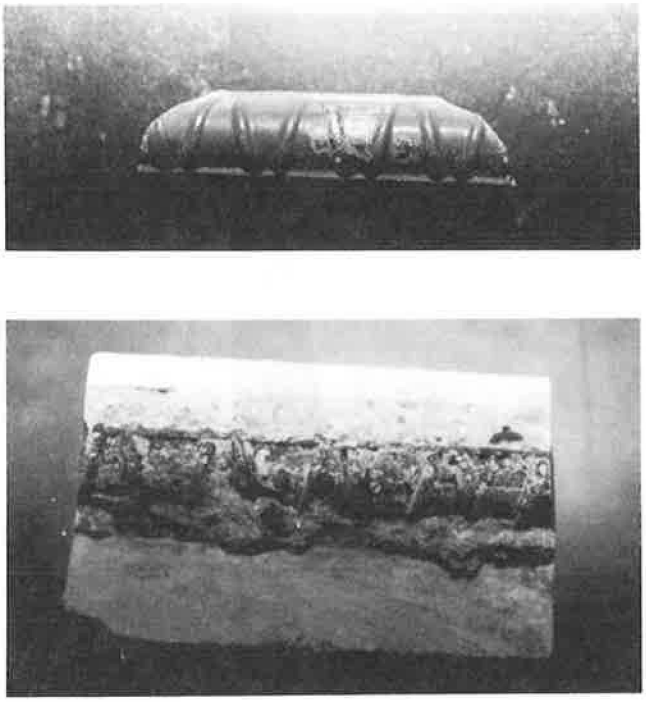

FIGURE 11 Autopsy photographs of slabs with epoxy-coated bars in top mat only. (*Top*: top bar. *Bottom*: bottom bar.)

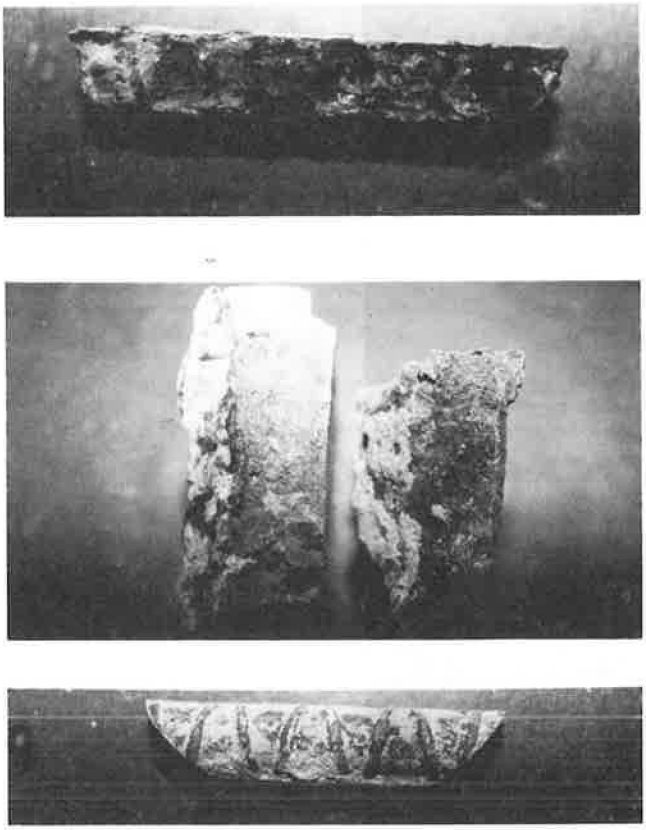

FIGURE 12 Autopsy photographs of slabs with black steel (uncoated) bars in both mats. (*Top*: top bar. *Middle*: top rebar trace. *Bottom*: bottom bar.)

steel in both mats for the slabs with coated bars in one mat and 100 times lower for the slabs with coated bars in both mats) that significant iron consumption and tensile stresses high enough to crack the concrete would not be expected for extended periods of time.

Some softening of the epoxy coating in top- and bottom-mat bars was found but no detrimental effect of the softening (i.e., no undercutting or rusting beneath the coating) or reduction in electrical resistance was noted. Future research should investigate physical and chemical changes that occur on the coating when exposed to a high-alkaline environment with oxygen and moisture present for extended periods.

Findings in this study concur with previous studies by NBS, FHWA and others, but conflict with statements in Florida Department of Transportation reports that concrete with epoxy-coated rebars is less resistant to corrosion damage than that with uncoated rebars.

ACKNOWLEDGMENT

This work was supported by the Concrete Reinforcing Steel Institute.

REFERENCES

1. D. P. Gustafson. Epoxy Update. *Civil Engineering*, Vol. 58, No. 10, 1988, pp. 38–41.
2. R. E. Weyers and P. D. Cady. Deterioration of Concrete Bridge Decks from Corrosion of Reinforcing Steel. *Concrete International*, Vol. 9, No. 1, 1989, pp. 15–20.
3. J. R. Clifton, H. F. Beeghly, and R. G. Mathey. *Nonmetallic Coatings for Concrete Reinforcing Bars*, Report FHWA-RD-74-18. FHWA, U.S. Department of Transportation, Feb. 1974.
4. K. C. Clear and Y. P. Virmani. *Research Update: Methods and Materials*. National Association of Corrosion Engineers, Sept. 1982.
5. K. C. Clear and Y. P. Virmani. *Corrosion of Non-Specification Epoxy-Coated Rebars in Salty Concrete*. Paper No. 114, Corrosion 83 (Anaheim, April 1983), National Association of Corrosion Engineers, Houston, Tex., 1983.
6. Y. P. Virmani, K. C. Clear, and T. J. Pasko Jr. *Time-to-Corrosion of Reinforcing Steel in Concrete Slabs*, Vol. 5: *Calcium Nitrite Admixture or Epoxy-Coated Reinforcing Bars as Corrosion Protection Systems*. Report FHWA-RD-83-012. FHWA, U.S. Department of Transportation, Sept. 1983.
7. R. Powers and R. Kesler. *Corrosion Evolution of Substructure, Long Key Bridge*. Corrosion Report 87-9A. Florida Department of Transportation, Gainesville, 1987.
8. R. Powers. *Corrosion of Epoxy Coated Rebars, Keys Segmental Bridges*. Corrosion Report 88-AA. Florida Department of Transportation, Gainesville, 1987.
9. A. M. Zayed, A. A. Saugues, and R. G. Powers. *Corrosion of Epoxy Coated Reinforcing Steel in Concrete*. Paper No. 379, Corrosion 89 (New Orleans, April 1989), National Association of Corrosion Engineers, Houston, Tex., 1989.
10. K. C. Clear. *Time-to-Corrosion of Reinforcing Steel in Concrete Slabs*, Vol. 4: *Galvanized Reinforcing Steel*. Report FHWA-RD-82-028, FHWA, U.S. Department of Transportation, Dec. 1981.

Publication of this paper sponsored by Committee on Performance of Concrete.

Penetrating Sealers for Concrete: Survey of Highway Agencies

DAVID WHITING

A survey on the use of penetrating sealers for portland cement concrete was conducted by distributing questionnaires to all U.S. and several Canadian highway agencies. Information was obtained on applications of penetrating sealers, extent of use, qualification of sealers and test procedures used, and problems of application and performance. Although the survey results indicated much interest by highway agencies in using penetrating sealers, applications are limited. Linseed oil is widely used in many localities. Results also indicated that test procedures used to qualify sealers vary widely among agencies, with some agencies relying on data supplied by vendors or on results of testing carried out by other organizations. There is currently little activity related to in-place field testing of penetrating sealers.

It is generally accepted that the ingress of sufficient amounts of moisture and chloride salts into portland cement concrete structures leads to corrosion of reinforcing steel and eventual degradation of the reinforced concrete. This problem has led to the development of various approaches to reduce or eliminate the ingress of chlorides and moisture into concrete. These include the use of waterproofing membranes, rigid cementitious overlays, polymer overlays, and various coatings and sealants (*1–3*). Membranes and overlays, although effective in many cases, are engineered systems that require considerable construction detailing and relatively high labor installation costs. Many of the available coatings may not be applicable to wearing surfaces. Although linseed oil-based materials have been used to seal concrete surfaces, their use has diminished recently because of their effects on surface color and reflectance of concrete and the need for frequent reapplication. The introduction of new types of sealers, commonly referred to as "penetrating sealers," has generated considerable interest as a relatively inexpensive and easy means of prolonging the life of reinforced concrete structures (*4,5*). The survey described in this paper aimed at developing current (1989) information on the use and application of penetrating sealers by highway agencies in the United States and Canada.

OBJECTIVES AND SCOPE

The survey described in this paper had the following objectives: (a) update information on extent of use of penetrating sealers, (b) delineate the major application areas for sealers, (c) obtain information on testing procedures used by highway agencies in qualifying penetrating sealers, and (d) note problems commonly occurring in application and performance of sealers. A questionnaire was the primary source of this information. In addition, reports submitted by the agencies surveyed, data from published literature, and follow-up calls were used to develop further information.

Construction Technology Laboratories, Inc., 5420 Old Orchard Road, Skokie, Ill. 60077.

QUESTIONNAIRE AND RESPONSES

A questionnaire about the use of penetrating sealers for concrete was sent to all U.S. and 11 Canadian highway agencies. The questionnaire was primarily composed of simple yes or no and multiple category questions. In a few cases, those surveyed were asked to supply copies of documentation, such as specifications, test procedures, and lists of products and approved vendors. In addition, respondents were given the opportunity to discuss any problems they had experienced with either the application or performance of penetrating sealers.

Responses were received from all agencies surveyed. Of the respondents, four U.S. and two Canadian agencies had not used penetrating sealers. Surveys from these agencies were not included in tabulations. The data base, therefore, consists of 46 U.S. and 9 Canadian highway agencies.

Responses to questions about use, applications, and qualifications of penetrating sealers are summarized in Table 1. Responses to questions concerning test procedures and problems are summarized in Table 2. Although U.S. and Canadian responses are presented as separate tables, statistics were developed on the responses of the 55 agencies combined.

DISCUSSION OF RESULTS

Extent of Use

The current use of penetrating sealers and linseed oil is summarized in Table 3. The categories listed (extensive, moderate, limited, and experimental) did not represent specific numbers or percentages of structures in any state or province, but simply represented the perceived use of such materials by the respondent's agency. The number of agencies claiming extensive use of linseed oil is greater than the number claiming extensive use of penetrating sealers. Most agencies are using penetrating sealers on a limited or experimental basis. Four agencies have recently discontinued use of linseed oil and two have discontinued use of penetrating sealers. Two of the agencies that discontinued use of linseed oil had used it extensively in the past. One of the agencies that discontinued use of penetrating sealers had used it extensively in the past, and

TABLE 1 SUMMARY OF RESPONSES—USE, APPLICATIONS, AND QUALIFICATIONS

STATE	EXTENT OF USE	APPLICATIONS	QUALIFICATION	PRODUCT LIST
AL	Lim.-L.O.	Decks	Prescription	NO
AR	Mod.-L.O./Exp.	Decks	Prescription	NO
CA	Ext.-L.O./Lim.	Decks,beams,piers,caps,appurtenances, barriers	Internal testing, vendor data	YES
CO	Lim.	Decks,sidewalks	Prescription	NO
CT	Mod.	Decks,appurtenances,barriers	Vendor data	YES
DE	Lim.	Decks,piers,caps,barriers,appurtenances	Vendor data	NO
FL	Lim.	Decks,beams,piers,caps,appurtenances	Internal testing ,vendor data	YES
GA	Ext.-L.O.	Decks	Prescription	YES
I D	Lim.-L.O.	Decks	Internal/external testing	NO
I L	Mod-L.O./Lim.	Decks,piers,caps,barriers appurtenances,pavements	Vendor data	YES
IN	Exp.	Decks	Internal testing	YES
I A	Mod.	Piers,caps,curbs,gutters	Internal testing	YES
KS	Ext.	Decks, appurtenances	Internal testing	YES
KY	Lim.	Decks	Vendor data	YES
LA	Exp.	Decks	Experimental only	NO
ME	Ext.-L.O./Lim.	Decks,piers,caps,barriers,appurtenances	Vendor and other data	NO
MD	Lim.-L.O.	Decks	Internal testing	NO
MA	Mod.	Appurtenances,barriers	Internal testing	YES
M I	Ext.-L.O./Lim.	Decks(L.O.),Piers	Internal/external testing	YES
MN	Exp.	Decks,barriers	Experimental only	YES
MO	Ext.-L.O.	Decks,barriers,appurtenances	Internal testing	NO
MT	Mod.-L.O.	Decks,beams,appurtenances	Internal/external testing	NO
NE	Mod.	Decks	Internal testing,prescription	YES
NV	Exp.	Decks	Experimental only	NO
NH	Ext.	Beams,piers,caps,walls,appurtenances, barriers	External testing, vendor data	YES
NJ	Exp.	Decks	Internal testing,prescription	YES
NM	Ext.	Decks,beams,caps,appurtenances	Internal testing,vendor data	YES
NY	Mod.	Decks,piers,caps,appurtenances,barriers	Internal testing	YES
NC	Ext.-L.O./Lim.	Decks,appurtenances	Certification	NO
ND	Ext.-L.O./Lim.	Decks	Internal testing	YES
OH	Mod.	Beams,appurtenances	Vendor data	YES
OK	Ext.	Decks,piers,appurtenances	Internal testing	YES
OR	Lim.	Beams,piers,caps,appurtenances	External testing,vendor data	YES
PA	Lim.	Decks,piers,caps,barriers	Internal testing	YES
R I	Lim.	Appurtenances	Internal testing	YES
SC	Mod.-L.O.	Decks	Prescription	NO
SD	Ext.-L.O.	Decks	Internal testing,prescription	YES
TN	Lim.	Decks	Internal testing	NO
TX	Ext.-L.O.	Decks	Prescription	NO
UT	Exp.	Decks,piers,barriers,appurtenances	Experimental only	YES
VT	Ext.-L.O./Exp.	Piers,caps,barriers,appurtenances	Internal testing	NO
VA	Lim.	Decks,appurtenances,pavement	Internal testing	YES
WA	Exp.	Decks,beams,piers,caps	External testing	NO
WV	Ext.	Decks,beams,appurtenances	Vendor data	YES
W I	Ext.	Decks	Internal testing	YES
WY	Mod./Lim.	Pavement/decks	Internal testing,vendor data prescription	YES

PROVINCE	EXTENT OF USE	APPLICATIONS	QUALIFICATION	PRODUCT LIST
AB	Ext.	Decks,beams,piers,appurtenances	External testing,vendor data	YES
BC	Ext.	Decks, appurtenances	Internal testing, vendor data	YES
MB	Lim.	Decks, curbs	Vendor data,prescriptipn	NO
NB	Lim.	Decks, appurtenances	Internal/external testing	NO
NS	Lim.	Decks,barriers	Internal testing	NO
ON	Lim.	Beams,barriers	Internal testing	YES
QE	LIm.	Piers,barriers,appurtenances	Internal testing	YES
SK	Lim.	Decks,barriers,appurtenances	AB DOT data	YES
YT	Lim.	Decks,appurtenances	By recommendation	NO

Note-Use categories abbreviated as follows:

Ext.-Extensive use.
Mod.-Moderate use.
Lim.-Limited use.
Exp.-Experimental use only.
L.O.-Use category refers to linseed oil only (i.e. Mod.-L.O.)

TABLE 2 SUMMARY OF RESPONSES—TEST PROCEDURES AND PROBLEMS

STATE	TEST PROCEDURES USED	PROBLEMS		FIELD TESTS
		APPLICATION	PERFORMANCE	
AL	not tested routinely	NO	NO	NO
AR	AASHTO M233-L.O.	NO	NO	NO
CA	NCHRP 244,absorption	YES	n/a	NO
CO	not tested routinely	YES	YES	NO
CT	rely on vendor test data	NO	NO	NO
DE	rely on vendor test data	NO	NO	NO
FL	Impressed current	YES	NO	YES-Chloride sampling
GA	ASTM D260-L.O.	n/a	Questionable	NO
ID	NCHRP 244,pen.depth, vapor perm,skid no.	n/a	n/a	NO
IL	NCHRP 244, ASTM C 672	NO	NO	NO
IN	Field evaluation	NO	YES	YES-long term sampling
IA	AASHTO T259	NO	NO	NO
KS	ASTM C 642, AASHTO T259	YES	YES	YES-Chloride sampling
KY	rely on vendor test data	n/a	n/a	NO
LA	not tested routinely	NO	YES	YES-Chloride sampling
ME	rely on vendor and other DOT data	NO	NO	NO
MD	only use L.O.	YES	n/a	NO
MA	similar to NCHRP 244	NO	NO	YES-visual inspection
MI	AASHTO T 259	NO	NO	NO
MN	Field evaluations	YES	YES	YES-Chloride sampling
MO	ASTM C 672,C 642,AASHTO T 259	NO	NO	NO
MT	L.O. recently eliminated from specs.	n/a	n/a	NO
NE	AASHTO T 259	YES	NO	YES-Chloride sampling
NV	not tested routinely	NO	Unknown	YES-Chloride sampling
NH	NCHRP 244	NO	NO	NO
NJ	Saline absorption	NO	NO	YES-visual scale ratings
NM	ASTM C642, AASHTO T 259	NO	NO	NO
	OK DOTpen. depth,vapor perm			
NY	similar to NCHRP 244	NO	NO	NO
NC	not tested routinely	YES	YES	NO
ND	ASTM C642, AASHTO T 259	NO	NO	NO
	OK DOT pen. depth,vapor perm			
OH	rely on vendor test data	NO	NO	NO
OK	ASTM C642, AASHTO T 259	NO	NO	YES-water flood and
	pen. depth,vapor perm			observe
OR	NCHRP 244,ALB&FL tests	NO	NO	NO
PA	AASHTO T 259	n/a	n/a	NO
RI	Chloride intrusion	NO	Unknown	NO
SC	not tested routinely	n/a	Questionable	NO
SD	used as curing compounds only	YES	n/a	NO
TN	AASHTO T 259	n/a	n/a	NO
TX	not tested routinely	NO	NO	NO
UT	Freeze-thaw test	Unknown	Unknown	NO
VT	AASHTO T259(modified),absorption	NO	YES	YES-Chloride sampling
VA	ASTM C 666, AASHTO T 277	YES	YES	YES-field cores
WA	NCHRP 244	NO	YES	NO
WV	rely on vendor test data	NO	NO	NO
WI	AASHTO T 32, T 259, FL test	NO	n/a	YES-field cores
WY	ASTM C 642, OK DOT vapor prem,	NO	YES	YES
	pen. depth			

Note: L.O.- Linseed oil.

STATE	TEST PROCEDURES USED	PROBLEMS		FIELD TESTS
		APPLICATION	PERFORMANCE	
AB	Water absorption	NO	NO	NO
BC	AB and OK DOT test procedures	YES	n/a	NO
MB	rely on vendor test data	NO	NO	NO
NB	n/a	NO	YES	YES-water flood
NS	n/a	NO	YES	NO
ON	Water/saline absorption,ASTM C672	NO	YES	NO
	AASHTO T277			
QE	similar to NCHRP 244	YES	n/a	NO
SK	rely on AB DOT test data	NO	NO	NO
YT	not tested routinely	unknown	unknown	NO

TABLE 3 EXTENT OF USE OF PENETRATING SEALERS AND LINSEED OIL

Extent of Use	Number of Agencies	
	Penetrating Sealers	Linseed Oil
Extensive	7	9
Moderate	7	4
Limited	23	3
Experimental	9	0

discontinued use because of the sealer's apparent inability to reduce chloride ion infiltration into bridge decks.

Application Areas

As presented in Figure 1, the most widely used application of penetrating sealers is on concrete bridge decks.

This is an extremely interesting and significant statistic. Perhaps the most influential report on the performance of penetrating sealers, NCHRP Report 244 (*7*), states in its foreword, "The research concentrated on the protection of structural elements *other* than the top surface of the bridge deck." Indeed, the need for efficient and cost-effective means to protect non-wearing surfaces and substructural elements of bridges was the main impetus for funding the project under which NCHRP Report 244 was written. It was acknowledged that systems that provide adequate wearing surfaces (such as membranes and rigid overlays) were already available for protection of bridge decks, but could not be practically applied to substructures. However, it appears that aggressive marketing of penetrating sealers has lead to their increased use on wearing surfaces, although NCHRP Report 244 did not include abrasion subsequent to sealing in its test program, a procedure that is of vital importance in testing any materials for use on highway wearing surfaces.

About 30 percent of the respondents are using penetrating sealers in substructural elements such as piers, pier caps, and support beams. Again, this is probably because deck deterioration is still the primary problem in most areas, although occurrences of salt-induced damage to support and substructures has increased in recent years (*8,9*). About the same percentage of respondents apply penetrating sealers to median barriers in which deterioration problems have been noticed (*10*). Finally, 28 agencies reported use of penetrating sealers on appurtenance elements, which include parapets, abutments, railings, and sidewalks.

Qualification of Sealers

Highway agencies have traditionally relied on tests carried out within their own laboratories to qualify various products for use on their work. Recently, however, there has been a move toward accepting products on the basis of tests performed by or for manufacturers that demonstrate the product's compliance with ASTM, AASHTO, or specific agency specifications.

Data developed during the survey support these trends (Figure 2). Although most agencies still rely on internal testing to qualify sealers, many agencies use data submitted by vendors, prescribe sealers on the basis of prior testing experience, or utilize external testing agencies. The use of vendor data can be considered an indirect use of external testing agencies, because vendors often have their products tested by independent laboratories, and include these data in technical documentation submitted to highway agencies. Many agencies rely on a combination of various methods for qualification, often using internal or external testing, supplemented by vendor data, as one example. Finally, the category of "other" includes

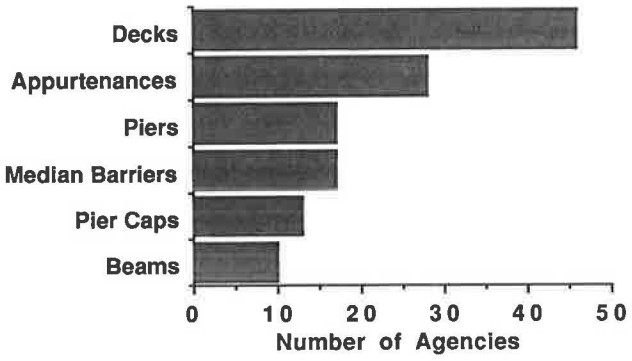

FIGURE 1 Application areas for penetrating sealers.

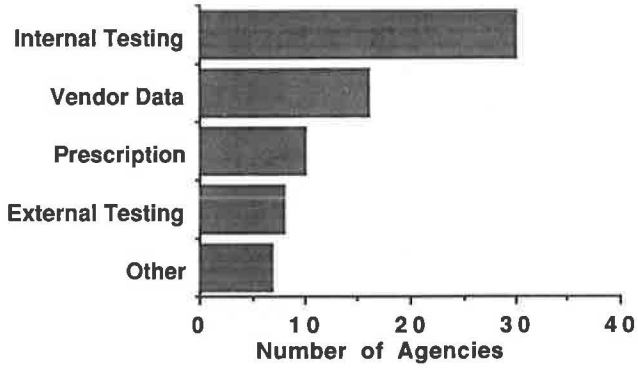

FIGURE 2 Procedures used to qualify penetrating sealers.

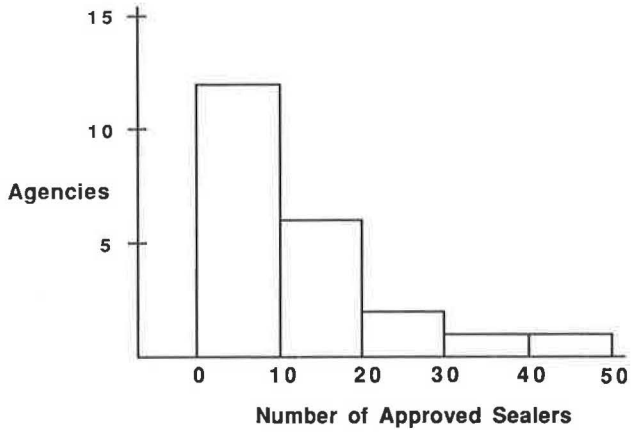

FIGURE 3 Number of penetrating sealers on approved product lists.

those agencies in which sealers were only used experimentally, in which lots of sealer were certified before use (linseed oil only), or in which data from other agencies were utilized.

Lists of Approved Products

Agencies were asked to list all approved penetrating sealers, including trade names and manufacturers. A few agencies had approved many products—Florida, Iowa, Ohio, and Pennsylvania each approved more than 20 products. Other agencies carried only a handful of sealers on their approved lists. A histogram summarizing these data is given in Figure 3.

Categorization of these data by generic type of sealer is difficult because the information was not available in many cases, and indeed, the quantity of such products on the market makes product categorization by sealer type a formidable task. However, familiarity with many of the products indicates that sealers with silane and siloxane bases predominated. Sealers with epoxy bases and other formulations are the next most common.

Test Procedures

Many agencies use more than one test procedure for their evaluations (Table 2). Additionally, a number of agencies rely on data submitted by vendors, and do not carry out their own tests.

A tabulation of test procedures in use by agencies, in decreasing order of usage, is given in Table 4. The most widely used procedure is AASHTO T 259, "Resistance of Concrete to Chloride Ion Penetration," which is commonly referred to as "90-day ponding." The second most widely used test is Series II of NCHRP Report 244 (7). This is not a standarized test method, but rather the report of a laboratory investigation. As such, considerable latitude in testing and interpretation of results is possible. ASTM C 642 "Standard Test method for Specific Gravity, Absorption, and Voids in Hardened Concrete" is the next most widely used method, along with other non-standard absorption methods. A number of techniques have been developed by the Oklahoma Department of Transportation, and are used by a number of other agencies. These techniques include tests for average penetration depth of sealers and vapor permeability. Finally, tests for deicer scaling resistance (ASTM C 672), freeze-thaw resistance (ASTM C 666), rapid chloride permeability (AASHTO T 277), and skid number are used by a small number of agencies.

Because of the wide variety of test procedures employed, it is extremely difficult to compare the performance of par-

TABLE 4 TEST PROCEDURES USED IN EVALUATION OF PENETRATING SEALERS

Test Procedure	Number of Agencies
AASHTO T 259	13
NCHRP 244[a]	9
ASTM C 642	6
Absorption (not ASTM C 642)	6
Rely on Vendor Data	6
Penetration depth[b]	5
Vapor Permeability[b]	5
Other Tests	5
ASTM C 672	3
AASHTO T 277	2
Freeze-Thaw Testing	2
Skid Resistance Testing	1

a) Most agencies utilize Series II testing as described in NCHRP Report 244 (7).
b) Test procedures developed by Oklahoma DOT.

ticular sealers with one another in examining results generated by different agencies. In addition, it is difficult to assign any degree of confidence to the data generated using varying methods, precision data resulting from standardized interlaboratory comparison tests are available for only one class of methods (freeze-thaw testing) and freeze-thaw methods are only used by two agencies in evaluating sealers. The precision of the two most widely used techniques, AASHTO T 259 and NCHRP Report 244, has not been determined.

Problem Areas

Agencies were asked to supply information developed in both the application and performance of penetrating sealers. Twelve agencies noted problems in applications, while 13 agencies noted problems in performance. Two agencies expressed the opinion that the performance of penetrating sealers was "questionable."

Various problems were reported by the respondents on the application of penetrating sealers. These problems included drifting and evaporation in hot and windy conditions, difficulty in obtaining specified coverage on newly placed concrete, slippery surfaces when linseed oil or other more viscous sealers were used, runoff during application, discoloration of concrete, flammability, non-uniform application, and little or no apparent penetration.

There were also certain areas in which respondents indicated performance of penetrating sealers to be less than desired. Several respondents indicated that many penetrating sealers were ineffective (or at least not as effective as claimed) in reducing infiltration of chloride ions into concrete. This was often manifested as a loss of effectiveness with time, and was especially bothersome on wearing surfaces in which effectiveness was expected to be about 3 years at most. Other performance problems included reduction of skid resistance (for those sealers that left a surface residue), failure to improve freeze-thaw and scaling resistance in non-air-entrained concretes, and failure to halt corrosion of reinforcing steel (as measured by half-cell potential surveys).

Field Test Procedures

Field testing of penetrating sealers has primarily consisted of periodic sampling of concrete for chloride ion penetration, using either core or drill samples. Although this does yield information on long-term effectiveness, the tests are destructive, time-consuming, and the number of samples that can reasonably be obtained from a given structure is limited. A second technique, used by at least two agencies, is to flood the treated sections with water and observe absorption of water into the concrete. If the water remains on the surface or "beads up," the sealer is judged to be effective; if it is rapidly absorbed into the concrete, the sealer is judged to be ineffective. Because this test is qualitative, it has significant subjective aspects. More rapid, quantitative field techniques are needed to assess the effectiveness of penetrating sealers.

CONCLUSIONS

There is keen interest in using penetrating sealers by most highway agencies in North America. The trend is moving away from such traditional products as linseed oil toward higher quality (and more expensive) materials such as silanes and siloxanes. Current use is limited, although several agencies are applying sealers to a significant number of structures. Qualification and test procedures for sealers vary from agency to agency, and more standardized acceptance methods are needed. There are problems in both application and performance of sealers, which must be resolved before highway agencies can be assured long-term performance.

ACKNOWLEDGMENTS

This research was funded by the Strategic Highway Research Program of the National Research Council through a subcontract with the Pennsylvania State University. The author would like to thank those representatives of state and provincial highway agencies who provided the data used in this paper.

REFERENCES

1. R. I. Frascoia. Vermont's Experience with Bridge Deck Protective Systems. *Chloride Corrosion of Steel in Concrete*. ASTM STP 629. ASTM, Philadelphia, Pa., 1977, pp. 679–81.
2. D. Whiting and W. Dziedzic. Chloride Permeabilities of Rigid Concrete Bridge Deck Overlays. In *Transportation Research Record 1234*, TRB, National Research Council, Washington, D.C., 1990, pp. 24–29.
3. M. M. Sprinkel. Comparative Evaluation of Concrete Sealers and Multiple Layer Polymer Concrete Overlays. Report FHWA/VA-88/R2. Virginia Transportation Research Council, Charlottesville, Va., 1987.
4. *The Use of Penetrating Sealers for the Protection of Concrete Highways and Structures*. Fosroc Preco, Plainview, N.Y., 16 pp.
5. S. Munshi and L. Millstein. *Low Cost Bridge Deck Surface Treatment*. Report FHWA/RD-84/001. FHWA, U.S. Department of Transportation, 1984.
6. C. F. Crumpton. Field Performance of Chem-Trete in Kansas. Presented at the 65th Annual Meeting of the Transportation Research Board, Washington, D.C., 1986.
7. D. W. Pfeifer and M. J. Scali. *NCHRP Report 244: Concrete Sealers for Protection of Bridge Structures*. TRB, National Research Council, Washington, D.C., Dec. 1981, 138 pp.
8. D. W. Pfeifer, J. R. Landgren, and A. Zools. *Protective Systems for New Prestressed and Substructure Concrete*. Report FHWA/RD-86/113. FHWA, U.S. Department of Transportation, April 1987.
9. V. Novokshchenov. *Salt Penetration and Corrosion in Prestressed Concrete Members*. Report FHWA-RD-88-269. FHWA, U.S. Department of Transportation, Nov. 1988.
10. D. Whiting and D. Stark. *NCHRP Report 258: Control of Air Content in Concrete*. TRB, National Research Council, Washington, D.C., May 1983.

Publication of this paper sponsored by Committee on Performance of Concrete.

Optimization of Concrete Mixes for Cost-Effective Construction

BRYCE P. SIMONS

Performance concrete is developed by optimizing concrete mix designs to more easily produce concrete that meets all structural and performance requirements of a project using the most cost-effective materials. Two projects with severe performance requirements are described, to show the importance and utility of this process. Selection of the basic mix ingredients as a function of the ultimate demands of a project is discussed. Developing performance concrete is concluded to be the most cost-effective way to approach a project, and optimization must be an integral part of the development process.

The need to optimize concrete mixture designs is becoming more important. Solving problems of concrete performance cannot be accomplished simply by adding more cement. It is critically important to ensure that the quantities and types of ingredients not only provide the characteristics required, but are also present in the proper proportions. Without the proper balance, some or all of the performance characteristics required might be missing. Additional expenses that result can negate the advantages of using a performance-oriented concrete mixture.

To optimize any concrete mixture, the constituents must be present in the correct proportions. Optimization involves numerous mixture iterations in the laboratory and in the field. Optimization of the components of a concrete mixture is the key to developing effective performance concrete mixture designs.

A significant difference exists between "ordinary" concrete and performance concrete. Ordinary concrete is a mixture that is prepared using conventional materials, proportions, and quality control methods. These mixes are typically prepared using the levels of control appropriate for concrete mixes requiring compressive strengths of 2,000 to 2,500 psi. For these mixes, compressive strength normally ranges between 2,000 and 7,000 psi; standard deviations normally range between 450 and 700 psi; and coefficients of variation normally range between 6 and 10 percent.

Ordinary concrete mixes normally have cement contents ranging between 5 and 7 sacks/yd^3. Increased strengths are achieved with more cement, resulting in decreased water to cement ratios. Ordinary concrete mixes may use normal range water reducers and can sometimes use high range water reducers. They rarely contain pozzolans, and their paste volumes are usually greater than necessary.

The biggest difference between a performance concrete mixture and an ordinary mixture is the amount of attention and control it receives. A performance concrete mixture, with properly optimized proportions, is designed so that the material properties (both fresh and hardened) will not vary outside narrow ranges. The ranges include coefficients of variation less than 5 percent and within-test coefficients of variation less than 3 percent. Typical concrete mixes have coefficients of variation closer to 7–8 percent. In addition, one or more of a performance concrete mixture's properties are normally maximized to realize particular project objectives. Maximizing these properties commonly taxes the ability of the ready mix plant and the contractor. Table 1 compares an ordinary concrete mixture design with actual performance concrete mixture designs.

The increased effort required by the producer and contractor usually cause the unit cost of performance concrete to be higher than that of ordinary concrete. However, the overall cost of a project using performance concrete will be substantially less. In the free-market system, performance concrete mixtures will be used only if they result in decreased overall project costs. The cost savings result from the elimination or substantial reduction of required quantities of concrete and associated building materials, such as steel. The reduction is possible because of the improved properties of the performance concrete. Overall project savings of as much as 30 percent are common.

Performance concrete mixes must be properly developed if they are to be successful. Individual characteristics required on various projects include high slump, long-term durability, high compressive strength, high flexural strength, high modulus of elasticity, sulfate resistance, penetration resistance, workability, and hard trowel finishability. All of these characteristics will probably not be needed, or even wanted, on any given project.

Understanding of the internal mechanics of concrete is increasing, and properties are being achieved that have never been considered possible. These properties result from altering the constituents and proportions of standard concrete mixtures in new ways. Consequently, some negative effects are created in the process that are difficult to predict and often difficult to eliminate. Some of the negative side effects include excessive retardation, segregation, difficulty in mixing, plugging of hoppers at the plant or in the truck, plugging of pump lines, excessive plastic shrinkage cracking, and various placing difficulties.

Two examples of projects that successfully used demanding performance specifications are described to illustrate the different approaches that can be taken. The Pacific First Center project in Seattle, Washington, shows one way to develop a proper mixture. The second project is an example of the more common approach and its consequent problems.

Simons Engineering, Inc., 32510 Northeast 111th St., Carnation, Wash. 98014.

TABLE 1 TYPICAL CONCRETE MIXTURE PROPORTIONS

	Ordinary	10,000 psi	19,000 psi
Cement (lb-Type II)	611	799	893
Fly ash (lb-Class F)	0	160	135
Silica fume (lb-solid material)	0	-	90
Water (lb-total)	280	280	216
Sand (lb-SSD)	1,540	1,210	1,009
Gravel (lb-SSD)	1,650	1,650	1,814
Normal range water reducer	-	-	67 oz
High range water reducer	-	190 oz	268 oz

The mixture for the Pacific First Center project required a compressive strength of 14,000 psi at 56 days of age and a modulus of elasticity of 7.2×10^6 psi, and it had to be pumped to about 700 ft above the ground. The concrete was to be placed inside steel-encased columns by pumping the material into the bottom of the column. The maximum height of each column pour was to be 30 ft. These criteria are difficult to meet. If the components of the mixture were not present in exactly the right proportions, at least one of these requirements could not have been met.

Because of the stiffness requirement, the original project specifications required a minimum modulus of elasticity of 7.2×10^6 psi at 56 days. The requirement was waived because the ready mix supplier was certain neither of its ability to consistently produce a mixture with this modulus of elasticity nor of the ability of any testing laboratory to consistently test for this value with the dependability required for compliance documentation. The ready mix supplier therefore agreed to provide a mixture that would provide a compressive strength of 19,000 psi at 56 days instead of meeting the modulus and compressive strength requirements originally specified (see 19,000 psi mixture in Table 1). The mixture that was subsequently developed was placed easily and met all of the requirements.

To develop the performance concrete mixes, about 8 months was spent in the laboratory mixing various blends of concrete to assess their characteristics. This work was performed under contract to the structural engineer before any documents went out for bid. These mixes were initially designed using a special Type II cement, fly ash, silica fume, and a special gradation of sand. The cement was required to have a reduced amount of tricalcium aluminate and a maximized amount of dicalcium silicate; the fly ash was used to provide a more uniform gradation in the very fine range, to act as a water reducer, and to provide some pozzolanic reactivity; the silica fume was used for its extreme pozzolanic reactivity; and the sand was produced using a much coarser gradation than the standard ASTM building sand. Materials specifications included

- Cement: met minimum requirements of ASTM C 150, as well as
  - —C_2S, 20.0 percent minimum,
  - —C_3A, 6.0 percent maximum, and
  - —Blaine fineness, 350 m^2/kg minimum.
- Fine aggregate: complied with all material properties of ASTM C 33 and with gradation requirements of 1984 Washington State Department of Transportation Specification 9-03.1(2)B, except that the minimum amount of material passing the No. 50 Sieve was 5.0 percent.

Numerous mixes were prepared with various sizes of coarse aggregate, various sand to aggregate ratios, crushed versus rounded aggregates, various cement contents, and various cement to pozzolan ratios. In all cases, only one variable was changed at a time so that the results of the change could be more easily determined.

After a mixture had been developed that appeared to provide all the necessary characteristics, the first field trials were conducted. Field trials are necessary to determine whether the intended mixture can be used as desired. The trials also allow project personnel to familiarize themselves with the mixture in an environment that is not critical. It was necessary, therefore, to place the material in a manner similar to that planned for the project and to employ the same people who would be working on site.

Field trials were performed on this project using a 10-ft diameter "dummy" column 10 ft tall, similar to the 10-ft diameter columns used on the project. In addition, the field trial column was instrumented internally with thermocouples placed at the lower, middle, and upper sections. Embedded strain gauges were situated at the lower third and upper third points of the member to measure shortening. The maximum temperature measured was 201°F, and the maximum temperature differential was 18°F/linear ft. No strains were measured because the strain gauges were damaged during the placement.

The trial mixes were evaluated by trained laboratory personnel before being discharged into the pump. The material was then pumped through approximately 1,000 ft of line. Bends and loops were intentionally built into this run to simulate the pressure losses that would occur on site. The initial laboratory work proved to be effective for this mixture because all of the fine tuning was accomplished with just three field trials.

Approximately 10,000 yd^3 of this mixture were required to complete the project. The results of the compressive strength test from this mixture are presented in Table 2.

The second project shows what can happen if this procedure is shortcut. This project was a canal that was to carry varying levels of sediments, so both durability and abrasion resistance were important. Testing was conducted, under contract to the owner, to determine the relation between high-strength concrete and this type of abrasion resistance. A new test was developed to measure the effects of the high-shear forces typically developed by large rocks bouncing down the structure.

Abrasion tests were performed on five panels that represented potential linings for the project. The panels were cast using (a) ordinary concrete, (b) steel plate, (c) concrete with hardener (a topping mixture containing metal aggregates),

TABLE 2 HARDENED CONCRETE PROPERTIES FOR PACIFIC FIRST CENTER PROJECT (MEASURED WITH 4 × 8 CYLINDERS)

Age of Specimen (days)	Compressive Strength (psi)	Modulus of Elasticity (psi x 10 6)
7	12,020	6.7
28	16,830	7.2
56	17,960	7.6
91	18,370	8.0

(d) concrete with 20 percent Class F fly ash (high-strength), and (e) concrete with 20 percent silica fume (high-strength).

Drum sanders, 12 in. in length were placed on the surfaces with only the weight of the machine resting on the belt. A 20-grit Carborundum paper was used for grinding. The sander was maintained in exactly the same position during testing to ensure consistent results. To eliminate error resulting from sand paper wear, sanding belts were replaced every 30 min. The grooves that resulted from sanding were measured at each belt change to record the rate of growth of each groove (abrasion resistance). The panels were subjected to abrasion for 8 hr per panel. This test design revealed the resistance of concrete to both high-point and high-shear loads. The test results are presented in Table 3. The ordinary concrete displayed substantially greater spalling and dusting than both of the high-strength concrete mixtures.

Test results showed the necessity of using 20 percent fly ash, by weight of cement, in the mixture. This percentage of fly ash ensures an adequate level of impermeability and the subsequent strength development inherent to fly ash. In the author's opinion, the improved abrasion resistance of the high-strength concrete results from improved adhesion of the cement paste to the aggregate particles. Accordingly, the strength on this project was specified to be a minimum of 10,000 psi at 56 days. Because cracking was a primary concern in this project, the amount of cement permitted in the mixture was limited to 799 lb/yd^3.

The sand available from the ready-mix supplier was significantly finer than desired and because this plant was a dry batch operation, consideration had to be given to mixing. The effects on overall water demand of the mix because of the fine sand and problems in developing uniform mixes were boundary conditions.

Problems first arose when the owner-designer team assumed that the concrete mixture could be pulled off the shelf, similar to ordinary concrete mixtures. After discussion, the owner and designer were convinced that the ready mix supplier had to be given advance notice to prepare the mixture. The time was already short.

The ready mix plant made a similar mistake. The mixtures used for the research work were prepared with different materials than were planned for the project. However, the suppliers believed that because their plant was the best operation around, they could easily produce a mixture that would meet the specifications. The laboratory phase of the suppliers' concrete development process was eliminated because they believed that field-oriented equipment should be used because they were trying to simulate field conditions. The need to fine tune the mixes using small, controlled loads in the laboratory became apparent in time.

TABLE 3 RESULTS OF ABRASION TEST

	Depth of Groove (in.)	Width of Groove (in.)
Steel plate	0.088	1.704
Concrete with 20 percent SF	0.183	2.228
Concrete with 20 percent Fly Ash	0.168	2.075
Ordinary concrete	0.215	2.586
Concrete with hardener	0.250	2.421

The field-trial concrete prepared did not have the control exercised that is necessary. Because no one from the owner-design team had been told where field trials would occur, no one from the design team witnessed them. The trial slab was placed, went down easily, and finished well, but was placed without the level of batch plant control desirable for these procedures. Furthermore, the ready mix plant was unable to reproduce this mixture later on in the project.

The first placement took place about 2 weeks after the field trial. The 7-day compressive strengths from the field trial were low, and because the 28-day results were not available, another theoretical mixture was prepared that had a substantially lower water to cement ratio. There was no time to test the mixture, either in the laboratory or in the field. This new mixture had a water to cementitious ratio of .23. It was hard to pump, and was difficult to place. The contractor had to put as many as 6 men on a 12-ft screed to strike off the concrete. Finally, the admixtures used retarded the mixture so that it could not be finished. The project was shut down.

What followed should have occurred initially. A series of carefully controlled trial batches were prepared using various combinations of ingredients. It was finally discovered that the sand to aggregate ratio was not correctly balanced for the maximum-sized coarse aggregate used. The sand to aggregate ratio had been determined on the basis of a gravel with maximum-sized aggregates of ⅜ in. The ready mix producer instead used a gravel with maximum-sized aggregates of ⅞ in. The change in gravel size was made without changing the sand to aggregate ratio.

By changing the sand to aggregate ratio from 39 to 42 percent of the total aggregate volume in the mixture, and bringing the water to cementitious ratio up to .25, the new mixture became easy to pump, required substantially less admixture, and could be troweled off nicely.

The remainder of the project went smoothly, and the finish finally achieved was extremely good. However, the level of mental and physical anguish to the team members and the added costs need not have occurred.

The lessons learned from the two projects are not new. There appears to be an inherent human tendency to compare what is being said with one's personal experiences. If words do not fit with beliefs, then they are ignored. This commonly happens in the process of developing performance concrete. Performance concrete can work effectively only if the team handling it is assembled soon enough, the research and laboratory work necessary are properly performed, the field trials are correctly carried out, and all individuals are willing to listen and work together. The potential for substantially improved performance characteristics on any project is profound. There is no question that using performance concrete on projects will provide a significant edge, which will, in turn, provide an incentive to ensure that within 10 years, performance concrete will be in common use throughout the country. Performance concrete mixes must be properly developed in order to gain widespread acceptance. Optimization is the key to the development of performance concrete.

Publication of this paper sponsored by Committee on Chemical Additions and Admixtures for Concrete.

High-Performance Silica Fume (Microsilica)–Modified Cementitious Repair Materials

MARK D. LUTHER

Basic information about silica fume (microsilica), portland cement–based materials containing silica fume, and the use of these materials in the repair of structures is reviewed in this paper. Information is presented about high-performance (strength in excess of 20,000 psi) repair materials containing silica fume. Various applications are discussed, including those involving grout, underwater concrete, shotcrete, and concrete repairs.

This paper accomplishes two goals. The first is to present basic silica fume (microsilica) information and to introduce repair materials containing silica fume (SF). The second is to describe high-performance materials containing SF that usually achieve compressive strength around or in excess of 20,000 psi and that are suitable for many repair applications.

SILICA FUME BASICS

Also referred to as microsilica and as condensed silica fume, SF is the solid material collected from the exhaust gases of submerged electric arc furnaces during the production of silicon or silicon alloys. Before the mid-1970s nearly all SF was discharged into the atmosphere. After environmental concerns necessitated collecting and disposing SF in landfills, it became economically justified to use it in various applications.

SF particles are typically spherical, average about 0.15 micron in diameter, have a specific gravity of 2.2, and are gray in color. Usually, the particles are collected as a dry powder. The powder, which has a bulk density between 5 and 27 pcf, may be added as is to concrete. To improve handling characteristics and to make it more economical to ship, it may be either slurried with water or densified.

In the United States, SF is usually added to portland cement (PC) concrete in the range of 3.8 to 21 percent by weight of cement. Applications employing SF to improve corrosion protection of reinforcing steel tend to use 3.8 to 10 percent dosages. High-strength applications often use dosages between 7 and 21 percent and the 7½ to 20 percent dosage range covers most grout, chemical resistance, abrasion, abrasion-erosion, and cavitation resistance applications. In PC concrete, SF improves cohesion of the fresh concrete, and it enhances many of the hardened properties, like compressive strength, bond strength, abrasion resistance, abrasion-erosion resistance, cavitation resistance, permeability (reduced), frost resistance, and resistance to many chemical solutions.

Elkem Materials Inc., 10 Parkway View Drive, Pittsburgh, Pa. 15205.

It is beyond the scope of this paper to more fully describe SF and SF concrete. These topics have been treated in numerous publications (*1–6*). By mid-1989 over 700 articles about materials containing SF had been published.

SF-BASED REPAIR MATERIALS

To facilitate the discussion about repair materials containing SF, these materials are grouped into the general categories presented in Figure 1. The high-performance (compressive strength exceeding 20,000 psi) materials are the primary focus of this paper. The lower-strength repair materials containing SF are discussed first, presented by category.

Grout

Grouts containing SF have been employed by various state departments of transportation to improve the bond between base concrete and repair overlays (*7,8*). These SF bonding grouts have also been used during parking garage restoration work to improve the bond between overlays or patches and the base concrete. SF grouts used in these applications tend to employ a SF-to-cement ratio by weight between 7½ and 15 percent. In some cases water-reducing admixtures are used, and many of the grout formulations contain fine aggregate. SF grout is noticeably more cohesive (less segregation and bleeding) than plain PC grout. SF grout has been used in anchor applications.

Various proprietary bagged grout and patch products containing SF are commercially available. The SF is added to improve bond, increase strength, and reduce permeability.

Underwater Concrete

The cohesiveness of mixtures containing SF makes them suitable for underwater applications. Several successful underwater repairs of dams have been completed. The first such repair in the United States occurred in the summer of 1988 when 2,300 cubic yards (cy) of a maximum 1-in. coarse aggregate concrete containing 48 pcy of SF was placed in the Dashields Lock & Dam, Milepost 13.3, on the Ohio River. That same year, 127 cy of concrete containing about 93 pcy of SF and ¾-in. maximum-sized coarse aggregate was placed in the Point Marion Lock & Dam No. 8 on the Monongahela River.

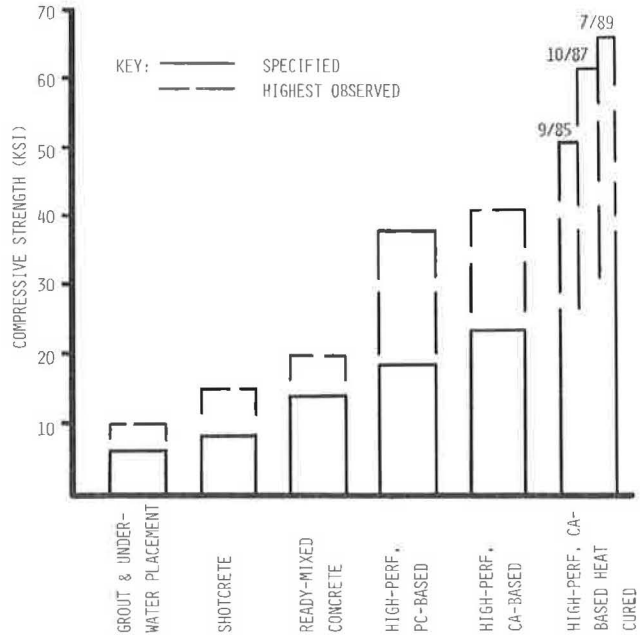

FIGURE 1 Strengths of SF concretes.

A smaller volume of similar SF concrete was used during a repair at the London Locks on the Kanawha River in West Virginia. The water-to-cementitious materials (W/C) ratio of these concretes varied between 0.34 and 0.40, and the concretes achieved 28-day strengths between 8,000 and 10,000 psi.

One project in England used an SF grout in a tremie placement in which the coarse aggregate was preplaced.

Shotcrete

SF shotcrete, both dry process and wet process, is used worldwide, and in some countries it is used extensively. For example, over 90 percent of the shotcrete used in Norway contains SF. Although most of the shotcrete work is in new construction, SF shotcrete has been commonly used as a repair material (*9,10*).

Reasons for choosing SF shotcrete include reduced rebound (hence reduced materials and clean-up costs), thicker placements, better bond, and improved durability. Usually SF dosages for shotcrete lie between 7½ and 10 percent, but dosages as high as 15 percent have been used. Strengths exceeding 15,000 psi were reported for trial work associated with the 1983 Bureau of Mines repair in Lake Lynn, Pennsylvania (*11*).

SF Concrete

Although research investigating the properties of SF concrete (concrete containing SF) began almost 40 years ago, and SF concrete has been used intermittently since the mid-1960s in Japan, SF has been commercially available for manufacturing concrete only since the mid-1970s in Norway and since the early 1980s in the United States. SF concrete is now routinely used for repair work in many countries and continents, including North and South America, Europe, Iceland, and Australia.

SF concrete has been used for repairs in many applications, and some of these are listed in Table 1 along with the SF dosages and several W/C ratios typically employed. Perhaps the largest volume of SF concrete is employed in repair applications to protect steel from corrosion. Decks of many parking garages and bridges have been either partially or completely replaced with SF concrete for this reason. Also, approach slabs, traffic barriers, sidewalks, and other portions of bridges have been replaced with SF concrete (*7*).

Some bridges, such as the over 1,200-ft-long Landon B. Hassler Memorial Bridge in Tennessee, used the high-early-strength property of SF concrete to enable rapid opening of structures to traffic. Portions of pavements in Norway have been replaced with SF concrete, and these have already significantly outlasted other pavements exposed to similar steel-studded tire loadings. In another abrasion-resistant application, an approach lane to a weighing platform at the New Enterprise Stone and Lime Company, Roaring Spring, Pennsylvania, has already survived more than three times longer than concrete previously in use.

Refractory Concrete

A relatively large volume of calcium aluminate (CA)–based SF concrete is used in the repair of refractories. SF often replaces some or all of the CA cement. Refractory SF concrete for repair work is usually chosen because it is more durable than many other refractory concretes.

HIGH-PERFORMANCE SF-BASED MATERIALS

PC-Based Mortar/Concrete

The SF materials previously discussed—grout, underwater concrete, shotcrete, and concrete—are high performance in the sense that strength and the other properties mentioned are usually significantly improved relative to non-SF reference mixtures. The remainder of this paper focuses upon materials that are high performance in the sense that strength exceeds 20,000 psi.

History

During the late 1970s, high-performance PC-based SF materials were developed in Denmark. By 1982 some of these materials had been patented and were being provided to users in Europe and North America. These materials have been used to repair concrete exposed to very severe environmental conditions.

Materials and Packaging

High-performance PC-based SF materials are typically packaged in 50-lb bags, which are used in whole-bag increments and usually contain all the mortar or concrete ingredients

TABLE 1 REPAIR CONCRETES CONTAINING SILICA FUME

Portland Cement-Based Repair Application	Silica fume dosage range commonly seen (% added by weight of cement)	W/(C + SF)[1]
Abrasion (industrial floors, loading docks, pavements)	7% - 15%	$\leq$0.45
Abrasion/erosion (stilling basins, spillways, sidewalls, baffles, river liners)	14% - 18%	<0.35, and in some cases <0.30
Cement replacement (low heat of hydration pier repair)	10%	<0.40
Chemical resistance (vats, floors, channels, slabs)	10% - 20%	$\leq$0.40
Corrosion protection of steel, primarily due to low permeability and increased electrical resistivity (parking garages, bridges, piles)	3.8% - 10%	$\leq$0.40
High early strength (bridges)	11% - 15%	$\leq$0.45
Lightweight concrete (parking decks)	7½%	$\leq$0.40
Marine environment (piers, docks, piles)	5% - 15%	$\leq$0.45

Note 1: W/(C + SF) = water-to-(cement plus silica fume)

except water. Rarely, additional high-range water-reducing admixture (HRWR) might be added. Although the aggregate size and mineral composition may vary from one specific product to another, one of the more popular products uses ¼-in. maximum size calcined bauxite aggregate. A special PC cement is used to develop very high strengths. None of 26 other cements achieved equivalent strength. SF for these products is undensified and comes from the production of silicon. The amorphous SiO_2 content of such SF is above 90 percent. A large dose of dry HRWR is used to obtain W/C ratios below 0.24 with slump exceeding 8 in. Steel fibers may be added to the concrete for applications requiring enhanced toughness. Most commonly, ¾- or 1-in.-long fibers are supplied. Proportions of these products have been published (*12*).

Concrete Mixing

The concrete is typically produced at the repair site in ½- to 1½ cubic foot (cf) batches using either horizontal axis mortar mixers or pan mixers. After the bag contents have been emptied into the mixer along with the amount of water recommended by the supplier, the concrete is mixed for 10 min. Next steel fibers are added, if required, and the concrete is mixed an additional 5 min. In cases needing increased workability, additional HRWR is added.

Properties of Fresh Concrete

The fresh properties are usually as follows for the described material: slump = 8 to 10 in.; air content = 3.3 percent; unit weight = 170 pcf; initial time of setting at 70°F is just under 1 day (the setting of these concretes tends to be retarded, which may be attributed to very high admixture content). The concrete is highly cohesive.

Placement and Curing

As with all overlay or patchwork, careful preparation of the base concrete is important. Preferred results are obtained when the base is meticulously clean and in a saturated surface-dry condition. The material should be consolidated using mechanical equipment. Best results for flatwork occur when a vibratory screed is used. In most cases, surface texturing and curing should begin immediately. Extended wet curing (for at least 3 days), preferably using wet burlap covered with plastic, is recommended.

Properties of Hardened Concrete

Table 2 presents the properties of hardened concrete. Compressive strengths exceeding 20,000 psi at 28 days are typical. At later ages a small strength gain is observed (Figure 2). The highest strength reported for this material was 38,000 psi (*12*), and the author has achieved 28,000 psi. To achieve 28,000 psi, a small amount of dolomite coarse aggregate (ASTM C 33 No. 67 grading) had been added to the concrete. In another instance, 30 percent by weight gravel (ASTM C 33 No. 8 grading) at SSD moisture condition was added to the basic

TABLE 2 HARDENED PROPERTIES OF HIGH-PERFORMANCE PC-BASED CONCRETE CONTAINING SILICA FUME

Property	Result	Associated Compressive Strength
Compressive strength (n=6)		
@ 7 days	17,670 psi	
@ 28 days	21,110 psi	
Flexural strength (single point)		
@ 28 days (n=2)	2,690 psi	22,070 psi
Static modulus of elasticity (16).	8,000,000 psi 7,690,000 psi[1]	24,000 psi 22,350 psi[1]
Poisson's ratio[1]	0.21	22,350 psi
Splitting tensile strength[1]	1,436 psi	22,350 psi
Direct tensile strength[1]	900 psi	22,350 psi
Double shear strength[1]	5,340 psi	22,350 psi
ASTM C666 procedure A, durability factor (n=2)		
Without air entrainment (3.3% air)	100[2]	20,000 psi[3]
With 12.0% air[3]	100[2]	11,660 psi[3]
AASHTO T277-83 Rapid Chloride Permeability	Very low	
Charge passed @ 42 days (n=3)	102 Columbs	18,140 psi

Note 1: Unpublished work conducted during 1984 by the Concrete Structures Bureau Laboratory, United States Bureau of reclamation, Denver, Colorado.

Note 2: No steel fibers used. All other mixtures used steel fibers.

Note 3: Air content was made high deliberately to determine the effect upon frost resistance. Associated strength of non-air-entrained prisms was nominally 20,000 psi.

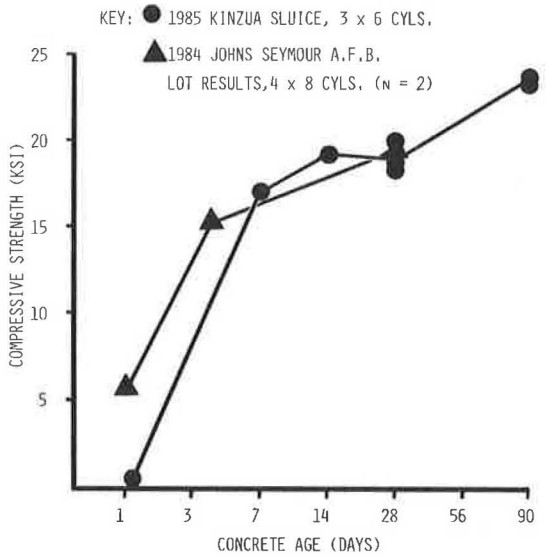

FIGURE 2 Two examples of strength development, high-performance PC-based SF-concrete.

product. Workability was improved in this case with only a small strength reduction, which was 20,060 psi (n = 4) for the modified mixture and 21,520 psi (n = 9 on three batches) for the initial mixture.

Flexural strengths higher than those of PC concrete have been observed. The mathematical expression for the flexural strength results shown in Table 2 may be expressed as follows: flexural strength = 18 (compressive strength)$^{1/2}$. Constants as high as 20 have been seen in mixtures in which steel fibers had been added. The factor for the dolomite-modified mixture was 20.1.

The results for static modulus of elasticity (E) are around 8 million psi. The ACI predictor equations for E somewhat overestimate the observed E by ½ to 3 million psi. Although at very high strength levels, this is also true for other PC concretes (*13,14*).

Poisson's ratio for the subject concrete, at 0.21, was the same as that found for the reference concrete.

The material shows clearly acceptable resistance to cycles of freezing and thawing even when air-entraining admixtures are not added.

The AASHTO T 277 rapid chloride permeability (RCP) result shown in Table 2 typifies those historically observed. The RCP shown in Table 2 is at the low end of the very low range.

The abrasion resistance results (Table 3) for the concrete were significantly better than those for the reference concretes. The favorable performance of the SF concretes in the field, however, suggests that the revolving disk-type abrasion tests understate the performance of very high-strength concretes (*15*). Comparative sandblasting testing has also indicated that the abrasion of the SF concrete is significantly higher than that of other concretes (*15*). Still another type of abrasion test was conducted in 1984 at the Waterways Experiment Station, Vicksburg, Mississippi, on the material that was ultimately supplied to a runway repair project. In this test a weight was dropped on a 1-in.-diameter steel cable under which panels of the steel-fiber-reinforced, high-performance PC-based material were placed. In these previously unreported tests, the SF material performed well even after sustaining 5,000 blows. The abrasion-erosion resistance results shown in Table 3 indicate that this property is over 14 times better than in conventional PC concrete.

The cavitation results, also shown in Table 3, indicate that having demonstrated a 99-fold improvement relative to the reference concrete, high-performance PC-based SF material may provide better cavitation protection than other PC-based materials.

Tests exposing the high-performance PC-based SF material to various chemical solutions—usually acids—were conducted, and it was found to outperform reference PC concrete (*15*). It is recommended, however, that if a chemically resistant repair material is needed, the concretes be evaluated first by testing them in the chemical solutions.

Concretes exceeding 10,000 psi have shown creep and shrinkage values less than those of lower-strength concretes (*12,14*). SF concretes have shown similar creep as PC concrete of comparable strength, although somewhat less shrinkage has been observed (*14*).

On the basis of the fresh and hardened properties of the high-performance PC-based SF material, it is believed that there are many transportation applications in which these materials can be used, like pavement patchwork and overlays in areas exposed to severe abrasion. Examples of projects that have used this material are described next.

TABLE 3 HARDENED PROPERTIES RESULTS FOR ABRASION, ABRASION-EROSION, AND CAVITATION TESTS

Property	Result For High-Performance SF Concrete	Result For Reference Concrete	Result Associated Compressive Strength
Abrasion			
° ASTM C779, procedure A, revolving disks, 60 min., mean depth of wear at 42 days. (n=3)	0.028 in.	0.038 in.	19,330 psi 6,000 psi
° DIN 52-108 (German wear test) mean mass loss on saw-cut from slabs. (n=2)	0.74%	1.43%	19,330 psi 6,000 psi
Abrasion/Erosion[1]	0.5%		24,000 psi
° CRD 63-80 volume loss of 12-inch-diameter specimens exposed to revolving steel balls in water for 72 hours (16).		>7%[2]	≤6,000 psi[2]
Cavitation[3]			
° Eight-hour exposure to venturi-type cavitation apparatus, subjecting nominal 4.5 by 4.2 by 12-in. prisms to an upstream pressure of 60 psi and a maximum water velocity of 70 ft/sec.			
Weight loss (n=2)	1.6 grams	131.5 grams	22,354 psi 8,090 psi
Volume loss (n=2)	0.035 in.	3.485 in.	22,354 psi 8,090 psi
Capacity of cavitation resistance relative to control	99X	1X	23,354 psi 8,090 psi

Note 1: From reference 16.

Note 2: Concrete manufactured without specialty or hard aggregate commonly shows losses in excess of 7%.

Note 3: Unreported work conducted during 1984 by Concrete Structures Bureau Laboratory, United States Bureau of Reclamation, Denver, Colorado.

Examples of Projects

During November 1982 a small repair was demonstrated at the Dashields Lock & Dam on the Ohio River. Approximately

9 cf of concrete was placed in a nominal 3-in.-thick overlay in an area of existing deterioration. The high-performance material, which did not contain steel fibers, was screeded and finished with a steel trowel. An inspection in 1988 revealed that there was no evidence of deterioration of the overlay, although the adjacent concrete had deteriorated severely.

In April 1985 about 9 cf of steel-fiber-reinforced concrete was placed in a cavitation damage repair in Sluice No. 4 at the Kinzua Dam in northwestern Pennsylvania. After batching, the concrete was lowered to a boat that transported it to the sluice. The concrete was then carried through the sluice about 130 ft to the repair location. The concrete was placed and internally consolidated. Inspection of the casting in 1988 revealed no evidence of damage. The compressive strength development curves for this concrete are shown in Figure 2.

Columns of high-strength concrete, specified to have a compressive strength of 12,000 psi, were cored and repaired with PC-based SF concrete in 1988. An upward-directed plastic elbow was attached to each horizontal hole. Then the concrete was placed, aided by an internal vibrator. On the following day, the elbows were removed, along with the remaining concrete, which was still weak enough to be easily trimmed. At 3 days, cylinders cast with the repair concrete exceeded 16,000 psi.

To obtain high resistance to abrasion, approximately 40 cf of high-performance material was placed under the arresting gear at the end of a runway at Seymour Johnson Air Force Base in October 1984. (See Figure 2.) Arresting cables, located at the end of runways, are about 1 in. in diameter, and are supported 2 to 3 in. above the runway. Aircraft engage the cables with a tail hook in an emergency. When the aircraft wheels pound the cable to the runway, the underlying concrete is damaged. The overlay, which was flush with the adjacent pavement, ranged between 2 and 5 in. deep and was about 3 ft wide. The runway was opened 48 hr after placement. The concrete performed well, outlasting other materials that had been tested or used previously. This concrete was subsequently employed in similar applications.

CA-Based Mortar/Concrete

CA-based materials containing SF were developed in the mid-1980s. These are manufactured, packaged, and batched similar to the way that PC-based SF materials are packaged and batched. The CA-based materials, however, use more SF in the formulations, and they develop higher strength than the PC-based materials. The CA-based materials also exhibit a faster setting time than the PC-based ones.

The CA-based materials have been used in applications where high abrasion resistance is required (like warehouse floors) and in repairs where materials will be exposed to heat.

Proprietary CA-Based Material with Special Curing

When the CA-based materials are exposed to a special curing process (after initial wet curing, the materials are dried and heated), the strength and heat resistance dramatically increase. Cubes 3 to 4 in. cast with the material have developed strength in excess of 65,000 psi. The progression of the strength records using this material is shown in Figure 1.

Repair applications that have used the specially cured materials include replacing parts of equipment where formerly steel parts were used. In addition, abrasion-resistant repair plates and shapes have been cast and used with success. In some cases, when a repair material will be exposed to high-temperature (over 1,000°F) environments, this material is used.

Price

The delivered price of SF currently available across North America ranges from around $0.20/lb for bulk material for large jobs to $0.50/lb for bagged formulated products used on small jobs. This means that the additional cost of SF to a cubic yard of concrete ranges from around $10/cy for large jobs with low dosage levels (see Table 1) to around $50/cy for small jobs at high dosage levels. Handling by the concrete suppliers increases the price.

The price of the high-performance (≥20,000 psi) PC-based bagged materials without coarse aggregate is often around $4,000/cy when used in small quantities. The price of the CA-based repair materials usually begins at $4,000/cy.

CONCLUSION

SF-modified concretes have been used successfully in a variety of repair applications. The strong bond strength, high compressive strength, low permeability, and good durability of silica fume grouts, mortars, and concretes make them appropriate repair materials.

High-performance PC-based materials containing SF have been used successfully in severe environments. These materials are suitable for repair work in cavitation, abrasion-erosion, abrasion, and some chemical environments.

Although high-performance CA-based materials containing SF have only recently become available, the high strength, heat resistance, and durability of these materials make them desirable for certain applications.

ACKNOWLEDGMENTS

Appreciation and thanks are expressed to Elkem Materials Inc. for financial support for writing this paper; Emily Cooper and Arleen K. Smith for typing the paper; Robert L. Robertson for assembling support information; Anton Krysa of the U. S. Army Corps of Engineers, Pittsburgh; Dennis Arney of the U. S. Bureau of Reclamation, Denver, Colorado; Tony Husbands, U. S. Army Corps of Engineers, Waterways Experiment Station, Vicksburg, Mississippi; Hans H. Bache, Aalborg Portland Cement, Denmark; Magne Dastol of Elkem Materials a/s, Kristiansand, Norway; and Celik Ozyildirim.

REFERENCES

1. *Condensed Silica Fume* (P. Aitcin, ed.). *Les Editions de l'Université de Sherbrooke*, (P. Aitcin, ed.), Sherbrooke, Quebec, Canada, 1983, pp. 25–27.

2. E. Sellevold and T. Nilsen. Condensed Silica Fume in Concrete: A World Review. Presented at International Workshop on Condensed Silica Fume in Concrete, Montreal, Canada, May 4–5, 1987.
3. ACI Committee 226. Silica Fume in Concrete. *ACI Materials Journal*, Vol. 84, No. 2, March-April, 1987.
4. M. D. Luther. Silica Fume Materials and Action in Concrete. In *Recent Advances in Concrete Technology, Proceedings, Concrete Technology Seminars* (P. Soroushian and S. Ravanbaksh, eds.), Michigan State University, East Lansing, Feb. 1–2, 1989, pp. 13.1–13.15.
5. M. D. Luther. Silica Fume (Microsilica) Production, Materials and Action in Concrete. In *Advancements in Concrete Materials* (Z. Bayasi and R. Bhatacharya, eds.), *Proceedings*, Bradley University, Peoria, Ill., March, 1989, pp. 18.1–18.21.
6. V. M. Malhotra, V. S. Ramachandran, R. F. Feldman, and P.-C. Aitcin. *Condensed Silica Fume in Concrete.* CRC Press, Inc., Boca Raton, Fla., 1987.
7. M. D. Luther. Silica Fume (Microsilica) Concrete in Bridges in the United States. In *Transportation Research Record 1204*, TRB, National Research Council, Washington, D.C., 1988, pp. 11–20.
8. *Bridge Special Provisions No. 16: Bridge Deck Concrete Overlays.* Illinois Department of Transportation, Springfield, 1987.
9. D. R. Morgan. Use of Supplementary Cementing Materials in Shotcrete. Presented at International Workshop on the Use of Fly Ash, Slag, Silica Fume and Other Siliceous Materials in Concrete, Sydney, Australia, 1988.
10. D. R. Morgan. Dry-Mix Silica Fume Shotcrete in Western Canada. *Concrete International*, Vol. 10, No. 1, Jan. 1988, pp. 24–32.
11. O. A. Opsahl. Bureau of Mines Protects Mine Entrance with Reinforced Microsilica Concrete. *Concrete*, Nov. 1983, pp. 36–40.
12. H. H. Bache. Densified Cement/Ultra-Fine Particle-Based Materials. Presented at 2nd International Conference on Superplasticizers in Concrete, Ottawa, Ontario, Canada, 1981.
13. *Requirements for Reinforced Concrete.* Report ACI 318-83, Section 8.5.1. American Concrete Institute, Detroit, Mich., 1986.
14. M. D. Luther and W. Hansen. Comparison of Creep and Shrinkage of High-Strength Silica Fume Concrete with Fly Ash Concretes of Similar Strength. *Proc., 3rd International Conference on Fly Ash, Silica Fume, Slag and Other Natural Pozzolans in Concrete*, Trondheim, Norway, Vol. 1, SP 114-27, June 1989.
15. M. D. Luther. Microsilica (Silica Fume) Concrete Durability in Severe Environments. *Proc., ASCE Structural Materials Congress*, San Francisco, Calif., 1989, pp. 95–105.
16. T. C. Holland. *Abrasion-Erosion Evaluation of Concrete Mixtures for Stilling Basin Repairs, Kinzua Dam, Pennsylvania.* U.S. Army Engineer Waterways Experiment Station, Miscellaneous Paper SL-83-16. Vicksburg, Miss., Sept. 1983.

Publication of this paper sponsored by Committee on Chemical Additions and Admixtures for Concrete.

Overview of the Use of Fly Ash Concrete in Highway Construction

WOODROW J. HALSTEAD

An overview of opportunities and concerns on the use of fly ash as a pozzolan in hydraulic cement concrete in constructing highways and other transportation facilities is presented. It is derived primarily from more detailed information given in *NCHRP Synthesis of Highway Practice 127.* Some of the early concerns related to the loss of entrained air in fly ash concrete, shipment-to-shipment uniformity of fly ash, and more careful selection of by-products marketed as pozzolans. Significant differences between the by-products from burning bituminous coal and subbituminous coal have been identified, and more fundamental information is being developed. The need to use a more rational method of proportioning ingredients for concretes containing fly ash based on performance characteristics is discussed. A more rational approach can provide opportunities for more efficient utilization of fly ash as a pozzolan in hydraulic cement concrete.

Probably the greatest drawback to full utilization of fly ash concrete in highway construction is a perception that substituting fly ash for part of the portland cement constitutes the addition of an adulterant to the product. The idea that 25 to 30 percent of a plentiful, inexpensive by-product can replace a more expensive, carefully manufactured material with the resulting end product having superior performance characteristics contradicts a widely held concept that "more expensive is better." Yet, this is basically the situation with respect to use of fly ash as a pozzolan in concrete. However, the use of fly ash in concrete for highways or other transportation facilities has both advantages and disadvantages. This paper reviews some of these and recent developments to provide a perspective on the optimum utilization of fly ash concrete in the construction of transportation facilities.

BACKGROUND

Renewed interest in the overall use of fly ash in concrete grew from efforts to increase the utilization of the ash from burning pulverized coal (*1*). In the United States, this renewed interest was triggered by passage of the Resources Conservation and Recovery Act (RCRA) in 1976. Worldwide interest has also been generated by the energy and environmental concerns of other countries.

The entire problem relates to potential uses for all of the coal ash. This is illustrated in Figure 1 using the information reported by Golden (*2*). He stated that the amount of such ash generated annually in the United States is 71 million tons, with expectations of substantial increases in the future. Approximately 57 million tons of this ash is fly ash, of which only about 15 million tons is used in any form, and only a small percentage of this is pozzolan usage in hydraulic cement concrete. Evidently, using fly ash as a pozzolan in concrete is only a small part of the total concern of power plants to develop suitable uses for their by-product, yet full development of its potential could have a significant impact on highway concrete technology.

Virginia Transportation Research Council, Box 3817 University Station, Charlottesville, Va. 22903-0817.

As a part of the implementation of RCRA, the Environmental Protection Agency issued guidelines for procuring concrete. These guidelines prohibit specifications that exclude the use of fly ash in materials used in federal construction projects unless a technical reason exists for such exclusions. This applies to all federal-aid highway construction.

Considerable efforts have been made by the Federal Highway Administration, the Transportation Research Board, the American Concrete Institute, the American Concrete Coal Ash Association, the Electric Power Research Institute (EPRI), and fly ash marketers to provide information on how best to utilize fly ash in day-to-day operations.

NCHRP Synthesis of Highway Practice 127: Use of Fly Ash in Concrete (*1*) reviews the history of the use of fly ash concrete in highway construction and summarizes potential advantages of using fly ash as well as the potential problems facing state transportation agencies in its use. That report summarized the state of the art at the beginning of 1986. Since its publication, the second conference on the use of fly ash, silica fume, slag, and natural pozzolans in concrete and the eighth international ash utilization symposium have been held (*3,4*). Although the large proportion of these conference papers dealt with matters other than the use of fly ash in concrete, those papers that were concerned with its utilization in concretes confirmed trends and concerns reported in Synthesis 127. The purpose of this paper is to briefly review some of the major concerns reported in Synthesis 127 and to evaluate recent developments affecting such concerns.

CONCERNS RELATING TO HIGHWAY APPLICATIONS

Potential for Air Entrainment Problems

In early trial uses of fly ash concrete, the need for an additional amount of air-entraining agent to incorporate the proper amount of air into the concrete was not recognized. Improper air entrainment resulted in early deterioration from freezing and thawing and economic losses resulting from having to replace portions of the concrete (*1*). Loss of entrained air after initial tests for air entrainment at mixing plants and job sites has

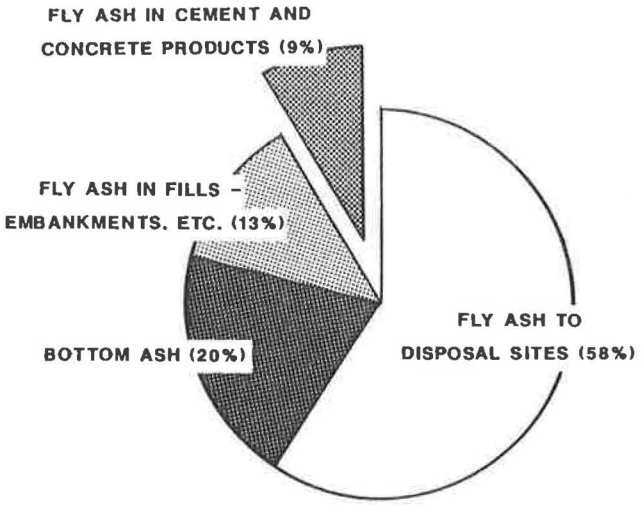

FIGURE 1 Estimate of coal ash in the United States in 1985 [Total Volume = 71 Million Tons (*2*)].

also been a problem (*5*). The magnitude of this problem apparently has been reduced by recent trends toward the lower carbon content (loss on ignition) of fly ash that has resulted from more efficient burning and the elimination of "upset load" projects from the fly ash to be sold as a pozzolan. Development of an air-entraining agent that is less affected by the carbon in the fly ash has also been reported (*6*). However, careful testing is still required to determine the air content of the concrete when placed until the pattern shown by the materials being used on a job has been established.

Uncertainties Relating to Uniformity of Fly Ash Supply

Uniformity of fly ash from the same source was a concern for many of the early users. Complete testing of the pertinent characteristics of each fly ash shipment was (and is) impractical, and the effect of variations in fly ash was not fully known. This problem has been lessened by the development of a fly ash marketing industry that is developing standards of acceptability and a willingness to certify uniformity within reasonable standards [see Appendix C, *NCHRP Synthesis of Highway Practice 127* (*1*)]. Such standards now generally provide adequate shipment-to-shipment uniformity of the product so that its effect on concrete characteristics does not vary significantly. Most organizations utilizing a certification acceptance procedure after complete initial testing have had satisfactory results. Generally, fineness [amount retained on a No. 325 (45-μm) sieve] and the loss on ignition are spot-checked during the construction of a project.

Cold and Hot Temperature Placements

In recognition of the known slowdown of pozzolanic reactions at low temperatures, state highway agencies customarily establish a cutoff date after which fly ash concrete is not placed in pavements or structures. However, in recent studies in West Virginia, the initiation of freeze-thaw tests on specimens 1 to 3 days old did not indicate poor performance (*7*). The fly ash concretes were at least as good as the control.

Although the extent to which cutoff dates could be eliminated or extended in other geographical areas cannot be determined from this result, reevaluation of cold weather limitations is indicated. At the other end of the scale, some studies at the Virginia Transportation Research Council have shown a large increase in the resistance of fly ash concrete to chloride-ion penetration when specimens were cured at 100°F rather than the standard 73°F (*8*). Although not yet confirmed by field tests, the implication is that use of fly ash in hot weather would avoid detrimental results known to occur with ordinary portland cement concrete when placed and cured at elevated temperatures.

Differences in Class F and Class C Fly Ashes

Before 1970, most of the literature on fly ash was concerned with materials designated as Class F in accordance with ASTM Specification C 618. This material is a by-product of the burning of bituminous or anthracite coal that acts as a pozzolan but has no self-hardening properties. Substantial use of subbituminous coal began in the United States in the 1970s. The fly ash from burning these coals often has very high lime (CaO) content and exhibits self-hardening characteristics. These are designated as Class C; however, a number of them would also meet the Class F requirements.

Class F and Class C fly ash have been shown to vary considerably in their effect when used in concretes. Many of the principles established for using the by-products from burning bituminous coal are not completely valid for by-products from burning subbituminous coals. This has confused the classification picture, and although a number of suggestions have

been made, no agreement has been reached concerning a classification system for fly ash that will better indicate its performance in concrete.

The recently completed comprehensive study sponsored by EPRI provides excellent data on characteristics of the fly ash now being produced in various regions of the United States (*9*). However, the predictive models for compressive strength of fly ash concrete developed in this study are not useful as a basis for a system that could classify fly ash by purpose.

Any evaluation of the efficiency of fly ash in developing strength in concrete must account for both the characteristics of the particular fly ash involved and the characteristics of the particular cement used. The same fly ash often reacts differently with different cements.

ECONOMIC LOSS OR GAIN

Cost savings resulting from the use of fly ash concrete are usually emphasized because a portion of the portland cement is replaced by fly ash, which on a ton-for-ton basis, costs less. However, other factors enter into the total cost of fly ash concrete.

1. Relative transportation costs. The distance fly ash must be hauled has a large effect on its cost and thus the cost of producing fly ash concrete.
2. Normally, a mass of fly ash greater than the mass of the cement replaced is added to the concrete mix.
3. Additional air-entraining agents are required when fly ash is used.
4. Additional production costs for the concrete producer result from the necessity of maintaining a separate storage facility for fly ash and an apparatus to add it to the concrete mixes.
5. Additional control and acceptance testing is required when fly ash is used.

Thus, depending on the circumstances, the bid price of fly ash concrete may be equal to or even greater than the bid price of portland cement concrete without fly ash.

DESIGN OF FLY ASH CONCRETE FOR OPTIMUM CHARACTERISTICS

Although many researchers have indicated a need for a rational design of concrete mixtures containing fly ash to ensure optimum concrete characteristics and cost-effectiveness, most state highway agencies establish maximum amounts of cement that can be replaced with fly ash in highway applications. It is also customary to require that the mass of fly ash added be greater than the mass of cement removed. In judging the suitability of the fly ash, the procedure most often used is to compare the strength difference at early ages between control concretes containing the usually specified minimum mass of cement with the fly ash concrete at the same water-to-cementitious-material ratio. This procedure overlooks two important facts. The first is that there are a number of ways in which strength of the fly ash concrete at early ages (1 to 27 days) can be increased; for example, water-to-cementitious ratios can be water-reducing admixtures, or other changes could be made in mix proportions. Thus, establishing the levels of performance needed in concretes at specific ages without regard to the amount of cement being replaced is necessary. This approach will probably demonstrate that present levels of fly ash usage are well below optimum and that restrictions on the fly ash-cement ratio for some applications prevent the use of optimum amounts of materials leading to maximum benefits.

The second fact overlooked is that different types and brands of cements may react differently with the same fly ash. Thus, the optimum conditions for different fly ash–cement combinations may be different. Despite the fact that this principle is well established, there appears to be a reluctance on the part of some state highway agencies to make trial mixtures with the actual fly ash–cement combinations that will be used in a project. A potential solution to this problem that is currently receiving considerable attention is the establishment of performance specifications. Such specifications would permit a concrete supplier much leeway in the materials used as long as performance requirements are met. It is necessary to consider the durability of the concrete as well as the strength. A strong concrete under laboratory test conditions may not perform satisfactorily if it is subjected to damage from chlorides and sulfates or damage from freezing and thawing.

DEVELOPING TECHNOLOGY

The increased interest in fly ash usage has led to more studies and improved evaluation of the potential benefits of fly ash in concrete. In particular, the special characteristics of self-hardening fly ash are being evaluated. In general, these materials contribute to high strengths but may not always provide the increased sulfate resistance that is expected from Class F materials (*10*,*11*).

Studies on the chemical reactions taking place during hydration and within the liquid solutions of the hardened concrete are being performed, and their relation to physical properties is being determined. Determinations are also being made about the effects of combining fly ash and slag or fly ash and silica fume and how these combinations could provide cost-effective solutions to problems. Early results of a Virginia Transportation Research Council study with combinations of fly ash and small amounts of silica fume indicate that very high resistance to chloride-ion penetration can be obtained at early ages, thus counteracting adverse effects from the addition of fly ash alone.

Although it is not possible to predict how this developing technology will ultimately affect the use of fly ash concrete in highway construction, better knowledge of fundamental reactions and interactions of different cements with different fly ashes should permit optimization of mixture proportions for designated performance requirements that will also provide optimum environmental and economic benefits.

REFERENCES

1. W. J. Halstead. *NCHRP Synthesis of Highway Practice 127: Use of Fly Ash in Concrete*. TRB, National Research Council, Washington, D.C., 1986.

2. D. M. Golden. EPRI Coal Ash Utilization Research. In *Proc., 8th International Ash Utilization Symposium*, Vol. 1, Electric Power Research Institute, Palo Alto, Calif., Oct. 1987, p. 1-1.
3. *Fly Ash, Silica Fume, Slag, and Natural Pozzolans in Concrete: Proceedings, 2nd International Conference, Madrid, Spain*. ACI SP-91. American Concrete Institute, Detroit, Mich., 1986.
4. *Proceedings, 8th International Ash Utilization Symposium*. Vols. 1 and 2. EPRI CS-5362. Electric Power Research Institute, Palo Alto, Calif., 1987.
5. R. C. Meininger. *Status Report on Effect of Fly Ash on Air Entrainment in Concrete*. Series J-153. National Ready-Mixed Concrete Association, Silver Spring, Md., 1979.
6. G. R. Burg. You Now Have a Choice of Air Entraining Admixtures. *Concrete Products*. Oct., 1985.
7. W. S. Head and J. Sajadi. *Early Age Durability of Fly Ash Concrete*. WVDOH RP69. Department of Civil Engineering, West Virginia University, Morgantown, W. Va., 1985.
8. C. Ozyildirim and W. J. Halstead. *Resistance to Chloride Ion Penetration of Concrete Containing Fly Ash, Silica Fume, or Slag*. VTRC 88-R11. Virginia Transportation Research Council, Charlottesville, 1988.
9. *Classification of Fly Ash for Use in Cement and Concrete*. EPRI CS-5116. Electric Power Research Institute. Palo Alto, Calif., 1987.
10. E. R. Dunstan Jr. Possible Method for Identifying Fly Ashes That Will Improve the Sulfate Resistance of Concretes. *Cement, Concrete, and Aggregates*. CCAGDP, Vol. 2, No. 1, 1980.
11. P. K. Mehta. Effect of Fly Ash Composition on Sulfate Resistance of Cement. *Journal of the American Concrete Institute*. Vol. 83, 1986.

Publication of this paper sponsored by Committee on Chemical Additions and Admixtures for Concrete.